Towards an improved thermodynamic modelling and enhanced efficiency of energy conversion systems

Silvia Lasala

Ecole doctorale SIMPPÉ

Sciences et Ingénierie des Molécules, des Produits, des Procédés et de l'Énergie

Towards an improved thermodynamic modelling and enhanced efficiency of energy conversion systems

Contribution à l'amélioration de la modélisation thermodynamique et à l'augmentation de l'efficacité des systèmes de conversion d'énergie

Mémoire présenté en vue de l'obtention du diplôme
d'habilitation à diriger des recherches

par **Silvia Lasala**

Maître de conférences à l'ENSIC-LRGP

Soutenance : le 18 mars 2024 à 9h00, amphithéâtre Donzelot, ENSIC, 1 rue Grandville, Nancy

Rapporteurs :

Prof. Maria Grazia DE ANGELIS, University of Edinburg, Royaume Uni

Dr. Paolo STRINGARI, Mines Paris–PSL, France

Prof. Eva THORIN, Mälardalen University, Suède

Examinateurs :

Prof. Paolo CHIESA, Politecnico di Milano, Italie

Prof. Jean-Noël JAUBERT, Université de Lorraine, France

Prof. Fabrice LEMOINE, Université de Lorraine, France

Prof. Isabella NOVA, Politecnico di Milano, Italie

Prof. Roland SOLIMANDO, Université de Lorraine, France

Summary

Preface

The field of "thermodynamics of energy conversion systems" represents the core of the activities covered by the university training, the doctoral and post-doctoral studies of the applicant, Silvia Lasala. Currently, she is assistant professor at *Université de Lorraine*, more precisely she teaches at the *Ecole Nationale Supérieure des Industries Chimiques* (ENSIC) and carries out her researches at the *Laboratoire Réactions et Génie des Procédés* (LRGP) of the *Centre National de la Recherche Scientifique* (CNRS) and *Université de Lorraine*.

The applicant is an Energy Engineer who carried out her university studies at Politecnico di Milano. She was initiated to the field of Research in 2011, with the development of her Master thesis in the R&D Combustion and Casings department of Rolls-Royce plc, in United Kingdom. With the necessity of reducing NO_x emissions of its aeronautic engines and addressing the related problem of induced combustion instabilities, Rolls-Royce appealed to Politecnico di Milano. In this context, the applicant was selected to develop an experimental combustion chamber and a semi-empirical model both used for the prediction of unstable modes occurring in full annular combustion chambers of aeronautic turbines operating with liquid kerosene. Dealing with the understanding of the interactions between the thermo-acoustics of the combustion chamber and the flame dynamics, this topic approached the applicant to the field and the rigour of scientific research.

In 2012, she started a doctoral European thesis [1] under the supervision of Prof. Paolo Chiesa, at Politecnico di Milano, and in collaboration with Prof. Jean-Noël Jaubert, at ENSIC-LRGP. Her doctoral research focused on the theoretical and experimental study of the thermodynamics of fluids involved in CO_2 capture and storage technologies. The four major contributions of this doctoral research [2–7] are: **1) the improvement of cubic equations of state.** Aiming at the definition of a thermodynamically accurate and consistent cubic equation of state, this work analyses and corrects theoretical inconsistencies in cubic equations of state applied to pure fluids and mixtures. More specifically, the theoretical development of equations of state for pure fluids has consisted in the derivation and application of theoretical criteria for defining the functional relationship between the energy parameter of an equation of state and temperature; with regard to the modeling of mixtures, this study has tested the accuracy of new mixing rules that couple the equation of state with the residual part of the Wilson Helmholtz excess energy model (mixing rules noted as "EoS/$a^{\text{E-Wilson}}{}_{\text{res}}$" in what follows). **2) Measurement of thermodynamic properties of mixtures in liquid-vapor equilibrium.** Optimizing and validating the proposed thermodynamic model (and every thermodynamic model available

today) requires experimental data. Due to insufficient available data, in this work it was carried out an experimental campaign to determine the thermodynamic properties of CO_2-O_2, CO_2-N_2, CO_2-Ar, CO_2-N_2-O_2, CO_2-N_2-Ar mixtures in liquid-vapor equilibrium for temperatures between 223 K and 293 K and pressures ranging from 10 bar to 200 bar. **3) Optimization and validation of the model developed in the study.** The thesis presents the optimization and comparison of two models: the Peng-Robinson equation of state modified by the application of the "EoS/$a^{E\text{-}Wilson}{}_{res}$" mixing rules proposed in the study (new model developed) and the standard Peng-Robinson equation of state (commonly used comparison model). In this work, these models were optimized on the experimental liquid-vapor equilibrium data available for the 36 binary mixtures resulting from the combination of 9 compounds typically present in CO_2 capture and storage mixtures: H_2, N_2, CO, Ar, O_2, CH_4, CO_2, H_2S, H_2O. Given the number of datasets available in the literature and those measured in this study, it was possible to optimize the model on 23 binary mixtures. Validation and comparison of the two models was carried out using data on ternary mixtures in vapor-liquid equilibrium, and data on mixing enthalpies and densities. The results confirmed the superiority of the model proposed in this study. **4) Assessment of the industrial impact of the accuracy of the applied thermodynamic model**. The effects of using more or less accurate models were quantified by means of considerations on the sizing and performance of a purification and compression unit for mixtures typically captured in post-combustion, pre-combustion and oxy-combustion processes. The main analyses concerned the following aspects: (1) purification by liquefaction and distillation; (2) determination of the CO_2 pressure to guarantee its transport in liquid or supercritical phase conditions; (3) calculation of the energy required to pressurize the CO_2-based mixture up to transport pressure. The most important effect related to the accuracy of the thermodynamic model used was observed when calculating the number of trays in a distillation column to reduce the level of oxygen present in the captured CO_2 stream to 100 ppm: the equation of state introduced by this study, rather than the models commonly used, predicts a number of trays needed to reach the target that is halved.

During her doctoral studies and at the beginning of her postdoctoral researches, the applicant also investigated, with some colleagues of "Politecnico di Milano" and "Università di Brescia", some effective ways to increase the efficiency of power cycles used to recover the thermal energy content of low-temperature heat sources (max. 400 °C) and, eventually, high temperature heat sinks (higher than 30 °C). More specifically, she contributed to the design, experimental characterization and thermodynamic modelling of **working fluids for power**

cycles. Firstly, she focused on the comparison of cycles operating with either CO_2 or organic molecules, considering different features of the thermal energy source (maximum temperature, and cooling degree). Some useful maps have been produced, suggesting the specific working fluid and cycle's configuration to be used depending on the heat source characteristics. During this fluid screening, the selection of working fluids with respect to their thermal stability (i.e., their capability of maintaining unchanged their molecular structure at a specific temperature), was based on a very uncertain hypothesis. Indeed, the thermal stability limit of organic molecules is rarely known. Thanks to the collaboration with Prof. Invernizzi, the applicant could then perform, at the University of Brescia, the experimental characterization of the thermal stability limit of different molecules of interest for either Organic Rankine Cycle applications (perfluorohexane, n-pentane, cyclo-pentane and toluene [8,9]) or CO_2-based mixtures, for supercritical and transcritical CO_2 cycles, that she conceived [10]. Although she designed a system to measure the thermal stability of mixtures, this experimental activity was unfortunately limited to the study of the thermal stability of pure fluids. However, the experimental investigation of the thermal stability of working fluids for power cycles and heat pumps, and the impact of a small (acceptable?) degree of molecular instability on the performance of plants is an open -and not sufficiently investigated- field of research which would deserve more attention from the scientific community.

Right after the doctoral thesis, in 2016, the applicant started a two-year postdoc at LRGP funded by Air Liquide, who appointed two main tasks. The first one consisted in the understanding of the modelling potential of thermodynamic and transport properties of the fluids involved in cryogenic processes for separating the main components present in **air (nitrogen, oxygen and argon)** [11]. A second topic was about the thorough study of the state of the art of hydrogen liquefaction catalytic processes. Hydrogen exists in two molecular forms of nuclear spin isomers called ortho-hydrogen (o-H_2) and para-hydrogen (p-H_2). The proportion between these two forms of hydrogen, dictated by the thermodynamic equilibrium of the o-H_2 ⇄ p-H_2 equilibrium reaction, varies with temperature: at the start of the hydrogen liquefaction process (at ambient temperature) the mixture consists of 75% o-H_2 and 25% p-H_2 (a mixture known as 'normal hydrogen'), in a gaseous state; at storage temperature (20 K) the mixture consists of 99.8% p-H_2, in a liquid state. The transformation of o-H_2 into p-H_2 is exothermic and characterised by a very low conversion rate. As a result of such slow kinetics, the hydrogen remains in its "normal" form throughout the liquefaction process, up to the storage temperature (20 K); the liquid thus obtained, composed of 75% o-H_2, undergoes a slow spontaneous

exothermic transformation which converts this 75% o-H_2 into p-H_2 with a release of heat that produces an undesirable partial evaporation of the liquefied hydrogen. To overcome this drawback, ortho/para-hydrogen conversion must be carried out during liquefaction using a suitable catalyst that increases the speed of the conversion reaction. The applicant was asked to thoroughly analyse the state of the art on the thermodynamics and kinetics of the **reaction ortho-hydrogen ⇄ para-hydrogen** [12] and on the catalytic effect of ferric oxide Fe_2O_3 on the kinetics of the reaction. She also developed a library that contains the selected kinetic model, optimized by Wilhelmsen et al. [13] which is currently used in the process simulator (ProSim) generally used at Air Liquide for liquefaction-H_2 simulations. The research on the thermodynamic modelling of hydrogen was then pursued in collaboration with a colleague, Prof. Ø. Wilhelmsen, of NTNU [14]. He proposed to collaborate with the aim of developing an accurate and thermodynamically consistent cubic equation of state (i.e., accounting for the consistency criteria of α-functions developed in the applicant's thesis and furthermore by Le Guennec et al. [4]) by applying a **quantum correction** to the hydrogen co-volume. The correction was extended to other quantum fluids and resulted in a sensibly higher modeling accuracy of pure quantum fluids and their mixtures.

In parallel to the above-mentioned postdoctoral subject, the applicant started developing her proper research project, that she defended in the occasion of the attribution of her chair of assistant professor, in 2018. This project pivots around a curious question that was introduced in 1957 by Prof. Lighthill [15] and then investigated by few authors, among which Prof. Angelino [16] of Politecnico di Milano: **what happens if we expand or compress fluids where a reversible chemical reaction takes place all along the expansion/compression transformation?** What is the effect of the simultaneous conversion of thermal (physical) and chemical energy in thermodynamic transformations and thus in thermodynamic cycles?

To answer this question in a generalized way (i.e., non-fluid-specific), the applicant proposed to define **fictitious gaseous reactive working fluids** and assessing the impact that the thermochemistry and the stoichiometry have on cycle's performance. The first conclusions were drawn on Baryton power cycles and quantified a breakthrough potential [17] that pushed the applicant to extend this study to other thermodynamic cycles (Brayton cycle-based heat pumps, Stirling power and heat pump cycles) that are being studied by a doctoral student under the (co)supervision of the applicant [18]. Also, the revealed high-potential and the limited availability of real suitable reactive fluids drove the applicant towards the submission (and

obtention) of an ERC-Starting Grant project (REACHER) aimed at designing and characterizing appropriate reactive working fluids, the corresponding optimal thermodynamic cycle architectures and validating in a micro-power plant. These are the main overall topics covered by the current research activity of the applicant, described in more details in the present document.

Other researches were undertaken in the last years, in collaboration with other national and international research groups. This manuscript presents the main past, present and future contributions of the applicant to fundamental and applied scientific research in thermodynamics and Energy Engineering. Their presentation follows a (non-chronological) thematic order, grouped in the following main axes.

- *Chapter 1.* Contributions to the **thermodynamic characterisation** of pure and multicomponent **inert fluids**.
- *Chapter 2.* Contributions to the **improvement of conventional thermodynamic cycles efficiency**.
- *Chapter 3.* Investigation and development of **thermodynamic cycles** operating with **reactive working fluids**, from fictitious to real reactive working fluids: the ERC project REACHER.
- *Chapter 4.* Modelling the **thermodynamics of reactive mixtures** (a first outcome of the ERC project REACHER, introduced in chapter 3)
- *Chapter 5.* Design of an **experimental micro – power plant** to validate the potential of using reactive working fluids (a second outcome of the ERC project REACHER, introduced in chapter 3)

1. Contributions to the thermodynamic characterisation of pure and multicomponent *non-reacting* fluids, at equilibrium.

Application to CO_2 capture and storage, quantum-fluids, and air-component separation processes

This chapter presents the contributions of the applicant to the thermodynamic modelling of inert pure and multicomponent fluids, produced during her doctoral (sections 1.1-1.5) and postdoctoral (sections 1.6 and 1.7) research activities. The main co-contributors to these activities with whom the applicant interacted the most are the professors: prof. Paolo Chiesa (supervisor of the doctoral thesis), Jean-Noël Jaubert, Romain Privat, Øivind Wilhelmsen.

<u>Current</u> supervision activity on this topic (2023-2026): Ehsan Asadi (doctoral student).

1.1. The thermodynamic modelling needs affecting CCS processes.

The target of reducing the worldwide level of greenhouse gases emitted by industries has diverted the focus of engineers and scientists towards the achievement of an increased efficiency of production processes, on the one side, and the design of innovative low-CO_2 emission energy systems, on the other. In this context, technologies have been developed to capture the CO_2 produced by energy-intensive industries, transport the captured carbon dioxide and either utilize it (for Enhanced Oil/Gas Recovery (EOR/EGR) or for its further conversion into energy) or sequestrate it in geological formations. Depending on the characteristics of the CO_2 capture technology, on the type of fuel and oxidant used within the energy conversion process, captured CO_2 streams contain different types and amounts of species (mostly, H_2O, Ar, N_2, O_2, CH_4, H_2, CO, H_2S, CO). This is schematically represented in Figure 1.

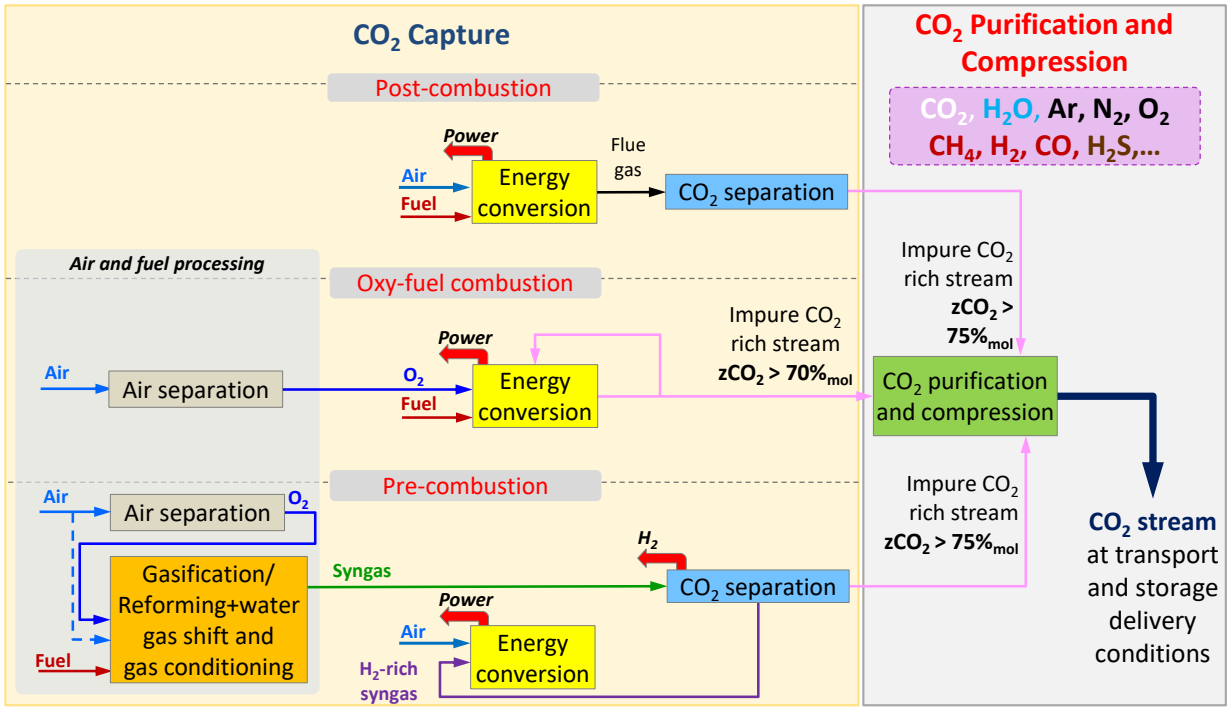

Figure 1. Capture processes and produced impure streams. In the figure, "zCO_2" represents the molar fraction of CO_2 in the stream. Figure collected from the defence support of the PhD thesis of the applicant.

Researchers identified, in the inaccurate and uncertain thermodynamic modelling of multicomponent fluids treated by CCS processes, one of the main sources of uncertainty for estimating costs associated to the CCS industry [19]. Indeed, both the attested inaccuracy of available thermodynamic models and the unknown uncertainty associated to inaccurate

thermodynamic calculations drive engineers towards the oversizing of equipment, to ensure the achievement of capture requirements.

The driver of this research was that, among the thermodynamic models which are present in the literature, their accuracy in describing the thermodynamic properties of interest for CCS processes is still not satisfying. Available cubic and molecular-based Equations of State (EoS), whether optimized over low and high pressure data, tend in fact to deteriorate the accuracy of low pressure calculations to improve their, however poor, capability in representing the critical region [20–22]. One of the most challenging thermodynamic tasks is represented, in fact, by the modelling of the critical region of typical high-pressure systems.

Considering the above, the doctoral research of the applicant has aimed to:

- improve the theoretical soundness of available cubic equations of state, in order to provide a theoretically consistent, accurate and, thus, reliable model applicable to mixtures containing CO_2, N_2, O_2, Ar, CO, CH_4, H_2, H_2S, H_2O;
- install an experimental apparatus for VLE measurements and provide high-pressure VLE data of binary and ternary systems containing CO_2, Ar, N_2, O_2;
- assess the impact of the accuracy of considered equations of state in designing and operating CO_2 conditioning and compression units of CCS processes.

In order to present more specifically these contributions, the following sections 1.2-1.5 briefly introduce: the main features of the considered cubic equations of state and considered experimental data (section 1.2), the proposed theoretical improvement to cubic equations of state (section 1.3), the VLE data measured in the doctoral work (section 1.4) and the optimisation and validation of the proposed model (section 1.5).

1.2. Theoretical gaps in the development of cubic equations of state

Equations of State (EoS) may be grouped in four classes: Virial EoS, cubic EoS, multi-parameters EoS, non-cubic molecular EoS. Among those, cubic EoS are the mostly applied by process engineers; and the reason for their widespread application lies in their recognized high capability and simplicity, compared to the other three groups, in modelling the thermodynamics of complex systems [23]. Furthermore, it is worth mentioning that the comparison performed by other authors [20,21,24] between cubic and molecular-based equations of state showed similar low accuracies in the calculation of equilibrium pressures, vapour phase compositions

and liquid densities of CCS mixtures. Cubic EoS have been considered in this work mainly because, despite the copious amount of scientific works aimed at investigating and exploiting the potentiality of such models, some theoretical improvements still could be performed over them [25]. The general formulation of a cubic equation of state is the following:

$$P = \underbrace{\frac{R \cdot T}{v - b_m}}_{\text{Repulsive term}} - \underbrace{\frac{a_m}{(v - r_1 \cdot b_m)(v - r_2 \cdot b_m)}}_{\text{Attractive term}} \quad (1)$$

where r_1 and r_2 are two universal constants which depend on the selected equation of state [26], a_m and b_m are respectively the energy and covolume parameters of the mixture, R is the universal gas constant, P, T and v are respectively the pressure, temperature and molar volume of the mixture.

The application of any cubic equation of state to mixtures requires to express energy and covolume parameters of the mixture, a_m and b_m, by means of mixing rules, as a function of, respectively, energy and covolume parameters of pure species that compose the mixture, a_i and b_i, and of the composition of the system. This means that at the basis of modelling complex systems through cubic EoS, there is the need of defining (i) pure components energy and covolume parameters (a_i, b_i) and (ii) mixing rules (MR).

The doctoral research has contributed to the theoretical improvement of the thermodynamic modelling of mixtures by cubic EoS focussing on their α-function models (directly related to energy parameters through the critical properties of i-th pure fluid $a_i(T) \propto \frac{T_{c,i}^{\,2}}{P_{c,i}} \cdot \alpha_i(T)$) and mixing rules.

Gaps in pure component modelling: focus on α-functions.

As already mentioned, this research work investigates systems containing components characterised by highly different volatilities. Indeed, CCS mixtures may simultaneously contain components being subcritical and supercritical, in their pure form. As it will be emphasised, the preliminary evaluation and comparison *in both subcritical and supercritical regions* of the different available α-function models, for each of the nine considered pure species, proved to be crucial.

As highlighted by [23], one of the most influential contributions in the prediction of vapour pressures of non-polar and slightly polar pure compounds has been the introduction of the Soave α-function [27]. Over the years, further modifications have been introduced to this functional form, mainly aimed at improving the correlation of vapour pressures. However, as stated by Poling et al. [28], most of the α-functions presented in literature have been developed without evaluating their predictive capability in the supercritical domain. According to Sengers et al. [23], one of the main targets, at the basis of the modifications to the Soave function, consisted in the "improvement of the behaviour in the supercritical domain", in addition to that of increasing its accuracy in correlating vapour pressures of any fluid. To complete such an observation, in this research work it is noted that the only attempt found in the literature, to improve the behaviour of α-functions in the supercritical region, consisted in optimizing the parameters of the function, separately, in the subcritical and supercritical domain. However, Neau et al. [29] showed that such distinctions between subcritical and supercritical regions, introduced in both Soave-type [27] and generalized-Twu [30] models, lead to an irregular behaviour of derived thermodynamic properties, such as enthalpies and heat capacities.

Any modification to the Soave α-function has been found that introduces a novel functional form being able to improve the predictions in both subcritical and supercritical regions, without distinguishing between parameters specifically applied in one of the two domains. To this modelling gap it was associated the lack, in the literature, of specific theoretically-based guidelines to define an α-function that could guarantee consistent predictions of the derived thermodynamic properties, in the whole temperature range.

One of the aims of this research was to contribute to fill this gap, as explained in section 1.3.

Gaps in mixture modelling: focus on mixing rules.

Over the years, different approaches were developed which have led to the definition of four main classes of mixing rules (MR): classical quadratic MR, composition-dependent MR, density-dependent MR and MR that incorporate local-composition activity coefficient models. Composition- and density-dependent MR has not been considered in this work. This is because the former only incorporates empirical modifications to the classical quadratic mixing rules and the latter does not improve the accuracy of the computed phase-equilibrium properties, with respect to density-independent MR [15].

Classical van der Waals quadratic MR have been considered in this work since, despite their limitations, they have stood the test of time. However, these models are limited: they are characterized by a low accuracy in modelling mixtures where interactions are strongly coupled to the local composition because they assume that intermolecular interactions between compounds are independent of each other (e.g. random mixing).

Mixing rules based on the local composition concept incorporate "local composition activity coefficient (γ) models" that account for preferential intermolecular interaction forces which lead the local composition to differ from the bulk one (e.g., Wilson [31], NRTL [32], UNIQUAC [33]). Historically, these mixing rules (Huron-Vidal (HV) MR [34], Modified Huron-Vidal (MHV) MR [35] and Wong-Sandler (WS) MR [36]) are called "MR derived from excess Gibbs energy model" [37], or "EoS+$g^{E,\gamma}$ MR", which take the general form:

$$\begin{cases} b_m \text{ (MR - dependent formulation)} \\ \dfrac{a_m}{b_m} = \displaystyle\sum_i z_i \frac{a_i}{b_i} + \frac{g^{E,\gamma}}{\Lambda_{\text{EoS, MR - depedent value}}} \end{cases} \tag{2}$$

where the three models differ on the basis of the mixing rule for the co-volume, b_m, and the parameter Λ, dependent on the selected equation of state and on the selected mixing rule (HV, MHV or WS). Their name, "EoS+$g^{E,\gamma}$ MR", originates from the fact that those are derived from equating the excess Gibbs energy derived from an equation of state and the one derived from a local activity coefficient model:

$$\left[g^{E,EoS}\left(T, P, \mathbf{z}\right) \right]_{P_{ref}} = g^{E,\gamma}\left(T, \mathbf{z}\right) \tag{3}$$

The cubic equations of state based on local composition mixing rules which have been applied before this work, in general and more specifically to CCS systems, are based on "EoS+$g^{E,\gamma}$ MR" [20,38]. However, streams treated by CCS processes, on the one side, and experimental data at the basis of the optimization of these EoS to model CCS fluids, on the other, may achieve very high pressures (higher than 150 bar).

When applied to high-pressure systems, "EoS+$g^{E,\gamma}$ MR" retain an inconsistency which could be avoided by recognizing that the pressure-independence of activity coefficient models present in the literature (e.g., Wilson, NRTL, UNIQUAC/UNIFAC) entails their being theoretically

sound excess Helmholtz energy models rather than pressure-dependent excess Gibbs energy ones. Thus, applying the following equality instead of (2):

$$\left[a^{E,EoS}\left(T,\mathbf{z}\right)\right]_{P_{ref}} = a^{E,\gamma}\left(T,\mathbf{z}\right) \tag{4}$$

Jaubert and Privat [39] obtained the following unique generic formulation of "MR derived from excess Helmholtz energy model" ("EoS+$a^{E,\gamma}$ MR"):

$$\begin{cases} b_m \text{ (any mixing rule)} \\ \dfrac{a_m}{b_m} = \displaystyle\sum_i z_i \frac{a_i}{b_i} + \frac{a_{res}^{E,\gamma}}{\Lambda_{EoS}} \end{cases} \tag{5}$$

which means that, providing any mixing rule for the covolume, the mixing rule for the energy parameter is univocally determined once the local composition model, $a^{E,\gamma}$, is specified. Moreover, only the energetic part of the excess Helmholtz energy model $a^{E,\gamma}$ is included in the mixing rule for a_m, the so-called "residual ("*res*") contribution". Some open questions remained, such as their general modelling capability, the value of the parameter Λ_{EoS}, and the activity coefficient model to be adopted to compute the residual excess Helmholtz energy term.

This doctoral research work aimed at testing, for the first time, mixing rules in equation (5), applying them to CCS mixtures and preliminarily addressing the above-mentioned open questions, as explained in section 1.3.

Literature review of experimental data available for CCS systems

At the basis of the development of thermodynamic models there are data. This is why, in this section, it is summarised the result of a review about available experimental data for the CCS systems considered in the doctoral thesis of the applicant and being considered in an ongoing PhD thesis under the supervision of the applicant.

In the doctoral research of the applicant, available data were originally collected for binary and ternary systems containing CO_2, N_2, O_2, Ar, CO, H_2, CH_4, H_2O and H_2S. Data have been collected from review works [40–44] and from the NIST database, accessed through the software Aspen Plus®. For 13 of the 36 binary mixtures deriving from the binary combination of these 9 pure components (H_2O+CH_4, H_2O+O_2, H_2O+Ar, H_2O+CO, H_2O+N_2, H_2O+H_2, H_2S+H_2, H_2S+O_2, H_2S+Ar, CH_4+O_2, CO+H_2, CO+O_2, CO+Ar), as well as for most

multicomponent systems, vapour-liquid equilibrium data are not available or not sufficiently numerous either to optimize or to reliably validate models. Clearly, such a drawback reduces the accuracy of models calibrated over these limited data, and the reliability of their validation over multicomponent mixtures. This preliminary bibliographic review has also revealed the lack of uncertainties associated to available experimental data. It is worth observing that the reason of missing data for some of the mentioned systems is either their toxicity and/or their reactivity.

As said previously, during this doctoral research, the considered experimental data were limited to the consideration of the NIST database and available papers. A more thorough literature research is being performed in the context of the PhD thesis of Ehsan Asadi, currently under the direction of the applicant and of prof. Jérôme Sterpenich. In this work, the Dortmund Data Bank is used, and NO and SO_2 are added to the list of 9 components. Other binary systems for which thermodynamic data are missing are H_2S+SO_2, H_2S+NO, NO+Ar, NO+O_2.

1.3. Proposed theoretical improvements of cubic equations of state

As a result of a preliminary analysis performed on the capability of both Peng-Robinson (PR) and Soave-Redlich-Kwong (SRK) equations of state, to model the thermodynamics of the considered CCS pure species (CO_2, N_2, O_2, Ar, CO, H_2, CH_4, H_2O and H_2S), the PR equation of state has been preferentially selected rather than SRK since the PR model, with respect to the SRK one: (1) greatly improves the representation of liquid and vapour densities of carbon dioxide and of less volatile components; (2) partially improves the representation of vapour densities of components more volatile than CO_2 (except for N_2 and CO); (3) leads to errors in the calculation of saturation pressures being comparable with that of SRK; (4) slightly improves the prediction of enthalpies of vaporization (except for CO) and of specific isobaric heat capacities of saturated liquids of all 9 pure components.

Consistency criteria for α-functions

After selecting the Peng-Robinson as cubic EoS to be considered in the doctoral study, it has been assessed the possibility of improving its accuracy by comparing the results obtained by using the original PR α-function (the Soave model) with the Twu91 [45] α-function. Those models have been analysed in this work because they are considered, respectively, the most accurate generalized and component-specific α-functions, being both continuous in the whole temperature domain.

Figure 3a shows how similarly the Soave and Twu91 α-functions behave in subcritical conditions for argon and n-decane. However, Figure 3b shows that the two models follow a completely different trend in the supercritical domain. In this work, this issue has been detected and understood. The observed deviation is due to the empirical nature of α-function parameters, which are optimized by fitting the predictions of the applied equation of state to experimental data, (1) considering only subcritical properties (saturation pressures, heats of vaporization, liquid heat capacities) and (2) without imposing proper constraints to the behaviour of α-functions in the supercritical domain. Depending on the functional relationships that relate α-functions to their parameters, such an unconstrained optimization may lead to the generation of abnormal deviation when extrapolating to supercritical temperatures.

Clearly, the lack of theoretically-based guidelines that define consistent α-functions has always prevented from the definition of specific constraints to the α-function parameters under optimization. The demonstration of the consistent "positive - monotonically decreasing - convex function of temperature" of α-functions is briefly outlined below.

1) To avoid non-physical negative values of the attractive term of cubic equations of state:

$$\alpha(T) > 0 \quad \forall T \tag{6}$$

in particular, it can be observed that $\alpha(T_c) = 1$.

2) When temperature tends to infinite values, molecules move randomly without interacting, leading to:

$$\lim_{T \to \infty} \alpha(T) = 0 \tag{7}$$

3) When temperature is reduced, molecules are particularly prone to interact, upon collision, hence:

$$\frac{d\alpha}{dT} < 0 \quad \forall T \tag{8}$$

4) To understand how should an α-function behave at intermediate temperatures, consider the expression for $c_v^{res}(T^*)$:

$$c_v^{res} = -\frac{T}{(r_1 - r_2)b} \ln\left(\frac{v - r_1 b}{v - r_2 b}\right)\left(\frac{d^2 a}{dT^2}\right) \tag{9}$$

Where it can be observed that:

$$-\frac{T}{(r_1-r_2)b}\ln\left(\frac{v-r_1 b}{v-r_2 b}\right)>0 \quad \forall T \tag{10}$$

As a consequence, the eventual presence of inflection points of an α-function at a specific temperature T* would entail a zero $c_v^{res}(T^*)$:

$$\left.\frac{d^2 a}{dT^2}\right|_{T=T^*}=0 \Leftrightarrow c_v^{res}(T^*)=0 \tag{11}$$

Which would mean that the fluid would have the same heat capacity as the one of an ideal gas, in T^*. However, since $c_v^{res}(T^*)$ is pressure-independent, the validity of eq. (11) would entail that at the same temperature T^* the fluid would be characterized by the same heat capacity (that of an ideal gas) whatever the pressure would be $c_v(T,P)=c_v^{ig}(T)$, which is not supported by experimental evidence.

The first outcome of the theoretical part of this research is the demonstration that a theoretically consistent α-function must be a positive - monotonically decreasing - convex function of temperature, that is:

$$\begin{cases} \alpha(T)>0 \quad \forall T, \quad \alpha(T_c)=1 \\ \lim\limits_{T\to\infty}\alpha(T)=0 \\ \dfrac{d\alpha}{dT}<0 \quad \forall T \\ \dfrac{d^2\alpha}{dT^2}>0 \quad \forall T \end{cases} \tag{12}$$

This theoretical demonstration and result is presented in the doctoral thesis of the applicant [1], and has been published in [4] where the work has been further extended by the ThermE team, in the doctoral work of Dr. Le Guennec [46], under the supervision of prof. Jaubert and prof. Privat. With reference to these new defined guidelines, the Soave and Twu91 models have been then analysed. The mathematical formulations are shown in Figure 2.

T-overall formulation

Generalized parameters

Soave(*)

$$\alpha = \left[1 + m\left(1 - \sqrt{T_r}\right)\right]^2$$

where m are obtained from the following generalized formulations:

EoS	m	Ref
RK	0.480 + 1.574 ω - 0.176 ω^2	(*)
PR	0.37464 + 1.54226 ω - 0.26992 ω^2	(**)

(*) (Soave 1972)
(**) (Peng and Robinson 1976)

Component-specific parameters

Twu-91(*)

$$\alpha = T_r^{N(M-1)} exp[L(1 - T_r^{NM})]$$

with L,M,N being component-specific parameters. For components of this study:

EoS	Comp.	L	M	N	Ref
PR	Ar	0.036512	0.935460	3.97643	(**)
	n-$C_{10}H_{22}$	0.315303	0.811589	2.42062	(**)
	CO_2	0.040	0.943	8.538	(***)

(*) (Twu, et al. 1991)
(**) (Twu, Coon and Cunningham 1995) -PR
(***) (Privat, Visconte, et al. 2015)

T-domain-specific formulation

Generalized parameters

Gen.-Twu (*)

$$\alpha = \alpha^{(0)} + \omega(\alpha^{(1)} - \alpha^{(0)})$$

$$\alpha^{(i)} = T_r^{N^{(i)}(M^{(i)}-1)} exp\left[L^{(i)}(1 - T_r^{N^{(i)}M^{(i)}})\right]$$

with i ∈ {0;1}
with $L^{(i)}$,$M^{(i)}$,$N^{(i)}$ being domain-specific parameters:

EoS	Par.	Tr≤1		Tr>1	
		$\alpha^{(0)}$	$\alpha^{(1)}$	$\alpha^{(0)}$	$\alpha^{(1)}$
RK (*)	L	0.141599	0.500315	0.441411	0.032580
	M	0.919422	0.799457	6.500018	1.289098
	N	2.496441	3.29179	−0.20000	−8.00000
PR (**)	L	0.125283	0.511614	0.401219	0.024955
	M	0.911807	0.784054	4.963070	1.248089
	N	1.948153	2.812520	−0.20000	−8.00000

(*) (Twu, Coon and Cunningham 1995)-RK
(**)(Twu, Coon and Cunningham 1995)-PR

Mathias-Copeman (*)

$$\alpha = \left[1 + c_1\left(1 - \sqrt{T_r}\right) + c_2\left(1 - \sqrt{T_r}\right)^2 + c_3\left(1 - \sqrt{T_r}\right)^3\right]^2$$

with c_1,c_2,c_3 being component-specific and domain-specific parameters

Tr≤1	Tr>1
c_1	c_1
c_2	0
c_3	0

(*) (Mathias and Copeman 1983)

Figure 2. Classification of α-function models. The models proposed by Soave, Twu and Mathias-Copeman are presented, by way of example, to introduce the four groups of α-functions. (From Lasala [1])

Because of its quadratic form, the Soave α-function is always a positive - convex function of temperature but it is not monotonically decreasing in the whole temperature domain (see in Figure 3b: Soave for n-decane). However, the temperature at which it starts to increase is always far from the application range. Thus, in the interval of temperatures of engineering applications, the Soave α-function retains the required positive - monotonically decreasing - convex shape.

On the other hand, one of the most relevant outcomes of this part of the work is the observation of the detrimental effect, for some chemical pure species, of extrapolating the widely applied Twu91 model in the supercritical region, when using parameters present in the literature (e.g., [47] and in the original publication by Twu [30,45]). This is revealed in Figure 3b, by the occurrence of two inflection points, in the argon-Twu91 curve at $T_r \sim 1$ and $T_r \sim 2$. However, this is not the case for all components. For example, when this function applies to n-decane, it does not present any unexpected irregular behaviour. Twu91, in fact, is a component-dependent multi-parameters exponential function where the adoption of some sets of parameters, optimized only over subcritical properties, may lead to extremely unphysical results in the supercritical domain. With respect to this, Figure 3c aims at showing, practically, the concept anticipated above, about the physically absurd effect of inflection points of α-functions on the computation of residual molar heat capacities.

Moreover, Figure 4c shows how the incorrect modelling of pure components in the supercritical region, caused by the improper optimization of Twu91 α-function, affects the VLE calculations for the mixture CO_2-Ar at 253.1 K. In particular, it compares experimental isothermal VLE data to the optimized isothermal phase diagrams predicted by the Peng-Robinson equation of state, integrated with the advanced class of mixing rules introduced in this doctoral work, by selecting the Soave rather than the Twu91 α-function. Differently from α-Soave, which correctly correlates thermodynamic properties for both the pure components at 253.1 K, Twu91 fails at modelling the supercritical behaviour of argon, as shown in Figure 3b and Figure 4a. As a result, the critical point of the mixture is severely over-predicted and the bubble curve is misled. *Acknowledging that the problem is the modelling of the α-function, it is worth noting that the inaccurate representation of such VLE mixture properties lies in the incorrect modelling of the thermodynamics of pure components, rather than in the applied mixing rule.*

In the PhD thesis of the applicant, the (L, M, N)-parameters of the Twu91 have been re-optimized, for the 9 considered pure components, by imposing the correct positive - monotonically decreasing - convex form of the α-function (i.e. under constrained optimization). Figure 4c shows how the application of constraints to parameters of Twu91 α-function, to their optimization, improves VLE results and enables to obtain the consistent, desired, shape of the α-function. The generalized Soave and the constrained-Twu91 α-functions have been applied and compared in the thermodynamic models of the systems under analysis, finally justifying the conclusive preference of the application of the Soave model in this work. As a consequence,

the standard pure component formulation of the Peng-Robinson equation of state (originally based on the Soave formulation) has then been applied to model pure fluid parameters involved in mixture modelling. Also, it is specified that the mixing rule which has been used in this analysis to produce Figure 4(c) is the accurate "EoS+$a^{E}_{res}\gamma$-Wilson MR" introduced in the next section.

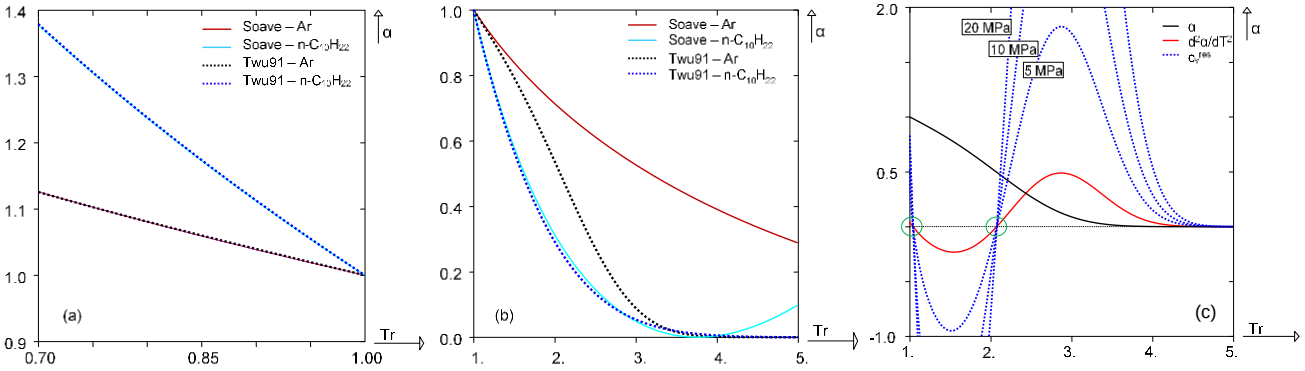

Figure 3. Comparison between PR-Soave and PR-Twu-91 α-functions in the subcritical (a) and supercritical (b) domains for argon and n-decane. For Twu91, the coefficients reported in [30] have been applied. (c) Effect of the presence of inflection points in α-functions, on residual heat capacities; in this figure, the model Twu-91 is applied to Argon (from Lasala [1]).

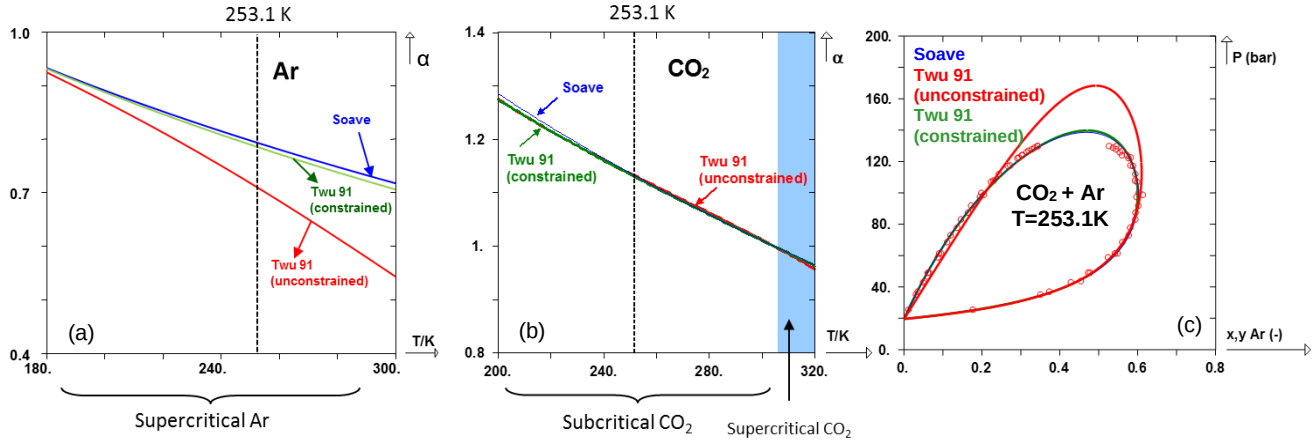

Figure 4. Comparison between Soave, Twu91 with parameters obtained from unconstrained or constrained optimization, applied to Argon (a), CO_2 (b) to Ar and CO_2 in the binary system Ar + CO_2 at 253.1K (c). (From Lasala et al. [2]).

The necessity of optimising α-function parameters considering the consistency criteria that have been derived has then been considered in further research works of the group [48,49] and is currently adopted by the scientific community.

Advanced mixing rules

The doctoral research shows the results of the first application of "EoS+$a^{E_{res}\gamma\text{-Wilson}}$ MR" local-composition mixing rules to CCS systems, proposing a proper formulation for the covolume mixing rule and assessing the application of the Wilson γ-model.

Table 1 summarizes the two classes of mixing rules applied, in this work, to the Peng-Robinson equation of state and then compared. As regards specification about the selected mixing rule for the covolume, for EoS+$a^{E,\gamma}$ mixing rules, the molecular-founded proposal of Lorentz [50] has been applied. In the considered models, empirical parameters are contained in the mixing rule for the energy parameter, a_m:

- quadratic Van der Waals mixing rule for a_m contains an empiric parameter for each pair of components present in the mixture. This is the k_{ij} symmetric (i.e., $k_{ij} = k_{ji}$) parameter mentioned in Table 2;
- the EoS/$a^{E_{res}\gamma\text{-Wilson}}$ mixing rule for a contains two binary, asymmetric, interaction parameters L_{ij} and L_{ji} which are included in the formulation of the activity coefficient model ($a^{E,\gamma\text{-Wilson}}$). Those are based on theoretical foundations; in fact, these parameters are an integral part of the local Boltzmann distribution around molecules, included in the Wilson local composition model.

In general, as justified in the thesis, these parameters should be optimized over experimental VLE data of binary systems. Considering that this thesis treats mixtures of, at most, 9 components, it results that 36 VLE binary systems have to be studied and, for each of them, VLE experimental data have been collected and/or measured, as it is mentioned in sections 1.2 and 1.4.

Table 1. Summary of the mixing rules applied in this work to the PR EoS

Name of the MR	***MR for the co-volume, b_m***	***MR for the energy parameter, a_m***	***MR parameters***
Classical quadratic vdW	$b_m = \sum_i z_i b_i$ (13)	$a_m = \sum_i \sum_j z_i z_j \sqrt{a_i a_j}\left(1 - k_{ij}\right)$ (14)	k_{ij}
EoS+ $a^{E_{res}\gamma\text{-Wilson}}$	$b_m = \sum_i \sum_j z_i z_j \left(\frac{b_i^{1/2} + b_j^{1/2}}{2} \right)^2$ (15)	$a_m = b_m \left[\sum_i z_i \frac{a_i}{b_i} + \frac{a_{res}^{E,\gamma\text{-Wilson}}}{\Lambda_{EoS}} \right]$ (16)	L_{12}, L_{21} (of the γ-Wilson model). For more details, refer to [3]

1.4. Measurement of VLE data

The doctoral work provides new isothermal Vapour-Liquid Equilibrium (VLE) data of binary and ternary mixtures of CO_2+O_2/N_2/Ar at temperatures and pressures ranging between 223 K-293 K and 10 bar–200 bar. The experimental setup used to perform such measurements and the procedure for the determination of experimental uncertainties have been described in [1,51] while the experimental data are published in [3,6,51]. As it can be observed from what has been mentioned in section 1.2, the systems which have been experimentally characterised in this work (CO_2+O_2/N_2/Ar) belong to the family of systems for which experimental data already exist; that is justified by the fact that the experimental set up was not equipped to treat systems not yet characterised, which are either toxic/flammable/explosive or non-dangerous but aqueous and thus highly challenging to characterize. As shown in section 1.7, a work is now in progress to characterise the VLE of mixtures containing toxic CCS compounds.

1.5. Model optimization, validation and application to CCS processes

The doctoral work presents the optimization of (1) the standard Peng-Robinson (PR78, based on one-parameter *van der Waals MR*) and (2) the one introduced in the thesis (PR78 with two-parameter EoS+$a^{E}_{res}\gamma$-Wilson MR). These models are optimized over VLE data of binary mixtures resulting from the binary combination of 9 typical CCS components (H_2, N_2, CO, Ar, O_2, CH_4, CO_2, H_2S, H_2O) for which experimental data are made available either from the literature or from this work (i.e., 23 systems), as introduced in section 1.2.

For the sake of brevity, Table 2 summarizes the type of collected experimental data and their final use within this work. More details about the number of data and their accuracy are available in the thesis [1] and the relative publication [5].

Table 2. Type and use of collected experimental data

Type of data considered:	**Binary VLE**	**Ternary VLE**	**Density**	**Enthalpy of mixing**
Used in the stage of:	Model optimization	Model validation	Model validation	Model validation

Figure 5 shows the improved accuracy of the novel EoS (Figure 5b), compared to the optimised PR78 (Figure 5a). This conclusion is confirmed even if temperature-dependent k_{ij} parameters are considered for the PR78 model.

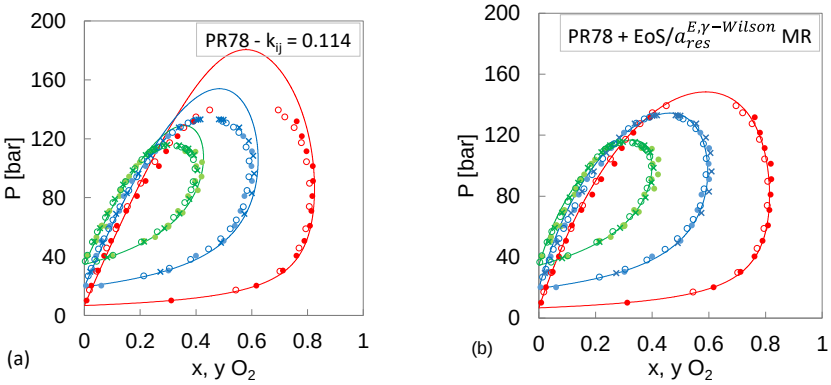

Figure 5. Phase diagrams of CO_2+O_2 at 223 K, 253 K, 273 K. Points (•, ×): data from lit. Points (o): data from this work. Lines: calculations with PR78 (a), with PR78 with optimized EoS+a^{E}_{res}γ-Wilson MR (b). (From [3])

The capability of the new model in representing most of CCS systems without introducing systematic errors has led to benefit, in this work, from the application of maximum likelihood optimization method: (i) whose results do not depend on the selected objective function; (ii) which accounts for the uncertainty of experimental data; (iii) which enable the characterization of the uncertainty of optimized parameters. These results led to capture the theoretical meaning of optimal parameters and could allow their predictive theoretical formulation. Results of this optimization process have been published in [52].

The 6th and last edition of The Properties of Gases and Liquids [53] **has considered this EoS/a^{E}_{res}γ-Wilson mixing rule, and associated it to the *tc*PR equation of state, also developed in the ThermE team** [54,55]**, which is a volume-translated version of the PR equation of state including the consistent Twu α-function. The comparison of this model with available equations of state (Refprop models, PC-SAFT, PR76, …) has led to the conclusion that tcPR+EoS/a^{E}_{res}γ-Wilson mixing rule "appears to provide the best capability for correlating VLE data of binary systems at low and high pressures".** One of the two databases used in the book to perform this comparison was developed by Jaubert et al. [56].

A further outcome of this research is the assessment of the impact of accounting for molar fraction uncertainties within the optimization process. This analysis has been published in a further paper [7]. The model validation, over ternary VLE, mixing enthalpies and densities, confirms the superiority of the new model. Results of this validation process have been published in [6].

The effect of applying differently accurate and uncertain models has been quantified by sizing and performance considerations on a CO_2 purification and compression unit, considering

mixtures produced by post-, oxy-fuel and pre-combustion capture processes: (1) purification by liquefaction and stripping; (2) determination of phase regime during CO_2 transportation; (3) definition of the pressurization level of purified CO_2 streams; (4) compression processes. For the sake of brevity, it is only reported the most evident impact, observed in designing stripping columns for the purification of CO_2 from O_2 up to a level of 100 ppm of O_2 (CCS with EOR restriction). The accuracy of the model has shown to relevantly affect the calculated number of column plates required to achieve the target purification level; indeed, the new model predicts half of the number of plates predicted by the less accurate model.

1.6. Further contributions to thermodynamic modelling during postdoctoral research

Modelling NO+SO₂ mixtures [57]

The postdoctoral research activities of the applicant were partially devoted to the further optimisation of the EoS+a^{E}_{res}γ-Wilson MR (eqs. (15) and (16)), to enable the characterisation of the VLE data of the binary system **NO+SO₂**, also relevant for CCS applications. More information can be found in the co-authored work of Creton et al. [57].

Extending the capability of E-PPR78 [22]

Moreover, the applicant has been working over the extension of the **Enhanced-Predictive-PR78** (E-PPR78), the predictive cubic equation of state proposed by Jaubert et Mutelet in [58]. This model is a modified version of the Peng-Robinson equation of state, where the binary interaction parameter, k_{ij}, in eq. (14) is calculated from the group contribution theory, with the following expression:

$$k_{ij}(T) = \frac{-\frac{1}{2}\left[\sum_{k=1}^{N_g}\sum_{l=1}^{N_g}(\alpha_{ik}-\alpha_{jk})(\alpha_{il}-\alpha_{jl})A_{kl}\left(\frac{298.15}{T/K}\right)^{\left(\frac{B_{kl}}{A_{kl}}-1\right)}\right]-\left(\frac{\sqrt{a_i(T)}}{b_i}-\frac{\sqrt{a_j(T)}}{b_j}\right)^2}{2\frac{\sqrt{a_i(T)a_j(T)}}{b_i b_j}} \quad (17)$$

where the a_i and b_i values are the energy and co-volume parameters of the Peng-Robinson equation of state, N_g is the number of different groups defined by the method and α_{ik} is the fraction of molecule i occupied by group k, and the group-interaction parameters, A_{kl} and B_{kl}, are symmetric, $A_{kl} = A_{lk}$ and $B_{kl} = B_{lk}$ (where k and l are two different groups), and empirically determined by correlating experimental data. Also, $A_{kk} = B_{kk} = 0$. The decomposition of two molecules in elementary groups (see Figure 6) and the knowledge of the group contribution parameters, A_{kl} and B_{kl}, enable the predictive determination of the binary interaction parameter

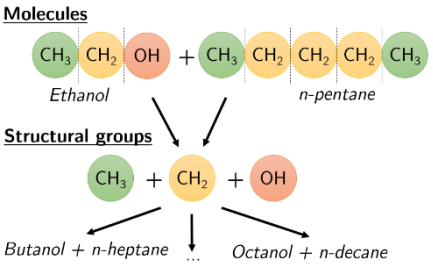

Figure 6. Group contribution concept.

for the couple of molecules forming the binary mixture. This model is known as the Predictive-PR78 (PPR78).

More precisely, **four new molecular groups** have been added to the matrix of group parameters: **"COS" (group 28), "NH_3" (group 29), "NO_2/N_2O_4" (group 30) and "N_2O" (group 31)**. The results of this work have been published by Xu et al. [22].

Discussing the power of including enthalpy and heat capacity of mixing data in model's optimisation: from PPR78 to E-PPR78 [59]

The applicant has written the last paper on the PPR78 model, aiming at presenting the reason why, in 2015, the model's group contribution parameters, A_{kl} and B_{kl}, are being optimized over enthalpy and heat capacity data other than VLE data, and changed its name to Enhanced-PPR78 (*E*-PPR78). This paper demonstrates that the **inclusion of enthalpy and heat capacity of mixing data in the process of optimization of the binary interaction parameters of the 40 groups of the *E*-PPR78** (i.e., its last version) leads to a remarkable reduction of the error on these properties, from 841.51% to 51.42%, while keeping almost constant the accuracy in the prediction of VLE data, 8.6% (without inclusion of mixing properties) to 8.8% (with inclusion of mixing thermal properties), on the basis of about 160 000 data. This work has been published in [59].

Improving the modelling of quantum fluids (hydrogen, helium, neon, deuterium) with cubic equations of state [14]

The consistency criteria proposed for the development of thermodynamically consistent α-functions (see section 1.3) positively led to consistent Twu α-functions for all species, except for quantum fluids, such as hydrogen and helium [4]. The reason was not understood, but was attributed to their negative acentric factors. Observing that for quantum fluids the co-volume parameter (which represents the size of a particle) of the equation of state, *b*, should be treated differently, a colleague from the NTNU, prof. Ø. Wilhelmsen, proposed to collaborate over the inclusion of temperature-dependent quantum corrections for the co-volume parameter and the re-optimization of their α-functions.

Indeed, quantum fluid properties are strongly influenced by the quantum effects: the size of a quantum particle increases at low temperature, as a consequence of the more pronounced wave-like nature of the particle, at those low temperatures. The constant-temperature co-volume of classical cubic equations of state does not allow to consider this so-called "quantum swelling" effect encountered when lowering temperature. In this work, the co-volume parameter was thus modified accounting for the temperature-dependent quantum swelling corrected form of the Feynman-Hibbs Mie potential. This was applied to model helium (^{4}He), hydrogen, neon and deuterium, and showed that the modification of the co-volume to account for quantum effects, not only resulted in the improved modelling of those pure fluids and their binary mixtures, but also in the obtention of re-optimized α-functions complying with consistency criteria. In this work, the task of the applicant was a minor one, since she was asked to validate the calculations performed by the team of NTNU.

Comparing available equations of state for air-component mixtures (Air Liquide need) [11]

A part of the postdoctoral research was funded by **Air Liquide** and devoted to the improvement of the knowledge and modeling potential of the thermodynamic and transport properties of fluids involved in cryogenic processes for the separation of components present in the air (**nitrogen, oxygen and argon**). In order to find the most precise equation of state for the representation of the thermodynamics of mixtures of oxygen, nitrogen and argon, this research has aimed to compare the performances of the three models, already available in the literature in their optimized form: two multi-parameter models, GERG-2008 and Bender, and the cubic Peng-Robinson equation of state. These models were compared on the basis of the deviations

observed between calculated values and experimental values of liquid-vapor equilibrium and density. This comparison made it possible to note the clear superiority of the GERG-2008 model and to show the impact of the deviations observed on the volume properties, on the precision of calculation of the transport properties (thermal conductivity and dynamic viscosity). The results of this work have been published in [11].

Improvement of REFPROP codes to model air-component mixtures (Air Liquide need)

The final objective of the research work funded by Air Liquide was the improvement of the computer codes developed by NIST, Refprop 9.1, in order to be able to reliably perform 10 different types of flash calculations needed by Air Liquide to model mixtures of N_2+O_2+Ar (T(temperature)-p(pressure), T-q(vaporization rate), p-q, T-h(enthalpy), T-s(entropy), p-h, p-s, p-ρ(density), ρ-s, ρ-u(internal energy)) with the GERG-2008 model. It is worth recalling that the so-called *flash* calculation enables the determination of thermodynamic states of a system associated to two known independent variables and the composition of the system. The analysis of Refprop source codes (written in Fortran) has allowed the understanding and the correction of some instabilities of its flash calculations, observed for different global compositions. Two problems have been detected:

1) At specific T-values, the two-phase region is predicted at pressures higher than bubble pressure ("Pb. 1" in Figure 7a), up to the calculated critical pressure.
2) In the very proximity of the critical region there is a discontinuity of the two-phase region ("Pb. 2" in Figure 7a).

The analysis of the TP-flash Fortran code has revealed that the observed problems are related to the facts that, to attest if the fluid is in two-phase or in single-phase, the subroutine TPFLSH compares the pressure of the system with dew and bubble pressures calculated by means of subroutines that, at some specific temperature values, fail in calculations (see incorrect bubble pressure calculations in Figure 7b). As a consequence, the two-phase region is misled. The problem has been fixed by modifying convergence criteria originally present in the subroutines for calculation of saturation pressures. The correction of this problem in bubble and dew pressure calculations has solved the issue, which was also affecting the other flash calculations. This modification has been included by NIST in Refprop 10, for which the applicant has worked as beta tester.

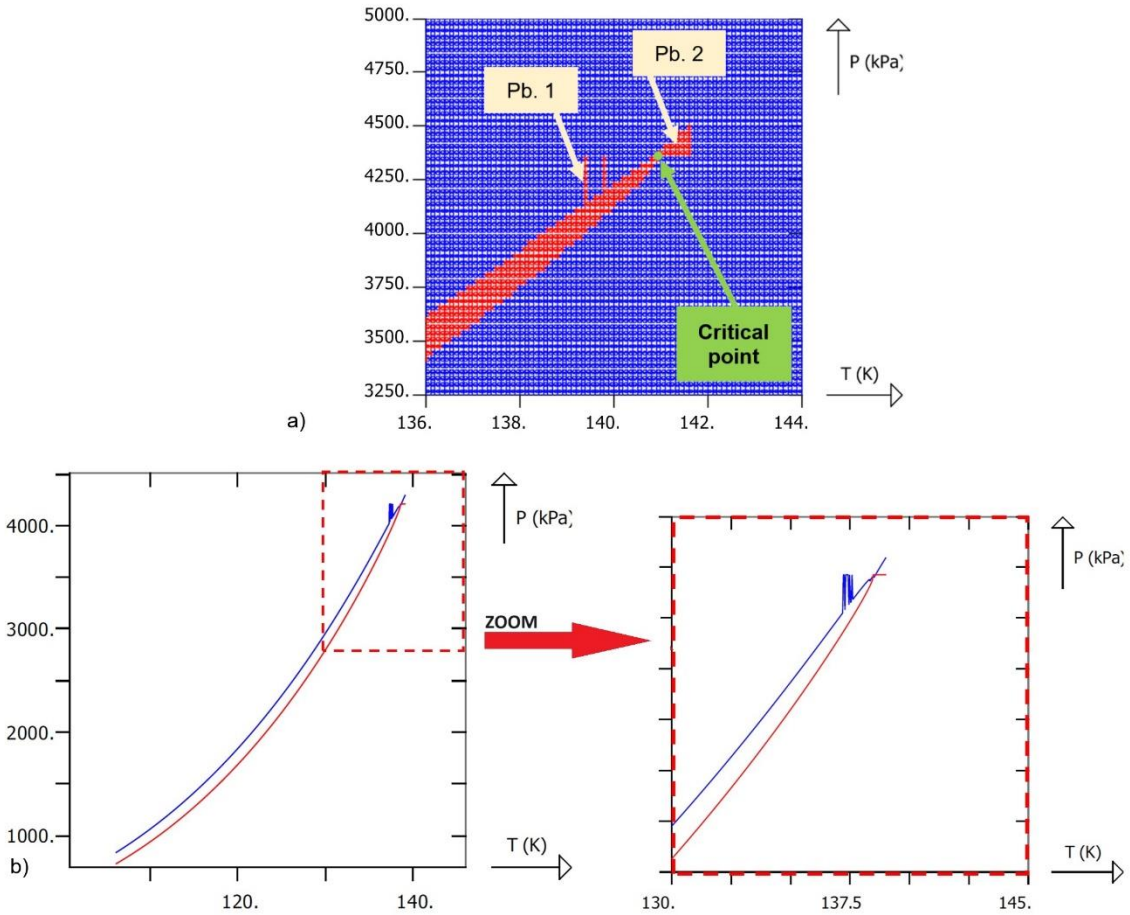

Figure 7. PT-flash calculations (fig. a) and bubble and dew pressure lines (fig. b) calculated with the Refprop, for a specific case-study (N_2 (50%mol) – O_2 (50%mol) – Ar (0%mol)).

1.7. Perspectives

Among all those studies aiming to develop the theoretical basis of cubic equations of state (with the introduction of thermodynamic consistency criteria for α-functions, EoS+$a^{E_{res}}\gamma$-Wilson mixing rules, E-PPR78), also extending their applicability to the modelling of CCS mixtures, there are still multiple open ways to be explored:

- The doctoral work has preliminarily shown that the temperature relationships of the binary interaction parameters incorporated in the γ-Wilson model reflect the intermolecular interaction energies of differently non-ideal systems. The logical extension of this work and of further conclusions obtained later by other authors [53] would lie in the research of a more theoretically-based definition of temperature dependent parameters and of their predictive formulation (based on group contribution theory?).

- The assessment of the impact of using speed of sound measurements in the optimization of thermodynamic models is a curiosity that is worth considering. With the aim to investigate that in a near future (2-3 years), the applicant has established a collaboration with Dr. David Vega-Maza of the University of Vailladolid, where accurate measurements of speed of sound are performed, and Prof. Martin Trusler of the Imperial College, expert in speed of sound modelling.
- An important gap in the experimental characterization of CCS mixtures lies in the scarce amount of data concerning toxic mixtures (containing NO, SO_2, H_2S, NO_x, …). Since 2016, the applicant collaborates with the laboratory GeoRessources of the University of Lorraine, supporting the theoretical modelling of mixtures for CCS applications containing toxic molecules that this laboratory characterizes experimentally [60]. Indeed, they have developed an experimental technique based on micro-capillary volumes and Raman spectroscopy measurements enabling the safe treatment of dangerous fluids. A new PhD thesis of Ehsan Asadi, under the (co)direction of the applicant, has started in 2023, aiming: 1) to measure vapour-liquid equilibrium data of toxic systems still totally unexplored, such as NO+Ar, NO+H_2S, H_2S+SO_2 and NO+O_2; 2) to set up a thermodynamic model for those mixtures (probably, the PR with EoS+$a^{E}_{res}\gamma$-Wilson mixing rule, which proved to be the most accurate for CCS systems).
- The team ThermE of LRGP owns an equipment [61] for the measurement of critical points of binary mixtures, which are pivotal properties to be used in the process of optimization of thermodynamic models. Since the arrival of the applicant in the ThermE team, she was appointed to make it operational, after a stop of 10 years. This still remains an objective that the applicant wants to address as soon as possible.

2. Contributions to the improvement of the efficiency of conventional thermodynamic cycles

Application to power and tri-generation cycles

This chapter includes the contributions of the applicant to the improvement of the efficiency of conventional thermodynamic cycles used for power and tri-generation. The main co-contributors to these activities with whom the applicant interacted the most are the professors: Davide Bonalumi (Politecnico di Milano), Marco Astolfi (Politecnico di Milano), Paolo Chiesa (Politecnico di Milano), Paolo Iora (Università di Brescia), Costante Invernizzi (Università di Brescia), Aldo Bischi (Università di Pisa), Riccardo Camerano (Tifeo), Jean-Noël Jaubert (Université de Lorraine), Romain Privat (Université de Lorraine).

<u>Main</u> supervision activity (2018-2019): work of Andrés Pina-Martinez in the context of the project REGEN-BY-2.

2.1. State-of-the-art on thermodynamic cycles

2.1.1. The historical role of thermodynamic cycles

At the time of the introduction of the theory of thermodynamic cycles, the priority of engineers was the design of powerful thermal engines being able to provide the energy output (useful mechanical work) required to drive industrial growth. Now that the priority has been diverted towards the necessary development of more environmentally friendly industrial and urban systems, with the aim to address climate change and reduce air pollution, the focus has become the design of efficient and cheap thermal engines. Although such a diversion of target's spotlight, thermal engines are still based on the same classical thermodynamic cycles, being used to exploit either fossil-fuelled or renewable thermal sources. To face nowadays' energy needs, engineers have also learnt to exploit thermodynamic cycles for refrigeration and heating purposes, by means of vapour compression refrigerators and heat pumps. Thermodynamic cycles thus constitute the backbone structure of all these thermal systems: fossil-fuelled and renewable thermal engines, vapour compression refrigerators and heat pumps.

2.1.2. Performance improvement by working fluid selection

Nowadays, efficiency improvement of thermal energy systems (thermal engines, compression refrigerators and heat pumps) is achieved by acting on three main technological aspects [62]: the optimal selection of the working fluid crossing the whole cycle, the modification of unit operations and of their arrangement. The improvement of classical fossil-fuelled power engines (steam cycles, gas turbines and combined cycles) concerns, mostly, the improvement of unit operations and, thus, their enhanced tolerance for more severe -but more efficient- thermodynamic conditions. On the other hand, the efficient adaptation of those engines to the exploitation of lower thermal grade renewable energies and waste heat sources both requires the optimal selection of the working fluid (some main examples are reported in Figure 8) and the re-design of unit operations [62,63]. In heat pumps and vapour compression refrigeration systems, the priority is twofold: the research of environmentally friendly, efficient and safe refrigerants (Mota-Babiloni et al. [64] presents a thorough review on this topic) and the efficient adaptation of the technology (equipment and control system) to those fluids.

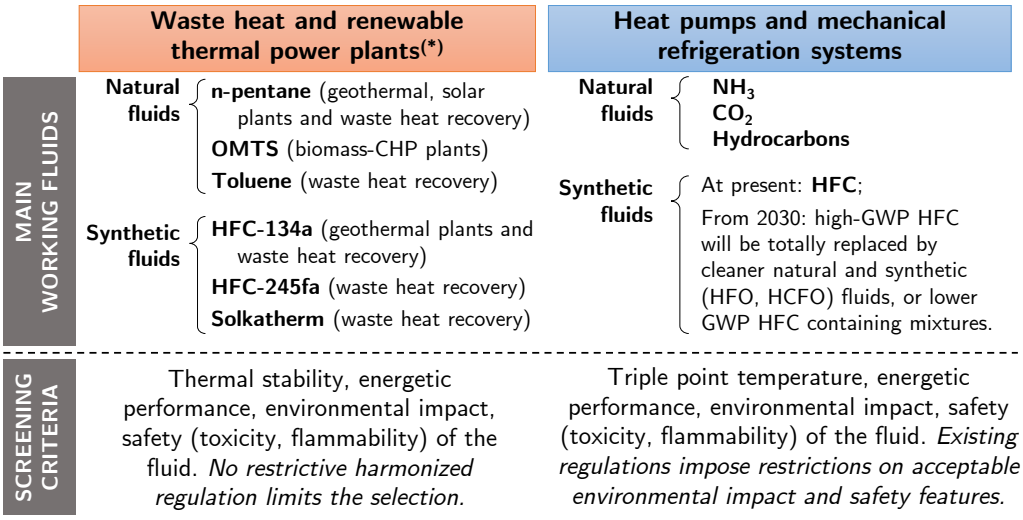

Figure 8. Main current working fluids and fluid selection criteria for power, refrigeration and heating applications. (*) Information collected from Quoilin et al. [62]

2.1.3. "Environmentally friendly – efficient – safe" working fluids? A variably-constrained trade-off

No regulation currently restricts the choice of working fluids for power applications. All types of fluids are currently accepted and used: flammable, toxic, high-GWP, etc. On the other hand, the selection of refrigerants in refrigerators and air-conditioning systems is limited, on the one side, by existing regulation [65], to fluids having low global warming potential (GWP) and zero ozone depletion potential (ODP) and, on the other, by impositions on safety (toxicity and flammability) characteristics [66]. However, environmental regulations and safety standards for refrigerant use evolve with scientific findings. McLinden et al. [67–69] have clearly stated that the selection of a working fluid is a matter of trade-off mainly because: (1) most performant fluids are flammable; (2) the acceptance of fluids characterized by non-zero but small ODP allows for an important reduction of GWP. The increasing priority of complying with both energetic efficiency and environmental requirements is smothering previous too strict limitations to: (1) non-flammable and non-toxic refrigerants, with the acceptance of "mildly flammable" gases (labelled as A2L by ASHRAE); (2) zero-ODP fluids, with the acceptance of small ODP (lower than 0.01 [70]) refrigerants (i.e., HCFO-1233zd(E), HCO-1130(E)).

2.1.4. Efficiencies of Best Available Technologies

Despite the numerous efforts of researchers, the efficiencies of thermal engines, vapour compression refrigerators and heat pumps remain far from the maximum achievable ones [71]. Exergy analysis of most performant operational fossil-fuelled power plants (natural gas combined cycles) shows that their thermal efficiency (about 60%) is at 65% of the maximum

attainable one; exergy efficiencies of waste heat and renewable thermal power plants achieve maximum values of about 50% (derived from thermal efficiencies declared by Wang et al. [63]). Best available technologies for vapour compression cooling and heating devices achieve exergy efficiencies of 30%. Moreover, the current state of the art shows a certain maturity for all these technologies [62], which mainly results from the limited possibility to further reduce thermodynamic irreversibility arising from the use of currently adopted working fluids and cycle architectures.

2.2. The implication of the applicant in state-of-the-art advancements

Since 2015, the applicant has been working over the investigation of the possible improvement of power cycles by **working fluid selection** (pure fluids: CO_2 versus organic fluids [72,73], fluids for novel trigeneration cycles [74]), **working fluid design** (inert binary mixtures – she has also co-patented a new class of mixtures for power cycles [75–77]) **and fluid characterization** (experimental study of the thermal stability of inert working fluids [8,9] and predictive modelling of their thermodynamic properties [78]). In the wake of the currently considered ways to further improve efficiencies [62], the applicant has also contributed to the development of innovative unit operations and tri-generation cycle architectures, in the context of an on-going H2020 European collaborative research project, REGEN-BY-2, coordinated by the University of Pisa [74]. Those contributions are summarized in the present section.

2.2.1. Optimal working fluids for power cycles exploiting medium grade heat sources (doctoral research period, but not included in the thesis)

During her doctoral studies, other than working on the subject of the thesis about CO_2 capture and storage (as presented in chapter 1), the applicant took advantage of the knowledge acquired in the thermodynamic modelling of fluids, to collaborate with her colleagues of the Group of Energy and Conversion Systems (GECOS) at Politecnico di Milano, on the optimal selection of working fluids for thermodynamic cycles.

Pure fluids (CO_2 versus organic fluids)

- *2015, at Politecnico di Milano*

This contribution is devoted to the definition of the optimal working fluid of power cycles for waste heat recovery, biomass and solar thermal applications. CO_2 and organic fluids are compared. Different medium grade thermal energy sources are modelled as hot streams of 30 MW_{th} having a maximum temperature comprised between 200 °C and 600 °C and being characterised by different cooling grade (from 0% to 100%). Either air- and water-cooled cycles

are considered. A preliminary study [73] was performed, and partially confirmed by a second one [72], where more cycle configurations were considered for the comparison. The first conclusion is that either CO_2 (in CO_2 supercritical or transcritical cycles) or organic fluids (in transcritical or subcritical organic Rankine cycles, ORC) can be of interest but, as expected, the specific advantage in their utilisation depends on the characteristics of the thermal source, heat sink and the adopted cycle configuration. The conclusion of the study is reported in Figure 9, where the use of either ORC or CO_2 cycles is suggested -from a thermodynamic efficiency point of view- according to the characteristics of the heat source, cooling source and minimum cycle pressure (indicated in Figure 9 with $p_{cond,min}$). In this work, specific best organic molecules have been identified and provided in the relative paper [72], together with the efficiency of each considered cycle (ranging between 14% and 31% for ORC, 10% and 40% for CO_2 cycles). Figure 9 (e)-(f) versus Figure 9 (a)-(b) also confirms what was mentioned in section 2.1, about the safety of working fluids: the increasing priority of complying with energy efficiency requirements appeals to the use of unsafe fluids; indeed, the additional constraint of using safe fluids results in the necessity of using less efficient CO_2 cycles (being more efficient than ORC cycles operating with safe fluids). In this work, the applicant contributed to the definition of the methodology of the work, with prof. Astolfi, and to the calculation of CO_2 recuperative and recompression cycles [73].

One of the priority over the design of more efficient and environmentally friendly low temperature power cycles should focus on the development of technologies being able to process unsafe fluids, minimising at most the risks for the user.

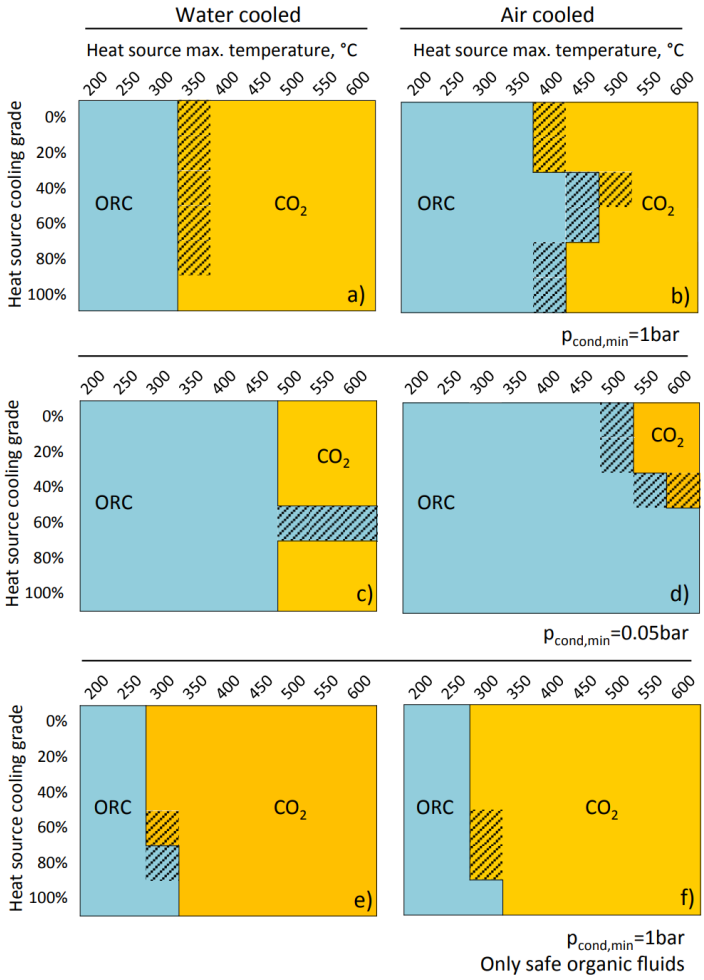

Figure 9. Selection maps ORC vs CO_2 for water-cooled and air-cooled power systems in three different cases: (a)-(b) ORC with minimum cycle pressure higher than 1 bar, (c)-(d) ORC with minimum cycle pressure higher than 0.05bar, (e)-(f) ORC minimum cycle pressure higher than 1 bar and non-flammable fluids. From Astolfi et al. [72].

<u>Binary mixtures as working fluid for power plants</u>.

- *2014-2015, at Politecnico di Milano and at the University of Brescia*

With the aim to improve the efficiency of supercritical carbon dioxide (S-CO_2) Brayton cycles, the applicant proposed, during her doctoral studies, the use of specific CO_2-based mixtures as working fluid to replace pure CO_2.

Although their application is still very limited and at R&D stage, thermodynamic calculations prove that supercritical carbon dioxide (s-CO_2) Brayton cycles offer the potential of equivalent or higher cycle efficiency compared to supercritical or reheated steam cycles at turbine inlet temperatures relevant for solar and nuclear energy conversion systems (higher than 500 °C). The efficiency of s-CO_2 cycles could be improved if the working fluid is condensed and

compressed in the liquid phase. However, due to low CO_2 critical temperature (about 30°C), the cooling of the fluid up to saturated liquid conditions would require the use of cooling water at rather low temperature (lower than 15 °C), which represents a relevant geographical limitation to the application of these power plants.

However, if CO_2-based binary mixtures characterized by higher critical temperatures are used as working fluids, instead of pure CO_2, condensation cycles could be feasible also in places lacking cooling water (i.e., in desertic regions, for Concentrating Solar Power applications). Because of their higher critical temperatures, these mixtures would allow the use of air as coolant and the achievement of higher cycle efficiencies.

The specific proposal of the applicant was to add to CO_2 a very small amount of a fluorocarbon, as a second component, that could allow the increasing of the critical temperature of the binary mixture, up to 40-50°C. Because of their assumed higher thermal stability and solubility in CO_2, compared to other fluorocarbon families, two perfluoroalkanes were proposed: the perfluorohexane (C_6F_{14}) and the hexafluorobenzene (C_6F_6) [10].

Different equations of state (Peng-Robinson, Soave-Redlich-Kwong, with different mixing rules, and PC-SAFT) were optimised on available (but limited) experimental vapour-liquid equilibrium data of the mixtures **CO_2+C_6F_{14}** and **CO_2+C_6F_6**. The optimised models led to comparable results and the first conclusion was that CO_2 based mixtures of **4%$_{molar}$ of C_6F_{14}** or of **2% $_{molar}$ of C_6F_6** have a critical temperature which is about 45 °C. The calculation of the efficiency of these cycles, for a maximum temperature equal to 400 °C, has shown a double interest, both in the **increased first-principle efficiency by 10%**, relatively to the efficiency of the pure CO_2 cycles (23% vs 21%), and in the reduced cycles minimum and maximum pressures. The vapour-liquid equilibrium properties of the CO_2+C_6F_{14} system have been measured by a master student that the applicant co-supervised [79].

Because of the calculated non-negligible performance improvement (higher for the mixture CO_2+C_6F_{14}), the applicant performed, in the period 2014-2015, **thermal stability tests** at the *Department of Mechanical and Industrial Engineering* of the *University of Brescia*, to experimentally evaluate the thermal stability limit of the pure C_6F_{14}. This assessment consists in the initial measurement of the saturation pressure of the pure fluid, followed by the fluid heating in an oven at a first stability test temperature kept stable for 80h (e.g., at 200 °C); then the saturation pressure of the fluid is measured again and the compared with the initial curve,

and if the deviation is considered within the experimental measurement error, the fluid is heated again at a second higher stability test temperature (e.g., at 250 °C) and temperature is maintained stable for 80h; then saturation pressure is measured again and compared to the initial one; this process continues until the deviation is considered higher than experimental error, and in this case the last tested stability temperature is the first observation of unstable behaviour (leading to fluid decomposition). The test, more specifically described in Lasala et al. [8] proved the **stability of C_6F_{14} up to 350 °C**. The personal contribution of the applicant was to analyse the experimental data obtained by the personnel of the Department and to perform an uncertainty analysis of the measurements, in order to provide the quantitative criterion that attests the beginning of fluid decomposition and the first unstable temperature. This analysis was performed to characterize the thermal stability of other molecules [9]: cyclohexane, n-pentane, and toluene.

In 2015, the collaboration with Dr. Davide Bonalumi and Prof. Ennio Macchi at Politecnico di Milano led to the proposal and characterisation of another CO_2-based mixture, containing $TiCl_4$. This system has been patented [80]. In this work, the applicant had the task to provide a computer program being able to perform thermodynamic calculations close to the critical point of the mixture **CO_2+$TiCl_4$** and thus to determine and optimise the performance of transcritical thermodynamic cycles. Indeed, Aspen Plus, generally used by the GECOS group, showed convergence issues around the critical region. The thermodynamic analysis of this system has been published [76,77]**.**

<u>Further developments of these works</u>

In 2019, the GECOS group of Politecnico di Milano was granted by a H2020 project, named SCARABEUS [81], aimed at thoroughly investigating the impact of using the some of the mixtures previously proposed (CO_2+C_6F_6) and characterized (CO_2+$TiCl_4$) by the applicant for the thermodynamic cycle of Concentrating Solar Power (CSP) plants. With high interest, the applicant read that further thermal stability tests have been performed on C_6F_6 and $TiCl_4$ and vapour liquid measurements, with the experimental apparatus that the applicant installed at LEAP laboratory during her PhD to measure vapour-liquid equilibrium properties of CCS fluids (see section 1.4) [82]. The cycle efficiency calculated in SCARABEUS attested improvements up to 7.4% [83], which is a value similar to the one previously quantified by the applicant at about 10% [10].

2.2.2. Optimal working fluids for a novel trigeneration cycle

The team ThermE of CNRS-LRGP is one of the partners of the Consortium of the European H2020 project named REGEN-by-2 ("Next REnewable multi-GENeration technology enabled by TWO-phase fluids machines"), started in 2020 and ending this year, 2024. The coordinator of this project is the University of Pisa [84]. The role of the applicant was to manage the scientific and some administrative activities of the team ThermE in the project.

This project aims at developing a trigeneration process, up to TRL4, starting from the idea patented by Dr. S. Briola [85] consisting in a cycle (a simplified version is shown in Figure 10) made of a unique thermodynamic loop (instead of usual cascade ones) enabling the transformation of available -medium temperature- thermal energy to electricity, cooling and heating. The advantage of this cycle is the high theoretical efficiency, which is close to the Carnot. The originality (and challenge) of this cycle is the fact that it operates with two-phase expanders (3-4, and 5-6) and compressor (7-8), which is currently not possible.

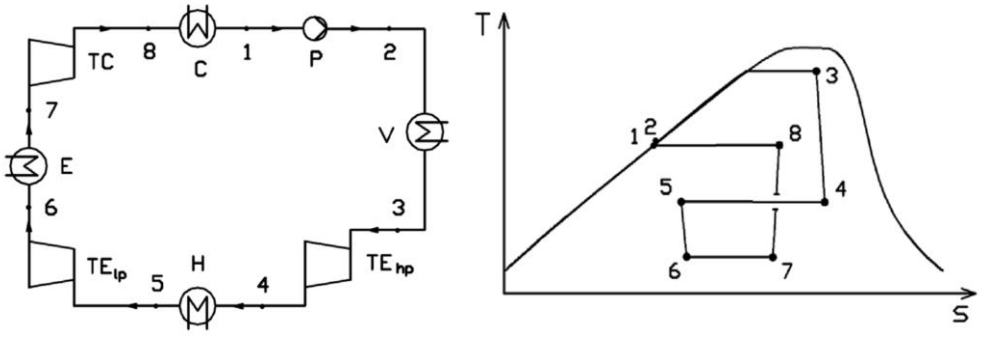

Figure 10. Simplified version of the Combined Cooling Heating and Power cycle treated in the REGEN-BY-2: process flow diagram, T-s diagram. From Briola et al. [86].

In REGEN-BY-2, the applicant worked as scientific responsible of the activities of the team ThermE. The main tasks of our team are:

1. The establishment of a methodology enabling the prescreening of the working fluids starting from a pool of about 66 000 pure fluids; that is, defining the thermodynamic, economic, environmental, and safety criteria for fluid selection, providing computational codes to quantify the criteria indexes and to perform the final prescreening. This step enabled to reduce the number of fluids to less than 50 species. The applied methodology has been published by Pina et al. [87].

2. The implementation of a thermodynamic package to be used by the other partners for the calculation of the thermodynamic properties of all the pre-screened fluids, with the aim of performing thermodynamic cycle calculations and selecting the final fluid leading to best performance indicators. The thermodynamic package, which is made available in under request, is called ThermeProp and is based on the predictive cubic equation of state developed by the team ThermE, the translated-consistent-Peng-Robinson equation of state (*tc*-PR) [88].
3. The assessment of the impact of adding up to $10\%_{massic}$ of oil in the selected optimal fluid, on the thermodynamic properties of the fluid. This work has been performed in collaboration with the *Centre of Thermodynamics of Processes* (CTP – Mines Paris, France), where experimental measurements were performed on the oil-working fluid mixture. The experimental data and their thermodynamic modelling are going to be published in the present year.

Unfortunately, the confidentiality of the results obtained in the project does not allow their dissemination, other than the content that we could publish in Pina et al. [87], where the methodology is applied to a similar cycle, but based on different users' needs, heat source features, and cycle's architecture.

3. The investigation and development of thermodynamic cycles operating with reactive working fluids

From fictitious to real reactive working fluids

A major contribution of the applicant concerns the study of an original type of thermodynamic cycles, where the novelty is the chemical reactivity of the working fluid: in these (closed) cycles, the working fluid is a reactive mixture undergoing a reversible "dissociation ↔ association" reaction, all along the cycle. This chapter firstly introduces the state of the art on this type of cycles (section 3.1). Then, it presents the analysis carried out by the applicant and her collaborators in order to preliminarily quantify the impact of the thermochemistry of reactive fluids on the performance of thermodynamic cycles, considering fictitious chemical reactions (section 3.2). Moreover, section 3.3 describes the project REACHER, funded by the European Research Council, in which the applicant represents the Principal Investigator.

<u>Main current</u> supervision activity:

- *2020-2024: Aya Barakat (doctoral student)*
- *2021-2025: Konstantin Samukov (doctoral student)*
- *2023-2025: Rachid Hadjadj (postdoctoral researcher)*
- *2023-2025: Sérgio Vilas-Boas (postdoctoral researcher)*
- *2024-2027: Luis Pinilla Monsalve (doctoral student)*

3.1. Introduction to reactive working fluids for thermodynamic cycles

As it was mentioned in the previous chapter 2, both pure fluids and mixtures are currently used as working fluids in thermodynamic cycles. For example, among the fluids reported in Figure 8, Solkatherm is an azeotropic mixture currently used as working fluid for waste heat recovery applications; refrigerants too are available in the form of mixtures [66]. The feature in common to all -used or proposed- working fluids is the fact that they are all inert fluids.

3.1.1. A neglected hint for scientific progress: concurrent thermal and chemical energy conversion

In 1957, Lighthill proposed [15] to convert the chemical energy like the "large energy change involved in dissociating gases" into work. Practically, he put forward the idea to use reactive working fluids, instead of inert ones, in closed power cycles. To appreciate the ground-breaking scientific nature of this idea, it is highlighted that current energy conversion systems for electricity production (schematically represented by the seven paths, 1-to-7, in Figure 11) are formed by one or more devices being the place of distinguished energy-type transformations: (1) wind turbines or marine technologies enable the transformation of the kinetic energy of wind or waves into mechanical energy and, by means of a generator, into electricity; (2) fuel cells and batteries enable the direct conversion of the chemical energy into electricity; (3) photovoltaic panels transform radiant energy into electricity; (4-7) thermal engines enable the conversion of thermal energies, from different sources, into mechanical energy by means of thermodynamic cycles where an inert working fluid undertakes modifications of its thermal energy content. **Lighthill's idea consists in a totally different energy conversion process: the transformation of an available thermal energy into mechanical one is made possible by the use of a thermodynamic cycle along which the original concurrent thermal and chemical conversion of the energetic state of a reactive fluid takes place** (numbered 4*-to-7* in Figure 11).

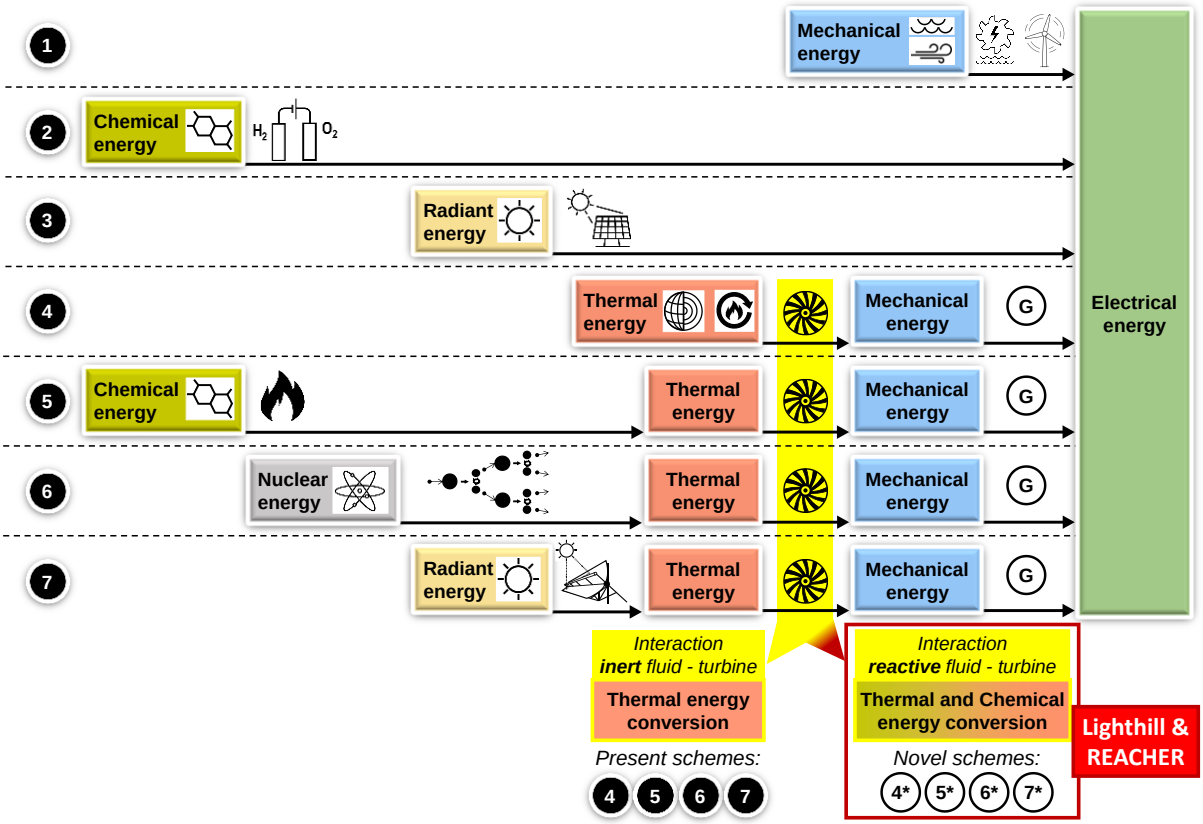

Figure 11. Summary of alternative energy conversion schemes for electricity production. Modified plot of Lasala et al. [31].

3.1.2. Preliminary studies on non-optimal existing reactive fluids for power cycles

From 1960s, some researchers have started to investigate, on paper, the performances of classical power cycles operating with 5 reactive working fluids: mainly, $N_2O_{4(g)} \rightleftarrows 2NO_{2(g)} \rightleftarrows 2NO_{(g)}+O_{2(g)}$ [16,89–92]; and, with a much lower level of details, $P_{4(g)} \rightleftarrows 2P_{2(g)}$ [93], $2NOCl_{(g)} \rightleftarrows 2NO_{(g)}+Cl_{2(g)}$ [94–97], $Al_2Br_{6(g)} \rightleftarrows 2AlBr_{3(g)}$ and $Al_2Cl_{6(g)} \rightleftarrows 2AlCl_{3(g)}$ [97,98]. Except for the last one, all these fluids are toxic. A complete review of these works is reported in a previous publication [17]. Although these researches have sampled the high potentiality of Lighthill's idea, the lack of a study intended to understand the theoretical relationship between reaction characteristics (stoichiometry, thermal and fluid-phase features) and its thermodynamic transformations along a cycle, as well as to search for less toxic fluids, has mostly smothered further research over this topic.

3.1.3. Reactive working fluids: why reconsidering them now?

Probably due to the fact that, at the time of these studies, the potential of inert fluids was not yet totally investigated, the more advanced idea of using reactive fluids was not fully appreciated and thus remained scientifically unexplored. Now that the use of inert fluids reveals

limitations in fulfilling, simultaneously, energetic performance, environmental and safety criteria, the applicant has proposed to revive Lighthill's idea.

3.2. Preliminary results with fictitious fluids for power cycles and heat pumps

Period 2018-2024

In 2017, during her postdoc, the applicant initiated a theoretical investigation intended to quantify the impact of using reactive working fluids on thermodynamic cycle performance. This work is still in process and pursued by Aya Barakat, a doctoral student co-supervised by the applicant. The first publication on this topic considered Brayton power cycles [17], the second one investigated heat pumps operating with a reverse Brayton cycle [18], and currently the last works about Stirling power and heat pump cycles are submitted to peer-reviewed journals. With the aim of considering a large spectrum of fluids, she proposed in all those works to preliminary consider fictitious working fluids, being the result of the application of a *chemical product design* approach, where the "product" is a *fictitious gaseous fluid being the place of a reversible chemical reaction*.

3.2.1. The definition of the fictitious reactive working fluids used in this work

With the aim to investigate the highest reactional effect of a chemical reaction, this analysis considers **reversible reactions** (hypothesis n. 1). That is, the reactive system is in chemical equilibrium and, thus, only thermodynamics governs the composition of the reactive system. Moreover, to quantify the influence of molecular dissociation (or association, in the inverse direction), different stoichiometries were considered, according to the following *dissociation* ↔ *association* structure:

$$A_{n(g)} \rightleftarrows {}^{n}/_{m}\, A_{m(g)}$$

where the specification of the number of atoms of the two molecules (or molecular groups), *n* and *m*, enables the definition of specific **stoichiometries of the reaction** (hypothesis n. 2). Once the stoichiometry of the reaction is fixed, its thermophysical and thermochemical characteristics must be defined to finalize the reaction design. This is detailed hereinafter. The studied reactive system has been modelled as an **ideal gas mixture** (hypothesis n. 3). The thermodynamic properties are thus computed accordingly [99]. Our choice for heat capacity, which is the basic property for the calculation of all other properties, is specified below. For simplicity, the specific heat capacity of each molecule has been considered constant with

temperature and provided by the equipartition theorem [100]: for monoatomic molecules, $c_{p,A} = 5/2 \cdot R$; for diatomic molecules, $c_{p,A2} = 7/2 \cdot R$; for polyatomic molecules, $c_{p,Ak\ (with\ k>2)} = 4 \cdot R$ (hypothesis n. 4). In this study, k = 4 is the maximum k-value that has been considered. Moreover, despite the reaction being at equilibrium, a conventional definition of the reactants and products is used in the following to refer to when mentioning the thermal and advancement characteristics of the reactions. A_n is the reactant, and A_m is the product ($A_n \rightarrow {}^{n}/_{m}\ A_m$). As specified before, the composition of the reactive mixture at each considered thermodynamic point is dictated only by the chemical equilibrium of the system, which corresponds to a zero-Gibbs energy of the reaction, $\Delta_R G$:

$$\Delta_R G\left(T, P, \mathbf{n}\right) \overset{\text{chemical equilibrium}}{=} 0 \tag{18}$$

where **n** is the vector containing the molar composition of the n_c types of molecules forming the system. It is possible to demonstrate [101] that, in the case of an ideal gas mixture, Eq.(18) corresponds to

$$K_{eq}\left(T\right) = \left(\frac{P/P_0}{n_{tot}}\right)^{\sum_{i=1}^{n_c} \nu_i} \prod_{i=1}^{n_c} \left(n_i\right)^{\nu_i} \tag{19}$$

where K_{eq} is the temperature-dependent equilibrium constant, P_0 is the standard pressure (1 bar), and ν_i are the stoichiometric coefficients of the considered species. The number of moles at a considered (T, P) condition can be calculated as a function of the value of the extent of the reaction at T and P, ξ(T, P), and of the initial number of moles (n_0) for each i-th component:

$$n_i = n_{i,0} + \nu_i \cdot \xi\left(T, P\right) \tag{20}$$

In the present case, Eq. (19) corresponds to the following:

$$K_{eq}\left(T\right) = \left(\frac{P/P_0}{n_{0,A_n} + n_{0,A_m} + \left(\frac{n}{m} - 1\right) \cdot \xi\left(T, P\right)}\right)^{\frac{n}{m}-1} \cdot \frac{\left(n_{0,A_m} + \frac{n}{m} \cdot \xi\left(T, P\right)\right)^{\frac{n}{m}}}{n_{0,A_n} - \xi\left(T, P\right)} \tag{21}$$

where the temperature-dependent formulation of the equilibrium constant for a considered reaction is given by [99,101] and is known as Ulich approximation [102] (hypothesis n. 5):

$$\ln K_{eq}(T) = a_R + \frac{b_R}{T} \tag{22}$$

<u>Demonstration of the Ulich approximation</u>. By combining the definitions of equilibrium constant and of Gibbs energy of reaction, one has:

$$\begin{cases} \ln K_{eq}(T) \triangleq -\dfrac{\Delta_R G°(T)}{RT} \\ \Delta_R G°(T) \triangleq \Delta_R H°(T) - T\Delta_R S°(T) \\ \qquad = \Delta_R H°(T^\bullet) + \displaystyle\int_{T^\bullet}^{T} \Delta_R c_p°(T)\, dT - T\left(\Delta_R S°(T^\bullet) + \int_{T^\bullet}^{T} \frac{\Delta_R c_p°(T)}{T}\, dT \right) \\ \qquad \text{where } T^\bullet \text{ is an arbitrary temperature.} \end{cases} \tag{23}$$

The Ulich approximation [102] *states that:*

$$\int_{T^\bullet}^{T} \Delta_R c_p°(T)\, dT - T\int_{T^\bullet}^{T} \frac{\Delta_R c_p°(T)}{T}\, dT << \Delta_R H°(T^\bullet) - T\Delta_R S°(T^\bullet) \tag{24}$$

Hence:

$$\boxed{\ln K_{eq}(T) \approx \frac{\Delta_R S°(T^\bullet)}{R} - \frac{\Delta_R H°(T^\bullet)}{R} \cdot \frac{1}{T}} \tag{25}$$

By comparing Eq. (22) and Eq. (25), the thermodynamic interpretation of a_R and b_R is straightforward:

$$\begin{cases} a_R = \dfrac{\Delta_R S°(T^\bullet)}{R} \\ b_R = -\dfrac{\Delta_R H°(T^\bullet)}{R} \end{cases} \tag{26}$$

In this study, $T^\bullet$ = 298 K has been considered. The equilibrium constant characterizing a reaction can be thus described as a function of its standard enthalpy and entropy of reaction $\Delta_R H°$ and $\Delta_R S°$ at a reference temperature (denoted $T^\bullet$). In addition to considering multiple stoichiometries, the parametric study accounts for a wide spectrum of possible ($\Delta_R H°$, $\Delta_R S°$)-coordinates. Quantitatively, this research investigates more than one reaction stoichiometries and two types of reaction design parameters (here called "reaction coordinates"), $\Delta_R H°(T^\bullet)$ and $\Delta_R S°(T^\bullet)$ (simply denoted $\Delta_R H°$ and $\Delta_R S°$ hereafter). Before specifying the numerical values attributed to these reaction coordinates, it is worth highlighting the following points.

- At a fixed temperature and pressure, the enthalpy-change of the reaction under standard conditions ($\Delta_R H°$) is positive for endothermic reactions and negative for exothermic reactions.
- The entropy-change of the reaction under standard conditions ($\Delta_R S°$) indicates how the orderliness of the reacting system is affected by the reaction. For a reaction taking place in the gas phase, this value is positive when the total number of product molecules is greater than the total number of reactant molecules and negative otherwise. For a gas-phase dissociation reaction, $\Delta_R S°$ is thus expected to be positive, and vice-versa for association reactions.
- An exothermic reaction in the forward direction is endothermic in the backwards direction and vice versa. Similarly, if the positive entropy change is positive in the forward direction, it is negative in the backwards direction and vice versa.

In this study, the specific values of $\Delta_R H°$ and $\Delta_R S°$ have been fixed referring to the direction leading to an increasing number of moles. On the basis of the above points, $\Delta_R H°$ and $\Delta_R S°$ can only be positive. According to the observation of reaction parameters of existing reactions, it has been agreed to vary $\Delta_R H°$ between 0 kJ/mol and 200 kJ/mol and $\Delta_R S°$ between 0 kJ/(mol·K) and 0.2 kJ/(mol·K).

The reaction design approach described in this section has been applied in Lasala et al. [17] and Barakat et al. [18] and has led to the results described in the following sections.

3.2.2. Results for Brayton power cycles

The analysis performed on Brayton power cycles [17] demonstrates that, with respect to comparable inert fluids (e.g., pure reactants or products or their inert mixtures), the use of specific reaction features (stoichiometry, reference standard enthalpy ($\Delta_R H°$) and entropy ($\Delta_R S°$) of reaction) may allow achieving much higher performances, with even classical (non-optimal) cycle architectures:

► Extremely high specific net power: an energy-intensive engine

This work has demonstrated that the expansion, in a turbine, of an equilibrated reactive fluid leads the equilibrium reaction to move towards the exothermic direction, providing thermal energy to the fluid on the one side and increasing the molar mass of the fluid during expansion on the other. The thermal effect due to the exothermic reaction leads the temperature of the system to reduce much less (during expansion) than if the fluid was inert; an isothermal

expansion can be observed (!). The antagonist effects on the volume (specific to the mass) that the higher average expansion temperature positively have, on the one side, and the higher molar mass negatively have, on the other side, result in a slightly positive (thermal) effect of the reaction on the expansion work. Vice-versa, the compression of an equilibrated reactive fluid shifts the equilibrium reaction towards the endothermic direction, (positively) cooling down the fluid and (negatively) increasing its molar mass, resulting in an overall reduction of the total amount of energy required for compression. Although positive, these two effects on the turbine and on the compression do not represent the key advantage of using reactive working fluids. The most positive effect related to the occurrence of the reaction comes from the combination of a compression and of an expansion process in a Brayton cycle. Indeed, the presence (according to Le Châtelier's principle) of a dissociation (endothermic) reaction mostly in the hot heat exchanger and of an association (exothermic) reaction occurring in the cold heat exchanger implies that molecules are dissociated at high temperature and are associated at low temperature, leading to the **desired expansion of simpler molecules** (i.e., monomers) and to the **desired compression of complex molecules** (i.e., dimers in the case of a dimerization reaction). Indeed, the difference in the molar specific heat capacity of simpler and complex molecules leads to the conclusion that it is favourable to compress complex fluids and to expand simple ones. The cumulation of these favourable (thermal and compositional) effects is quantified by the net specific work of the power cycle, which is the specific work released by fluid expansion reduced by the specific work required for fluid compression. To visualize the quantification of how much does the net work (W_{net}) of a closed Brayton cycle (Figure 12a) change with the thermal features ($\Delta_R H°$ and $\Delta_R S°$) of the reactive working fluid, Figure 12b shows the variation of its net specific work, as a function of the different couples of $\Delta_R H°$ and $\Delta_R S°$ of the fictive equilibrated reactive fluid $A_2 \rightleftarrows 2A$. It is highlighted that each point of this map represents a specific reactive fluid, whose specificity is dictated by the different $\Delta_R H°$ and $\Delta_R S°$ characteristics. Firstly, it is pointed out that the blue regions in Figure 12b (at high-$\Delta_R H°$ and low-$\Delta_R S°$, or, low-$\Delta_R H°$ and high-$\Delta_R S°$) represent the net specific work of chemically inert reactive fluids; indeed, it is shown that these ($\Delta_R H°$, $\Delta_R S°$)-features of the fluid (which quantify the temperature-dependent equilibrium constant of the reaction) make the reaction being completely shifted towards either 100% (inert) reactants, or 100% (inert) products, in the whole temperature and pressure domain of the cycle.

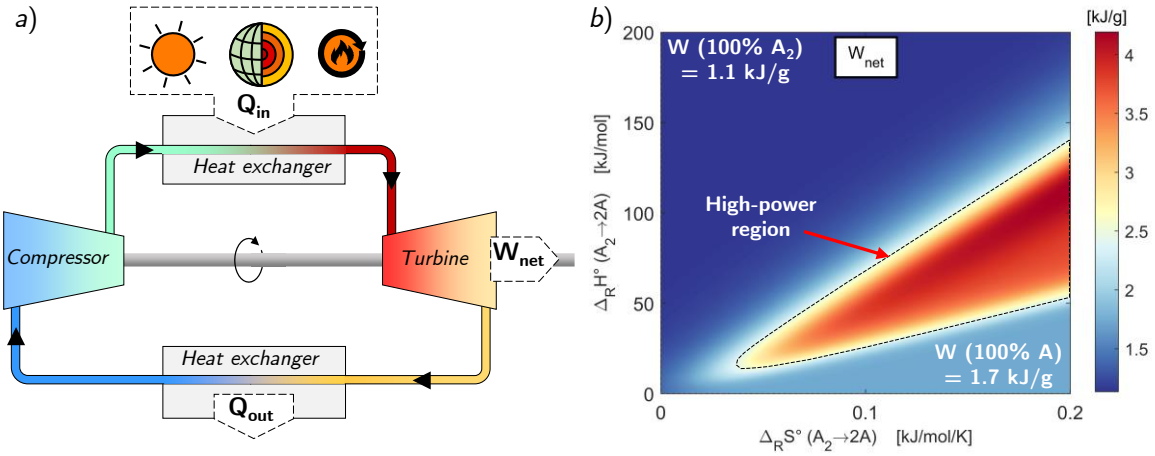

Figure 12. Brayton cycle (fig. a) and its net specific work (fig. b) resulting from the use of fictive fluids of stoichiometry $A_2(g) \rightleftarrows 2A(g)$ and different thermodynamic coordinates ($\Delta_R H°$, $\Delta_R S°$). See Lasala et al. [31] for details.

Having said that, it is now clearer that these "inert" fluids represent, in this study, the best term of comparison to understand and quantify the advantage of using reactive fluids with respect to inert ones: ***by comparing the net specific work resulting from the use of chemically reactive fluids (red region) with the one of inert fluids (blue regions) it can be observed that the former entails a more than doubled net specific work***.

- <u>High thermal efficiencies, with proper cycle architectures.</u>

The extremely high power that a thermodynamic cycle is thus able to release by operating with reactive fluids suggests the potential of very high thermal efficiency, which is the ratio between the net output mechanical power and the cycle's input thermal power. However, ***the input thermal power required to heat up a fluid undergoing an equilibrated reaction is higher than the one required to heat up an inert fluid.*** In fact, when a reversible reaction undergoes an isobaric heating process under thermodynamic equilibrium conditions, the chemical equilibrium shifts towards the endothermic direction, thus demanding more thermal energy to achieve a specific targeted outlet temperature. This is a drawback that affects cycle's efficiency, counter-balancing the positive effect of the higher net power.

On the other hand, the heat rejected by such a cycle into the environment is also higher, because the temperature reduction of a reactive fluid entails that equilibrium shifts in the exothermic direction. Such an observation suggests why ***the use of cycle architectures including a regenerator is crucial to achieve very high efficiencies***: the adoption of a regenerator, shown in Figure 13 would enable to recover such a higher thermal energy rejected by the cycle to

preheat the fluid before it enters the primary heat exchanger, counter-balancing the higher amount of thermal energy required to heat up the reactive fluid in the primary heat exchanger.

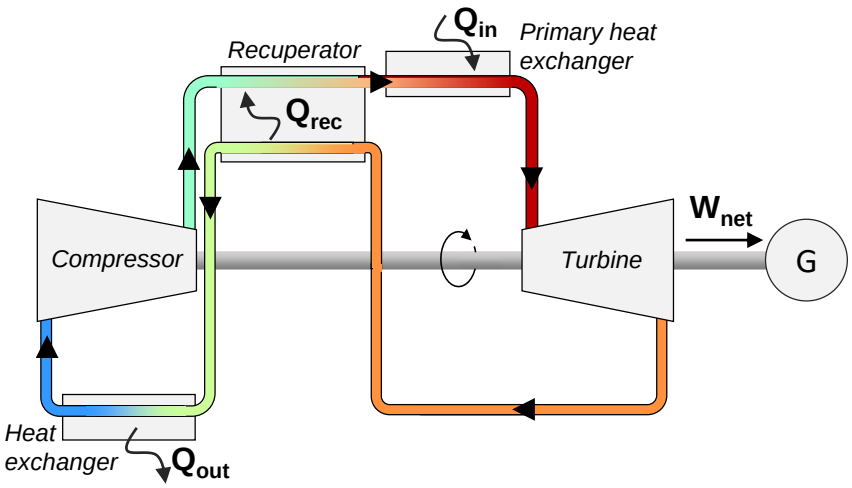

Figure 13. Regenerative Brayton cycle configuration. From Lasala et al. [31]

However, this preliminary work also shows that ***the peculiar thermodynamic properties of equilibrated reactive fluids entail that the heat recoverable in a regenerator is limited by a pinch-point placed inside the heat exchanger***. Consequently, the efficiencies attained with a regenerative Brayton cycle configuration (up to **+33% or +27%**, with respect to inert fluids, for a cycle operating with a maximum temperature of, respectively, 400 K or 700 K [17]) are not the highest and could be increased if the regeneration process is optimised.

To conclude:

- These considerations have led to the important conclusion that ***the redesign of the cycle architecture is necessary to achieve efficiencies that, fully, take advantage from the extremely high net specific work generated from the engine***.
- To understand the break of this potential with respect to the state of the art, it is highlighted that the highest declared efficiency improvement for next generation high-temperature organic Rankine cycles operating with (inert) zeotropic mixtures is **+16%** for heat sources of 150 °C, and **+6%** for heat sources of 250 °C[103]; as said, the use of specific reactive fluids in even with non-optimised cycle configurations could result in an efficiency increased by **+33%** with respect to best comparable inert fluids.

3.2.3. Results for Brayton heat pumps

A similar study [18] has been performed on heat pumps operating with the fictitious gaseous reactive working fluids defined as discussed in the beginning of this section. A vapour compression heat pump has been considered and the main schematics is shown in Figure 14.

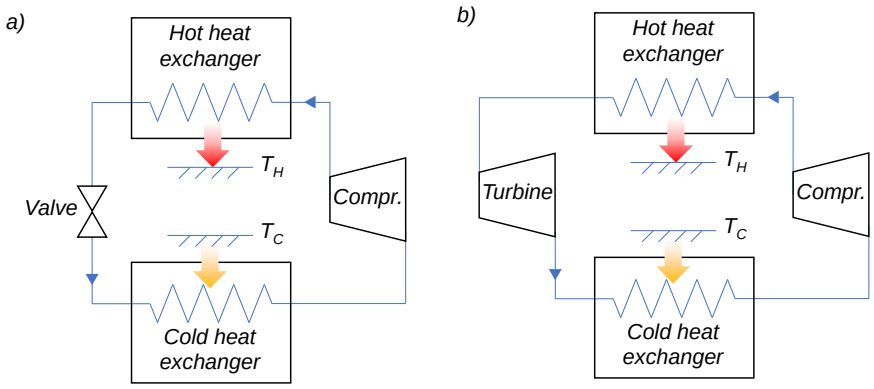

Figure 14. Schematics of a heat pump aiming at heating an environment at T_H, taking thermal energy from a cold external environment at T_C. Fig. (a) represents a typical configuration of vapour compression heat pump. Fig. (b) represents the configuration used in this study.

It is highlighted that a turbine (Figure 14 (b)) has been placed instead of a valve (Figure 14 (a)) mainly because, the fluid being a mixture of ideal gases and the valve being by definition isenthalpic, the thermodynamic transformation through the valve would be isothermal, which is not feasible. Indeed, the fluid's temperature at the outlet of the valve would be higher than the temperature of the cold environment (T_c) and the heat transfer in the cold heat exchanger, from the environment at T_c to the fluid right after the outlet of the valve, would be interdicted by the second law of thermodynamics.

The main results are summarised in the following:

- The reaction in the hot side heat exchanger and in the cold side heat exchanger is, respectively, exothermic and endothermic, for all considered reactive working fluids and operating conditions. This is a straightforward conclusion from the Le Chatelier principle.
- The reactions in the compression and in the expansion processes are, respectively, endothermic and exothermic, for most of considered reactive working fluids and operating conditions. As for the previous point, these results agree with the results obtained in the Brayton power cycle discussed above.

- In this study, the best performing inert fluid, among either A_2 or A, is A_2. Thus, A_2 is the fluid that is compared, in the following point, to the reactive fluid in terms of performance of a heat pump operating either inert or reactive fluids.
- Considering a heat pump providing a specific output thermal power, either using reactive or inert fluids:

$$\dot{Q}_{H,react.} = \dot{Q}_{H,A_2}$$

it has been observed that if the heat pump operates with reactive fluids, the coefficient of performance can be doubled with respect to the inert A_2. The higher COP of reactive working fluids can be explained by observing the temperature-entropy diagrams of the cycle, in Figure 15, where the higher COP fluids present diagrams where q_H and q_C (kJ/kg) are very small and the diagram shapes as a Carnot cycle.

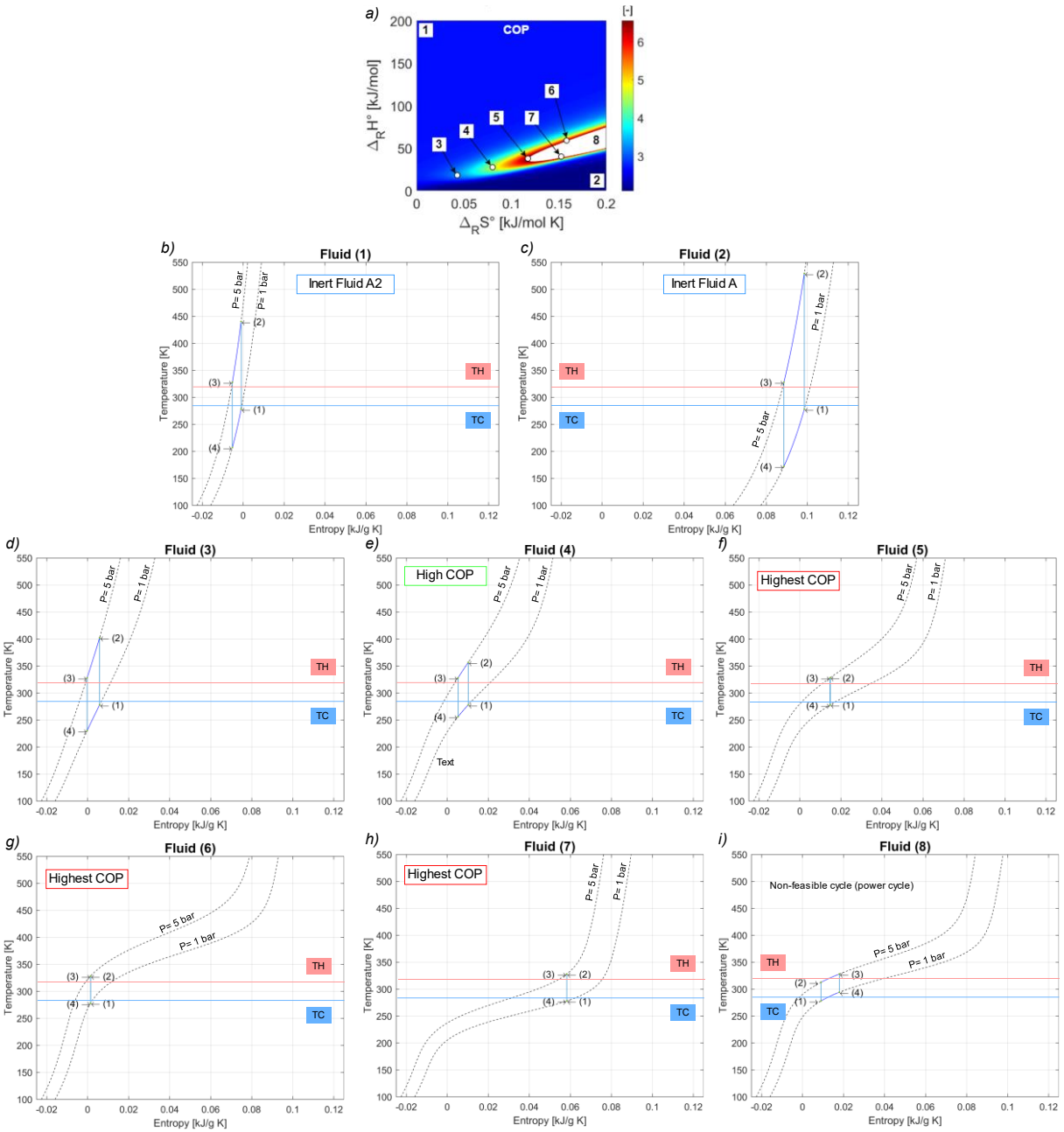

Figure 15. T-s diagrams (figures (b)-(i)) of fluids 1-8 characterized by the different reaction coordinates represented in figure (a) for the reaction stoichiometry $A_{2(g)} \rightleftarrows 2A_{(g)}$ *and the following operating conditions: T_1=5°C, T_3=55°C, P_1=1 bar, P_2=5 bar; where points (1) – (4), represent in Figure 14: (1) compressor's inlet; (2) compressor's outlet; (3) turbine's inlet; (4) turbine's outlet. Modified plot from Barakat et al. [18].*

However, the lower specific heat q_H and q_C of high performing reactive fluids entail that, to provide the same outlet thermal power, $\dot{Q}_H$, as the inert fluid, the mass flow rate of the cycle operating with reactive fluids must be higher:

$$\uparrow \frac{COP_{reactive}}{COP_{A_2}} \mapsto \downarrow \frac{q_{H,reactive}}{q_{H,A_2}} \overset{\dot{Q}_{H,react.}=\dot{Q}_{H,A_2}}{\Rightarrow} \uparrow \frac{\dot{m}_{reactive}}{\dot{m}_{A_2}}$$

Where $\dot{Q}[W] = \dot{m}[g/s] \cdot q[kJ/g]$.

Quantitatively, Figure 16 shows that the COP with best performing reactive fluids can be more than doubled if the mass flow rate of the reactive working fluid heat pump is 10 times the one of the heat pump operating with inert fluids: $\frac{COP_{reactive}}{COP_{A_2}} = 2.4$. It can also be observed that the increase of the mass flow rate by 10%, $\frac{\dot{m}_{reactive}}{\dot{m}_{A_2}} = 1.1$, would be sufficient to double the coefficient of performance.

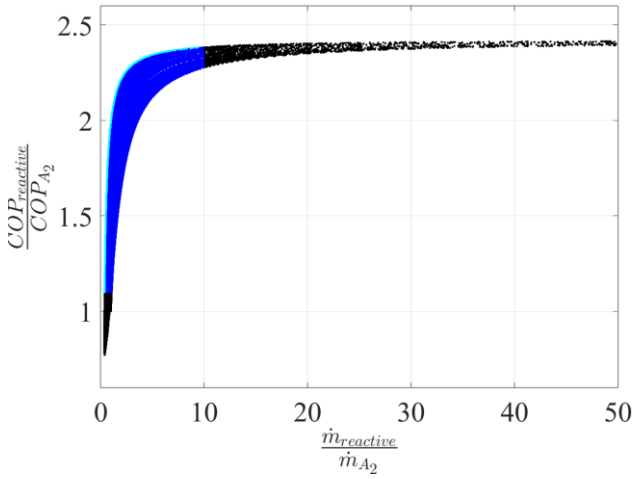

Figure 16. COP of the heat pump cycle operating with all the reactive fluids considered to trace the map in Figure 15(a), with respect to to inert A_2, with respect to the relative mass flow ratio (reactive vs. inert A_2), at the following operating conditions: T_1=5 °C, T_3=55 °C, P_1=1 bar, and P_2=5 bar. Suitable reactive working fluids that satisfy the conditions $COP_{reactive} / COP_{A_2} \geq 1.1$ and $\dot{m}_{reactive} / \dot{m}_{A_2} \leq 10$ are marked in blue; the optimal points (Pareto front) of this region lie on the cyan curve. Modified plot from Barakat et al. [18].

3.2.4. Results for Stirling power cycles

Although it can be easily shown that *ideal* Stirling cycles (i.e., where only *reversible transformations* are considered) operating with inert fluids have the highest (Carnot) efficiency, the performance of Stirling cycles operating with reactive working fluids has been analyzed. Figure 17 and Figure 18 recall the schematic and P-v diagram of a Stirling cycle.

The complete analysis of this work is reported in a paper recently submitted to the Energy Conversion and Management Journal X [104]. In the following, the main conclusions are summarised.

This work has shown that, as expected, the maximum achievable efficiency is the Carnot one, both with inert fluids and with some reactive working fluids. However, reactive fluid cycles may have lower efficiencies and slightly higher (or lower) net work, as shown in Figure 19 (a) and (b), respectively. The reasons why reactive working fluids can lower the efficiency of Stirling cycles with respect to the inert fluid – Carnot – one is that, differently from the operation with inert fluids, 1) the regeneration process can not be reversible because of the presence of finite temperature differences between the heat exchanging media (see the temperature profiles in Figure 20 and the consequent entropy generated in the colormap in Figure 21); 2) the regenerative process can not be adiabatic, otherwise temperature profiles would cross, which is not possible according to the second principle of Thermodynamics.

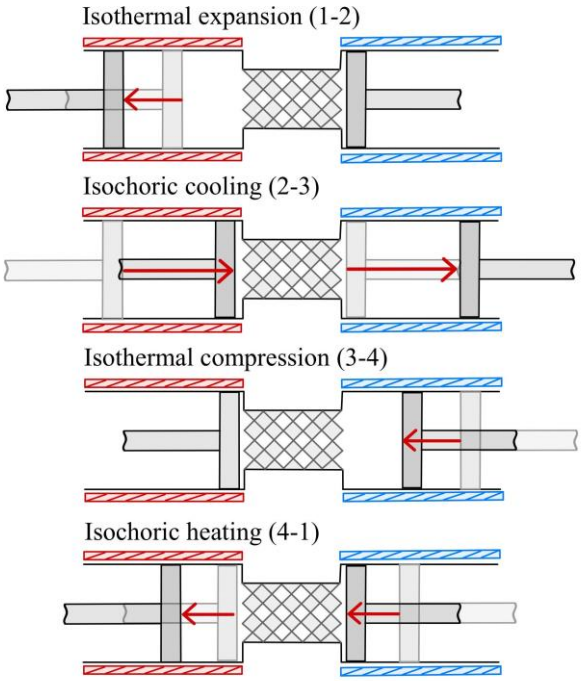

Figure 17. A schematic of the Stirling engine's four processes. From Barakat et al. [18].

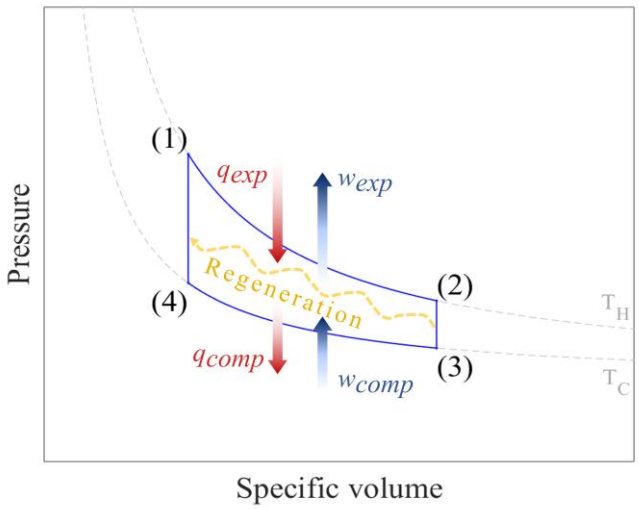

Figure 18. P-v diagram of the ideal Stirling cycle operating with an inert ideal gas (from [104])

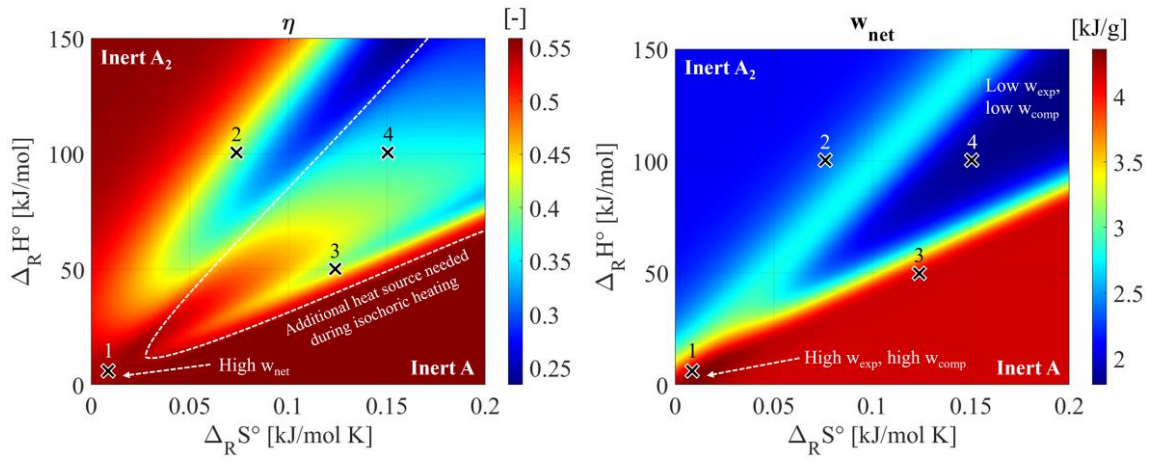

Figure 19. Performance of the Stirling cycle operating with theoretical ideal gas mixture $A_{2(g)} \rightleftarrows 2A_{(g)}$*, for different reaction coordinates* $(\Delta_R S°, \Delta_R H°)$*; thermal efficiency* η*, Fig. a; net specific work output* w_{net}*, Fig. a. Four chemically reactive fluids are marked for further T-q diagram analysis. This figure is taken from Barakat et al. [104].*

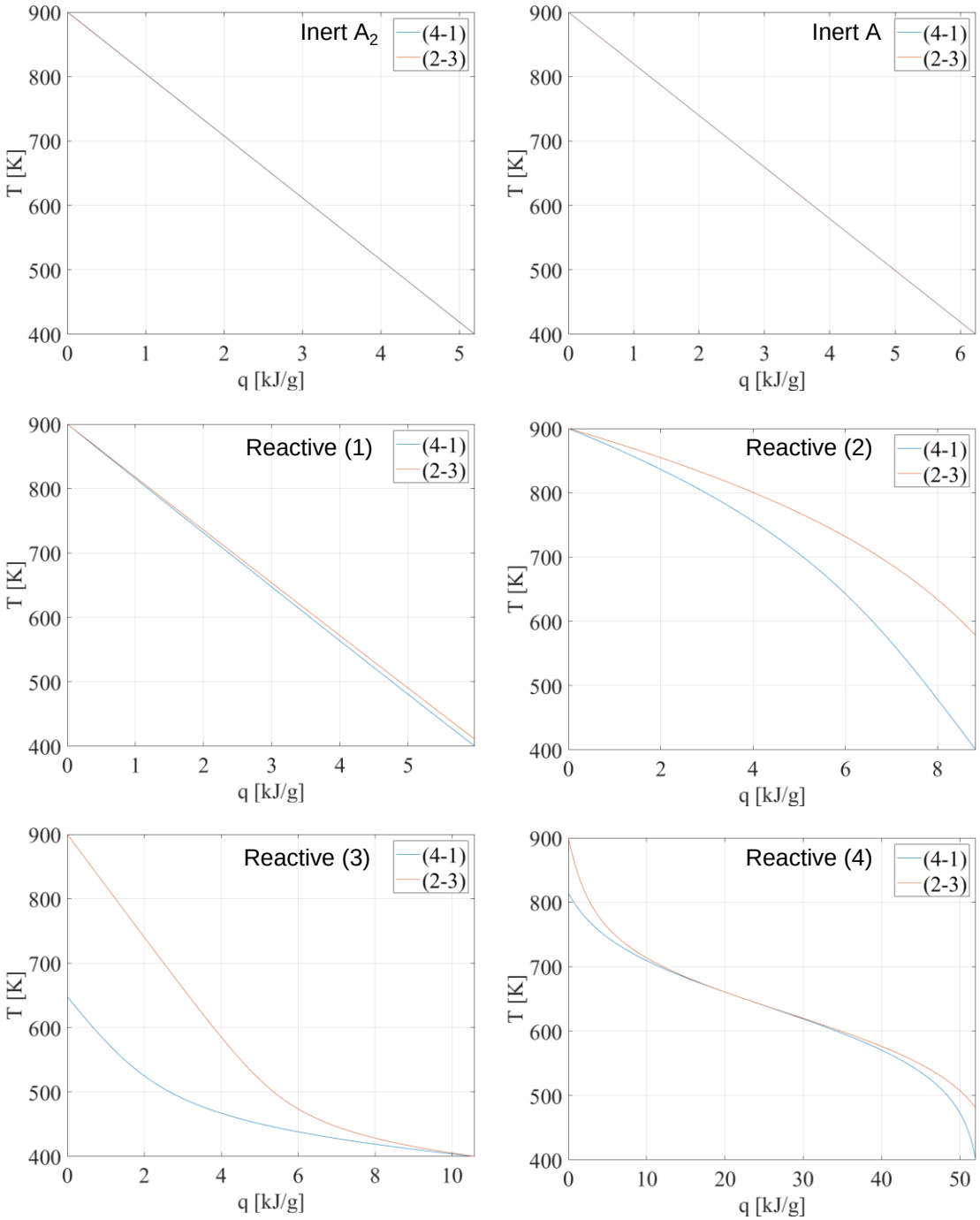

Figure 20. T-q diagrams of six theoretical working fluids: two corresponding to inert fluids (A and A_2), and four corresponding to selected chemically reactive fluids (1)-to-(4). These fluids are identified and numbered on the colormaps presented in Figure 19. This figure is taken from Barakat et al. [104].

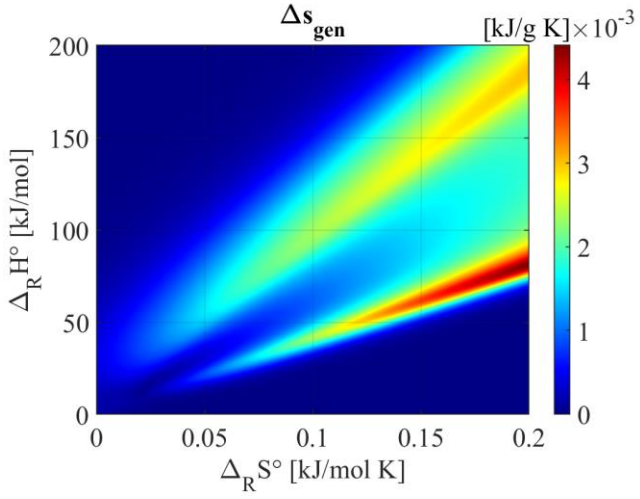

Figure 21. Specific entropy generated in the regenerator for the theoretical reactive working fluids considered. This figure is taken from Barakat et al. [104].

3.2.5. Results for Stirling heat pumps

Similar to the conclusion derived from the study of power Stirling cycles, the efficiency of Stirling cycle operating as heat pumps (i.e., the coefficient of performance) results to be lower than the one of the same cycle operating with inert working fluids. The conclusion of this study is thus that, from a performance point of view, the use of reactive instead of inert working fluids in Stirling cycles is not convenient. However, it is highlighted that all these studies have been performed considering ideal thermodynamic cycles; a "real cycle" analysis could lead to a different conclusion. The paper on this work is being drafted by Aya Barakat, under the supervision of the applicant.

3.3. From fictitious to real fluids: an introduction to the ERC project REACHER

Period: 2022-2027

Although only theoretical, the preliminary work presented in the previous section 3.2 has: (1) demonstrated the ground-breaking potential in engine performance of Lighthill's idea, (2) presented the main barrier to be overcome (searching for suitable real reactive fluids), (3) introduced the ways for further efficiency improvement (defining new optimal cycle configurations).

The main issue that prevented the demonstration of the -only theoretically sampled- potentiality of this process in substantially increasing the efficiency of energy conversion

systems based on thermodynamic cycles **is the apparently limited availability, in nature, of suitable reactions**.

To fill this gap, in the year 2021 the applicant submitted a proposal to the ERC Starting Grant programme, named REACHER: "*Reactive fluids for intensified thermal energy conversion*". This project, funded at its first submission, has started the 1st of April 2022 and will end the 31st of March 2027.

REACHER aims to achieve a two-level target: the search for, design of and characterisation of reversible reactions, by means of an original thermodynamic and kinetic predictive methodology making use of ab-initio Quantum Chemistry calculations, molecular Monte Carlo simulations, Machine Learning, and equations of state and in-house computational programs (primary-level target), in order to allow the exploration of a new energy science domain, based on the exploitation of chemical energy in closed thermodynamic cycles (secondary-level target). More details about the applied methodology are provided in the following section.

3.3.1. The methodology of the project REACHER

REACHER implements a methodology that consists in four work packages (WP), schematically represented in Figure 22 with a focus on WP2, the key WP of the project. Work packages are thoroughly detailed in the sections that follow. The first phase of the project (WP1) consists in the development of a thermodynamic predictive computational tool, that will be used in WP2 and in WP3. WP2 defines and characterizes a list of thermodynamically and kinetically suitable reaction. On the basis of that list of fluids and by means of the thermodynamic tool developped in WP1, WP3 implements a methodology to optimize thermodynamic cycles operating with those fluids. Finally, WP4 is devoted to the experimental observation and analysis of the behaviour of reactive fluids in a pilot consisting in a micro-power cycle.

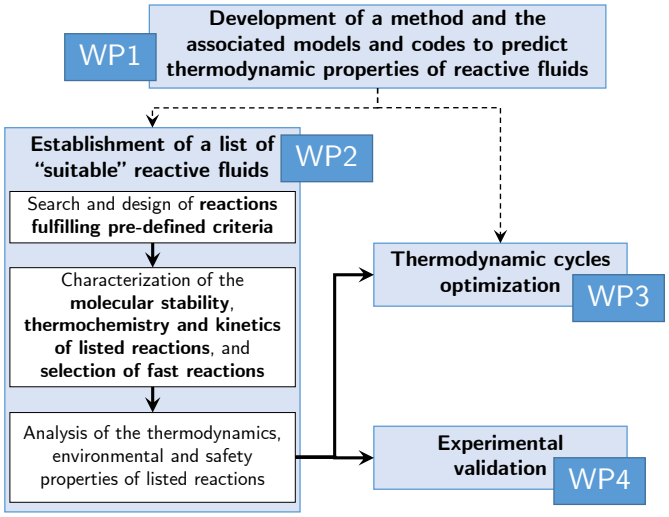

Figure 22. Overview of the methodology of the project REACHER.

WP1) Development of a computational tool for the prediction of thermodynamic properties

The achievement of REACHER's targets relies on the design of a robust computational tool to calculate the thermodynamic properties of reactive fluids. The steps that are planned are listed in the following.

(1.a) Selection and development of equations of state for the predictive thermodynamic modelling of reactive mixtures

The calculation of energetic and volumetric thermodynamic properties of real fluids requires the knowledge of a real-fluid equation of state, other than of the ideal gas heat capacity of the molecules forming the mixture. Most of the fluids considered in the study are designed from scratch and thus no experimental data are available. As a consequence, the use of a predictive equation of state is required where, with the term "predictive", it is meant that the intermolecular interactions are not quantified by empirical parameters fitted over experimental data, but theoretically calculated by the model.

The predictive model which is initially considered is the one studied in the PhD thesis of the applicant, which is the Peng-Robinson equation of state associated to advanced EoS+ $a_{res}^{E,\gamma}$ mixing rules, where, a zero-residual excess Helmholtz energy part, $a_{res}^{E,\gamma}$, is considered for this work. The use of a zero residual excess Helmholtz energy leads to a model free of semi-empirical binary interaction parameters to be adjusted (otherwise present in the residual excess Helmholtz energy model) and will thus work in a predictive way. This model will be mainly

applied to model mixtures for which no data are present in the literature and no other modelling alternatives exist (more details are given in the next chapter 4). For mixtures for which experimental data exist, more precise models will be applied, either predictive equations of state (e.g., Enhanced-Predictive-Peng-Robinson78 [22], Volume-Translated-Peng-Robinson [105], UMR-PRU) or semi-empirical models to be optimised over the experimental data. These equations of state are being implemented in the thermodynamic calculation code under development.

Finally, the *required inputs* for the use of each of these models are the critical pressure, the critical temperature and the acentric factor of all species forming the reactive mixture of interest. The related challenge is that the reversible reactions to be characterised (composed by at least 2 components), are constantly at chemical equilibrium and the measurement of the properties of the components participating to the reactions, in their pure form, is not feasible. Other required properties to perform thermodynamic calculations of reactive systems are the standard enthalpy of formation, the standard molar entropy and the specific heat capacity in the ideal gas state, for all species forming the reactive mixture. The paragraph about WP3 introduces and Chapter 4 details the methodology, based on multi-scale thermodynamic tools, we are applying to determine all those input properties.

(1.b) Implementation of an algorithm for chemical (reaction + fluid phase) equilibrium algorithms

The program which is under development implements the algorithms for chemical equilibrium calculations, including simultaneous phase and reaction equilibrium. These algorithms will be developed to enable the simultaneous occurrence of no more than two chemical reactions and four components. Indeed, in REACHER, the aim is to consider simple reactive systems presenting a maximum of two simultaneous reactions. The description of vapour-liquid equilibrium in reacting mixtures is important in this project to perform thermodynamic calculations in the two-phase vapour-liquid equilibrium region.

WP2) Establishment of a list of "suitable" reactive fluids

The successful development of this work package will lead to a list of reactions, and associated thermodynamic and kinetic data, considered as suitable (but definitely not optimal) for the set of studied applications.

(2.a) Quantification of thermochemical criteria to define "suitable" reaction.

This step consists in establishing preliminary acceptable joint ranges of standard enthalpy and entropy of reaction (thermodynamically acceptable "chemical space", or "($\Delta_R H°$; $\Delta_R S°$)-space") which, together, define the temperature-dependent formulation of the equilibrium constant of the reaction. The acceptation (or not) of these joint reaction coordinates depends on the evolution of a reaction in the considered ranges of temperature and pressure taken by the reactive working fluid along the considered thermodynamic cycle. In fact, suitable reactions must progress along the cycle and not behave as inert reactants or inert products. To assess the "thermodynamically acceptable chemical space" of reactions to be selected, REACHER applies the following methodology (schematically represented in Figure 23).

(2.a.1) Definition of at least 2 different *fictive* stoichiometries (for example, A_2=2A and A_3=3A).

(2.a.2) Definition of a preliminary rectangular ($\Delta_R H°$; $\Delta_R S°$)-space ($\Delta_R H°_{min}$, $\Delta_R H°_{max}$, $\Delta_R S°_{min}$, $\Delta_R S°_{max}$) in which searching for the "thermodynamically acceptable ($\Delta_R H°$; $\Delta_R S°$)-space"; in a previous work [17] it was already presented the guided selection of these values. It is emphasized that *each point* of this space identifies the thermodynamic coordinates that, whether associated to specific fictive stoichiometry (e.g., the three stoichiometries defined in (2.a.1)), define a specific fictive reaction.

(2.a.3) Definition of preliminary temperature and pressure intervals, (T_{min}, T_{max}) and (P_{min}, P_{max}), in which the reactive fluid will operate in typical thermodynamic cycles: the minimum and maximum temperature of the cycle are related to the hot source and cold sink of the considered application. For example, typically, T_{min} = 20 °C and T_{max} = 900 °C for high-temperature power cycles, T_{min} = 20 °C and T_{max} = 400 °C for medium-temperature power cycles, T_{min} = -15 °C and T_{max} = 70 °C for residential heat pumps, T_{min} = 20 °C (or higher) and T_{max} = 200 °C for industrial heat pumps, T_{min} = -30 °C and T_{max} = 30 °C for refrigeration cycles; the minimum and maximum pressure values generally are (in a gaseous cycle) dictated by optimisation considerations. Concerning pressure, a minimum and a maximum acceptable pressure are fixed by preliminary considerations.

(2.a.4) With the thermodynamic tool developed in the preliminary work leading to results published in [17,18], this step aims to calculate, for each reaction resulting from the coupling of the fictive stoichiometries defined in (2.a.1) and the points of the ($\Delta_R H°$; $\Delta_R S°$)-space defined in (2.a.2), the equilibrium composition of the system in the four (T,P)-extrema of the temperature and pressure domain defined for each of the four applications: (T_{min}, P_{min}), (T_{min}, P_{max}), (T_{max}, P_{max}), (T_{max}, P_{min}).

(2.a.5) The sum of the modules of the variations of the extent of reaction ($\Sigma|\Delta_i\xi|$, with i = 1-4) from point (T_{min}; P_{min}) to point (T_{min}; P_{max}), $\Delta_1\xi$, from point (T_{min}; P_{max}) to point (T_{max}; P_{max}), $\Delta_2\xi$, from point (T_{max}; P_{max}) to point (T_{max}; P_{min}), $\Delta_3\xi$, from point (T_{max}; P_{min}) to point (T_{min}; P_{min}), $\Delta_4\xi$, will be plotted on the z-axis of a diagram representing that overall variation ($\Sigma|\Delta_i\xi|$) as a function of the thermodynamic reaction coordinates ($\Delta_R H°$ - the x-axis; $\Delta_R S°$ - the y-axis) and for the considered reaction stoichiometry that the ($\Delta_R H°$; $\Delta_R S°$; $\Sigma|\Delta_i\xi|$)-diagram refers to. That will enable to find out, for each considered stoichiometry, the region of ($\Delta_R H°$; $\Delta_R S°$) leading to a non-negligible variation of the extent of reaction. **Belonging to so-identified thermodynamically acceptable ($\Delta_R H°$; $\Delta_R S°$)-chemical spaces represents the first thermodynamic criterion for pre-screening of real reactions.** Other criteria will impose, for example, the exclusion of molecules being in the solid state at the considered operating conditions.

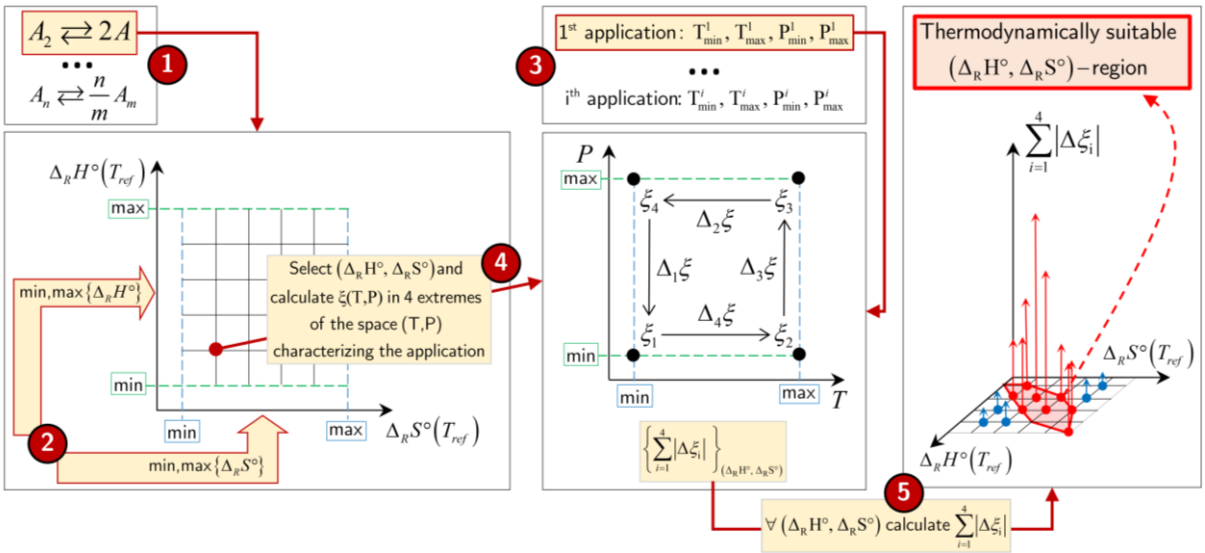

Figure 23. Definition of thermodynamic criteria for reaction searching and design.

These optimality maps will be derived for a fluid being: 1) in the gaseous phase, in the whole (T,P)-domain (i.e., in the 4 extrema of the considered (T,P)-domain) or 2) in the gaseous phase in all the extrema except in (T_{min}; P_{min}), where the fluid is in saturated liquid phase.

(2.b) Search and design of reactions fulfilling pre-defined thermodynamic criteria.

(2.b.1) Research of existing fast chemical reactions, and related data. That is done accessing the databases of the ThermE team (NIST-TDE, DDB and DIPPR).

(2.b.2) Design of reactions suiting specific molecular structure criteria. More details are provided in section 3.3.3.

(2.b.3) Assessment of the molecular stability of the designed molecules and calculation of the ideal gas thermochemical properties of the reactions (the standard enthalpy of formation, $\Delta_f H^{\circ}_{i,298.15K}$ at 298.15 K, the molar entropy, $S^{\circ}_{i,298.15K}$, at 298.15 K and the ideal gas heat capacity as a function of temperature, $c^{ig}_{p,i}(T)$), by Quantum Mechanics calculations. More details about Quantum Mechanics calculations are provided in chapter 4. Finally, it is specified that machine learning methods are also applied in order to obtain in a way independent of Quantum Mechanics calculations, $\Delta_f H^{\circ}_{i,298.15K}$ and $S^{\circ}_{i,298.15K}$. This is done in order to strengthen the reliability of the obtained results or to quantify their uncertainty.

(2.b.4) Selection of reactions having an enthalpy and an entropy of reaction belonging (or close) to the ($\Delta_R H°$; $\Delta_R S°$)-spaces pre-defined in section (2.a). At the end of this step, a list of thermochemically suitable reactions will be released.

(2.b.5) Validation of the above procedure by selecting designed reactions for which thermochemical are available in the literature and comparing these data with calculated properties.

(2.c) Characterization of the kinetics of reactions listed in (2.b), and further selection of fast reactions.

Reactions that will be finally selected as "suitable" must be *fast and reversible*, that means, be characterised by a relaxation time lower than the lowest residence time measurable in cycle

components (typically, expansion devices). To allow the further screening of reactions on the basis of kinetics criteria, the kinetics of these systems has to be assessed, in section (2.c.1) and (2.c.2).

(2.c.1) Evaluation of the kinetics of designed reactions

If a dimer A_2 exists in a stable form, the determination of the rate coefficient of a simple association reactions of the form $2A \rightarrow A_2$ is quite straightforward, since the energy of the transition state is negligible. As a consequence, the activation energy E_{act} of the dissociation reaction $A_2 \rightarrow 2A$, given by the sum of the activation energy of the association reaction and the enthalpy of reaction, is approximated with the enthalpy of reaction.

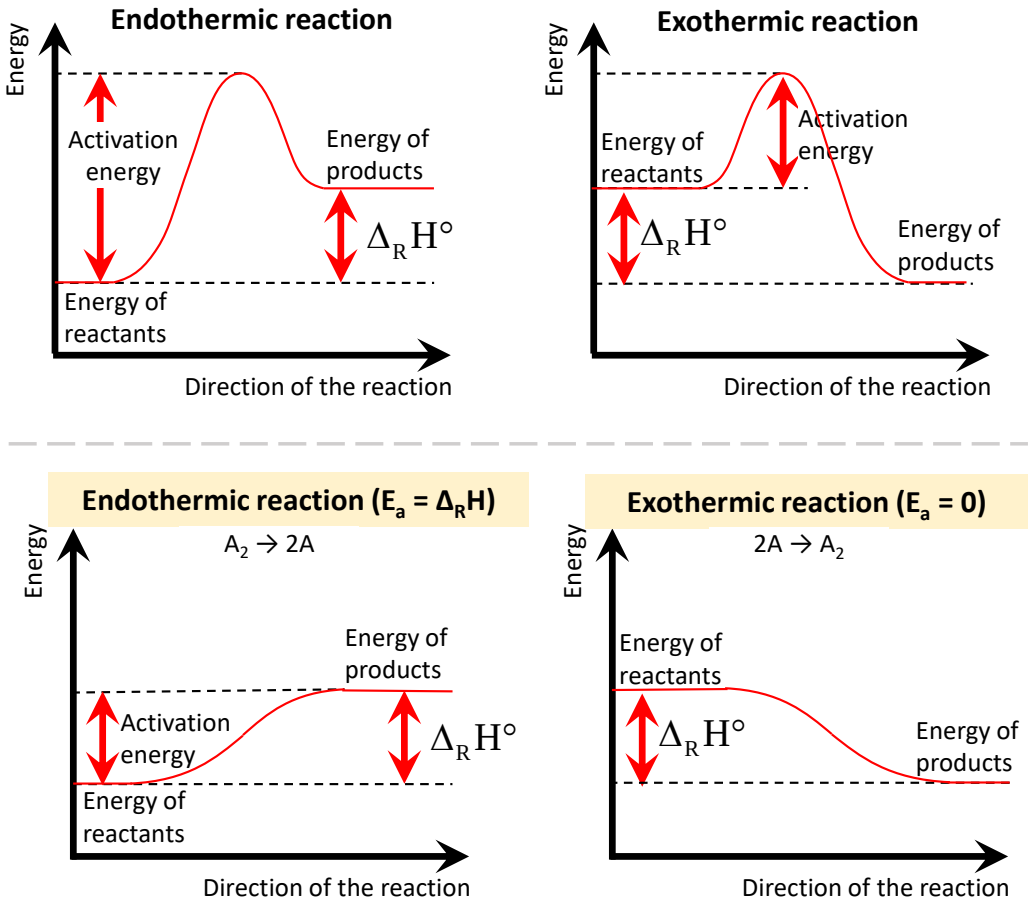

Figure 24. Reaction energy schematics

Knowing the standard enthalpy of reaction at 298.15 K, the rate constant of the reaction $A_2 \rightarrow 2A$ can thus be calculated in a straightforward way from the Arrhenius equation:

$$k_{A_2 \to 2A} = A \cdot \exp\left(-\frac{E_{act}}{R \cdot T}\right) \sim A \cdot \exp\left(-\frac{\Delta_R H°}{R \cdot T}\right) \quad (27)$$

considering as a first approximation the pre-exponential factor, A, equal to 10^{16} 1/s. The kinetic rate constant of the backward reaction $2A \rightarrow A_2$ can be calculated from the equilibrium constant, considering that:

$$\frac{k_{A_2 \to 2A}}{k_{2A \to A_2}} = K_{eq, A_2 \rightleftharpoons 2A} \quad (28)$$

and that the equilibrium constant is determined from $\Delta_R H°$ and $\Delta_R S°$ (at a 298.15 K) as shown in equation (25). Having computed the thermochemistry by Quantum Mechanics, the kinetics can be directly assessed.

The reliability of these calculations (i.e., of the assumption of negligible activation energy of the association reaction) and the validity of equation (27), is checked for some systems, by calculating by Quantum Mechanics the transition state energy of the association reaction.

(2.c.2) Exclusion of reactions characterized by a low reaction rate.

Reactions whose relaxation time result sensibly higher than the lowest residence time measurable in cycle's components are excluded. In thermodynamic cycles, the unit operations characterized by the lowest residence time are expansion devices. In general, the residence time of a fluid crossing a unit operation depends on the considered application (on the size of the component and the operating conditions). However, in this project, a value of 0.7 ms will be considered as an indicative residence time characterizing single-stage micro-turbine; this value has been estimated considering a single-stage micro-turbine that DEPRAG has designed and manufactured under the request of the applicant, for a low-temperature power cycle designed for experimental purposes (see chapter 5 for more details). This turbine is also used in the experimental activity of REACHER (in WP4).

The indicative residence time of 0.7 ms is used in this stage of the project as a reference value to allow exclusion of reactions characterized by too slow kinetics. Depending on the uncertainty of the predicted or found kinetic model of each reaction, an acceptable margin is applied to the value of 0.7 ms.

(2.d) Analysis of the thermodynamics, environmental and safety characteristics of the reactions belonging to the defined list of reactions.

As a result of the previous steps, a list of thermochemically and kinetically suitable reactions is now available, together with the relative thermochemical data needed to characterize the ideal gas properties of the reaction. This part of the methodology aims at characterising the real fluid thermodynamics, environmental and safety characteristics.

(2.d.1) Thermodynamic characterisation

As highlighted in the methodology, at point WP1-(1.a), the thermodynamic characterisation of the real fluid properties requires, in general, the use of equations of state and the inputs that their application needs (critical point coordinates and acentric factor of each molecule forming the mixture). So, the first thermodynamic properties that must be assessed in order to be able model the reactive mixture properties are the ones of the pure species forming the mixture.

Indeed, the novelty of most of reactive fluids (the designed ones) and the impossibility of measuring the pure component properties of the molecules participating to reversible reactions (see Chapter 4) requires the use of predictive computational tools. In this work, we perform **Monte Carlo (MC)** [106] simulations to determine the pure fluid VLE properties (T- $P^{sat}(T)$-$\rho_L(T)$-$\rho_V(T)$) and deduce their critical point properties and acentric factor. These calculations require some inputs (e.g., optimised molecular geometries, partition functions, …) from the **Quantum Mechanics** calculations performed in part (2.b.3) of this methodology. Also, Monte Carlo simulations are performed on the reactive system, to determine (T-$P^{vle}(T)$-$\rho_L(T)$-$\rho_V(T)$-x(T)-y(T))-properties for mono-variant binary reactive systems at VLE conditions -see Chapter 4-, or (T-P-$\rho_L(T,P)$-$\rho_V(T,P)$-x(T,P)-y(T,P))- properties, for bivariant ternary reactive systems at VLE conditions. With those data, the thermodynamic calculation package developed in WP1 can be used to calculate energetic and VLE properties of all fluids by cubic equations of state. This whole methodology has recently been applied and validated on the well-known system $N_2O_4 \rightleftharpoons 2\ NO_2$ and is described in Chapter 4.

The applicant is acquiring competences on Monte Carlo simulations thanks to a collaboration that she started in 2023 with Prof. Thijs J. H. Vlugt working at the Process

& Energy Department TU Delft, who gave her the possibility to spend one week in his team. During this -short but intense- period, she learned how to use Brick-CFCMC [107], a Monte Carlo code built by this team that was used then used by the applicant to perform the calculation on the $N_2O_4 \rightleftharpoons 2\ NO_2$ system, as discussed in Chapter 4. This collaboration has led to two major papers under publication [108,109], where the publication [108] is fully presented in Chapter 4.

What has been omitted above is that force field-based MC calculations require an additional input: the parameters of the all-atoms force field (for example, the Lennard-Jones force field model) of considered molecule forming the mixture (see par example Figure 25). Nowadays, those are always optimised on experimental data. For $N_2O_4 \rightleftharpoons 2\ NO_2$, force field parameters were present in the literature and MC calculations could be performed. However, for the designed molecules, for which no data are a priori available, those parameters are unknown. An iterative procedure, shown in Figure 26, is proposed in this project in order to be able to obtain force field parameters and Monte Carlo simulation results. Before describing the procedure, it is worth saying that the Brick-CFCMC code originally based on all-atoms force field was simplified. Indeed, in the modified version of the code molecules are represented as single LJ particles (see Figure 25), molecules thus accelerating the calculations. The impact of such a simplification on the properties of the studied (quite simple) systems, by MC simulation, has revealed to be sufficiently small to allow its application [109].

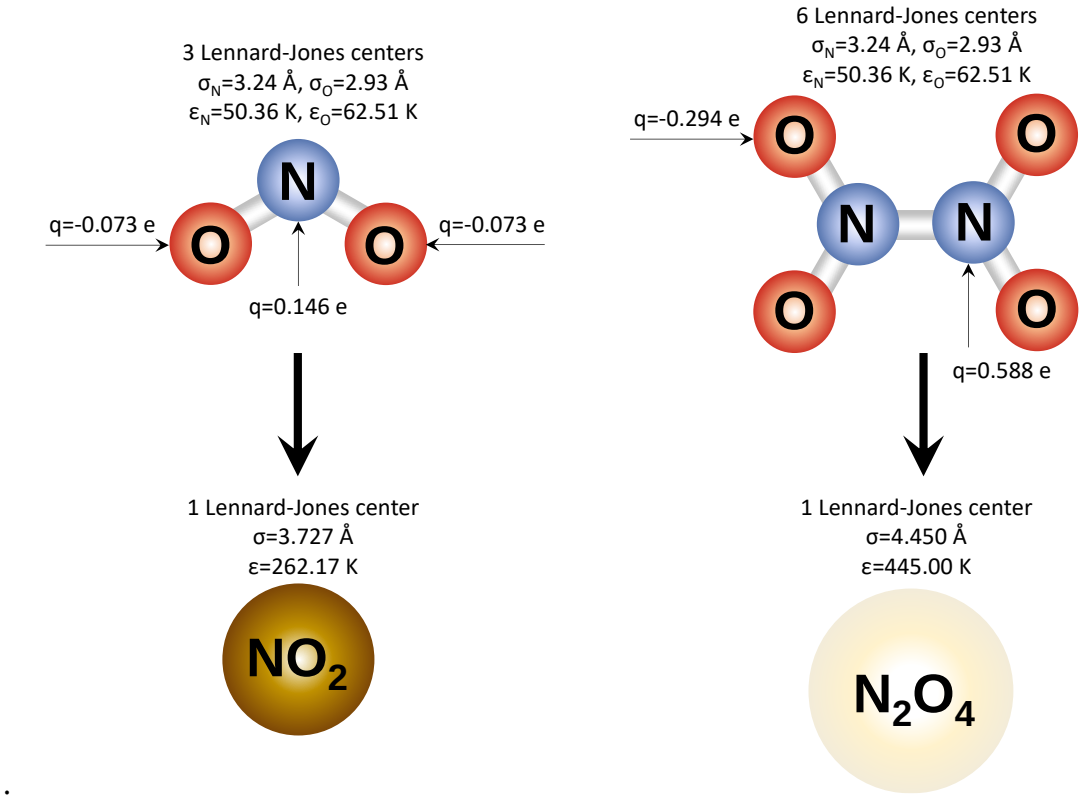

Figure 25. From all-atom to single-particle force fields.

Based on the use of the software COSMO-RS and the Monte Carlo software Brick-CFCMC [107], the following procedure has been designed (but not yet tested) in order to perform MC simulations starting from initially guessed force field parameters. This procedure:

1. Initially uses COSMO-RS program to estimate the normal boiling temperature, T_{boil}, and the hard-sphere volume V_{COSMO} in order to calculate, by specific correlations reported in the User Manual [110] and in Figure 26, the critical temperature T_c and molar volume v_c of the considered molecule.
2. Calculates the Lennard-Jones parameters, σ and ε, from available correlations [111] that relate those parameters to the critical properties (see Figure 26).
3. Perform MC simulations with the modified (single LJ particles)-Brick-CFCMC code, to obtain VLE and saturation density data (with NPT and NVT ensembles).
4. Estimate the critical properties by applying scaling laws, as shown in a recent paper by Lasala et al. [108] and in Chapter 4.
5. Compare the obtained critical properties with the ones of the previous iteration. If the difference is sufficiently low (the convergence criterion is going to be

defined during the first tests of this procedure), the procedure has converged and the results of the final iterations are the final one. If not, the obtained critical properties are used to recalculate, at point 2 of the procedure, σ and ε and the procedure continues up to convergence.

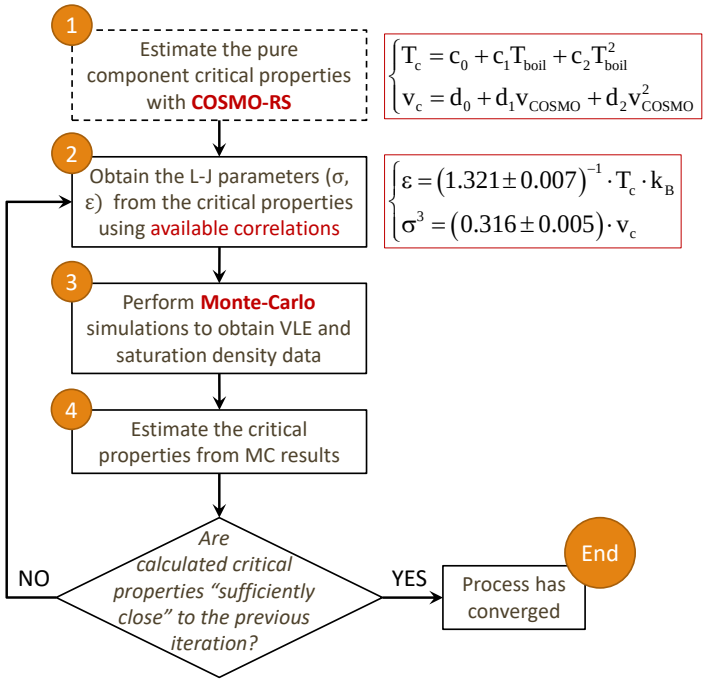

Figure 26. Methodology proposed to calculate critical point properties of pure fluids without knowing input Lennard-Jones parameters.

(2.d.2) Environmental, toxicological and safety characteristics

Environmental data such as Global Warming Potential (GWP) and Ozone Depleting Potential (ODP) will be either collected from the literature or estimated: GWP will be estimated from available -and eventually improved- simple group contribution techniques [112] or more rigorous methods based on the analysis of IR spectra of molecules available from Quantum Mechanics calculations [113], and from the knowledge of the molecular structure of the species involved in the reaction; molecules containing high-ODP potential atoms (bromine, chlorine and iodine) will be considered but penalized in the fluid selection process.

Toxicological data of molecules will be either collected from the Globally Harmonized System of Classification and Labelling of Chemicals (GHS) or, eventually, estimated by machine learning techniques [114].

WP3) Optimization of a thermodynamic cycle based on reactive fluids.

The availability of a list of thermodynamically suitable and equilibrated reactive fluids represents the starting point for the system optimisation, consisting in assessing the optimal fluid and cycle architecture for a specific application.

(3.a) Process and product optimisation (neglecting kinetic effects)

Considering a specific application of power, heating or cooling, and specifications by reference users, in REACHER, the optimization of the overall system (fluid and cycle architecture) consists in 4 steps.

(3.a.1) For each application and detected suitable fluids: optimisation of the cycle architecture and operating conditions.

Firstly, a process design method will be applied to determine the optimal cycle's architecture which corresponds to each fluid of the list defined in WP2. The most comprehensive process-design optimization method would consist in the definition of a process flowsheet (a so-called "superstructure" [115], see Figure 27 taken from [116]), representing the alternative structures by means of decision switches, and the determination of the optimal design by Mixed Integer Non-Linear Programming optimization. This is one of the competences of the Axis PRIMO of the laboratory LRGP. A collaboration with Dr. Andrés Pina-Martinez would help to realise this work.

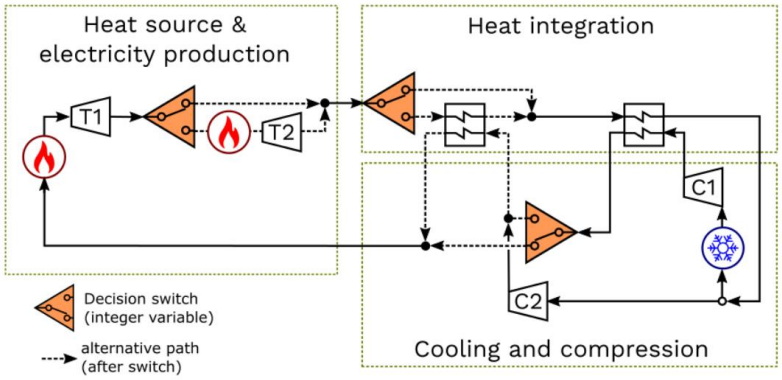

Figure 27. Superstructure used for identifying an optimal Brayton with the aim of maximizing the cycle efficiency [116]

However, it is likely that such a MINLP optimisation results to be computationally difficult due to the necessary simultaneous resolution of (potentially long)

thermodynamic calculations. In alternative, different possible cycle architectures will be predefined (no more, superstructures) and their operating conditions optimised in parallel.

(3.a.2) For a specific application: definition of the best "fluid-architecture" system.

Then, a comparison between all these optimized systems, on the basis of their performance indicators, will provide the best "fluid-architecture" system. The analysis of the obtained results will enable the identification, and thus the understanding, of possible correlations between reactive fluid characteristics and resulting optimal cycle configurations.

(3.a.3) Optimisation with inert working fluids.

The same process design method will be applied considering a list of 10 inert working fluids, preliminary screened from three thermodynamic databases (DDB, DIPPR, NIST [117–119]), already available at ThermE team, containing properties for more than 80 000 pure fluids. In particular, those 10 fluids will be selected considering two steps: 1) Considering all the pure fluids for which specific parameters enabling the application of a preliminary selected equation of state are available, a pre-screening of fluids is initially performed; 2) specific screening criteria (e.g., on critical temperature, triple temperature, saturation pressure at the minimum and maximum cycle temperatures - whether applicable-, environmental and safety features, …) will be applied to the pre-screened fluids, on the basis of the specific application. A similar screening has been realised in the on-going REGEN-BY-2 project, where we came up with a list of 10 fluids for a three-generation cycle, starting from an initial pull of more than 60 000 molecules (see section 2.2.2).

(3.a.4) Comparison reactive versus inert working fluids.

Optimal solutions obtained with inert and reactive working fluids will be compared *to quantify REACHER's gain*.

(3.b) Impact of the kinetics on optimality results

Optimizations performed in (3.a) neglect the actual kinetics of reactions: each point of the thermodynamic cycle is at thermodynamic equilibrium. The next phase consists in selecting one of these optimal cases and analysing the effect of kinetics, over a high number of cycles undergone by the fluid. Non-stationary effects will be studied, by assessing the temporal variation of fluid composition, in each point of the cycle. It also specified that the calculation code will be entirely realized, in Fortran, by the research team of REACHER.

WP4) Observing the transformation of thermal and chemical energy into work

An important part of this project is devoted to the experimental observation of the energy conversion undergone by a reactive fluid in an adiabatic expansion process taking place along a micro-axial turbine that the applicant acquired in a regional research call. WP4 is organized as it follows:

(4.a) Design and test of a closed power cycle operating with a selected reactive working fluid.

Firstly, at least two candidate reactive fluids are chosen, from the designed list of suitable fluids being commercially available. Non-toxic and non-flammable fluids are preferably considered. An experimental power cycle is realised, enabling to observe how does the reactive fluid behave along the cycle and to validate the performance calculations. The cycle, a closed loop represented in Figure 28 where the fluid circulates, is composed of, mainly, 4 unit operations:

- a primary heat exchanger, where the reactive working fluid is heated up to 180 °C (from point n. 1 to n. 2);
- the 3.5 kW_{el} micro-turbine mentioned above, which is designed to expand 80 g/s of CO_2 from 180 °C and 4.5 bar to 1.5 bar (from point n. 2 to n. 3);
- a cooling system, to reduce the temperature of the fluid up to 25 °C (from point n. 3 to n. 4);
- an oil-free compressor which increases the pressure of the fluid before it enters the primary heat exchanger (from point n. 4 to n. 1).

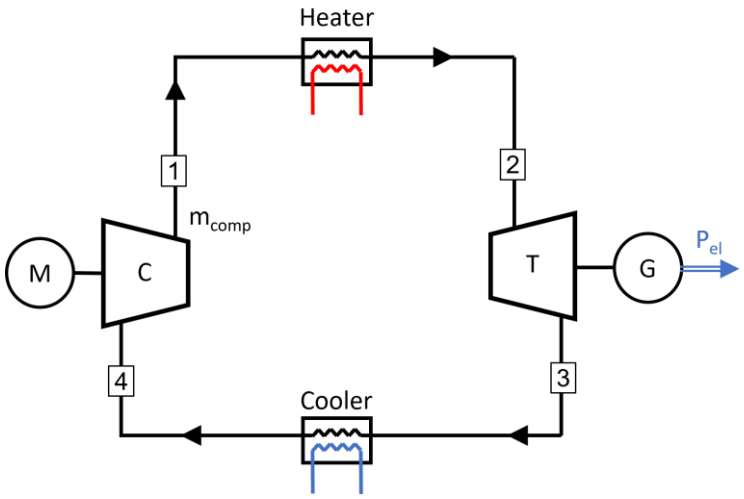

Figure 28. The pilot (simplified schematic) of the closed Brayton cycle.

The turbine, connected to a generator by its shaft, has been designed to expand 80 g/s of pure CO_2, with an inlet temperature and pressure of 180 °C and 4.5 bar, and an outlet pressure of 1.5 bar. In this experimental activity, the idea is to progressively increase the amount of reactive fluid in an inert environment (pure CO_2) and to validate calculations by: 1) experimental observing, with online Raman spectroscopy, the variation of the equilibrium composition between the inlet and the outlet of the turbine and, 2) measuring the electrical energy produced by the generator.

Given the fact that the turbine is designed to run with CO_2, its use to expand another fluid is not optimal. However, the sensibly higher net power that is expected to be produced by the turbine, as a result of the addition of the selected reactive fluid, should entail a remarkable increase of mechanical energy although the turbine will not operate in optimal conditions (i.e., with other fluids than pure CO_2). Online Raman spectroscopy compositional measurements will be also performed at the inlet and at the outlet of the compressor, so that the composition will be characterized in all the points of the cycle. This will also enable to analyse the behaviour of the fluid in crossing the heat exchangers and the compressor.

(4.b) Spectrometer calibration

The use of a Raman spectrometer to measure the composition of reactive fluids requires the design of both an experimental equipment and a specific experimental methodology to analyse and calibrate the Raman signals.

(4.c) Experimental campaign

The final step of this work package consists in running the pilot in three conditions:

1) Open cycle: the pilot is tested with ambient air as working fluid and the inlet of the compressor directly takes the air from the environment, while the outlet of the cold heat exchanger discharges air in the atmosphere. This configuration is operated in order to test the behaviour of the unit operations (turbine, compressor, heat exchangers).
2) Closed cycle operating with a pure fluid: the pilot is tested with a pure fluid to check the dynamics and control of the system in a closed loop, that is when the outlet of the cold heat exchanger is connected to the inlet of the compressor.
3) Closed cycle operating with a mixture of pure fluid (CO_2 or N_2) + reactive fluid: the pilot is used for the purpose for which it has been designed, that is to assess the performance of the cycle operating with reactive working fluids. Each test will take one day and the stationarity of the system will be verified.

Risk analysis and feasibility assessment

REACHER is a high conceptual-risk project mainly because of the potential difficulty of finding suitable reactive working fluids for thermodynamic cycles ("suitable" means that the fluid fits thermodynamic, kinetic, environmental and safety criteria). Such a risk is related to the breakthrough character of the project and its occurrence could potentially lead to the conclusion that reactive fluids can not be used in thermodynamic cycles (if all discovered fluids result to be thermodynamically and kinetically unsuitable), or that fluids being unsafe but thermodynamically and kinetically suitable should be used. The reason why the activity must be pursued despite the “unsuitable” toxicological characteristics of these fluids is related to the impact of REACHER. The novel **intensified** energy conversion system under investigation will involve the use of an extremely reduced amount of working fluid, with respect to state-of-the-art technologies, because of its smaller size. Considering that current technologies for power production and refrigeration purposes also use unsafe fluids (being toxic and flammable) or environmentally harmful fluids, the completion of the whole study is fundamental to fully evaluate the potential of this concept with respect to the state-of-the-art. Table 3 reports four main risks and actions proposed both to minimize and to overcome the occurrence of the main risks identified in REACHER, guaranteeing the feasibility of the methodology.

Table 3. Main risks associated to the project. Risk assessment grades: Low risk - Medium risk - High risk.

ID	Risk item	Effect of the risk	Causes of the risk	Grade	Actions to minimize the risk
1	*Failure in the establishment of a sufficiently long list of reactions (>10 fluids).* ***Risk in WP2****.*	Constrained or even impossible selection of fluids.	■ Too restrictive screening criteria. ■ Long quantum chemistry computational time. ■ Too uncertain procedure for the determination of thermodynamic criteria (WP2).	High risk	■ Understanding of the effect of the relaxation of imposed thermodynamic and kinetic screening criteria on the number of fluids forming the list. ■ Improvement of the reliability of the initialisation of QC calculations. ■ Post-processing validation of the procedure applied in WP2: once the list of fluids is defined, the term quantifying the overall variation of the extent of reaction in the cycle, $\Sigma\lvert\Delta_i\xi\rvert$, (see WP2(2.a)) is recalculated considering real fluid properties, to confirm its significant amount.
	This risk is graded as "high" *mainly because* ***it could conceivably happen*** *and because* ***its impact on the project in case of occurrence is severe.*** **Alternatives in case of occurrence of RISK 1**: If, despite the actions applied to minimize the risk, the application of the methodology outlined in WP2 leads to a poor (or empty) list of reactive fluids associated to a specific application: 1) thermodynamic and kinetic *constraints will be relaxed* and the same methodology will be applied again; 2) since current power technologies use inert fluids that might be toxic and/or flammable (see Fig. 2), unsafe fluids will a-priori not be excluded in the project; in this case, to reduce toxicity or flammability, *the addition of an inert fluid* to the reactive one will be proposed. **Consequence of the implementation of alternatives in the methodology**: With respect to the implementation of the two above-mentioned alternatives: 1) the relaxation of thermodynamic and kinetic criteria will probably lead to the selection of less suitable reactive fluids; in the case of necessary implementation of this alternative, a thorough study will be performed to evaluate the impact of the use of those, discovered or found, less "thermodynamically and kinetically" suitable reactive fluids; 2) With respect to this point, it is worth highlighting that the use of toxic or flammable fluids in these cycles would probably be less dangerous with respect to their use in current technologies; this is because thermodynamic cycles using reactive fluids would have significantly reduced sizes and this would imply the load of a significantly lower amount of working fluid in the cycle. In case an inert component will be added to limit unsafety features, this fluid-selection process will be guided by an intense study aiming to assess the impact of the addition of an inert fluid in a reactive one, on the cycle's performance and on the overall resulting safety of the application. Therefore, if this risk occurs, only WP2 will be modified, while the methodology implemented in WP1, WP3 and WP4 will remain unchanged.				
2	*Unreliable prediction of the kinetics of reactions.* ***Risk in WP2.***	Uncertain kinetics of selected reactions.	Unavailable data required to reliably initialize and/or to validate the predictive method.	Medium risk	■ Analysis of multiple databases. ■ Intensification of discussions with Dr. Herbinet, to reliably validate the kinetic properties assessment.
	This risk is graded as "medium" *mainly because* ***it could conceivably happen*** *and because* ***its impact on the project in case of occurrence is noticeable.*** **Alternatives in case of occurrence of RISK 2**. If the procedure of validation of the kinetics predictive methodology leads to the conclusion that performed quantum mechanics calculations are too uncertain for the considered fast reactions, the number of reactions for which it will be necessary to calculate the kinetics by quantum mechanics will be reduced, prioritizing the reactions whose kinetics data are still absent in the literature. That will allow the use of more sophisticated (but more time consuming) levels of quantum theory to predict kinetic models. Also, with the aim to better select reactions that are likely to have a fast kinetics, machine learning methods will be tested and eventually used to help in classifying fast and slow reactions. **Consequence to the implementation of alternatives in the methodology**. The prediction of kinetics will require a longer time spent in the suitable tuning of predictive quantum chemistry methods.				
3	*Optimal reactive cycle configurations unchanged with respect to traditional ones.* ***Risk in WP3.***	Limitation to the improvement of cycle efficiency.	■ Too simple superstructure architecture. ■ Demonstrated impossibility of improving the cycle configuration.	Low risk	■ Increase the complexity of the superstructure, to maximise the number of possible configurations. ■ Optimise parallel configurations, instead of an overall superstructure.

ID	Risk item	Effect of the risk	Causes of the risk	Grade	Actions to minimize the risk
	This risk is graded as "low" mainly because it is very unlikely to happen. **Alternatives (and related consequences) in case of occurrence of RISK 3:** If this risk occurs, the optimisation of the cycle configuration will take more time than expected and the sole consequence of that action is the necessity of reducing the time originally planned for other activities. As for risk 2, that will allow to respect the overall schedule.				
4	*Unsuccessful calibration of the composition of reactive fluids.* ***Risk in WP4.***	Limited measurement of the composition of the working fluid.	Difficult calibration of the spectrometer, due to the sensible or not visible variation of the composition with temperature and pressure of the sample.	Low risk	■ During the calibration process, temperature and pressure conditions will be controlled in order to avoid bias in the calibration process. ■ Accurate thermodynamic models will be used to calculate mixture compositions necessary to calibrate the spectrometer.
	This risk is graded as "low" mainly because it is very unlikely to happen. **Alternatives (and related consequences) in case of occurrence of RISK 4:** If this risk occurs, it will not be possible to quantify the composition of the system. However, it will be possible to analyse the spectra in a qualitative way and to follow: 1) their variation along the cycle, comparing the 4 spectra on the cycle (each spectrum corresponding to one point of the cycle) and 2) their variation over time. This eventuality will not affect the feasibility of the experimental activity, since the measurement of the torque will be possible and that will enable to measure the mechanical energy converted during the expansion of the fluid along the turbine.				

3.3.2. The research team

The project is hosted by the "Laboratoire Réactions et Génie des Procédés" (LRGP) of University of Lorraine (UL), in Nancy (France). The ERC funding enables to enrol: *two Ph.D. students* (36 p.m. for each Ph.D.) with strong basis in thermodynamics (***PhD1***) and energy engineering (***PhD2***); and *three post-doctorate researchers* (24 p.m. for each PostDoc) having a solid background in chemical engineering (***Postdoc1*** and ***Postdoc2***) and skills in experimental tests on power cycles (***Postdoc3***). The implication of the personnel is summarized in Figure 29.

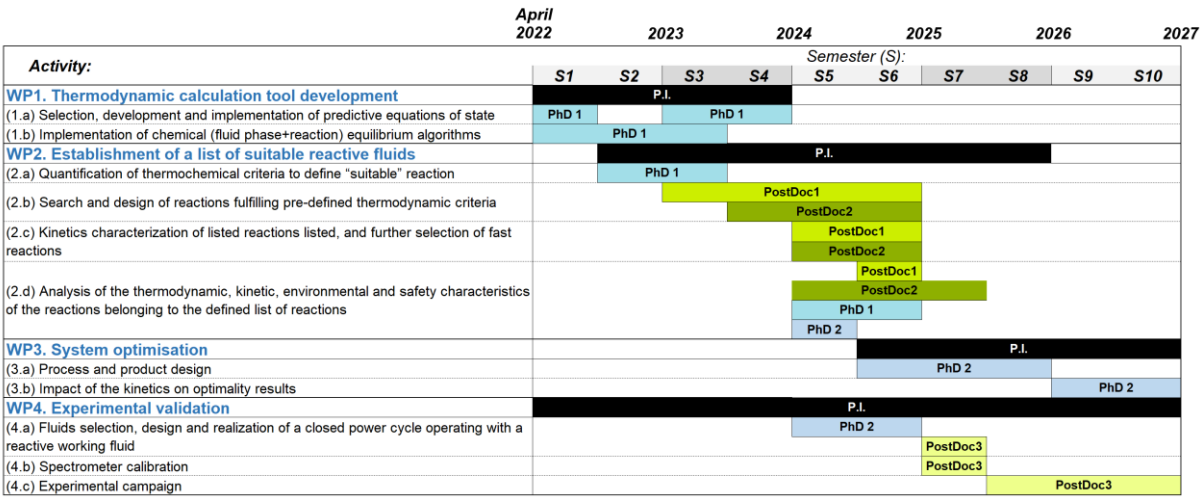

Figure 29. Gantt diagram and tasks allocation.

As for the applicant, she is dedicating 42 p.m. of her work to manage this five-year project. She is managing each phase of the project, in the full awareness of the responsibility that she has in its successful realization, which highly depends on her capability to -humanely and scientifically- conduct, coordinate and supervise the activities carried on by the scientific team.

3.3.3. Current state of progress and short term perspectives of the project

The project started in April 2022 and this is the almost the end of its second year. According to the planning, the team is currently composed of the following members:

- Konstantin SAMUKOV, employed for the period April 2022 - March 2025, is addressing the tasks mentioned for "PhD 1" in section 3.3.2. He is involved in WP1.
- Rachid HADJADJ, employed for the period June 2023 - May 2025, is addressing the tasks mentioned for "Postdoc 1" in section 3.3.2. He is involved in WP2.
- Sérgio VILAS BOAS, employed for the period November 2023 - October 2025, is addressing the tasks mentioned for "Postdoc 2" in section 3.3.2. He is involved in WP2.
- Luis PINILLA MONSALVE, employed for the period November 2023 - October 2025, covering the role of "PhD 2" in section 3.3.2. He will be involved in WP3.

The following colleagues are also collaborating on the project:

- Olivier HERBINER (WP2 and WP4)
- Jean-Noël JAUBERT (WP1 and WP3)
- Romain PRIVAT (WP1)
- Philippe ARNOUX (WP4)

This section explains briefly the state of progress of the project, for the different WPs, with the presentation of some preliminary results. The more thorough description of WP1, WP2 and WP4 follows in the next chapters, 4 and 5.

<u>WP1. Development of a computational tool for the prediction of thermodynamic properties</u>

The computer program for the calculation of thermodynamic properties of reactive mixtures is being developed, in Fortran language. <u>At present</u>, the code enables the thermodynamic characterisation (*volumetric, energetic, compositional properties* - in vapour-liquid equilibrium and single-phase conditions) of reactive binary mixtures being the site of a single reversible elementary dissociation/reassociation of the form $A_n \rightleftharpoons (n/m)\ A_m$ (e.g., $N_2O_4 \leftrightarrow 2\ NO_2$). Some of the results obtained from the use of this code, as well as the theoretical analysis, are presented

in **Chapter 4** [108]. This code is being developed by the doctoral student K. Samukov, under the supervision and with the contribution of the applicant, R. Privat and J.-N. Jaubert. In the next 2 years, the code will be developed to allow the thermodynamic characterisation of systems where **more than one reversible reaction** takes place and **one inert component** may be present. The code will allow performing calculations in equilibrium conditions and accounting for kinetic effects.

WP2. Establishment of a list of "suitable" reactive fluids

As presented in section 3.2, the postdoctoral activity of the applicant and the doctoral work of A. Barakat have enabled the investigation and coding of Brayton and Stirling cycles, power plants or heat pumps, operating with gaseous fictitious fluids. These codes are being used to address task (WP2.a), that is, to determine preliminary **suitable thermochemical characteristics** ensuring an acceptable evolution of the reaction in a thermodynamic cycle operating within specific temperature and pressure intervals.

Furthermore, the **research of reversible reactions** in the literature (W2.b.1) has led to the conclusion that reactions similar to $N_2O_4 \rightleftharpoons 2\ NO_2$, where a central covalent bond is broken in the reaction, are very limited and, except for N_2O_4, not well characterised. The scarce level of details provided in the present document about considered reactions is due to confidentiality reasons (two patents are currently under filing). The activity of **designing suitable chemical reactions** (WP2.b.2) has started in 2023 and is realized by the postdoc R. Hadjadj, under the supervision of the applicant. A methodology, as well as the relative Fortran code, is being realised to generate dimers being able to monomerise, according to a simple dissociation reaction $A_2 \rightleftharpoons 2A$, where A is a monomer and A_2 is the relative dimer. The specific design criteria and the generated molecules can not be disclosed in this document because two patents are currently under filing. Once patented, all the results will be provided to the scientific community. In parallel, the postdocs S. Vilas Boas and R. Hadjadj are performing **Quantum Mechanics** simulations, supervised by the applicant and Dr. Herbinet, to assess the stability of the designed molecules and to calculate the standard enthalpy of formation, standard molar entropy, specific heat capacity of perfect gas (WP2.b.3), and the kinetics of the generated reactions (WP2.c).

In collaboration with the axis *Génie des Produits* of LRGP, a remarkable work has just been concluded about the use of **machine learning** methods to predict standard enthalpy of

formation and standard molar entropy [120,121]. This application originated from the need in the project REACHER of predicting these properties with different independent tools (Quantum Chemistry and Machine Learning), in order to have an idea of their possible variability. A doctoral thesis is going to start in the next few months in order to continue this prediction work on other properties (critical point coordinates), as well as to pursue the collaboration between Dr. D. Meimaroglou, Dr. O. Herbinet and the applicant.

Concerning the calculation of the thermodynamic properties, a methodology has been designed and validated on N_2O_4. This methodology requires the appeal to Quantum Mechanics calculations, Monte Carlo simulations and equations of state. All the details are provided in chapter 4.

WP3. Optimization of a thermodynamic cycle based on reactive fluids.

According to the planning, this part of the work is going to start in March 2024, with the PhD thesis of Luis Pinilla. Initially, Luis will be asked to familiarize with the calculation of different thermodynamic cycles operating with inert fluids, and the concept of cycle optimisation. Then, he will be introduced to the thermodynamic calculation code developed in the thesis of K. Samukov, and will start treating reactive working fluids.

WP4. Observing the transformation of thermal and chemical energy into work.

According to the initial planning, the design of the experimental apparatus should have started in April 2024. However, the design has been anticipated in order to ensure the complete realization before the end of the project. As it is more precisely described in chapter 5, the design of the power plant is almost completed and all operation units have been acquired. Also, a Raman spectrometer and 4 Raman probes have been acquired. Some Raman tests are being performed and some systems are being characterised, thanks to the collaboration with two colleagues, Dr. P. Arnoux and Dr. O. Herbinet of LRGP, and the work of some students of ENSIC (the Chemical Engineering School where the applicant teaches) who realised their research project on Raman measurements. For example, some closed ampoules containing $N_2O_4 = 2\ NO_2$ in vapour-liquid phase equilibrium have been bought and some preliminary Raman spectra have been measured. The experimental campaign will start in 2025, after multiple tests of the pilot to be performed in 2024.

4. Modelling the thermodynamics of reactive mixtures

First outcome of the project REACHER (WP1&2)

Application of thermodynamics at different scales to describe the behaviour of fast reacting binary mixtures in vapour-liquid equilibrium

Silvia Lasala[1,*], Konstantin Samukov[1], H. Mert Polat[2], Véronique Lachet[3], Olivier Herbinet[1], Romain Privat[1], Jean-Noël Jaubert[1], Othonas A. Moultos[2], Kevin De Ras[4], and Thijs J. H. Vlugt[2,**].

[1] Université de Lorraine, CNRS, LRGP, F-54000 Nancy, France.

[2] Engineering Thermodynamics, Process & Energy Department, Faculty of Mechanical Engineering,

Delft University of Technology, Leeghwaterstraat 39, Delft 2628CB, The Netherlands.

[3] IFP Energies nouvelles, 1 et 4 avenue de Bois-Préau, 92852 Rueil-Malmaison, France.

[4] Ghent University, Laboratory for Chemical Technology (LCT), Technologiepark 125, B-9052 Ghent, Belgium.

Corresponding authors:

* silvia.lasala@univ-lorraine.fr

** t.j.h.vlugt@tudelft.nl

Paper published in the Chemical Engineering Journal [108].

Abstract

The use of reactive working fluids in thermodynamic cycles is currently being considered as an alternative to inert working fluids, because of the preliminarily attested higher energy-efficiency potential. The current needs to simulate their use in thermodynamic cycles, which may operate in liquid, vapour or vapour-liquid state, are an accurate real-fluid equation of state and ideal gas thermochemical properties of each molecule constituting the mixture, to calculate the equilibrium constant. To this end, the appeal to a multi-scale theoretical methodology is paramount and its definition represents the objective of the present work. This methodology is applied and validated on the system $N_2O_4 \rightleftharpoons 2NO_2$. Firstly, the equations solved for simultaneous two-phase and reaction equilibrium are presented. Secondly, ideal gas thermochemical properties of N_2O_4 and NO_2 are computed at atomic scale by quantum mechanics simulations. Then, to apply the selected cubic equation of state, pure-component properties of the species forming the reactive mixture (critical point coordinates and acentric factor) are required as input. However, these properties are not measurable, since NO_2 and N_2O_4 do not exist in nature as pure component. To get around this difficulty, the methodology relies on molecular Monte Carlo simulations of the pure N_2O_4 and NO_2, as well as on the reactive $N_2O_4 \rightleftharpoons 2NO_2$, enabling the determination of those missing pure-component properties and thus the calculation, on a macroscopic scale, of the reactive mixture properties. Finally, the comparison of calculated mixture properties with available experimental data leads to validate the accuracy of the proposed methodology.

Keywords: Reactive mixtures, vapour-liquid equilibrium, Monte Carlo simulations, Quantum Mechanics simulations, equations of state.

4.1. Introduction

There exist few reversible chemical reactions which evolve *very rapidly* towards chemical equilibrium, whether subjected to a modification of their intensive properties, such as temperature and pressure. According to the specific use of such fluids, the high reaction rate can be approximated as being infinite and thus the chemical equilibrium state considered as being instantaneously attained.

One of those few systems is formed by the molecules N_2O_4 and NO_2, whose proportion is dictated by the chemical equilibrium achieved by the reversible reaction $N_2O_4 \rightleftharpoons 2\ NO_2$, at the temperature and pressure of the system. At present, the NO_2/N_2O_4 gas mixture is used as a powerful hypergolic oxidizer of fuels like hydrazine, N_2H_4, in space and military rockets [122,16,97]. Between the years 1950 and 1990, the possible exploitation of the chemical properties of such a reactive fluid has also been explored in power plants, proposing it as a working fluid of thermodynamic cycles [16,97,123,124,91,125–127,89,128,94,129]. Indeed, the spontaneous, fast and reversible evolution of the chemical reaction when the fluid undergoes a modification of its temperature and pressure, while crossing the unit operations (turbine, heat exchangers, pumps, compressors, etc.), implies the involvement of chemical energy in the thermodynamic transformations, with significant effects on the performance of the thermodynamic cycle and on the sizing of units, such as the turbine [89]. Many studies have been conducted on the effect of using such a working fluid (commonly called "dissociating gas" in the literature) in power cycles, or on the characterisation of its thermochemical and thermophysical properties.

The above-mentioned works have theoretically demonstrated that the thermodynamic efficiency of supercritical (Brayton) and subcritical (Rankine) cycles operating with reactive working fluids, mainly N_2O_4, is larger than the efficiency of cycles operating with specific inert fluids, such as water, ammonia, helium or CO_2. However, the comparison between, for example, the dissociating molecule N_2O_4 and the inert molecule H_2O is not straightforward, as multiple molecular aspects should be considered, not only related to the chemical reaction but also to molecular heterogeneity (N_2O_4/NO_2 vs. H_2O). To enable a fairer comparison between reactive and inert fluids, other more generalised studies have considered fictitious chemical reactions ($A_n \rightleftharpoons (n/m)\ A_m$) and investigated the effect of the reaction stoichiometry (n, m) and thermochemistry (enthalpy and entropy of reaction) on the performance of the Brayton power cycles and heat pumps, with respect to pure fluids (reactants or products) [18,130]. Two main

conclusions were that the use of reactive working fluids may lead to the improvement of +30% in the efficiency of power plants [130] and a more than doubled coefficient of performance of heat pumps based on a gaseous inversed Brayton cycle [18]. The reliability and advantages related to the use of N_2O_4 have been experimentally validated at the Nuclear Power Institute of the Academy of Science, in Byelorussia, in mock-ups of 100 – 1000 kW_{th} [131]. After 1986, with the Chernobyl disaster, Byelorussia stopped activities related to nuclear research and thus those studies on dissociating fluids were discontinued too. Not a single experimental or full-scale power plant operates with N_2O_4, nor with other similarly proposed dissociating gases, such as $Al_2Cl_6 \rightleftharpoons 2\ AlCl_3$ and $Al_2Br_6 \rightleftharpoons 2\ AlBr_3$. A more complete review of past technological studies about reactive fluids and their applications is provided in Lasala et al. [130].

Theoretical studies on the use or characterization of reactive fluids potentially usable to enhance the performance of unit operations or thermodynamic cycles are nowadays again under development. Heat transfer properties of reactive N_2O_4 are investigated by computational fluid dynamics in various heat exchangers [132,133]. One of the main conclusions is that the presence of the N_2O_4/NO_2 chemical reaction in the heat exchange process enhances the heat transfer coefficient by 600% with respect to non-reactive fluids. The problem underlying the limited spreading of using reactive working fluids in thermodynamic cycles is the scarce availability of similarly reversible fast chemical reactions, other than N_2O_4. Taking that into consideration, a research project named REACHER [134,135], funded by the European Research Council, aims to discover novel working fluids, characterise their thermodynamic and kinetic properties, to optimise the thermodynamic cycle architecture and, finally, to validate cycle's performance calculations on an experimental micro-power plant.

The high number of studies performed in the past has made many thermodynamic data available on the reactive N_2O_4/NO_2, $Al_2Cl_6/AlCl_3$ and $Al_2Br_6/AlBr_3$. Most of the measured data are collected in the Thermo Data Engine database (TDE 10.1) [136] and in the Dortmund Data Base (DDB2020) [119]. The thermodynamic modelling of N_2O_4 is more investigated than Al_2Cl_6 and Al_2Br_6. Calculations of thermodynamic properties of N_2O_4 have been performed in different works, with the use of semi-empirical equations of state [137–145] or Monte Carlo simulations [146]. Stai et al. [137] used a modification of the Wohl equation to describe volumetric properties of gaseous N_2O_4, but the specifications for the critical coordinates are not explicitly provided. Seshadri [138] used virial equation of state parametrized over experimental data points and calculated the fugacity coefficients with the model developed by Hougen and

Watson [139]. McCarty et al. [140] performed calculations using the Peng-Robinson equation of state, and optimised the coordinates of the critical point of the molecules forming the reactive mixture over available volumetric experimental data and assigned, as a preliminary assumption, the same acentric factor to NO_2 and to N_2O_4. Also, McCarty [140] optimised the 32 parameters of a modified Benedict-Webb-Rubin equation of state to reproduce experimental P-ρ-T data of the equilibrium mixture, treating it as a pseudo-pure component. With the aim to perform calculations on a power cycle, Binotti et al. [141] and Manzolini et al. [142] also modelled the system as a pseudo-pure component and modelled it with the Peng-Robinson equation of state. Vapor-liquid equilibrium of N_2O_4/NO_2 was calculated by De Souza and Deiters [143], with both a hard sphere attractive model and a semiempirical equation of state optimized over experimental and Monte Carlo data. Then, Belkadi et al. [144] modelled VLE with soft-SAFT equation of state, without considering reactional equilibrium but treating the molecule NO_2 as a self-associating component.

Moreover, Monte Carlo simulations have been performed on similar reactive mixtures being in phase and reaction equilibrium. MC codes including Gibbs and reaction Monte Carlo were introduced by Johnson et al [147], who treated the equilibrium of the reactive $(NO)_2/NO$, and Smith and Triska [148]. The reactive system N_2O_4/NO_2 system has been previously characterised by MC reaction and Gibbs ensembles by Bourasseau et al. [146], who also provided force field parameters optimized over experimental data.

Recently, Lemmon et al. [145] produced a thorough review work on the thermodynamic modelling and experimental characterisation of this system, and also developed a highly accurate multiparameter equation of state being specific to the reactive N_2O_4. This equation of state also accounts for the occurrence of the higher temperature reaction $NO_2 \rightleftharpoons 2NO + O_2$, other than $N_2O_4 \rightleftharpoons 2NO_2$. In this model, authors used the pure-component critical temperature and density they determined for pure N_2O_4 and pure NO_2 by Monte Carlo Gibbs ensemble simulations, using the open source code Cassandra 1.2.5 [149] and force-field parameters from Bourasseau et al. [146]. Moreover, the parameters of the considered Helmholtz-based equation of state have been optimised on the basis of a high number of available experimental data that they reviewed in the same work [145].

As a matter of fact, at the basis of the development of equations of state there are experimental data. However, when designing and characterising the thermodynamics of novel fluids, experimental data are not available because not yet measured or not physically measurable.

More specifically to this work, the design and characterisation of novel reversible chemical reactions to be used as working fluids in thermodynamic cycles, as an alternative to N_2O_4, requires to set up a predictive methodology.

In this context, this paper presents a methodology, that we have implemented to the mentioned scope, and applied to the well-known system $N_2O_4 \rightleftharpoons 2\ NO_2$. It is worth noting that, in the presence of these two molecules, this is the only reaction taking place between 300 K and 410 K. However, between 410 K and 1150 K a second chemical reaction, $2NO_2 \rightleftharpoons 2NO + O_2$, occurs. In the interval of about 410 K – 600 K these two reactions take place simultaneously. In this preliminary work, the second reaction is not considered because we limit our discussion and calculations to a temperature range where this reaction does not occur. In this work, the definition of a thermodynamic model to enable the characterization of these systems is based on the complementary use of quantum chemistry, force field-based Monte Carlo simulations and equations of state. The only semi-empirical inputs to the methodology here presented are the force fields of NO_2 and of N_2O_4, which are taken from Bourasseau et al. [146] and, as mentioned above, are optimised to reproduce experimental data.

The structure of the paper is presented in the following. Section 4.2.1 introduces the singular thermodynamic behaviour of bi-component reversible reactions, such as $N_2O_4 \rightleftharpoons 2NO_2$, being characterized by phase equilibrium features similar to the ones of pure components, such as a unique critical and triple point, and a single vapour-liquid equilibrium (VLE) curve in the pressure-temperature space [150,151]. Sections 4.2.2 and 4.2.3 present, respectively, the set of equations applied to solve for chemical equilibrium in the presence of two coexisting phases and one chemical reaction, and the applied predictive equation of state. Section 4.2.4 introduces the way the ideal gas thermochemical properties (standard enthalpy of formation at 298.15 K, standard molar entropy at 298.15 K, heat capacities) and critical point coordinates of pure NO_2 and of N_2O_4 (required as an input to the equation of state) have been calculated by Quantum Mechanic (QM) simulations and force field-based Monte Carlo simulations. Section **4.2.5** presents the methodology applied to perform force field-based Monte Carlo (MC) simulations on the studied reactive binary systems at VLE conditions, with a focus on the reactive $N_2O_4 \rightleftharpoons 2NO_2$, to characterize their phase equilibrium and volumetric properties of the coexisting vapour and liquid phases. Finally, section 4.3 presents the results obtained from QM and MC, and the final exploitation of those results in the application of equations of state, with

the aim to characterize the full thermodynamics of binary reactive mixtures. Our findings are finally summarized in Section 4.4.

4.2. Methodology

Let us consider a binary system (A-B) undergoing the following general reversible reaction at its chemical equilibrium state:

$$\nu_A (A)_{g/l} \rightleftharpoons \nu_B (B)_{g/l} \tag{29}$$

The implementation of mass, energy and entropy balances in thermodynamic cycles operating with reactive working fluids requires (*i*) the availability of an equation of state for mixtures, (*ii*) algorithms enabling the resolution of chemical equilibrium, considering the presence of chemical reactions and, eventually, of coexisting vapour and liquid phases, (*iii*) ideal-gas standard enthalpy of formation at 298.15 K, ideal-gas standard molar entropy at 298.15 K and ideal-gas molar heat capacity as a function of temperature for each of the components present in the mixture. The latter properties are needed to calculate the equilibrium constant at any temperature, while the ideal gas heat capacities are also used to calculate the enthalpy and/or the entropy of a system containing the reactive fluid with an equation of state.

4.2.1. The number of degrees of freedom of the system

By definition, the number of degrees of freedom of a system, or its variance, is the number of intensive independent variables of its phases which must be fixed, in order to characterize all the intensive variables of the phases of the whole system. It can be demonstrated that the variance, υ, of a mixture composed by c-molecular species, r-chemical reactions and φ-fluid phases, is given by [101]:

$$\upsilon = 2 - \varphi + c - r \tag{30}$$

If we consider binary and reactive systems such as the one considered in this paper, $N_2O_4 \rightleftharpoons 2\ NO_2$, i.e. a system involving only one reaction, it turns out that the variance of the system is equal to:

$$\begin{cases} \upsilon = 2 \text{ if } \varphi = 1 \\ \upsilon = 1 \text{ if } \varphi = 2 \end{cases}, \quad \text{with } c = 2 \text{ and } r = 1 \tag{31}$$

This result coincides with the variance of a system composed by one single molecular species (where $c=1$ and $r=0$). The latter explains why the pressure-temperature relation of this system in vapour liquid equilibrium conditions is qualitatively similar to the vapor pressure of a pure component (Figure 30).

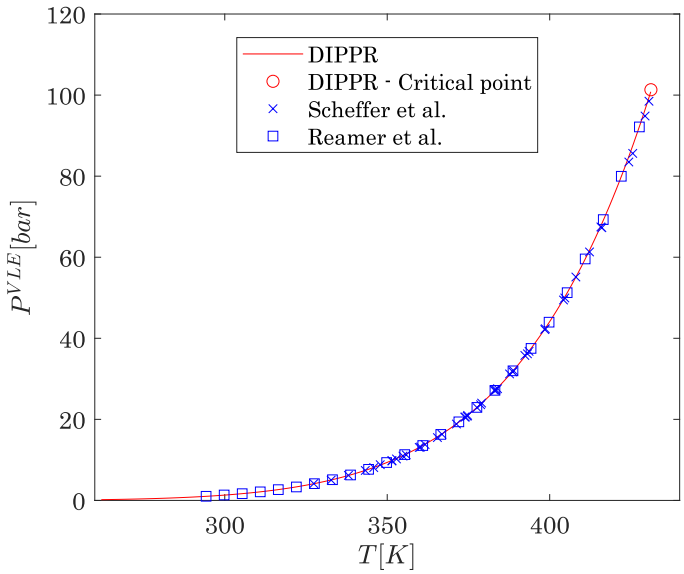

Figure 30. Vapour-liquid equilibrium pressure (P^{VLE}) as a function of temperature (T) for the reacting binary mixture $N_2O_4 \rightleftharpoons 2NO_2$. Blue points are experimental data from Scheffer and Treub [152] and Reamer and Sage [153]; red line and its end critical point (circle) are from DIPPR [154]. As expected, such a curve is very similar to the vaporization curve of a pure component.

4.2.2. Fluid phase and reaction chemical equilibrium

Let us consider the chemical reaction reported in eq. (29). The chemical equilibrium condition states that the Gibbs energy of reaction of the system, $\Delta_R G$, equals zero:

$$\Delta_R G \triangleq \sum_{i=A,B} \nu_i \bar{g}_i = 0 \tag{32}$$

That is,

$$\nu_B \bar{g}_B - \nu_A \bar{g}_A = 0 \tag{33}$$

In which $\bar{g}_i$ is the partial molar Gibbs energy (chemical potential) of species i and vi the algebraic stoichiometric coefficient. If the system is single phase, eq. (33) applies to that phase (liquid or vapour) and eq. (33) becomes:

$$\nu_B \bar{g}_B^{liq} - \nu_A \bar{g}_A^{liq} = 0 \tag{34}$$

Or

$$\nu_B \bar{g}_B^{vap} - \nu_A \bar{g}_A^{vap} = 0 \tag{35}$$

In the case the system is in vapor-liquid equilibrium (VLE), the fluid-phase equilibrium condition between the vapour and the liquid phase dictates that the partial molar Gibbs energy of each species is the same in all phases [101]:

$$\begin{cases} \bar{g}_B^{liq} = \bar{g}_B^{vap} \\ \bar{g}_A^{liq} = \bar{g}_A^{vap} \end{cases} \tag{36}$$

As a consequence, equations (34) and (35) are simultaneously satisfied which demonstrates that the chemical reaction takes place in the two phases, simultaneously; indeed, it results:

$$\Delta_R G^{liq} = \Delta_R G^{vap} = 0 \tag{37}$$

In other words, for a two-phase system, the condition $\Delta_R G^{vap} = 0$ is sufficient to impose that $\Delta_R G^{liq} = 0$, and vice-versa.

The expression of the Gibbs energy of reaction, $\Delta_R G$, is recalled in the Supplementary Materials of this paper [108] (section S1) as a function of:

- ideal gas properties (ideal gas standard molar enthalpy of formation at 298.15 K, ideal gas standard molar entropy at 298.15 K, and ideal gas isobaric heat capacity of each species of the mixture) obtained at the atomic level using ab-initio calculations

and

- real fluid properties (the fugacity of each species) determined by an equation of state.

<u>The resolution of simultaneous reaction and fluid phase equilibria</u>

The system of equations that needs to be solved to determine the chemical equilibrium of the binary reactive system in VLE can be written as follows:

$$\begin{cases} \bar{g}_A^{liq} = \bar{g}_A^{vap} \\ \bar{g}_B^{liq} = \bar{g}_B^{vap} \\ \Delta_R G = 0 \ i.e. \ K - \mathscr{P} = 0 \end{cases} \tag{38}$$

where, $\mathscr{P} \triangleq \prod_{i=A,B} \left(\frac{\hat{f}_i}{P^\circ} \right)^{\nu_i}$, $\hat{f}_i$ is the fugacity of component *i*, P° is the standard pressure, $P^\circ = 1 \, bar$, and *K* is the reaction equilibrium constant, related as follows to the standard Gibbs energy of reaction, $\Delta_R G^\circ$,

$$\ln K(T) \triangleq -\frac{\Delta_R G^\circ(T)}{RT} \tag{39}$$

In our case, the previous system of equations will be solved by an equation of state so that the uniformity of the chemical potential equation ($\bar{g}_i^{liq} = \bar{g}_i^{vap}$) is simply replaced by the isofugacity equation ($\hat{f}_i^{liq} = \hat{f}_i^{vap}$). However, in doing so, 2 new variables appear: the molar volumes of the liquid (v^{liq}) and vapor (v^{vap}) phases since the fugacity $\hat{f}_i$, derived from an equation of state, depends on temperature, composition and molar volume. It is therefore necessary to add 2 mathematical equations to reflect the fact that the variables T, P, v and composition are linked in each phase by the equation of state (EoS). Finally, we get:

$$\begin{cases} \hat{f}_A^{liq}(T, v^{liq}, \boldsymbol{x}) = \hat{f}_A^{vap}(T, v^{vap}, \boldsymbol{y}) \\ \hat{f}_B^{liq}(T, v^{liq}, \boldsymbol{x}) = \hat{f}_B^{vap}(T, v^{vap}, \boldsymbol{y}) \\ K(T) - \mathscr{P}(T, v, \boldsymbol{z}) = 0 \\ P - P_{EoS}(T, v^{liq}, \boldsymbol{x}) = 0 \\ P - P_{EoS}(T, v^{vap}, \boldsymbol{y}) = 0 \end{cases} \tag{40}$$

In eq. (40), $\mathscr{P}(T, v, \boldsymbol{z})$ can be calculated for either the liquid or gas phase since $\mathscr{P}(T, v^{liq}, \boldsymbol{x}) = \mathscr{P}(T, v^{vap}, \boldsymbol{y})$. $\boldsymbol{x}$ and $\boldsymbol{y}$ denote the composition of the liquid $\boldsymbol{x} = \{x_A, x_B = 1 - x_A\}$ and vapor phase $\boldsymbol{y} = \{y_A, y_B = 1 - y_A\}$ respectively. $P_{EoS}(T, v, \boldsymbol{z})$ is the pressure of the system, calculated as a function of temperature, *T*, molar volume, *v* and molar composition, ***z***, either of the liquid (***z***=***x***) or of the vapour phase (***z***=***y***) with a specifically selected EoS. The EoS model applied in this work is presented in the next section. To conclude this section, we recall that the reactive system in VLE is monovariant. It is therefore necessary to specify an intensive variable

before solving the system of equations. As an example, if the temperature is specified, the 5 equations make it possible to calculate P, v^{liq}, v^{vap}, x_A and y_A.

4.2.3. The proposed predictive equation of state

The cubic Peng-Robinson equation of state [155], given by eq. (41), is used in this work, to estimate the fugacities of each component:

$$P(T,v,z)=\frac{R\cdot T}{v-b_m}-\frac{a_m}{v\left(v+b_m\right)+b_m\left(v-b_m\right)} \tag{41}$$

Where $\boldsymbol{z}$ is the vector of the molar composition, T is the temperature, R is the universal gas constant and a_m and b_m are the mixing energy and co-volume parameters. The latter are calculated in this work with advanced mixing rules [156]:

$$\begin{cases} b_m=\sum_{i=1}^{NC} z_i b_i \\ \dfrac{a_m}{b_m}=\sum_{i=1}^{NC} z_i \dfrac{a_i}{b_i}+\dfrac{a_{res}^{E,\gamma}}{\Lambda_{EoS}} \end{cases} \tag{42}$$

where, $a_{res}^{E,\gamma}$ is the residual part of an excess Helmholtz energy model calculated from an activity coefficient (γ) model, Λ_{EoS} is a numerical parameter being a function of the considered equation of state [156], the pure component energy and co-volume parameters, i.e. a_i and b_i, respectively, are calculated using eq. (43).

$$\begin{cases} R=8.314472\ J\cdot mol^{-1}\cdot K^{-1} \\ X=\left[1+\sqrt[3]{4-2\sqrt{2}}+\sqrt[3]{4+2\sqrt{2}}\right]^{-1}\approx 0.253076587 \\ b_i=\Omega_b\dfrac{RT_{c,i}}{P_{c,i}}\ \text{with: } \Omega_b=\dfrac{X}{X+3}\approx 0.0777960739 \\ a_i(T)=a_{c,i}\alpha_i(T)\ with \begin{cases} a_{c,i}=\Omega_a\dfrac{R^2T_{c,i}^2}{P_{c,i}}\ \text{and } \Omega_a=\dfrac{8\left(5X+1\right)}{49-37X}\approx 0.457235529 \\ \alpha_i(T)=\left[1+m_i\left(1-\sqrt{\dfrac{T}{T_{c,i}}}\right)\right]^2 \end{cases} \\ \text{if } \omega_i\le 0.491 \text{ then } m_i=0.37464+1.54226\omega_i-0.26992\omega_i^2 \\ \text{if } \omega_i>0.491 \text{ then } m_i=0.379642+1.48503\omega_i-0.164423\omega_i^2+0.016666\omega_i^3 \end{cases} \tag{43}$$

More precisely, a zero-residual excess Helmholtz energy part, $a_{res}^{E,\gamma}$, is considered for this work. In other words, the NO_2/N_2O_4 binary system is assumed to be athermal because the intermolecular forces between non-polar N_2O_4 molecules are weak, as well as between N_2O_4 and NO_2. Clearly, the interaction between NO_2 radicals is strong at low temperature and gives rise to the association reaction, which is indeed accounted for as being a chemical reaction in the system. The use of a zero residual excess Helmholtz energy leads to a model free of semi-empirical binary interaction parameters to be adjusted (otherwise present in the residual excess Helmholtz energy model) and will thus work in a predictive way.

4.2.4. *The determination of thermochemical and thermophysical properties of pure fluids (N_2O_4 and NO_2)*

It is worth recalling that while the use of an equation of state is sufficient to perform VLE calculations, the ideal gas heat capacity, $c_{p,i}^{ig}(T)$, of each species is needed for the determination of derived thermodynamic properties, such as the enthalpy or the entropy of a given phase [157]. Moreover, as recalled in eq. (S7) of the Supplementary Materials of this paper [108], the calculation of the ideal-gas standard enthalpy and entropy of reaction requires the knowledge – for each species – of the standard enthalpy of formation, $\Delta_f H_{i,298.15K}^{\circ}$ at 298.15 K, the molar entropy, $S_{i,298.15K}^{\circ}$, at 298.15 K and the heat capacity as a function of temperature.

The temperature-dependent ideal gas heat capacity, the standard enthalpy of formation and the standard molar entropy of the pure components can be obtained by QM calculations, as explained in this paragraph, where the case of $N_2O_4 \rightleftharpoons 2NO_2$ is considered as an example.

Also, as shown in the previous section 4.2.3, the application of the Peng-Robinson equation of state (eqs. (41)-(43)) requires the knowledge of the temperature and pressure of the critical point of the two species forming the mixture, $T_{c,i}$ and $P_{c,i}$, and their acentric factors, ω_i. Since the species forming any fast and reversible chemical reaction, i.e. N_2O_4 and NO_2 in the $N_2O_4 \rightleftharpoons 2NO_2$ system, do not exist in their pure form, the experimental measurement of such properties is physically not feasible. To overcome this problem, force field-based Monte Carlo simulations have been performed in this work, with two available MC software (Brick-Continuous-Fractional-Component-Monte-Carlo (CFCMC) [107] and Monte Carlo GIBBS [158]) to determine *P-ρ-T* properties of the pure NO_2 and N_2O_4 and, thus, to deduce their critical point

properties and acentric factors. This is explained in the sections below devoted to Monte Carlo simulations.

Quantum mechanics simulations

The thermochemical properties of NO_2 and N_2O_4, i.e. the ideal gas standard enthalpy of formation (at 298.15 K), standard molar entropy (at 298.15 K), and heat capacity, have been calculated using software Gaussian 09 (revision B.01) [159] and the GPOP post-processing software suite from Miyoshi [160].

QM calculations were performed at the CBS-QB3 level of theory [161]. A conformational analysis was performed for N_2O_4 at the B3LYP/6-31G(d) level [162], to determine the most stable conformer, that is the conformer corresponding to the lowest electronic energy. The conformational analysis consists in varying the considered dihedral angle by step of 10° and re-optimizing all degrees of freedom except the dihedral angle, at each step. Also, internal modes are treated as harmonic oscillators in Gaussian; the conformational analysis enables to understand the validity of the Gaussian's harmonic oscillator assumption for internal rotation of moieties around simple bonds, such as the N – N bond in the N_2O_4 molecule. In general, if the conformational analysis shows that the highest energy gap between adjacent maximum and minimum energies, represented as an example in Figure 31, is lower than $R \cdot T$ (where R is the universal gas constant), then the harmonic oscillator model is not valid because internal rotation can occur. In such a case, the results have to be corrected accounting for the hindered rotor model [163]. In this work, this treatment is done with GPOP and requires as an input the Gaussian's rotational hindrance potential. The post-processing is also performed with GPOP and enables the estimation of the standard enthalpy of formation and of the standard molar entropy.

To determine the equilibrium constant of the reactive system, and thus perform Monte Carlo simulations for the reactive system as shown in section 4.2.5, it is necessary to calculate the partition function of the isolated molecules. Those can be obtained from available thermochemistry data (JANAF tables) or from quantum mechanical calculations (with Gaussian), from which it is possible to determine the atomisation energy and the rotational and vibrational temperatures used as an input to the calculation of the partition function of the isolated molecules.

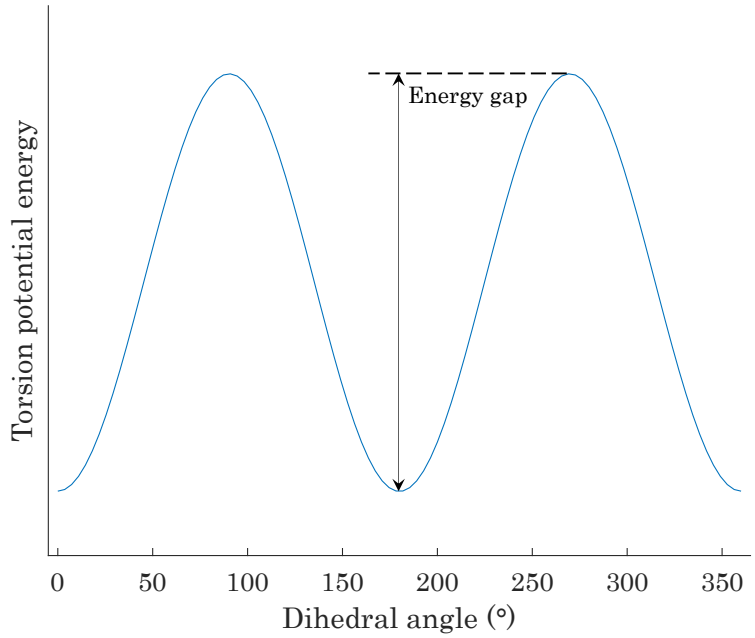

Figure 31. Example of correlated torsion potential energy obtained in Gaussian by varying the dihedral angle of the molecule.

Monte Carlo simulations with Brick-CFCMC software

To perform Monte Carlo simulations of N_2O_4 and NO_2, a classical force field is used in which interatomic interactions are described by both Lennard-Jones (LJ) and electrostatic interactions. NO_2 is treated as a rigid molecule. Concerning the N_2O_4 molecule, this molecule is rigid as well, except when the rotation of NO_2 moieties is considered and the rotational hindrance potential is then required as additional input for the MC simulations. The potential is deduced by optimising the parameters of a cosine series, on the rotation energy scan obtained with Gaussian.

Lennard-Jones interactions are truncated at 12 Å and analytic tail corrections are used [106]. Electrostatics are computed using the Ewald summation technique with a relative precision of 10^{-5}. The force field parameters of NO_2 and N_2O_4 are taken from Bourasseau et al. [146] and are also listed in Table S1 of the Supplementary Materials of this paper [108]. For atoms that are not identical, the Lorentz-Berthelot mixing rules [106,164] are used. The intermolecular coordinates of NO_2 and N_2O_4 are respectively listed in Table S2 and Table S3 of the Supplementary Materials of this paper [108]. Three-dimensional systems with periodic boundary conditions are considered in all simulations.

Pure component Gibbs ensemble simulations using the Continuous Fractional technique [165–167] were performed using the Brick-CFCMC software [107,168]. In the constant volume-constant temperature (NVT) version of the Gibbs ensemble [106,164], there are two simulation boxes that can exchange volume, energy, and molecules, in such a way that the simulation boxes resemble the coexisting phases at equilibrium. Molecule transfers between both simulation boxes are facilitated using a single fractional molecule per component [169]. The interactions of such a fractional molecule are determined by an order parameter λ, with λ=0 when the fractional molecule has no interactions with the surrounding molecules, and λ=1 when the fractional molecule has full, unaltered interactions with the surrounding molecules. Besides thermalization trial moves (molecule translations, molecule rotations, and volume changes), the simulation requires three additional trial moves [169]: (1) attempts to change the value of λ; (2) attempts to transfer a fractional molecule from one simulation box to the other one; (3) attempts to transform the fractional molecule into a whole molecule, and simultaneously, transform a "whole" molecule in the other simulation box into a fractional molecule, at the same value of λ. Biasing using the Wang-Landau algorithm [170] is needed to ensure that the probability distribution of λ is flat in both boxes, and that fractional molecules are equally likely to be in the simulation boxes. The chemical potential of component *i* in simulation box A follows directly from [107,168,171]:

$$\mu_i{}^A = k_B T \left(-\ln\left(\frac{q_i}{\Lambda_i^3 \rho_0} \right) + \ln\left(\frac{\rho_i^A}{\rho_0} \right) - \ln\left(\frac{p(\lambda_i{}^A = 1)}{p(\lambda_i{}^A = 0)} \right) \right) \tag{44}$$

in which kB is the Boltzmann constant, T is the absolute temperature, qi is the intramolecular part of the isolated molecule partition function of molecule type i (excluding the translational part), Λ_i is the thermal wavelength of molecule type *i*, ρ_0 is an arbitrary reference density set to 1 molecule per cubic Angstrom, ρ_i^A is the number density of component i in simulation box A, and p(λ_i^A) is the Boltzmann probability distribution of the value of λ of component *i* in simulation box A. The term q_i/Λ_i^3 can be obtained either from QM simulation or thermochemical tables (e.g. the JANAF tables), see Refs. [107,168,172] for details. At phase equilibrium, chemical potentials of component i are equal in both simulation boxes. As the Brick-CFCMC software does not compute pressures, a series of simulations in the constant temperature-pressure (NPT) ensemble are carried out around the density of the gas phase box. The coexistence pressure is calculated by matching the gas phase density to the NPT

simulations via interpolation. For more details on the simulation technique and the derivation of the accepted probabilities of the trial moves, the reader is referred to Refs. [107,168,169].

Monte Carlo simulations with GIBBS software

In this paper, other Monte Carlo results are presented for N_2O_4 and NO_2. These molecular simulations have been performed using NVT Gibbs ensemble Monte Carlo (MC) [173], with the "GIBBS Monte Carlo" code [158], to determine the saturation densities and pressures of pure N_2O_4 and pure NO_2. In this MC algorithm, the sampling of the configurational space is ensured by three Monte Carlo moves: rigid body translations or rotations of molecules, and volume changes. More specifically, differently with respect to the calculations performed in this work with Brick-CFCMC software, NO_2 and N_2O_4 molecules have been both represented as rigid molecules. Thus, in these simulations, N_2O_4 is not allowed to make torsional rotations, while in Brick the torsional potential is modelled as determined from Quantum Mechanics simulations. However, the force field parameters in these simulations coincide with the ones from Bourasseau et al. [146], like in settings used in Brick. In all simulations performed with GIBBS code, a cutoff for LJ intermolecular interactions equal to the half of the simulation box length has been used to reduce the computing time. Beyond the cutoff, standard long-range corrections have been employed. For more details on the simulation technique or on the molecular models used to determine these latter MC results, the reader is invited to refer to some previous works [57,146,174,175].

The derivation of critical coordinates and acentric factors

The determination of the critical point properties by MC is not straightforward, since the Gibbs ensemble is not applicable in the vicinity of the critical region [106]. To localize the critical point, we have proceeded as described below.

Once *P*-ρ-*T* properties in saturation conditions are calculated by MC, the critical temperature $T_{c,i}$ of the pure compounds, NO_2 and N_2O_4, are obtained by extrapolation from the sub-critical simulation points, assuming the following scaling law:

$$\rho_i^{liq}(T) - \rho_i^{vap}(T) = B_i \left(T_{c,i} - T\right)^{\beta} \tag{45}$$

Where $\rho_i^{liq}(T)$ and $\rho_i^{vap}(T)$ are the densities of component *i* at temperature *T* in the liquid and the vapor phases, respectively, calculated with Monte Carlo simulations, while β is the critical exponent, equal to 0.32 +/- 0.01 [176]. The critical temperature of each i-th component, T_{ci}, and its parameter B_i, also component-dependent, have been regressed by least square method minimizing the following objective function, *O.F.*:

$$O.F.: \min_{T_{c,i},B_i} \left\{ \sqrt{\sum_{k=1}^{NP} \left(\rho_k^{liq,MC}(T_k) - \rho_k^{vap,MC}(T_k) - B_i \left(T_{c,i} - T_k \right)^{\beta} \right)^2} \right\} \tag{46}$$

Where *NP* is the number of data points. The critical density, $\rho_{c,i}$, is then calculated with the application of the law of rectilinear diameter,

$$\frac{\rho^{liq}(T) + \rho^{vap}(T)}{2} = \rho_{c,i} - A_i \left(T_{c,i} - T \right) \tag{47}$$

and the least square optimization,

$$O.F.: \min_{\rho_{c,i},A_i} \left\{ \sqrt{\sum_{k=1}^{NP} \left(\frac{\rho_k^{liq,MC}(T_k) + \rho_k^{vap,MC}(T_k)}{2} - \rho_{c,i} + A_i \left(T_{c,i} - T_k \right) \right)^2} \right\} \tag{48}$$

Moreover, from the calculated P-T saturation points of the two pure fluids, a correlation $P_i^{sat}(T)$ is determined

$$\ln P_i^{sat}(T) = \alpha_i + \frac{\beta_i}{T} \tag{49}$$

where, parameters α_i and β_i are determined by minimizing:

$$O.F.: \min_{\alpha_i,\beta_i} \left\{ \sqrt{\sum_{k=1}^{NP} \left(\exp\left(\alpha_i + \frac{\beta_i}{T_k} \right) - P_i^{sat}(T_k) \right)^2} \right\} \tag{50}$$

and $P_{c,i}$ can be finally calculated from the optimized correlations, as a function of $T_{c,i}$.

Once $T_{c,i}$ and $P_{c,i}$ are obtained, the acentric factor ω_i is calculated from its definition:

$$\omega_i = -log_{10} P_{r,i}^{sat} - 1 \quad (51)$$

where $P_{r,i}^{sat}$ is the reduced vapor pressure ($P_i^{sat} / P_{c,i}$) at a reduced temperature ($T/T_{c,i}$) equal to 0.7.

4.2.5. The determination of thermodynamic properties of $N_2O_4 \rightleftharpoons 2\ NO_2$

To study the VLE phase coexistence of the reactive system $N_2O_4 \rightleftharpoons 2\ NO_2$, Monte Carlo simulations in the reactive Gibbs Ensemble [147,148,171,177,178] are performed with Brick-CFCMC [107]. In these simulations, the constant-volume Gibbs Ensemble setup previously introduced (paragraph "Monte Carlo simulations with Brick-CFCMC software" in section 4.2.4) is coupled to a grand-canonical reservoir of molecules of NO_2 and N_2O_4. The imposed chemical potentials of NO_2 and N_2O_4 are set such that the system is at chemical equilibrium so $\mu_{N_2O_4} = 2 \cdot \mu_{NO_2}$ and the exchanges from the reservoir are such that the total number of atoms of each type in the system is conserved. A fractional group is added to the vapor box of the Gibbs Ensemble, which contains fractional molecules of either the reactants or the reaction products [171]. Note that this group of fractional molecules is completely independent from the fractional molecules required for molecule transfers between the simulation boxes (as used in the CFCMC version of the Gibbs Ensemble described in section 4.2.4). In addition to the trial moves of the CFCMC version of the Gibbs Ensemble (section 4.2.4), the following trial moves (which all operate in the vapor box) are used for the molecules in the fractional group: (1) attempts to change the order parameter λ_R for the molecules in the fractional group. $\lambda_R = 0$ means that the molecules in the fractional group have no interaction with the surrounding molecules, and $\lambda_R = 1$ means that the molecules in the fractional group have full, unaltered interactions with the surrounding molecules; (2) attempts to transform the molecules in the fractional group from reactants into reaction products, or vice-versa. This requires the terms q_i / Λ_i^3 for NO_2 and N_2O_4; (3) attempts to transform the fractional molecules in the group into "whole" molecules, and simultaneously, transform "whole" molecules into a fractional group, in such a way that the fractional group changes from reactants to reaction products (or vice versa). In this trial move, the value of λ_R is unchanged. Biasing is needed to ensure that it is equally likely that the fraction group contains a single fractional molecule of N_2O_4, or two fractional molecules of NO_2, and that each value of λ_R is equally likely. At combined chemical equilibrium and phase equilibrium, we have $\mu_{N_2O_4} = 2 \cdot \mu_{NO_2}$ for both simulation boxes A and

B, and $\mu_i^A = \mu_i^B$ for both NO_2 and N_2O_4. The coexistence pressure is obtained by performing a series of NPT simulations at the average composition of the gas phase box, and use interpolation to match the simulated gas phase density from the Gibbs ensemble simulation in the reaction ensemble. For more details about the simulation setup and the derivation of the acceptance rules, the reader is referred to Refs. [107,171]. The isolated molecule partition function for both NO_2 and N_2O_4 were obtained in this work both from QM simulations, by using Gaussians outputs reported in Table S4 of the Supplementary Materials of this paper [108], and the thermochemical results reported in JANAF tables [107]. The calculated partition functions are shown in Figure 32, where V_0 = 1 Å^3. Two correlations that correlate the JANAF values are proposed below,

$$\ln\left(\frac{qV_0}{\Lambda^3}\right)_{NO_2} = \frac{110983.613}{T} + 16.403 \tag{52}$$

$$\ln\left(\frac{qV_0}{\Lambda^3}\right)_{N_2O_4} = \frac{228591.177}{T} + 23.218 \tag{53}$$

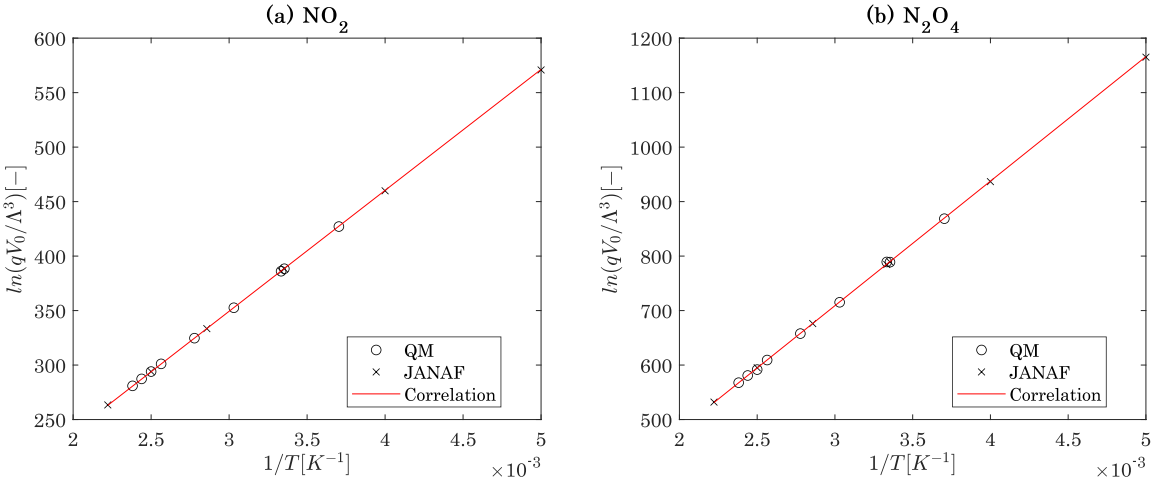

Figure 32. Natural logarithm of the partition functions, q, divided by the thermal wavelength, for NO_2 (fig. (a)) and N_2O_4 (b). Data obtained from the JANAF tables. Correlations are eqs. (52) *and* (53)*.*

4.3. Results

This section presents the results obtained from molecular simulations, as well as the calculations performed with the cubic equation of state and enabled by the calculated equation of state's input critical temperature, pressure and acentric factor of the pure fluids NO_2 and N_2O_4.

4.3.1. Thermochemical and thermophysical properties of N_2O_4 and NO_2

Quantum Mechanics results

Figure 33 shows the geometries of NO_2 and N_2O_4, optimised with Gaussian as discussed in section 4.2.4. It is worth noting that the length of N=O bonds and the N=O=N angles are very similar in both NO_2 and N_2O_4, which indicates that very limited rearrangements occur in moieties when N_2O_4 splits into two NO_2 moieties. The main specificity of N2O4 is the length of the N-N bond which is particularly long for such a bond: 1.797 Å compared to 1.487 Å for the N-N bond in hydrazine (value obtained at the CBS-QB3 level of theory with software Gaussian) and which can be attributed to an inductive effect of the vicinal oxygen atoms. This has consequently an impact on the energy of that particular bond as discussed further. Figure 34 shows the result of the conformational analysis that was performed to verify that the optimized geometry obtained for N_2O_4 corresponds well to the conformer with the lowest energy. The optimal coefficients for the torsion potential N_2O_4 are shown in Table S5 of the Supplementary Materials of this paper [108]. As expected, two distinct stable conformations exist for N_2O_4: a planar one with the lowest energy, and a skew one with an energy ca. 30 kJ/mol higher than that one the planar conformer. As it will be confirmed by MC simulation results considering the torsion of N_2O_4, the calculated potential barrier shows that the actually observed conformations are plane or almost plane. Some studies [179] focused on the origin of the greater stability of the planar conformer, but this is beyond the scope of the present work.

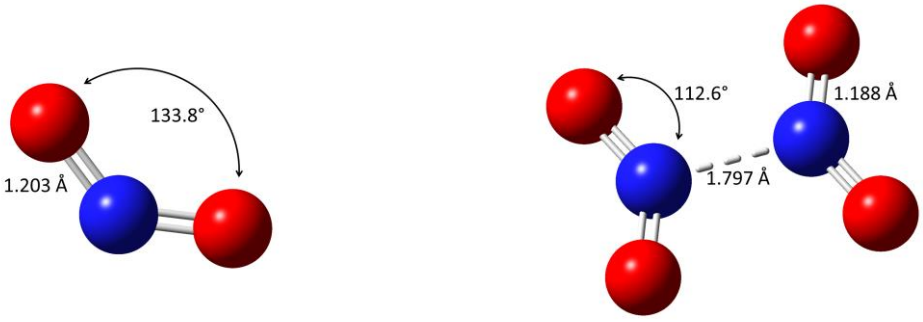

Figure 33. Optimal geometry of NO_2 and N_2O_4. Atomic coordinates are reported in Table S2 and S3 the Supporting Information.

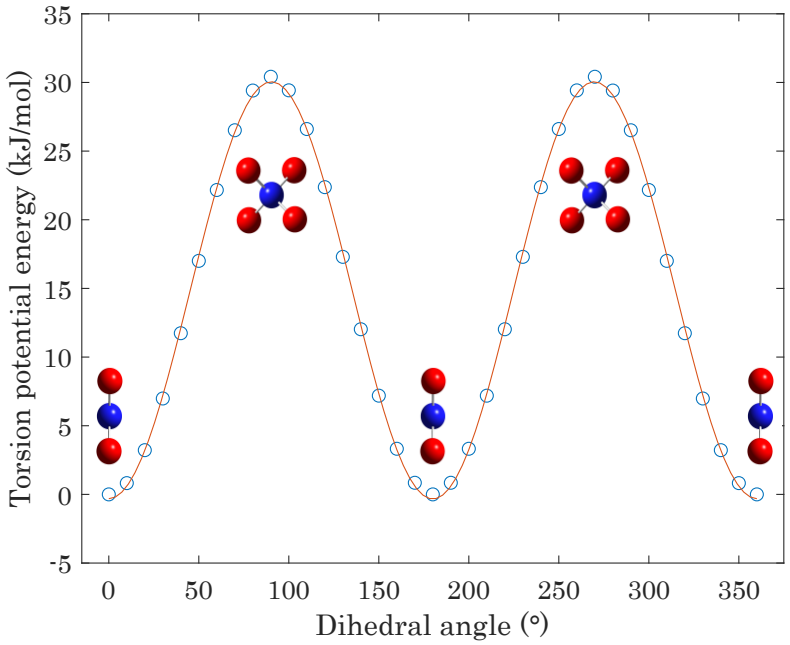

Figure 34. Conformational analysis of N_2O_4. The points in the figure represent Gaussian results, while the line is the cosine series fitted to the QM results.

As enthalpies provided by the Gaussian software are relative to a reference that is specific to the method used, they need to be rescaled. For NO_2, we considered in the present work the fictive reaction $2\ NO_2 + N_2 \rightleftharpoons 4\ NO$ leading to $\Delta_f H^{\circ}_{i,298.15K}$ equal to 34.20 kJ/mol, which compares well to the data available in the NIST database [180] (33.1 kJ/mol). For N_2O_4, the fictive reaction considered was $N_2O_4 \rightleftharpoons 2\ NO_2$ leading to $\Delta_f H^{\circ}_{i,298.15}$ equal to 9.99 kJ/mol, to be compared with the value of 9.08 kJ/mol provided in the NIST database. This leads to an enthalpy of reaction of 56.2 kJ/mol for the reaction of dissociation of N2O4 into two NO2 moieties (57.12 kJ/mol using the NIST data), confirming that the value of the N-N bond is unusually low and in line with the bond length of 1.797 Å.

For the ideal-gas standard molar entropy, $S^{\circ}_{i,298.15K}$, assuming an external symmetry number of 2 for NO_2, the value derived with postprocessing Gaussian results with GPOP, as briefly described in section 4.2.4, is 240.03 J/mol/K which compares very well to the data in the NIST database (240.04 J/mol/K). For N_2O_4, assuming an external symmetry number of 4, the calculated standard entropy is 297.65 J/mol/K, which is a bit lower than the data provided in the NIST database (304.38 J/mol/K) but still within the acceptable range. At such a low temperature, the difference in entropy for the $-NO_2$ rotor is only 0.54 J/mol/K between the harmonic oscillator approximation and the hindered rotor one, as a consequence of the fact that

the highest energy gap between adjacent maximum and minimum energy (i.e., the torsional barrier) is higher than $R \cdot T = 2.47$ kJ/mol at 298.15 K and thus the harmonic oscillator assumption is still valid (see section 4.2.4). The results obtained are summarised in Table 4.

Another result obtained from the postprocessing step is the ideal gas isobaric specific heat capacity, which has been correlated to the DIPPR correlation n. 107:

$$c_{P,i}^{ig}(T) = c_0 + c_1\left(\frac{c_2/T}{\sinh(c_2/T)}\right)^2 + c_3\left(\frac{c_4/T}{\cosh(c_4/T)}\right)^2 \quad (54)$$

The coefficients optimised in this work for NO_2 and N_2O_4 are reported in Table 5 and shown in Fig. S1 and S2 of the Supplementary Materials of this paper [108].

Table 4. Ideal gas standard properties at 298.15 K, obtained in this work by Quantum Mechanics.

	NO_2	**N_2O_4**
$\Delta_f H^{\circ}_{i,298.15}$ (kJ/mol)	34.20	9.99
$S^{\circ}_{i,298.15K}$ (J/mol/K)	240.03	297.65

Table 5. Coefficients for the calculation of the isobaric specific heat capacity of NO_2 and N_2O_4 by eq. (54).

	c_0 [J/mol/K]	c_1 [K]	c_2 [K]	c_3 [K]	c_4 [K]
NO_2					
QM, this work	33.631	24.566	1.1684	10.4065	0.6063
DIPPR [154]	33.261	24.919	1.1122	9.2534	0.5592
N_2O_4					
QM, this work	67.574	56.723	0.72373	13.722	2.0934
DIPPR [154]	65.796	58.428	0.69602	11.887	2.0748

Monte Carlo results

The MC simulations performed with Brick-CFCMC enabled the computation of coexisting densities and saturation pressures of the two pure compounds, NO_2 and N_2O_4, at different temperatures. Results are presented in Table 6 as well as in Figure 35 - Figure 38. MC simulations of N_2O_4 have shown that the most probable conformer is the planar one, according to the potential barrier calculated in Figure 34.

More precisely, Figure 35 and Figure 36 show the densities of the liquid and vapour phase of, respectively, NO_2 and N_2O_4, as a function of temperature. A comparison between the results of

the two different sets of simulations show an excellent agreement between the two methods. Main quantitative differences between the results of Brick-CFCMC and GIBBS may derive from slightly different implementation of the Ewald summation, or from a different cutoff and from the additional consideration (in Brick-CFCMC calculations) of torsion potential of N_2O_4. Moreover, these figures show the predicted critical points ($T_{c,i}$, $\rho_{c,i}$) of both NO_2 and N_2O_4, optimized over the two sets of data. It can be observed that despite simulations performed with Brick-CFCMC did not converge close to the critical point, the prediction of the critical point obtained from this set of data is acceptably similar to the one obtained with GIBBS code which better converges close to the critical point. It is highlighted that the uncertainties of MC simulations from Brick-CFCMC are not shown in Figure 35 and Figure 36, for the sake of simplicity, but are reported in Table 6.

Table 6. Results of MC simulations obtained for pure NO_2 and N_2O_4, obtained in this work by the use of Brick-CFCMC. "u" denotes the uncertainty of the calculated variables. These uncertainties correspond to the standard deviation between the results of MC simulations performed at each temperature to calculate saturation densities and pressures.

T [K]	P^{sat} [bar]	$u(P)$ [bar]	ρ_{liq} [kg/m^3]	ρ_{vap} [kg/m^3]	$u(\rho_{liq})$ [kg/m^3]	$u(\rho_{vap})$ [kg/m^3]
			NO_2			
240	25.07	0.45	985.6	74.9	1.3	1.9
245	28.60	0.31	960.9	86.6	1.6	1.5
250	32.82	0.84	935.0	101.4	2.3	4.1
255	37.11	0.52	905.5	116.8	1.9	2.9
260	42.42	1.01	875.4	138.3	3.5	6.2
265	47.39	1.33	838.7	158.6	3.5	8.9
270	52.10	0.92	791.7	177.3	6.2	7.0
			N_2O_4			
260	0.107	0.020	1537.6	0.454	1.9	0.085
270	0.175	0.036	1516.5	0.72	1.3	0.15
280	0.332	0.026	1494.1	1.31	1.1	0.10
290	0.457	0.038	1472.2	1.75	0.7	0.15
300	0.752	0.101	1449.0	2.80	0.5	0.38
310	1.046	0.093	1424.8	3.79	1.1	0.34
320	1.55	0.12	1401.8	5.47	1.1	0.43
330	2.23	0.20	1377.4	7.71	1.0	0.72
340	2.90	0.17	1352.3	9.85	0.3	0.63
350	4.11	0.14	1326.0	13.8	1.0	0.52
360	5.04	0.12	1299.3	16.6	0.7	0.45

370	6.67	0.13	1269.40	21.8	0.73	0.48
380	8.51	0.31	1240.68	27.6	2.40	1.13
390	10.63	0.35	1210.22	34.5	1.50	1.30
400	13.17	0.38	1176.49	42.4	1.66	1.48
410	16.55	0.18	1141.44	52.9	0.99	0.71
420	19.76	0.35	1098.91	63.2	1.39	1.47
430	22.97	0.40	1050.68	73.8	5.37	1.67
440	26.54	0.68	989.79	85.8	6.12	2.89

Table 7. Results of MC simulations obtained for pure NO_2 and N_2O_4, obtained with GIBBS code. "u" denotes the uncertainty of the calculated variables. These uncertainties correspond to the standard deviation between the results of MC simulations performed at each temperature to calculate saturation densities and pressures.

T [K]	P^{sat} [bar]	$u(P)$ [bar]	ρ_{liq} [kg/m^3]	ρ_{vap} [kg/m^3]	$u(\rho_{liq})$ [kg/m^3]	$u(\rho_{vap})$ [kg/m^3]
			NO_2			
220	13.1	0.29	1087.5	38.7	1.02	2.77
230	17.7	0.4	1043.1	51.9	1.49	3.43
240	24.1	0.43	1001.8	71.8	1.83	3.98
250	31.2	0.53	947.9	94.4	2.54	4.86
260	40.3	0.68	889.3	127	3.42	6.13
270	51.0	0.84	819.4	174	4.83	6.84
275	56.5	0.73	765.8	200	5.91	9.41
280	63.8	0.66	708.9	242.7	7.31	18.53
			N_2O_4			
300	0.7	0.04	1462.8	2.7	0.17	5.49
350	4.4	0.11	1346.0	15	0.45	3.7
400	13.6	0.46	1202.2	44.4	1.71	5.11
450	35.9	1.05	1018.8	129.4	6.12	8.57
475	52.8	1.39	848.2	219.8	11.62	30.35

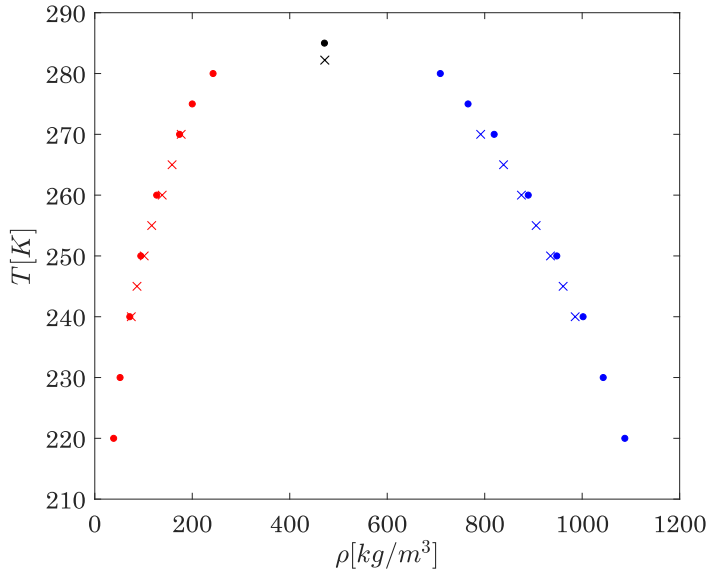

Figure 35. Liquid–vapor coexisting densities of pure NO_2 obtained by MC simulations. Crosses denote the results obtained in this work with Brick-CFCMC as described in section 4.2.4 and reported in Table 6, while points denote the results obtained with GIBBS reported in Table 7. Black symbols represent the critical point predicted as detailed in section 4.2.4, using the two sets of data.

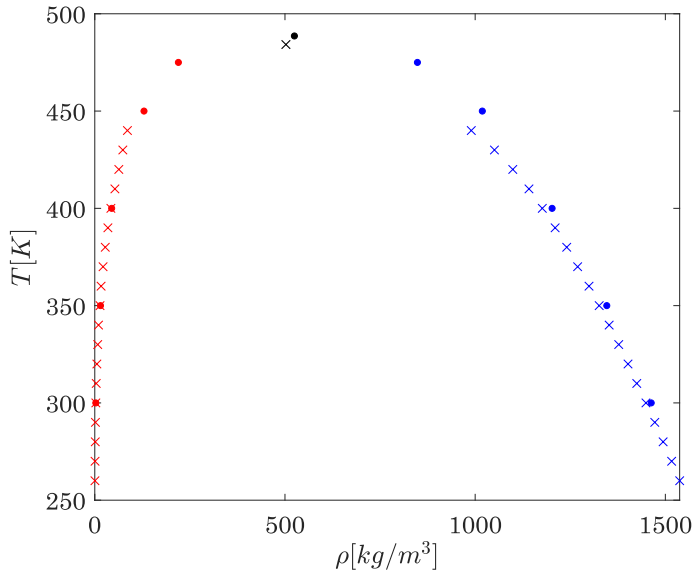

Figure 36. Liquid–vapor coexisting densities of pure N_2O_4 obtained by MC simulations. Crosses denote the results obtained in this work with Brick-CFCMC as reported in Table 6, while points denote the results obtained with GIBBS reported in Table 7. Black symbols represent the critical point predicted in this work using the two sets of data.

The calculated saturation pressures for the pure components are shown in Figure 37 and Figure 38, for NO_2 and N_2O_4 respectively. The correlation in eq. (49) has been optimized for both components, over the experimental data obtained by Brick-CFCMC, and this is also reported

in these figures. Coefficients of the correlations are shown in Table S6 of the Supplementary Materials of this paper [108]. With those correlations, the critical pressure could also be determined (see section 4.2.4), and this is reported in these figures too.

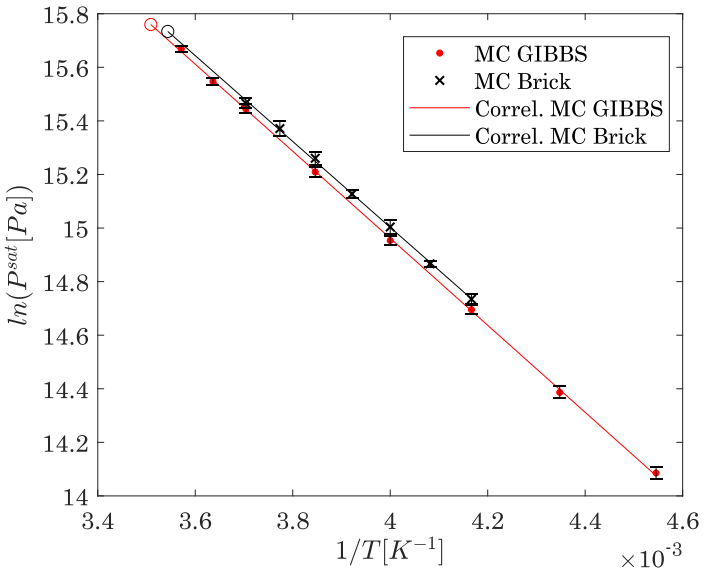

Figure 37. Vapor pressures of pure NO_2 obtained by MC simulations and the resulting correlations. The empty circles represent the critical point predicted as detailed in section 4.2.4, using the set of data obtained in this work.

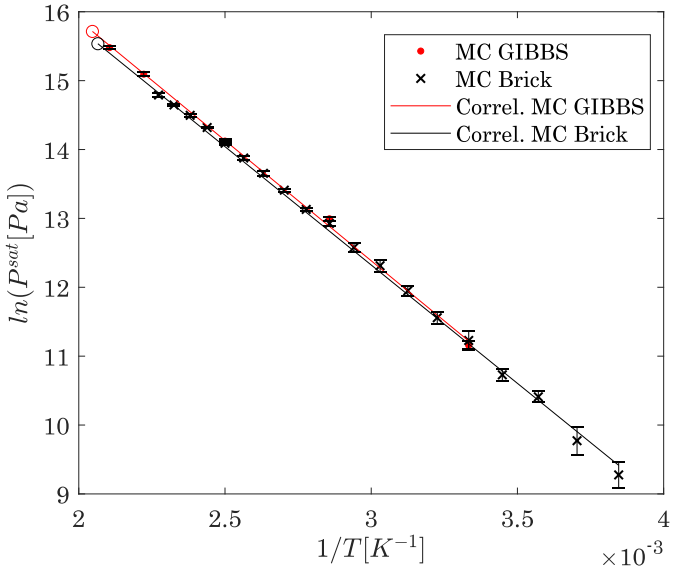

Figure 38. Vapor pressures of pure N_2O_4 obtained by MC simulations and the resulting correlation. The empty circles represent the critical point predicted as detailed in section 4.2.4, using the set of data obtained in this work.

The critical coordinates and acentric factors determined as described in section 4.2.4 are reported in Table 8. It can be observed that the values determined in this work are very different

with respect to the critical coordinates previously obtained by McCarty et al. [140], also reported in Table 8, who made the assumption of equal acentric factor between the two molecules.

Table 8. Critical coordinates and acentric factor of NO_2 and N_2O_4 obtained from the molecular simulation results.

	T_c [K]	ρ_c [kg/m^3]	P_c [bar]	ω [-]
NO_2 / This work, from results of MC Brick-CFCMC	282.2	471.80	68.2	0.0565
N_2O_4 / This work, from results of MC Brick-CFCMC	484.2	502.44	55.9	0.3212
NO_2 / This work, from results of MC GIBBS	285.0	471.20	69.9	0.0611
N_2O_4 / This work, from results of MC GIBBS	488.6	524.79	66.7	0.3306
NO_2 / Results from McCarty et al. [140]	239.3	-	103.3	0.01413
N_2O_4 / Results from McCarty et al. [140]	547.5	-	221.0	0.01413

4.3.2. Thermodynamic properties of $N_2O_4 \rightleftharpoons 2\ NO_2$

Monte Carlo results

The thermodynamic properties of the reactive mixture determined by MC simulations with Brick-CFCMC, as detailed in section 4.2.5, are presented in Table 9 and in Figure 39 - Figure 41. Figure 39 shows that the calculated VLE pressure of the reactive system is in very good agreement with available experimental data and with the correlation provided by DIPPR. The same consideration is valid for the other calculated properties: the composition of the vapour and liquid phase, in Figure 40, which is compatible with the MC results obtained by Bourasseau et al. [146], and the T - ρ_{liq} - ρ_{vap} data points reported in Figure 41, are also in good agreement with the experimental data.

It is worth noting that the P-$\{\boldsymbol{x},\boldsymbol{y}\}$ diagram reported in Figure 40 has two unique features that derive from the mono-variance of this binary reactive system in VLE (see section 4.2.1): (*i*) The diagram is a *unique* and *non-isothermal* P-$\{\boldsymbol{x},\boldsymbol{y}\}$ diagram for this system; indeed, at each specified pressure (between the triple point pressure and the critical pressure of the reactive system) corresponds a different temperature and different mole fractions in each phase. (*ii*) The diagram is not closed at the lowest pressure (the triple point pressure of the reactive fluid), because the condition of pure N_2O_4 ($x,y_{NO2} = 0$) is not compatible with the occurrence of the chemical reaction, whose extent of reaction is non-zero at those pressure levels.

Table 9. Results of MC simulations obtained for reactive $N_2O_4 \rightleftharpoons 2\ NO_2$, obtained in this work by the use of Brick-CFCMC. "u" denotes the uncertainty of the calculated variables. These uncertainties correspond to the standard deviation between the results of MC simulations performed at each temperature to calculate saturation densities and pressures. Molar fraction uncertainties are determined from the calculated standard deviations of molecules number in the simulation boxes resulting from each simulation, by applying the propagation error law.

T [K]	P^{sat} [bar]	$u(P)$ [bar]	ρ_{liq} [kg/m^3]	ρ_{vap} [kg/m^3]	$u(\rho_{liq})$ [kg/m^3]	$u(\rho_{vap})$ [kg/m^3]	x_{NO_2} [-]	y_{NO_2} [-]	$u(x)$ [-]	$u(y)$ [-]
260	0.124	0.033	1537.59	0.47	1.01	0.13	0.000025	0.023	0.000037	0.012
270	0.230	0.041	1515.67	0.85	0.82	0.16	0.000088	0.045	0.000069	0.013
280	0.42	0.10	1493.65	1.43	0.68	0.35	0.00030	0.115	0.00012	0.014
290	0.65	0.10	1471.78	2.11	0.57	0.36	0.00082	0.205	0.00021	0.017
300	1.21	0.17	1448.61	3.77	1.07	0.59	0.00192	0.275	0.00024	0.018
310	1.76	0.10	1424.68	5.19	1.20	0.33	0.00358	0.3483	0.00010	0.0082
320	2.82	0.18	1400.51	7.92	1.06	0.59	0.00557	0.385	0.00018	0.013
330	4.12	0.16	1375.94	11.15	0.77	0.50	0.00820	0.4066	0.00036	0.0067
340	6.06	0.31	1348.55	15.52	0.99	0.96	0.01312	0.4577	0.00045	0.0093
350	8.75	0.33	1320.12	21.71	1.03	1.00	0.01960	0.4875	0.00070	0.0074
360	12.45	0.38	1290.56	30.23	1.14	1.15	0.02793	0.5060	0.00077	0.0032
370	17.81	0.45	1257.53	42.41	1.70	1.44	0.04080	0.5309	0.00170	0.0057
380	24.10	0.70	1219.54	56.36	1.00	2.27	0.05746	0.5573	0.00085	0.0076
390	32.63	0.55	1178.09	76.73	1.90	2.07	0.0784	0.5636	0.0014	0.0046
395	37.95	1.01	1152.09	89.27	2.20	3.68	0.0952	0.5768	0.0025	0.0080
400	44.34	0.24	1128.36	104.85	2.03	0.87	0.1096	0.5834	0.0014	0.0011
405	50.45	1.39	1096.56	121.37	3.27	6.79	0.1295	0.586	0.0038	0.012
410	58.34	1.26	1062.98	141.98	5.36	5.79	0.1511	0.5861	0.0051	0.0085
415	67.35	1.77	1029.43	170.26	3.90	9.75	0.1718	0.580	0.0030	0.012

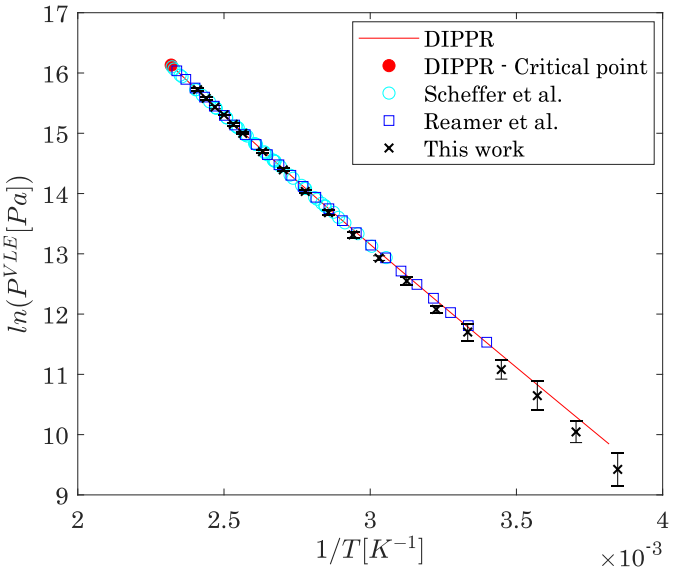

Figure 39. VLE pressures of the coexisting vapour and liquid phases of the reactive mixture containing N_2O_4 and NO_2. Crosses are points calculated by MC with Brick-CFCMC. Data of Scheffer and Treub [152] and Reamer and Sage [153] are also shown for comparison.

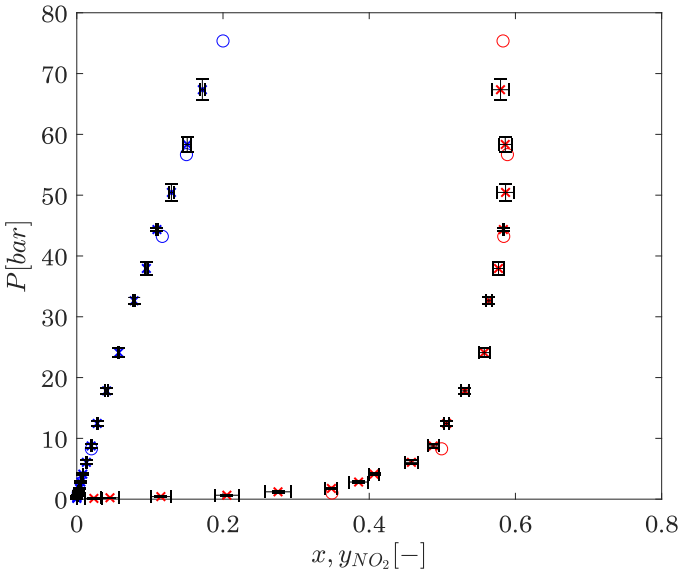

*Figure 40. P-{**x**,**y**} diagram of the reactive mixture containing N_2O_4 and NO_2. Crosses are the points determined with Brick-CFCMC, with the relative uncertainties; circles are points from MC simulations published in Bourasseau et al. [146].*

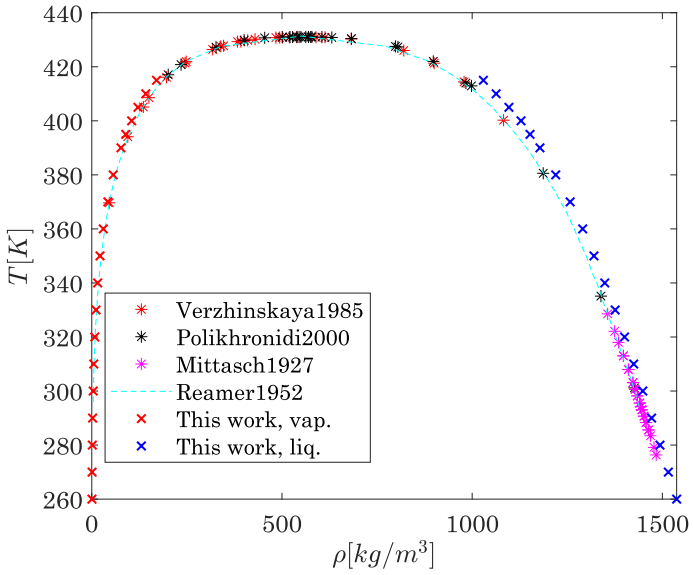

Figure 41. Vapour and liquid densities of the coexisting phases of the reactive mixture containing N_2O_4 and NO_2, as a function of temperature. Crosses represent results from Brick-CFCMC while the other are experimental data from the literature [153,181–185].

Thermodynamic calculations

The determination of the ideal gas standard enthalpy of formation (at 298.15 K), standard molar entropy (at 298.15 K) and isobaric heat capacity (as a function of temperature) of NO_2 and of N_2O_4, by quantum mechanics, as well as their critical point coordinates and acentric factors by force-field based Monte Carlo simulations allows the further application of a predictive thermodynamic model to fully characterize the properties of this system: the equation of state presented in section 4.2.3.

The first computed results are shown in Figure 42, where the global phase equilibrium diagram (GPED) [186] is represented for this system, and is calculated with two sets of critical coordinates: the solid lines represent the results of the equation of state with the critical coordinates obtained from MC simulations of Brick-CFCMC (see Table 8), also called in the following "EoS 1", while the dashed lines are results of calculations performed with the critical coordinates obtained from MC data obtained from GIBBS, also called in the following "EoS 2". Moreover, the GPED shows:

- the vaporisation curves of the pure NO_2, ending at their critical point (represented by the circle mark) – pink lines;
- the vaporisation curves of the pure N_2O_4, ending at their critical point – black lines;

- the locus of critical points of the binary non-reactive mixture formed by N_2O_4 and NO_2 – green lines;
- the VLE pressure of the reactive binary mixture, which is a line instead of a surface because of the mono-variance of this system (see section 4.2.1), ending at their critical point – blue lines; moreover, the red line and the light blue points on it represent, respectively, the DIPPR correlation and the experimental VLE pressures for the reactive system already shown in Figure 30. Black crosses are the MC results obtained with Brick-CFCMC (see Table 9 and Figure 39).
- the triple temperature of the system – the light blue dashed line.

Considering the fact that not a single mixture parameter has been optimised in the used equation of state for this work and that the model works in purely predictive form, the saturation pressure of the reactive mixture is appropriately represented.

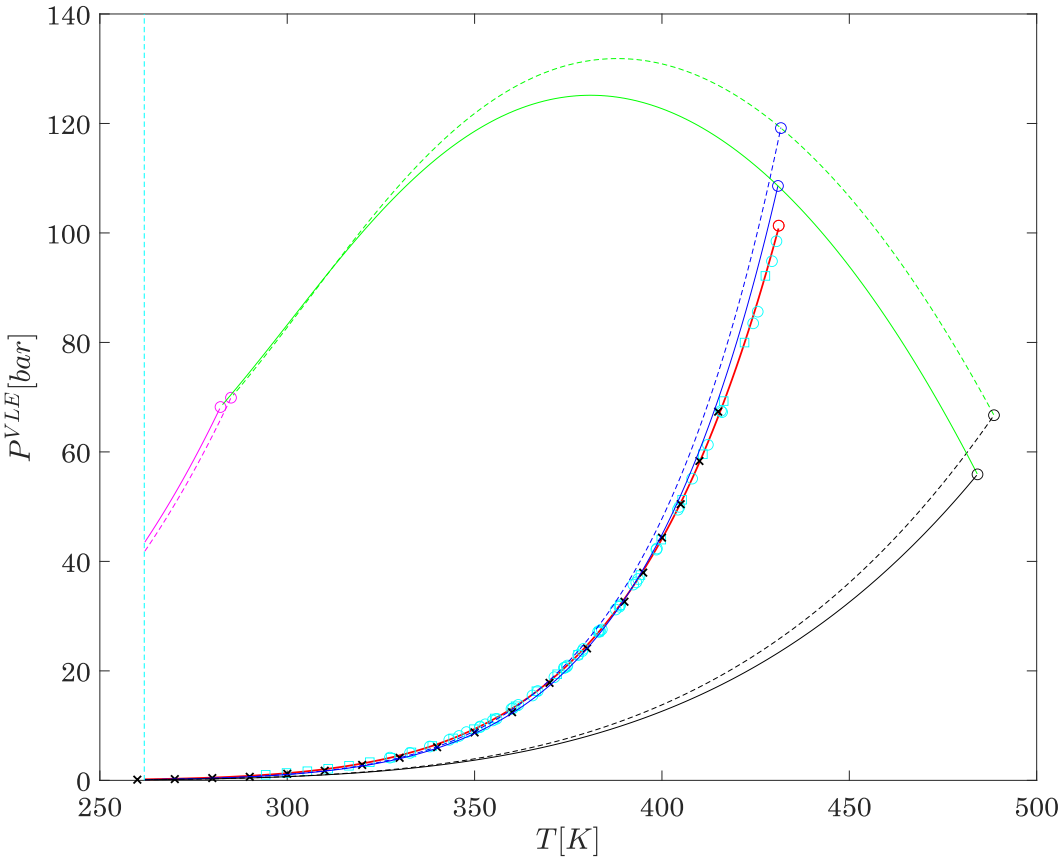

Figure 42. Global phase equilibrium diagram of the reactive mixture. The legend of this plot is detailed in the main text.

Furthermore, although the quantitative representation of the Monte Carlo results on the P-{$\boldsymbol{x}$,$\boldsymbol{y}$} diagram in Figure 43 is not well reproduced by the equation of state, the qualitative assessment of the phase behaviour of this system by the use of such a non-optimised equation of state is highly satisfactory. The modelling of vapour and liquid-phase densities is also acceptable, considering that the representation of the liquid phase density by cubic equations of state -without a translation term [187,188]- is known to be inaccurate.

To conclude, the comparison of the results obtained by the two sets of critical coordinates and acentric factors leads to the observation that the impact of their accuracy on the P-ρ-T-{$\boldsymbol{x}$,$\boldsymbol{y}$} is non-negligible and that their further optimisation over both pure component and mixture data is suggested. However, it is possible to observe that the impact on derived properties such as entropy (Figure 45) and enthalpy (Figure 46) is lower and that the energy and entropy balances will probably be less affected by the uncertainty on the critical coordinates of the pure components forming the mixture.

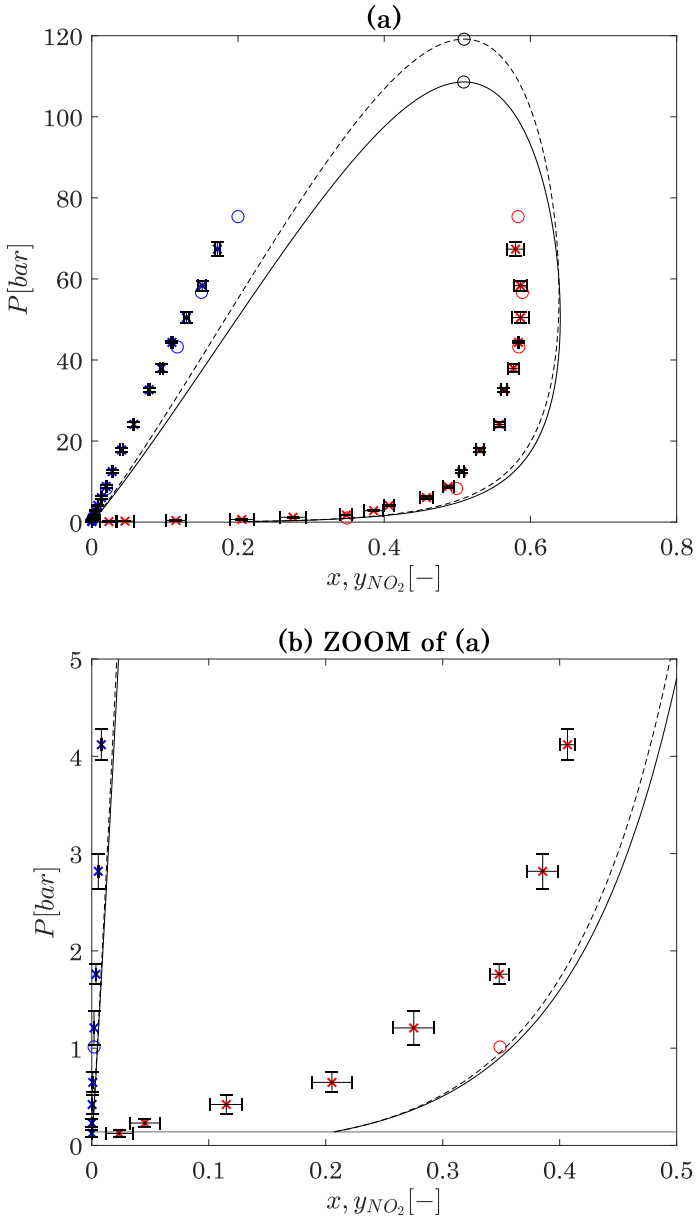

*Figure 43. P-{**x**,**y**} diagram of the reactive mixture containing N_2O_4 and NO_2. Fig. (a) represents the entire figure, Fig. (b) represents the ZOOM of Fig. (a). In the figures, crosses are the points determined with Brick-CFCMC, with the relative uncertainties; circles represent points published by Bourasseau et al. [146]; lines represent calculations with the equation of state associated to the two different sets of critical coordinates, solid lines represent EoS 1, while the dashed line represent EoS 2.*

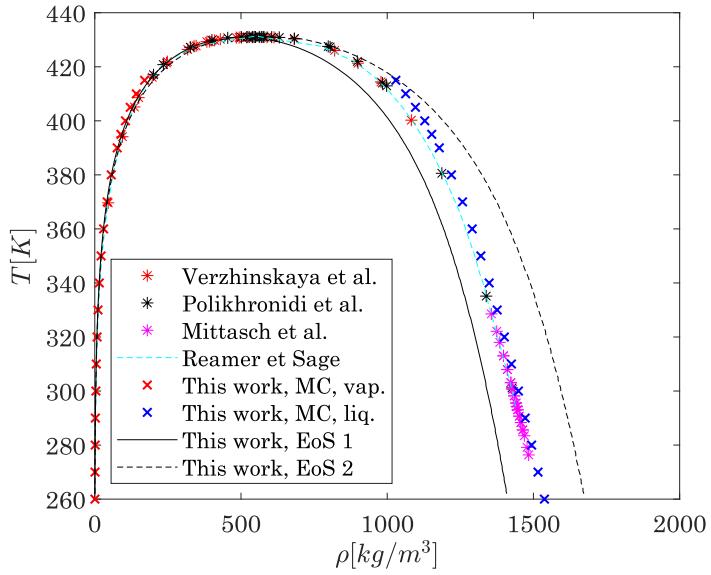

Figure 44. T-ρ^{vap}- ρ^{liq} diagram of the reactive mixture containing N_2O_4 and NO_2. Crosses are the points determined with Brick-CFCMC, with the relative uncertainties; lines represent calculations with the equation of state associated to the two different sets of critical coordinates. The other data points are the same already reported in Figure 41.

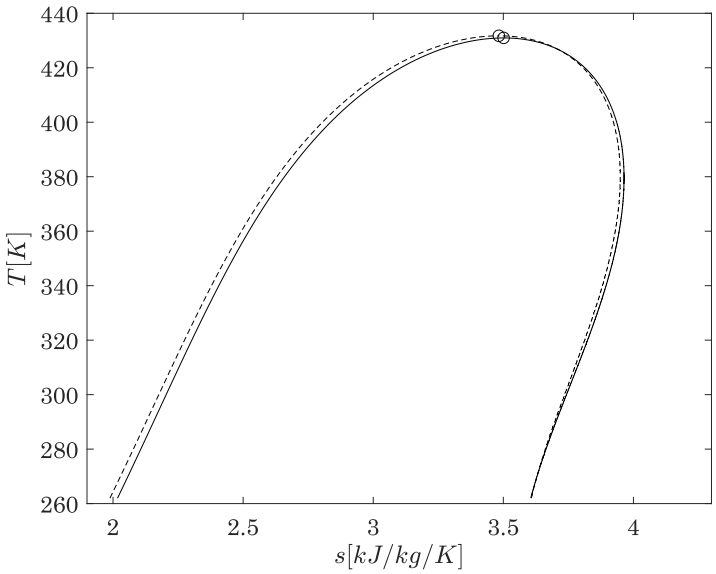

Figure 45. T-s diagram of the reactive mixture containing N_2O_4 and NO_2, calculated with the thermodynamic model defined in this work.

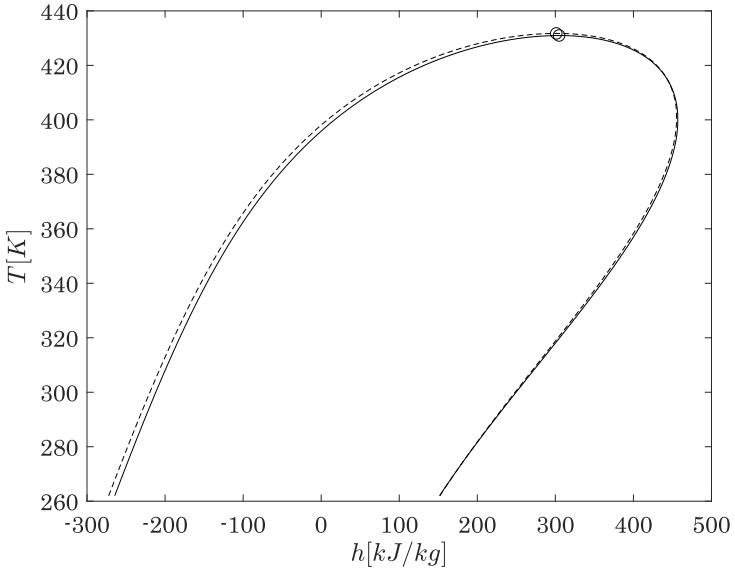

Figure 46. T-h diagram of the reactive mixture containing N_2O_4 and NO_2, calculated with the thermodynamic model defined in this work.

To conclude, Figure 47 shows the unique and non-isothermal phase equilibrium diagram of the reactive NO_2+N_2O_4 system (the black line – also shown in Figure 43 with the continuous line) and 5 isothermal phase equilibrium diagrams of the binary mixture of NO_2+N_2O_4 without reaction, calculated at 5 different temperatures (the coloured lines). This plot also shows isobaric lines corresponding to the saturation pressure of the reactive system at the 5 different temperatures at which the isotherms of the inert mixture have been traced. It can be seen that the phase diagram of the reactive system and each of the phase diagrams of the non-reactive system intersect in two points at equal pressure (the relative saturation pressure of the non-reactive isothermal system). Those two points are, respectively, the bubble and the dew point whose compositions are the solution of reactive system under vapour-liquid equilibrium at the considered temperature (and corresponding calculated pressure). For completeness, it is also specified that the equation of state used to generate all these diagrams is the model described in section 4.2.3, while the critical coordinates are the ones obtained in this work from results of MC Brick-CFCMC and reported in Table 8.

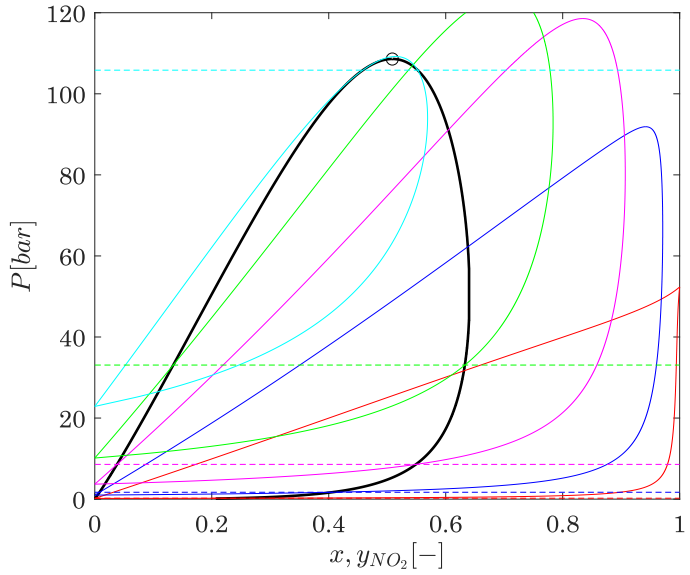

*Figure 47. Phase equilibrium diagrams (solid lines) of: the **reactive** NO_2-N_2O_4 mixture (unique non-isothermal phase equilibrium diagram) - black line; the **inert** NO_2-N_2O_4 mixture - coloured lines at 270 K (red), 310 K (blue), 350 K (magenta), 390 K (green), 430 K (light blue). Isobars (dashed lines) corresponding to the VLE pressures calculated for the reactive system at the 5 temperatures above considered to build the phase equilibrium diagrams of the inert mixture.*

4.4. Conclusion

This work introduces a methodology enabling the assessment of the VLE and energetic properties of reactive fluids being characterised by one reversible reaction at chemical equilibrium, for example $N_2O_4 \leftrightarrow 2NO_2$. These systems are known to be highly specific because, the reaction reaching instantaneously the chemical equilibrium composition dictated by the system's temperature and pressure, it is never possible to characterise experimentally the pure N_2O_4 and the pure NO_2 at pre-defined conditions. We have initially recalled in this paper some singular thermodynamic behaviours of these systems (such as the uniqueness of its single P-T curve in VLE condition and thus its unique critical point) and related that to the equal variance of such a binary and mono-reaction system with respect to a mono-component (inert) fluid.

To calculate thermodynamic properties, the Peng-Robinson equation of state associated to the predictive advanced mixing rules $EoS + a_{res}^{E,\gamma}$, with a zero-$a_{res}^{E,\gamma}$ term characterising athermal solutions, is applied. The required input critical temperature, pressure and acentric factors of the pure N_2O_4 and NO_2, being their experimental determination impossible, have been optimised in this work from force field-based Monte Carlo results of Gibbs and NPT ensemble

simulations, using the force field-based simulation codes Brick-CFCMC and GIBBS. The comparison of the two sets of simulation results obtained with the two codes has proved their high compatibility. Although GIBBS allows performing simulations closer to the critical point than CFC methods, the impact on the prediction of the critical point remains limited.

Moreover, using reaction ensembles, Brick-CFCMC has also enabled the determination of reactive mixture properties, that we have then used to assess the capability of Monte Carlo calculations to reproduce experimental data. Considering the reported uncertainty of MC simulations, this comparison has resulted in a highly satisfactory reproduction of experimental data points. The calculation of energetic properties for this reactive system (enthalpies and entropies) requires the calculation of the thermochemical properties of the molecules forming the reactive mixture (ideal gas standard enthalpy of formation, molar standard entropy and heat capacity). Those properties have been determined from ab-initio quantum mechanics simulations.

Furthermore, thermodynamic calculations have been finally performed on the reactive system, with the selected predictive equation of state, and its input T_c, P_c and ω of NO_2 and of N_2O_4 optimised on MC results of the two respective systems, with the required $\Delta_f H^{\circ}_{i,298.15K}$, $S^{\circ}_{i,298.15K}$ and the ideal-gas heat capacity temperature-dependent correlation obtained from Quantum Mechanics. The comparison with available P-ρ-T experimental data of the reactive system in VLE conditions has shown a very good agreement. However, a high sensibility of the accuracy of the equation of state to the critical coordinates used in this work, either obtained from MC simulations performed with Brick-CFCMC or with GIBBS, has been observed. That paves the way to a future investigation, intended to explore the possibility to optimise critical coordinates of NO_2 and N_2O_4 on MC of both pure components and reactive mixture data.

To conclude, the presented methodology has proven to be able to accurately determine the chemical equilibrium properties of $N_2O_4 \rightleftharpoons 2NO_2$, and is thus proposed to preliminarily predict the thermodynamic properties of other similar reactive systems.

5. Design of the experimental micro – power plant

Second outcome of the project REACHER (WP4)

In collaboration with:

- *Service SIEL (David BRUNELLO, Franck GIOVANELLA) – Pilot realization*
- *Service SIEL (Charly KOENIG and the team of SERM) – Pilot realization*
- *Mr. Alexis SESMAT (General Electric – Association APSIIS) – Pilot design*
- *Dr. Olivier HERBINET - Raman spectroscopy*
- *Dr. Philippe ARNOUX - Raman spectroscopy*

In the context of Work Package n. 4 (see section 3.2), an experimental micro-power plant is being designed. It is reminded that the purpose of running the pilot is the experimental validation of the calculated gain of using **reactive working fluids instead of inert fluids**. The objective is NOT to build an efficient power plant (because the constraints of the laboratory do not allow the achievement of sufficiently high temperatures and pressures) but to measure the **relative improvement**: in its operation with inert fluids, the pilot will globally require electricity; here, the aim is to show that in its operation with reactive fluids, the pilot will either require a much lower amount of electricity, or produce electricity.

5.1. The operating conditions

The aim of the pilot is to validate the effect of the fluid reactivity on the performance of a power cycle. The operating conditions selected for the cycle must ensure the evolution of the chemical reaction. In this pilot, a mixture of an inert fluid and of the reactive N_2O_4 will be tested as working fluid (except if other reactive fluids will be found among the commercially available ones).

If a **mixture of an inert fluid and of the reactive N_2O_4** is selected, a minimum temperature of 10 °C and a maximum temperature of 180°C, a minimum pressure of 1.5 bar and a maximum pressure of 4.5 bar will enable observing the evolution of the reaction and thus the effect on performances. Figure 48 shows the T-s diagram of pure N_2O_4. The isobars present an inflection point in the entropy interval 4 - 5 kJ/kg/K, in the vapour phase. This is due to the presence of the chemical reaction(s): $N_2O_4 = 2\ NO_2 = 2\ NO + O_2$. The temperature and pressure dependence of the evolution of the composition of the system (liquid, equilibrium vapour-liquid, vapour phases) is shown in Figure 49. In the temperature range 10 – 180 °C, the reaction $N_2O_4 = 2\ NO_2$ is almost complete. This temperature interval has thus been considered for the pilot application. The low-pressure level was selected in order to minimise leakages.

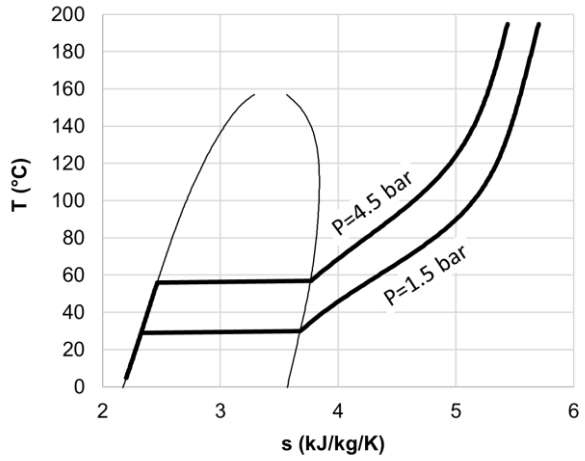

Figure 48. T-s diagram of pure N_2O_4, with two isobars at 1.5 bar et 4.5 bar. The diagrams are performed with the accurate multiparameter equation of state provided in confidential form by Lemmon et al. [145] and integrated in Refprop 10.1.

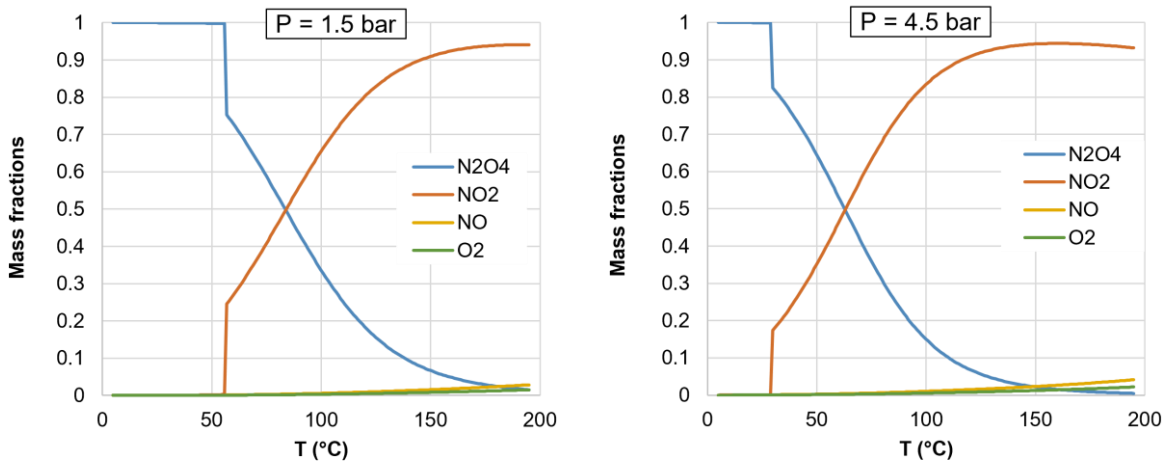

Figure 49. Evolution of the composition of N2O4, as a function of temperature and pressure. The diagrams are performed with the accurate multiparameter equation of state provided in confidential form by Lemmon et al. [145] and integrated in Refprop 10.1.

The calculations of the thermodynamic properties of the final mixture inert + reactive will be performed with the code which is under development by the team REACHER. However, in the temperature-pressure range here considered the mixture containing a minimum of 98%$_{molar}$ of inert (CO_2 or N_2) will be in the gaseous phase. A Brayton cycle can thus be designed operating at less than 5 bar and 10 – 180 °C.

More details about the preliminary calculations and thus the expectations of the pilot performance operating in these conditions are presented in section 5.3.2.

5.2. The starting point: the turbine acquired in 2019

The design of the pilot started in 2019, well before the applicant was granted with the ERC-REACHER project. The initial idea was to build a closed Brayton cycle operating with CO_2 (inert) + N_2O_4 (reactive). **The initial operating conditions have been then retained for the development of the final power plant, in the REACHER project**.

It is worth highlighting that the design of the pilot was highly constrained by the (limited) surface that was available at LRGP for its installation. The pilot is being designed to meet with space-noise-vibrations-weight-safety constraints.

The power plant has to operate within a minimum temperature of 10 °C (or 20°C, depending on the heat sink temperature) and a maximum temperature of 180 °C. The two (minimum and maximum) nominal pressure levels, the nominal mass flow rate and the nominal power output were defined iterating with the supplier of the turbine (described in the following).

The turbine that was designed by DEPRAG is a 3.5 $kW_{el,n}$ axial turbine without reaction. The turbine is directly connected to a synchronous generator, which is hermetically mounted on the shaft of the turbine. The turbine and the generator are shown in Figure 50.

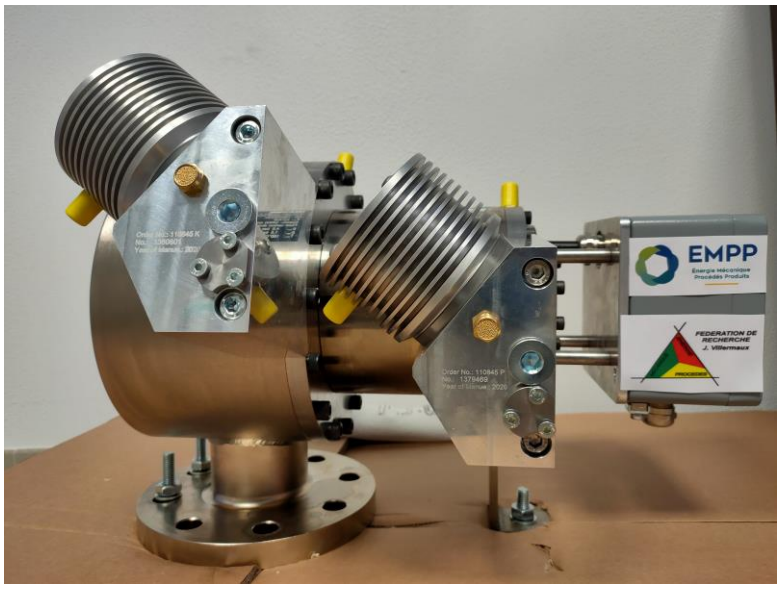

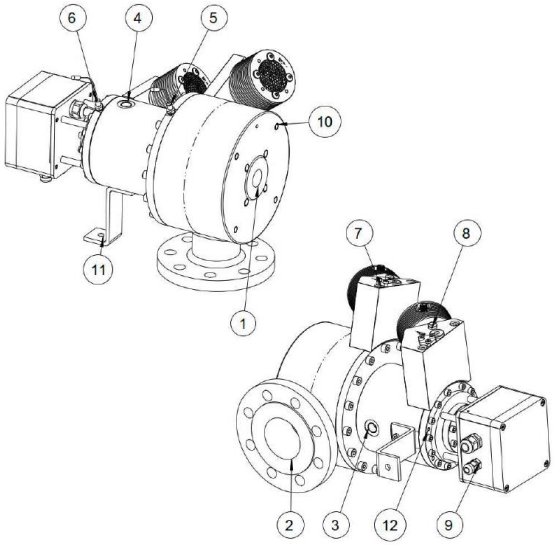

Position	Name
1	inlet flange DN25 PN25
2	outlet flange DN65 PN25
3	inlet cooling liquid G3/8
4	outlet cooling liquid G3/8
5	measuring point T.FL
6	measuring point T.LL
7	lubrication system FL
8	lubrication system LL
9	terminal box
10	fixing points M12
11	fixing point Ø10
12	grounding point M5

Figure 50. Turbine layout

This turbine is designed to operate:

- with a mass flow rate **80 g/s of CO_2**,
- at an **inlet temperature of 180 °C** and an **inlet pressure of 4.5 bar**,
- at an **outlet pressure of 1.5 bar**,
- with a **rotational speed of 35 000 rpm**.

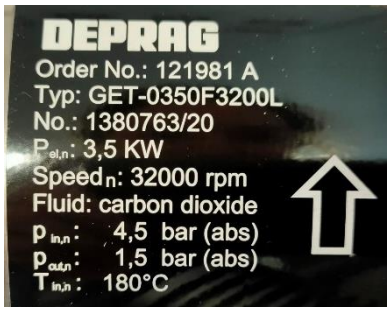

Figure 51. Data printed on the turbine.

For this nominal condition, the supplier calculated an outlet temperature of 119.1 °C and a turbine efficiency of 64.9%, for a turbine output of 4.4 kW (called $P_{mec.}$ in Figure 52) and an electric output of 3.5 kW (called $P_{el.}$ in Figure 52).

Considering the calculated thermodynamic properties of CO_2 (Table 10), the mass flow rate of 80 g/s of CO_2 and the inlet (DN25, A_{in} = 531 mm^2) and outlet (DN65, A_{out} = 3421 mm^2) cross sections of the turbine, this leads to the calculation (by eq. (55)) of the **power of the real expansion equal to 4.7 kW** (called $P_{real\ exp.}$ in Figure 52) and the one of the **iso-entropic expansion equal to 6.8 kW**, which results in an **iso-entropic efficiency equal to about 69.0%**. Indeed, it is reminded that the power of the real expansion is calculated as:

$$P_{\substack{real \\ exp.}} = \dot{m} \cdot \left(h_{in} - h_{out} + \frac{v_{in}^2 - v_{out}^2}{2} \right)_{\substack{real \\ exp.}} \tag{55}$$

Where $v_{in/out}$ is the velocity at the inlet or at the outlet:

$$v_{in/out} = \frac{\dot{m}}{\rho_{in/out} \cdot A_{in/out}} \tag{56}$$

And iso-entropic efficiency of a turbine is defined as the ratio between the real expansion work divided by the reversible (iso-entropic) expansion work:

$$\eta_{is,T} = \frac{\left(h_{in} - h_{out} + \frac{v_{in}^2 - v_{out}^2}{2} \right)_{\substack{real \\ exp.}}}{\left(h_{in} - h_{out} + \frac{v_{in}^2 - v_{out}^2}{2} \right)_{\substack{iso-s \\ exp.}}} \tag{57}$$

The turbine efficiency provided by the supplier (64.9%) is the ratio of the turbine output (4.4 kW) divided by the iso-entropic expansion power (6.8 kW), which gives 64.7% (the difference 64.7% vs. 64.9% is probably due to different thermodynamic calculations and neglected decimals of turbine power output).

*Table 10. Thermodynamic properties of **CO_2** at the inlet and outlet conditions of the turbine. Yellow columns are input from the turbine supplier, white columns are calculated in this work.*

Point	T (K)	P (bar)	density (kg/m^3)	enthalpy (kJ/kg)	entropy (kJ/kg/K)
IN	180	4.5	5.283	647.07	2.836
OUT real	119.1	1.5	2.0301	589.73	2.907
OUT iso-s	90.1	1.5	2.1941	562.93	2.836

Being the turbine power output (which is equal to the real expansion power reduced by organic losses) equal to 4.4 kW, the **mechanical losses are** 4.7 kW – 4.4 kW = **0.3 kW** and the **mechanical efficiency** is thus equal to 4.4 kW / 4.7 kW = **93%**. The **efficiency of the generator** is equal to 3.5 kW / 4.4 kW = **80%**. It will be shown in Figure 55 that the measured mechanical losses are a bit higher, about 0.4 kW.

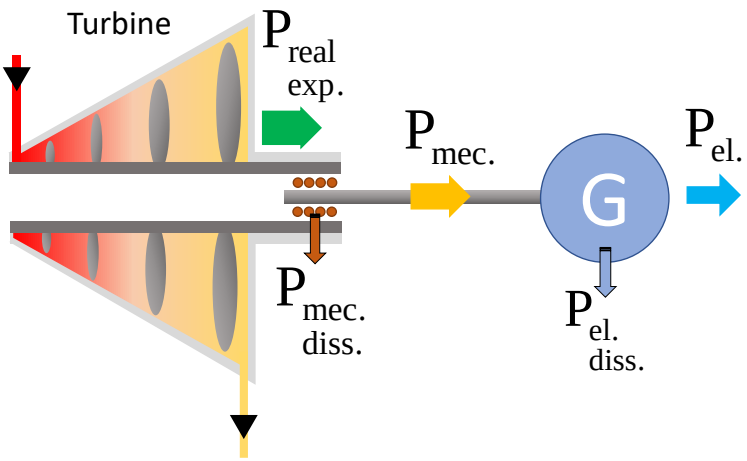

Figure 52. Chain of power losses ($P_{diss.}$) and converted power in the turbine, from fluid expansion to output electrical power. "G" is the generator.

The lines of CO_2 real (irreversible) and ideal (reversible) expansion are shown in Figure 53.

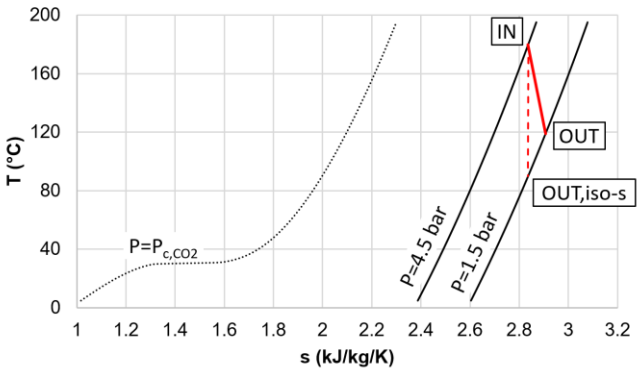

Figure 53. T-s diagram of CO_2. Black lines are isobars of CO_2, at the critical pressure (P_c = 73 bar) of CO_2, at the inlet pressure of the turbine (4.5 bar) and at the outlet pressure of the turbine (1.5 bar). Red lines represent the expansion line of CO_2, real expansion (solid line) and iso-entropic expansion (dotted line).

Considering that at nominal operation the turbine is in choked conditions, it is possible to estimate the critical (choked) section area:

$$A_c = \frac{\dot{m}_{choked}}{\sqrt{\rho_{in} \cdot P_{in} \cdot \gamma \cdot \left(\frac{2}{\gamma+1}\right)^{\left(\frac{\gamma+1}{\gamma-1}\right)}}} = 79.35\ mm^2 \qquad (58)$$

The critical cross section, A, measured by the supplier is 82.84 mm²

The turbine will be firstly tested with ambient air. In this (open cycle) operation mode, the outlet pressure (P_{out}) is the atmospheric pressure (1 bar) and, keeping constant the inlet temperature and pressure conditions, the inlet choked mass flow rate is modified by the different fluid properties. The mass flow rate can thus be recalculated, considering the properties of the other fluid (air ~ N_2), and the previously calculated critical cross section, A_c, of the turbine:

$$\dot{m}_{choked,N_2} = A_c \sqrt{\rho_{in,N_2} \cdot P_{in} \cdot \gamma_{N_2} \cdot \left(\frac{2}{\gamma_{N_2}+1}\right)^{\left(\frac{\gamma_{N_2}+1}{\gamma_{N_2}-1}\right)}} \qquad (59)$$

In case the inlet turbine conditions are equal to the nominal one even when using air, the resulting mass flow rate is equal to 0.067 kg/s. For this operating mode with air (N_2), for different inlet conditions, DEPRAG provided the outlet temperature (outlet pressure is always equal to 1 bar), shown in Table 11, and the relative efficiency of the turbine, the electric power and the mass flow rates, in Table 12. It is also reminded that the power of the real expansion

and the isentropic efficiency are calculated, respectively, as shown in eqs. (55) et (57). The mechano-electrical efficiency is given by: $\eta_{mec-el} = \frac{P_{el.}}{P_{\substack{real \\ exp.}}}$.

*Table 11. Thermodynamic properties of **nitrogen** at the inlet and at the outlet of the turbine, considering different operating conditions, for the operation at nominal rotational speed (32 000 rpm). Yellow columns are input from the turbine supplier, white columns are calculated in this work.*

Turbine inlet					**Turbine outlet**					**Turbine outlet (iso-entropic expansion)**				
P (MPa)	T (°C)	h (kJ/kg)	s (kJ/kg/K)	ρ (kg/m^3)	P (MPa)	T (°C)	h (kJ/kg)	s (kJ/kg/K)	ρ (kg/m^3)	P (MPa)	s (kJ/kg/K)	T (°C)	h (kJ/kg)	ρ (kg/m^3)
0.45	180	470.88	6.83	3.34	0.1	80	366.56	5.61	0.95	0.1	6.83	22.06	306.21	1.14
0.4	180	470.91	6.86	2.97	0.1	85	371.78	5.60	0.94	0.1	6.86	32.18	316.74	1.10
0.35	180	470.95	6.90	2.60	0.1	90	376.99	5.59	0.93	0.1	6.90	44.06	329.12	1.06
0.3	180	470.98	6.95	2.23	0.1	96	383.25	5.58	0.91	0.1	6.95	58.34	344.00	1.02
0.25	180	471.02	7.00	1.86	0.1	105	392.64	5.57	0.89	0.1	7.00	76.06	362.46	0.96
0.2	180	471.05	7.07	1.49	0.1	120	408.30	5.55	0.86	0.1	7.07	99.00	386.38	0.91

*Table 12. Characteristics of the turbine operating with **nitrogen**, at different operating conditions, for the operation at nominal rotational speed (32 000 rpm). Yellow columns are input from the turbine supplier, white columns are calculated in this work. Mechanical power, P_{mec}, is calculated by subtracting the previously determined mechanical power losses (0.4 kW – considered constant at fixed rotational speed of 32 000 rpm) to the real expansion power.*

Turbine inlet		**Turbine outlet**		**Turbine characteristics**							
P (MPa)	T (°C)	P (MPa)	T (°C)	$\dot{m}_{choked}$ (kg/s)	$P_{el.}$ (kW)	$\eta_{is,T}$ from eq. (57)	$P_{real\ exp.}$ (kW) from eq. (55)	$P_{mec.}$ (kW)	η_{mec}	η_{el}	$Q_{diss\ mec-el}$ (kW_{th})
0.45	180	0.1	80	0.067	5.7	63.44%	7.0	6.6	94%	86%	1.3
0.4	180	0.1	85	0.06	4.9	64.41%	6.0	5.6	93%	88%	1.1
0.35	180	0.1	90	0.052	3.9	66.37%	4.9	4.5	92%	86%	1.0
0.3	180	0.1	96	0.045	3	69.23%	4.0	3.6	90%	84%	1.0
0.25	180	0.1	105	0.037	2.1	72.35%	2.9	2.5	86%	83%	0.8
0.2	180	0.1	120	0.03	1.3	74.31%	1.9	1.5	79%	87%	0.6

It is worth observing that the mass flow rate provided by the supplier in Table 12 is equal to the mass flow rate that could be found in choked conditions (by applying eq. (59)) considering different inlet conditions.

For an ideal inert gas passing through an orifice, the mass flow rate depends on the occurrence (or not) of the choked condition at the critical section. The calculated mass flow is shown in eq. (60).

$$\begin{cases} 1)\ if\ \left(\frac{P_{out}}{P_{in}}\right) < \left(\frac{2}{\gamma+1}\right)^{\left(\frac{\gamma}{\gamma-1}\right)} \Rightarrow choked\ conditions \\ \qquad \Rightarrow \quad \dot{m}_{choked} = A_c \sqrt{\rho_{in} \cdot P_{in} \cdot \gamma \left(\frac{2}{\gamma+1}\right)^{\left(\frac{\gamma+1}{\gamma-1}\right)}} \\ 2)\ if\ \left(\frac{P_{out}}{P_{in}}\right) \geq \left(\frac{2}{\gamma+1}\right)^{\left(\frac{\gamma}{\gamma-1}\right)} \Rightarrow non-choked\ conditions \\ \qquad \Rightarrow \quad \dot{m}_{non-choked} = A_c \left(\frac{P_{out}}{P_{in}}\right)^{\frac{1}{\gamma}} \sqrt{\frac{2\gamma}{\gamma-1} \cdot \rho_{in} \cdot P_{in} \cdot \left[1 - \left(\frac{P_{out}}{P_{in}}\right)^{\frac{\gamma-1}{\gamma}}\right]} \end{cases} \quad (60)$$

Depending on the ratio between inlet and outlet pressure, the inlet of the turbine can be in non-choked conditions. In case of non-choked conditions, the specific mass flow rate (lower than the one defined by choked conditions) is defined by the compressor operation, while the inlet pressure of the turbine (if discharging in the environment, at ambient pressure) will result from equation (60).2 and the entering mass flow rate.

The supplier also provided the value of the (roughly) estimated high and low pressure transversal lengths, respectively, 100 mm and 150 mm.

This turbine could be started in two alternative modes:

1. Driven by a motor: a drive (frequency converter) by Sieb&Meyer has been electrically connected to the generator. This system enables the use of the generator in motor mode and guarantees the turbine ramp up to its nominal speed (32000 rpm). Once the motor is at nominal speed, the fluid is sent into the turbine and the motor is converted back to generation mode, to convert the energy of the expanding fluid into electricity. The turbine has been tested at LRGP without load, from 5 000 and 30 000 rpm (Figure 54), and the results of the running have allowed to calculate the power of the drive (Figure 55), required to run the turbine without load. The total power required by the drive enables to balance the energy dissipated in the bearings (mechanical energy losses, equal to about 300-400 W as shown above in this section), the electrical energy dissipated by the drive, the energy that compresses the (low amount of) air sucked by the turbine during motor operation.

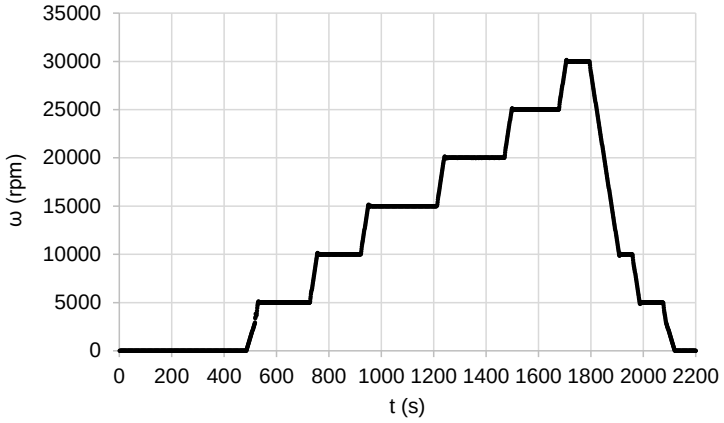

Figure 54. Test of turbine ramp up and stabilisation at 5000, 1000, 15000, 20000, 25000, 30000 rpm.

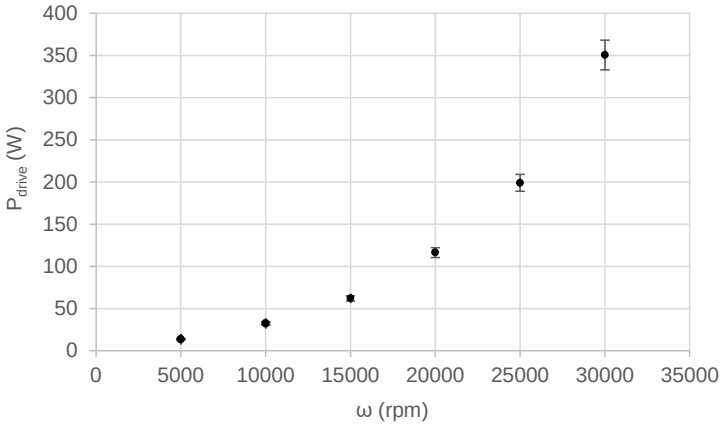

Figure 55. Drive power (product of output current and tension) required to run the turbine at 5000, 1000, 15000, 20000, 25000, 30000 rpm.

2. Driven by the fluid, stabilising at nominal 32 000 rpm. This mode requires a precise knowledge of how mechanical losses change with rotational speed, and of the inertia of the turbine. The eventuality of running in this mode will be confirmed by the possibility of braking the turbine's shaft and of measuring the rotational speed. At the moment, mode 1 is envisaged.

The **generator** needs to be **preheated** (before turbine ramp up) and **cooled down** (during stationary operation). To this aim, the generator must be preheated at 65 °C before starting the test, and kept at 65 °C during the test. This is done by circulating hot water whose temperature is controlled at 65 °C by a **thermostatic bath** which has been acquired and connected to the generator by points 3 and 4 indicated in Figure 50. Finally, the generator is connected to an

electrical resistance which enables the dissipation of the produced electrical energy into thermal energy.

5.3. The design of the pilot, coupled with the available turbine

To use the turbine described in the previous section, the pilot had to be equipped with three unit operations (a compressor (C), to provide the needed mass flow rate, an electric heater, to heat up the fluid before entering the turbine, a cooler, to cool down the fluid before entering the compressor), with two regulation valves (a bypass normally open (NO) valve V1 and a normally closed (NC) valve V2). The position of these components in the cycle is shown in Figure 56 and their characteristics are described in the following sections. Metric systems are also present in the pilot and shown in Figure 56, to measure the mass flow rate at the turbine inlet (Coriolis mass flow meter), 6 temperature probes PT100, 6 pressure transducers, 4 Raman probes to measure the composition (z).

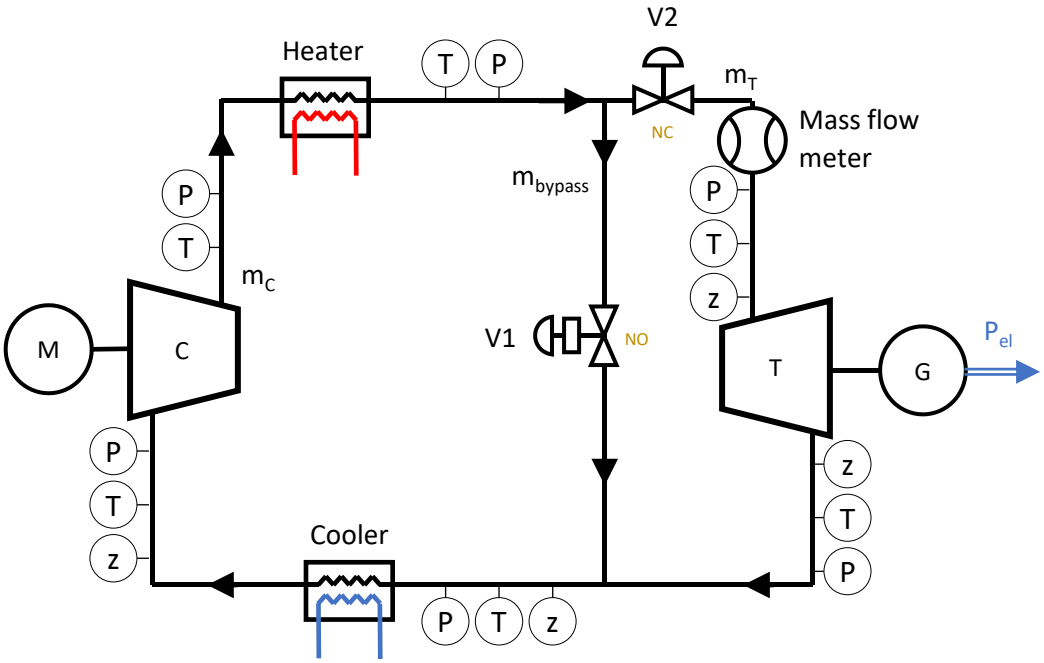

Figure 56. Schematic of the power plant, in closed cycle configuration.

To test the pilot, the following steps are followed:

1. Test of the cycle in open configuration (see Figure 57), operating with ambient air and, thus, a minimum pressure of the cycle equal to ambient pressure (1 bar).
2. Test of the cycle in (the definitive) closed cycle configuration (see Figure 56), operating with the selected inert fluid (originally CO_2, finally see section 5.3.3– N_2).

3. Test and running the cycle in (the definitive) closed cycle configuration, operating with the selected mixture of inert + reactive fluid.

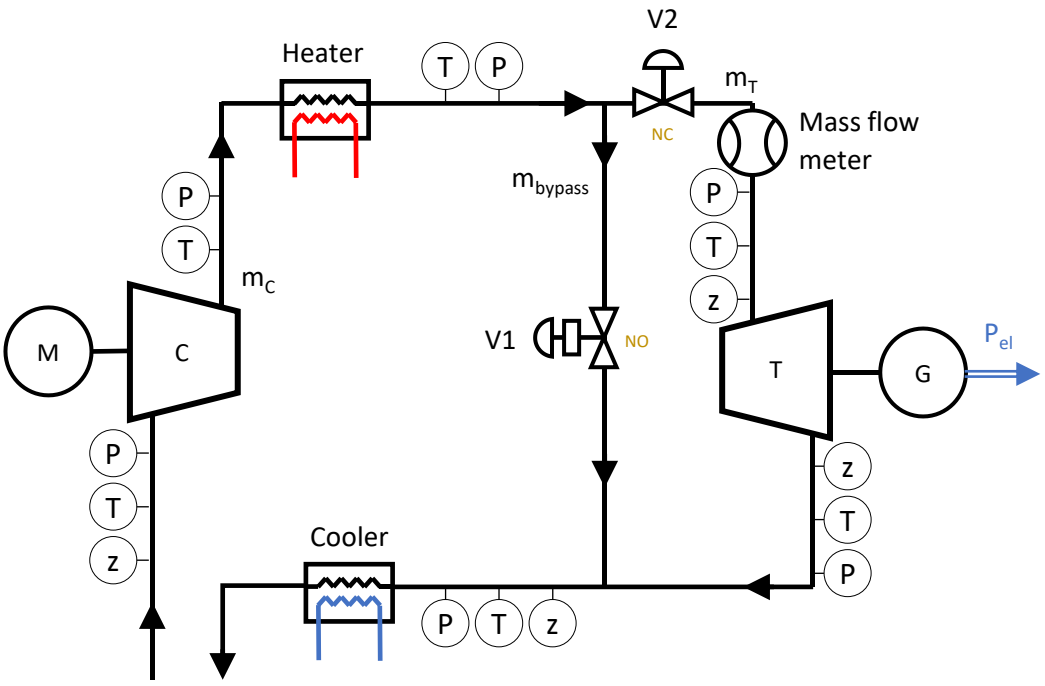

Figure 57. Schematic of the power plant, in open cycle configuration.

5.3.1. The compressor

An oil-free compressor, enabling to compress 80 g/s of CO_2 from 1.5 bar to 4.5 bar (the conditions by turbine design) was searched within the available commercial models (contacting about 20 potential suppliers) and types (screw rotary, centrifugal, reciprocating, axial type). In this selection, many constraints were necessarily imposed: limitation of the fluctuations in the pressure output, oil-free, non-intercooled (to limit the electrical heating of the fluid after compression process), required electric power lower than 15 kW, maximum weight of 1 t, designed to operate with CO_2, maximum 80 dB of noise, acceptable cost, hermetic.

Unfortunately, **no available CO_2 compressors have been found for this application and the choice was diverted to the use N_2, instead of CO_2**. As demonstrated in the previous paragraph, the use of a different gas in the turbine, while keeping the same inlet temperature (180 °C) and pressure (4.5 bar), requires the modification of the mass flow rate, $\dot{m}_{N_2} = 67\ g/s$, to ensuring choked conditions at the inlet of the turbine. However, also for N_2 the compressor availability was limited, because the combination of the requested differential pressure and mass flow rate were in a sort of "grey region" among the available models, and the imposed constraints too

limiting. For example, hermetic reciprocating compressors exist but their outlet pressure fluctuations and noise level are too high, while non-reciprocating available models (designed for air compression) keep acceptable vibrations, pressure fluctuations and noise, but have a high leakage rate.

A non-hermetic, displacement screw, oil-free, non-intercooled compressor from AERZEN (Delta Screw VM8R model) was selected, enabling to compress 67 g/s of N_2 from 1.5 to 4.5 bar, with an electrical motor of 18.5 kW_{el} equipped with a variator to enable the modification of the rotational speed and thus of the mass flow rate provided by the compressor (see Figure 58). It has thus been necessary to make important electrical modifications to the laboratory and to verify the resistance of the laboratory slab to support the compressor weight of 1.5 t.

Figure 58. Screw compressor of Aerzen (indicative model).

Figure 59 shows the thermodynamic characteristics of the compressor (the mass flow rate it provides, the mechanical power it needs, the calculated is-entropic efficiency, the outlet temperature of the fluid) as a function of the rotational speed of the motor. According to these characteristics, the mechanical power which is required to compress 67 g/s of nitrogen (the mass flow rate of nitrogen in turbine choked conditions – see section 5.2) from 20 °C and 1.5

bar to 4.5 bar is equal to 13.2 kW. The calculated mechanical efficiency of the compressor is almost independent of the rotational speed and is equal to 85.1(±0.5)%. The outlet temperature of the compressor could ideally be higher than the inlet temperature of the turbine (see Figure 59), which means that we would not even need to heat up the fluid before entering the turbine (but on the contrary, to cool it down). However, we need to ensure that the outlet of the compressor has a temperature lower than 180 °C. To do that, the inlet temperature of the compressor will be reduced to 10-15 °C, by acting on the regulation of the mass flow rate of cooling fluid (cold water) passing through the cooler of the cycle (see section 5.3.3).

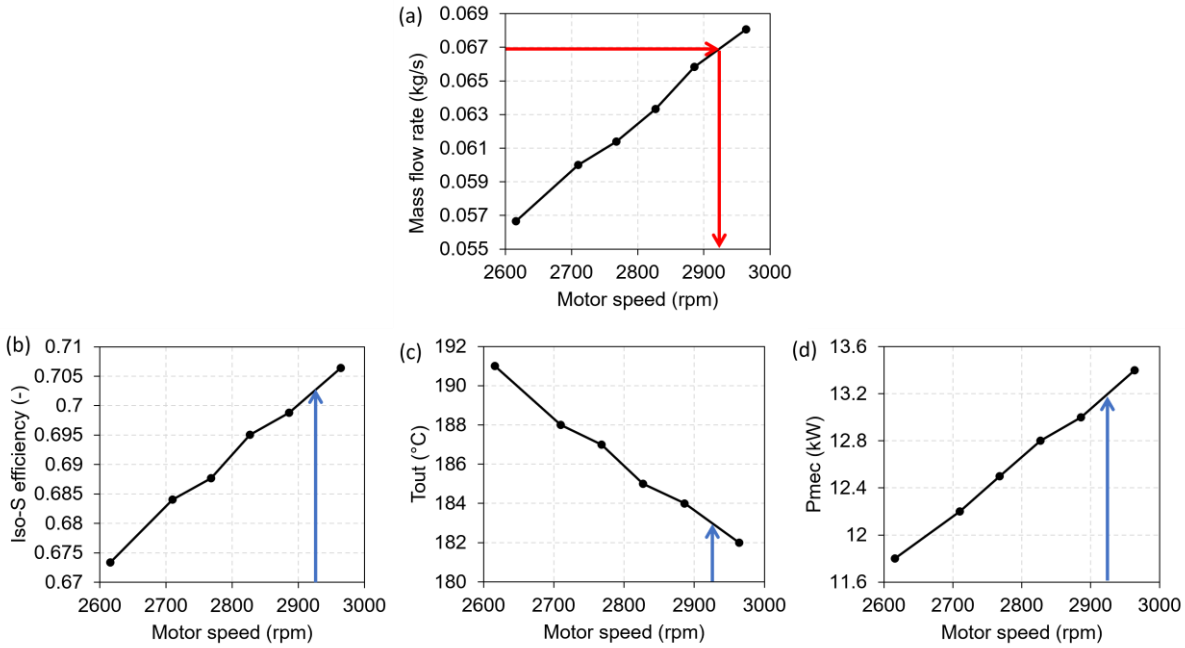

Figure 59. Characteristics of the compressor, operating with nitrogen, considering an inlet temperature and pressure of 20 °C and 1.5 bar and an outlet pressure of 4.5 bar. The arrows show the motor speed providing the mass flow rate of nitrogen defined by the design of the turbine (fig. (a)), and the corresponding iso-entropic efficiency (calculated in this work, fig. (b)), the outlet temperature of the compressor (provided by the supplier, fig. (c)), the mechanical power of the compressor (provided by the supplier, fig. (d)).

Similar curves have been built (from the data provided by the supplier) to analyse the behaviour of the compressor if the inlet is at 1 bar and not at 1.5 bar. A transfer function is being defined by the applicant in order to assess the behaviour of the compressor if it operates in open cycle configuration (that is, sucking ambient air) or in close loop, where the inlet pressure is a function of the equilibrium condition of the whole cycle.

The inlet/outlet piping of the compressor are DN 125 at the inlet, DN 65 at the outlet.

5.3.2. Thermodynamic coupling of turbine and compressor at nominal conditions

Some **preliminary** calculations to understand the coupling of the turbine and of the compressor have been performed, in order to quantify the need of heating and of cooling systems needed to close the cycle. An Excel spreadsheet has been created in order to calculate either **the output electrical net power** of the cycle and the needed mass flow rate (defined as "calculation mode n. 1" and described below) to ensure a specific pressure distribution along the cycle, or **the maximum pressure of the cycle (P_1)** and the needed mass flow rate (defined as "calculation mode n. 2") to provide a specific output electrical net power. These preliminary cycle calculations have been performed with inert or with a mixture of inert + reactive (N_2O_4) fluid.

In the following, the calculation modes (1) and (2) are presented, referring to the schematic and point numbering presented in Figure 60.

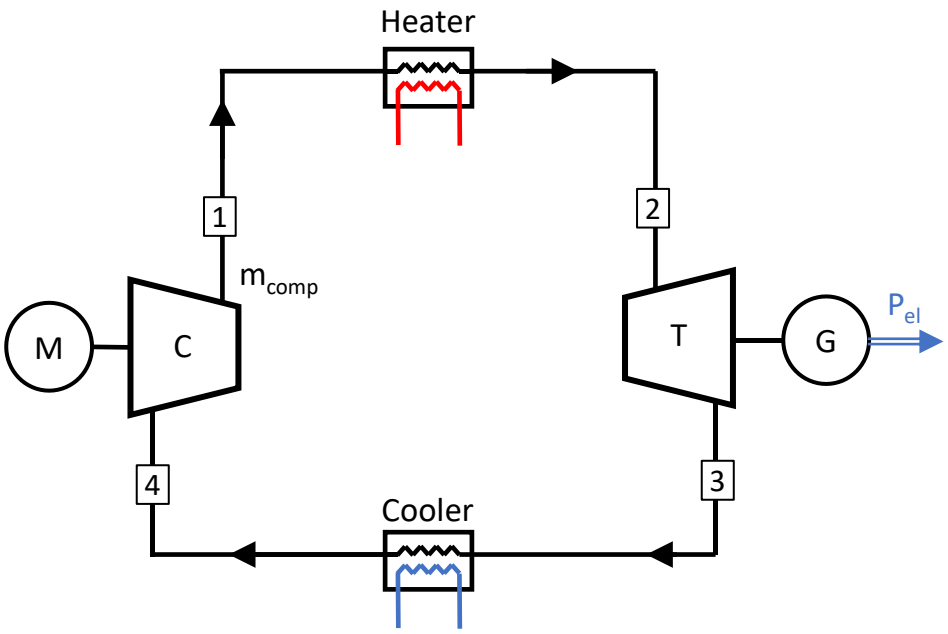

Figure 60. Schematic of the cycle for preliminary calculations.

Calculation mode 1 (with reference to Figure 61)

Hypothesis and input data for the calculations:

1. No pressure drops in pipes are present
2. **The inlet temperature and pressure of the compressor, T_4 and P_4, are known**
3. **The outlet pressure of the compressor, P_1, is given** and, according to assumption n. 1, is equal to the inlet pressure of the turbine, P_2

4. According to assumption n. 1, the outlet pressure of the turbine, P_3, is equal to the -given- inlet pressure of the compressor, P_4
5. **The inlet temperature of the turbine, T_2, is known**
6. The critical section of the turbine is given (as calculated in section 5.2), A_c
7. The iso-entropic efficiency and the mechanical efficiency of the rotor (for both turbine and compressor) and the electrical efficiency of the generator are given and are equal to the nominal one calculated in section 5.2.
8. The assumption of ideal gas underlies the thermodynamic calculations. Temperature-dependent ideal gas specific heat capacities, standard molar enthalpy of formation and molar entropy for the involved molecules are collected from DIPPR.
9. The speed of sound of the reactive mixture is preliminarily calculated considering the formula valid for inert ideal gas mixtures: $a = \sqrt{\gamma R_g T}$, where R_g is the universal gas constant divided by the molar mass of the reactive mixture, γ is calculated for the reactive mixture from its isobaric and isochoric heat capacities, $\gamma = c_p/c_v$. But it has been shown analytically by Lemmon et al. [145] that the calculation of the speed of sound of reactive mixtures differs from $a = \sqrt{\gamma R_g T}$.
10. Since the pilot runs at less than 180 °C, only the reaction $N_2O_4 = 2\ NO_2$ is modelled, while the higher temperature $2\ NO_2 = 2NO + O_2$ is not considered for these preliminary calculations.

The **unknowns of this calculation mode are the mass flow rate and the output mechanical powers** and the methodology is summarized in Figure 61.

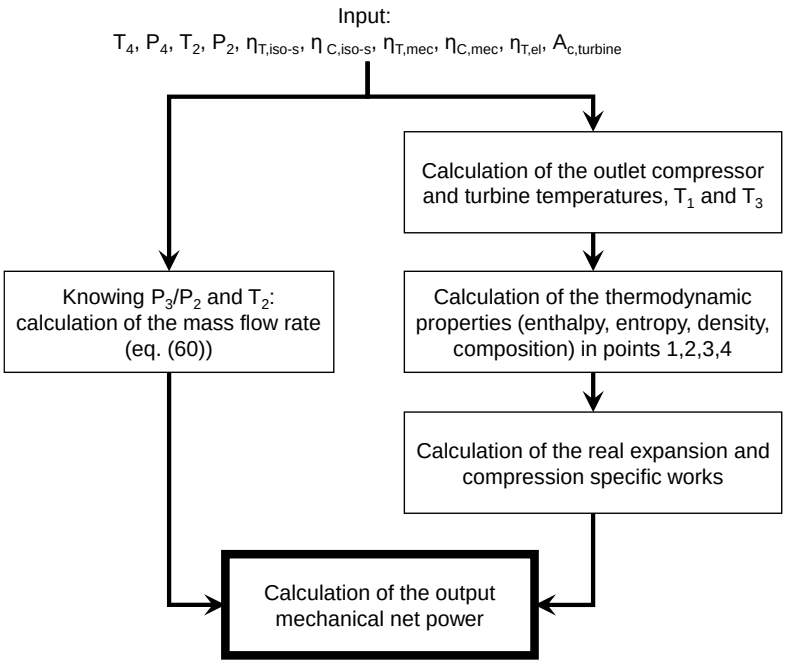

Figure 61. Calculation mode n. 1.

Mode 2 (with reference to Figure 62)

Hypothesis and input data for the calculations:

1. No pressure drops in pipes are present.
2. **The electric power output of the turbine, $P^{calc}_{el,T}$ is fixed.**
3. **The inlet temperature and pressure of the compressor, T_4 and P_4, are known.**
4. According to assumption n. 1, the outlet pressure of the turbine, P_3, is equal to the inlet pressure of the compressor, P_4.
5. **The inlet temperature of the turbine, T_2, is known.**
6. The critical section of the turbine is given (as calculated in section 5.2), $A_{c,turbine}$.
7. The iso-entropic efficiency and the mechanical efficiency of the rotor (for both turbine and compressor) and the electrical efficiency of the generator are given and are equal to the nominal one calculated in section 5.2.
8. The assumption of ideal gas underlies the thermodynamic calculations. Temperature-dependent ideal gas specific heat capacities, standard molar enthalpy of formation and molar entropy for the involved molecules are collected from DIPPR.
9. The speed of sound of the reactive mixture is preliminarily calculated considering the formula valid for inert ideal gas mixtures: $a = \sqrt{\gamma R_g T}$, where R_g is the universal gas constant divided by the molar mass of the reactive mixture, γ is calculated for the

reactive mixture from its isobaric and isochoric heat capacities, $\gamma=c_p/c_v$. But it has been shown analytically by Lemmon et al. [145] that the calculation of the speed of sound of reactive mixtures differs from $a=\sqrt{\gamma R_g T}$.

10. Since the pilot runs at less than 180 °C, only the reaction N_2O_4 = 2 NO_2 is modelled, while the higher temperature 2 NO_2 = 2NO + O_2 is not considered for these preliminary calculations.

The **unknowns are the mass flow rate, the inlet turbine pressure, P_2**, and the resulting net power output of the coupling turbine + compressor. The methodology is summarized in Figure 62.

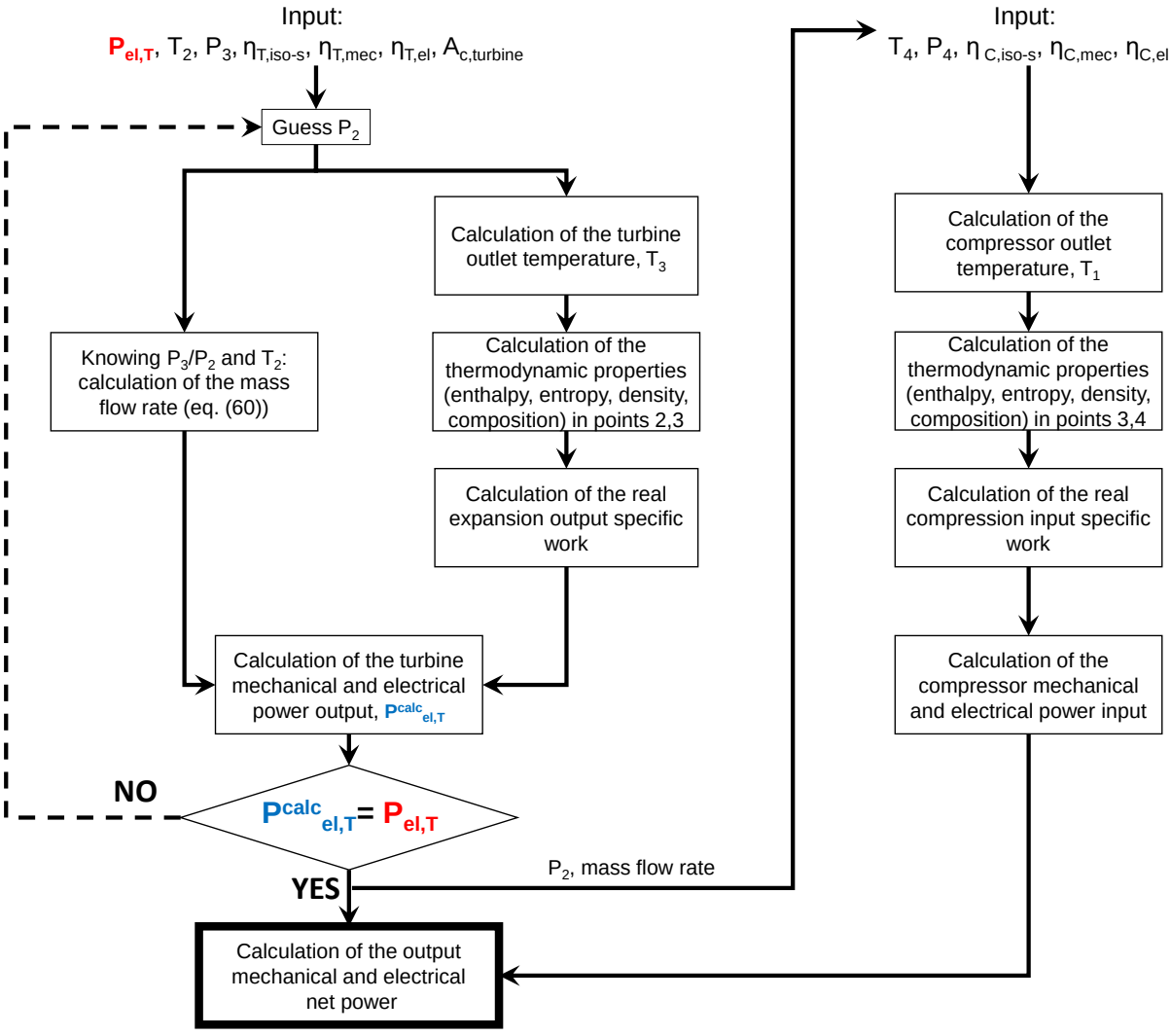

Figure 62. Calculation mode 2.

The results of a simulation with inert and reactive fluid, according to Mode 1 (with either a pressure P_2 equal to 4.5 bar or 2.5 bar) and to the conditions in Table 13, are shown in Figure

63. The observed negative net power was expected since the beginning of the design, because of the low pressure of the gaseous working fluid. As it can be noticed, the effect of the addition of the reactive fluid is the inflection of the isobars and thus the marked differentiation of the compressor and turbine specific works, leading to a less negative power output (- 2364 W versus - 9093 W, for the case with P_2 = 4.5 bar, and – 410 W versus – 1941 W, for the case with P_2 = 2.5 bar). Moreover, Figure 64 leads to the observation that the reaction $N_2O_4 = 2NO_2$ (modelled as an ideal gas reactive mixture) at low pressure (1 - 5 bar) mostly occurs at low temperature 0 - 100 °C. This explains why: 1) fluid compression (at low temperature) is much more favourable for reactive fluids than for inert ones; 2) fluid expansion does not beneficiate of reaction advantages and the molecule N_2 provides more specific work than the mixture of 80% N2 + 20% of (predominant) NO_2 (as shown by the h-s diagram in Figure 63).

It is worth highlighting that the addition of a small amount ($5\%_{molar}$) of reactive fluid is sufficient to observe the impactful improvement of the net power output (or, better, in this case the net power input). **This is what we want to observe experimentally.**

Table 13. Data to perform the simulation in mode n. 1.

P_2 (=P_1) [bar]	4.5 or 2.5
P_3 (=P_4) [bar]	1.5
T_2 [°C]	180
T_4 [°C]	10
$\eta_{T,iso-s}$	69%
$\eta_{T,mec}$	93%
$\eta_{T,el}$	80%
$\eta_{C,iso-s}$	69%
$\eta_{C,mec}$	85%
$\eta_{C,el}$ (assumed because not available)	90%
A_c [mm^2]	79.35
d_1 [mm]	70
d_2 [mm]	72.1
d_3 [mm]	29.7
d_4 [mm]	164

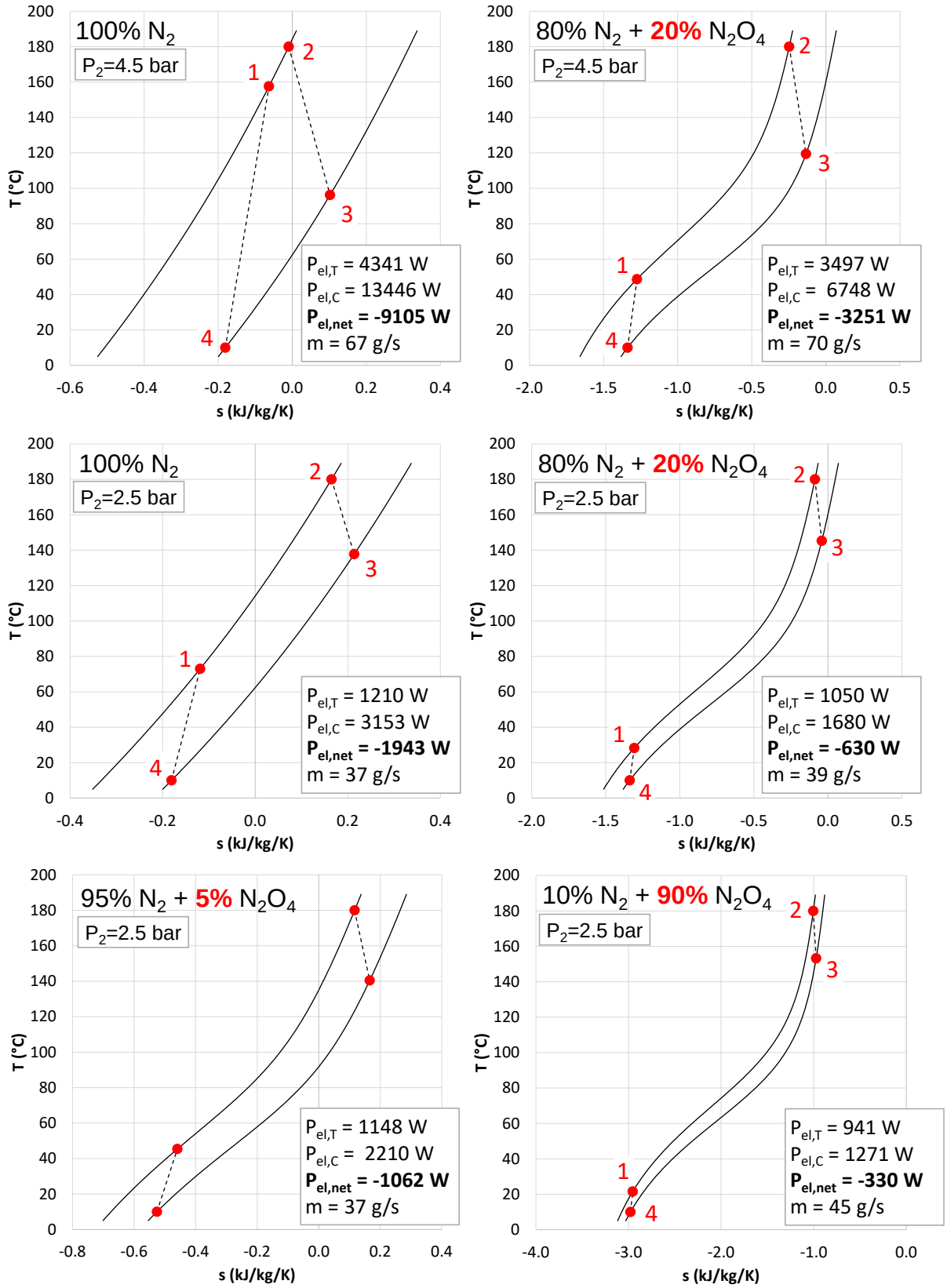

Figure 63. Temperature (T) vs. entropy (s) diagrams showing the calculation of the thermodynamic points, turbine and compressor power, for different conditions, according to calculation mode n. 1. Different molar compositions are shown in the treated cases.

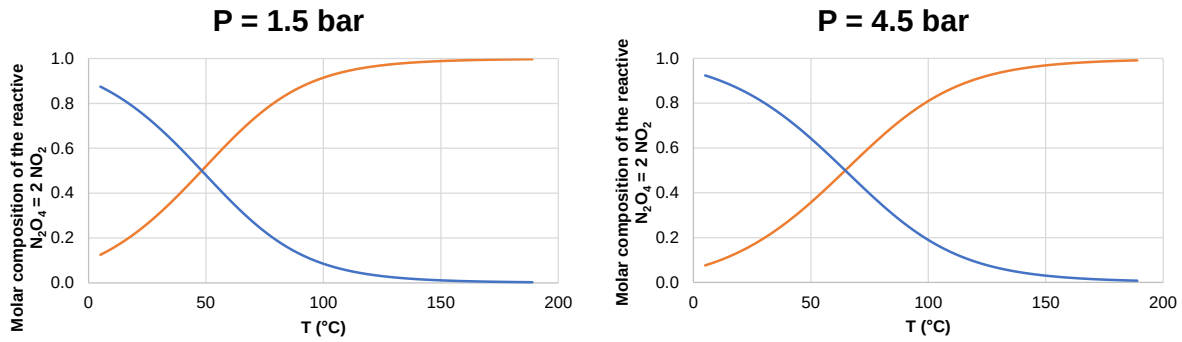

Figure 64. Evolution of the composition of the reactive fluid N_2O_4 = $2NO_2$, in the temperature range 0-190°C. Coherently with the calculations performed in this section, the ideal gas mixture assumption has been made to produce these results.

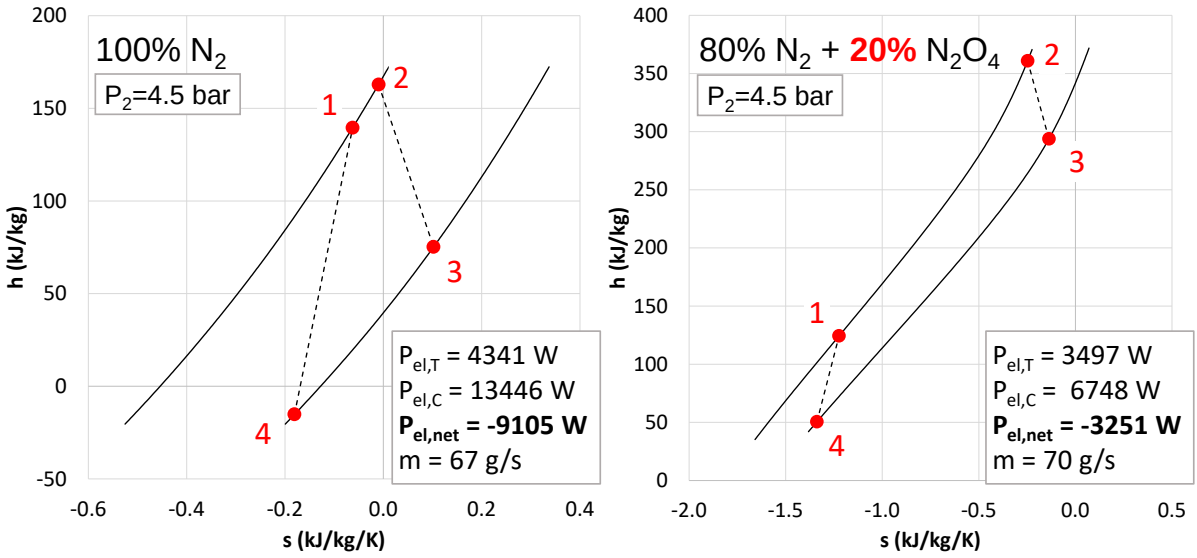

Figure 65. Enthalpy (h) vs. entropy (s) diagrams showing the calculation of the thermodynamic points, turbine and compressor power, for different conditions, according to calculation mode n. 1.

5.3.3. The electric heater and the cooler

Considering the different cases in Figure 63, and the fact that the pilot will operate either with pure N_2 or with maximum $5\%_{molar}$ of N_2O_4 in 95% of inert, a 8.5 kW_{el} **electric heater** will be sufficient to heat the fluid up to 180 °C. A regulation of the heat provided to the cycle will be performed to ensure the achievement of the inlet turbine temperature of 180 °C.

The electric heater has been bought and has an inlet and outlet diameter of DN 65.

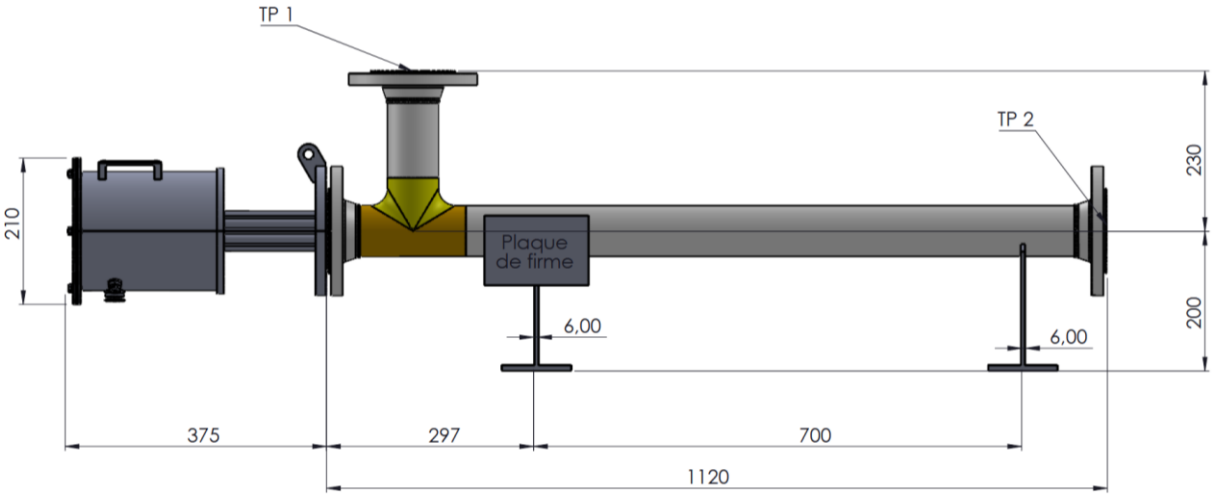

Figure 66. Electric heater by SELETECH EQUIPEMENT SAS. Sizes are in millimetres.

A shall and tube cooler has been acquired, in order to cool down the gas exiting the turbine, with cold water coming from a centralised (close loop) refrigeration system of the laboratory, delivering water at 7 °C. The inlet and outlet diameters of the heat exchanger are DN125.

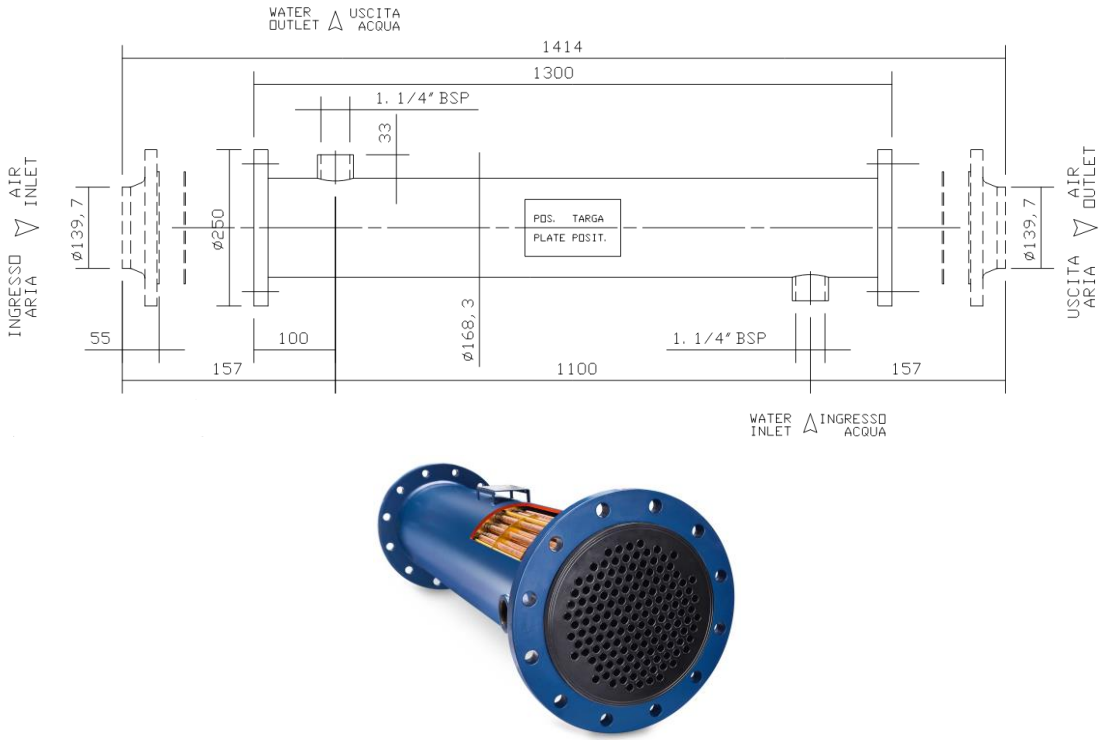

Figure 67. The shell-and-tubes heat exchanger, by Parker. Sizes are in millimetres.

5.3.4. The operation of the pilot and the regulation valves

The starting-up of the pilot as well as the more flexible coupling of the compressor and of the turbine have led to the necessity of including two regulation valves: V1 and V2 shown in Figure 56 and Figure 57. The procedure to operate the pilot in ***open cycle configuration*** (Figure 57) is described below.

Start-up phase

1. Initial condition: valve V1 is 100% open, valve V2 is closed, the generator is preheated at 65°C.
2. The compressor is switched on (100% of its flow rate crosses the by-pass and the outlet pressure of the compressor is defined by the ambient pressure, increased by the pressure drops in the line from the compressor to the outlet, passing through the bypass).
3. Once stationary conditions are attained, the drive feeds the turbine and allows the ramp of the turbo-generator up to 32 000 rpm.
4. The valve V2 is opened progressively at 100%. The opening time will be defined during first operations.

Operation at full load

5. Once stationary conditions are attained, measurements are recorded (condition with V1 and V2 100%-open).
6. The regulation (increase) of the electrical power of the turbine, to test different conditions, is then performed by progressively closing V1.

Turbo-generator shutdown

7. The valve V1 is progressively opened at 100%
8. The valve V2 is progressively closed.

The valves have been chosen, as outlined below, so that the above-mentioned procedure can be operated. Selecting a regulation valve consists in defining its K_{vs} (i.e., the valve coefficients that defines the pressure loss at 100% open condition).

Choice criteria for V2. For a given mass flow rate of the valve V2, it is necessary that the pressure drop through the valve is very low when it is 100% open. That means that the coefficient K_{vs} of the valve V2 must be high. Also, it has been necessary to guarantee that this valve, **in 100% open position and V1 totally closed**, enables the achievement of at least **2 kW of turbine outlet electric power**.

Choice criteria for V1. Concerning the valve V1, K_{vs} is selected so that **when both valves are 100% open, the output turbine electric power is maximum equal to zero.**

The quantitative characterisation of suitable valves has required the modelling of the cycle operating with the regulation valves and thus the assessment of the mass flow distribution in the bypass and in the turbine branch. The overall procedure for the calculation of the open cycle

configuration, represented in Figure 68, is summarized in the scheme in Figure 69 and introduced below.

Let us fix a desired outlet electric turbine power. As it has been shown in section 5.3.2 (Figure 62), given a specific outlet turbine pressure and inlet temperature, the inlet pressure of the turbine and the mass flow rate crossing the turbine can be calculated to ensure the production of the specific power output. In the case of the open cycle shown in Figure 68, the outlet pressure of the turbine is a function of the ambient pressure (pressure of point 4) and of the pressure drops in the pipes, which are in turn a function of the mass flow rate of the turbine and of the compressor. The mass flow rate in point 1 is imposed by the compressor and is fixed by the rotational speed of the screw motor. The calculation of the cycle is thus iterative and a summary of the process is shown in Figure 69. It is pointed out that pressure drops in each element of the system had to be modelled. Pressure drops in pipes, heat exchangers, elbows, diameter restrictions, etc., have been modelled according to the models present in the book by Idel'cik [189].

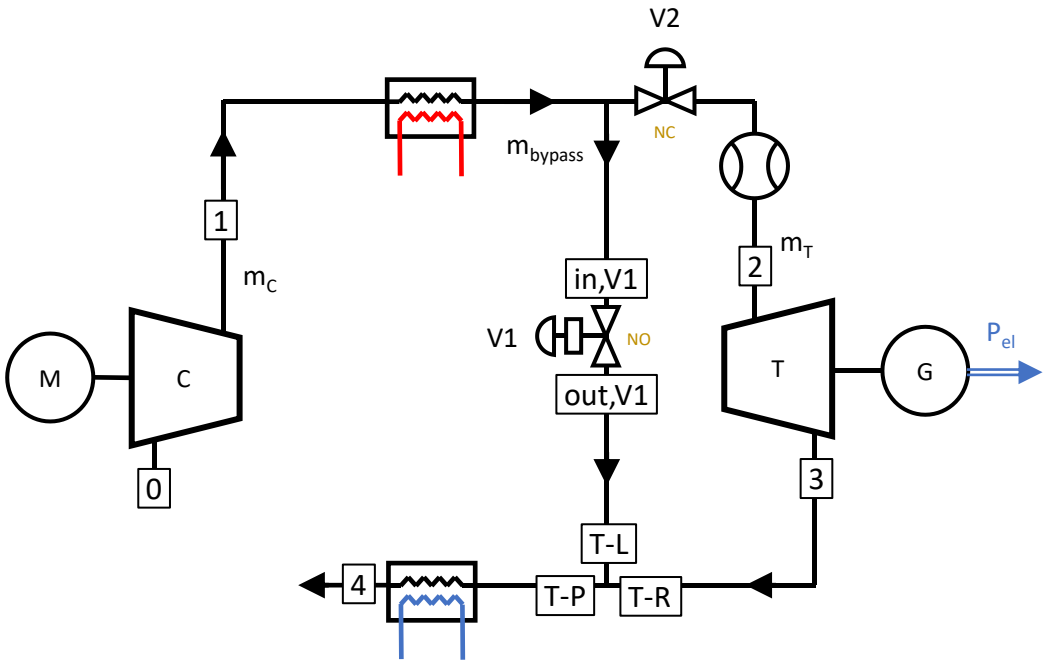

Figure 68. Layout of the pilot, with the nomenclature of points used in the process described in Figure 69.

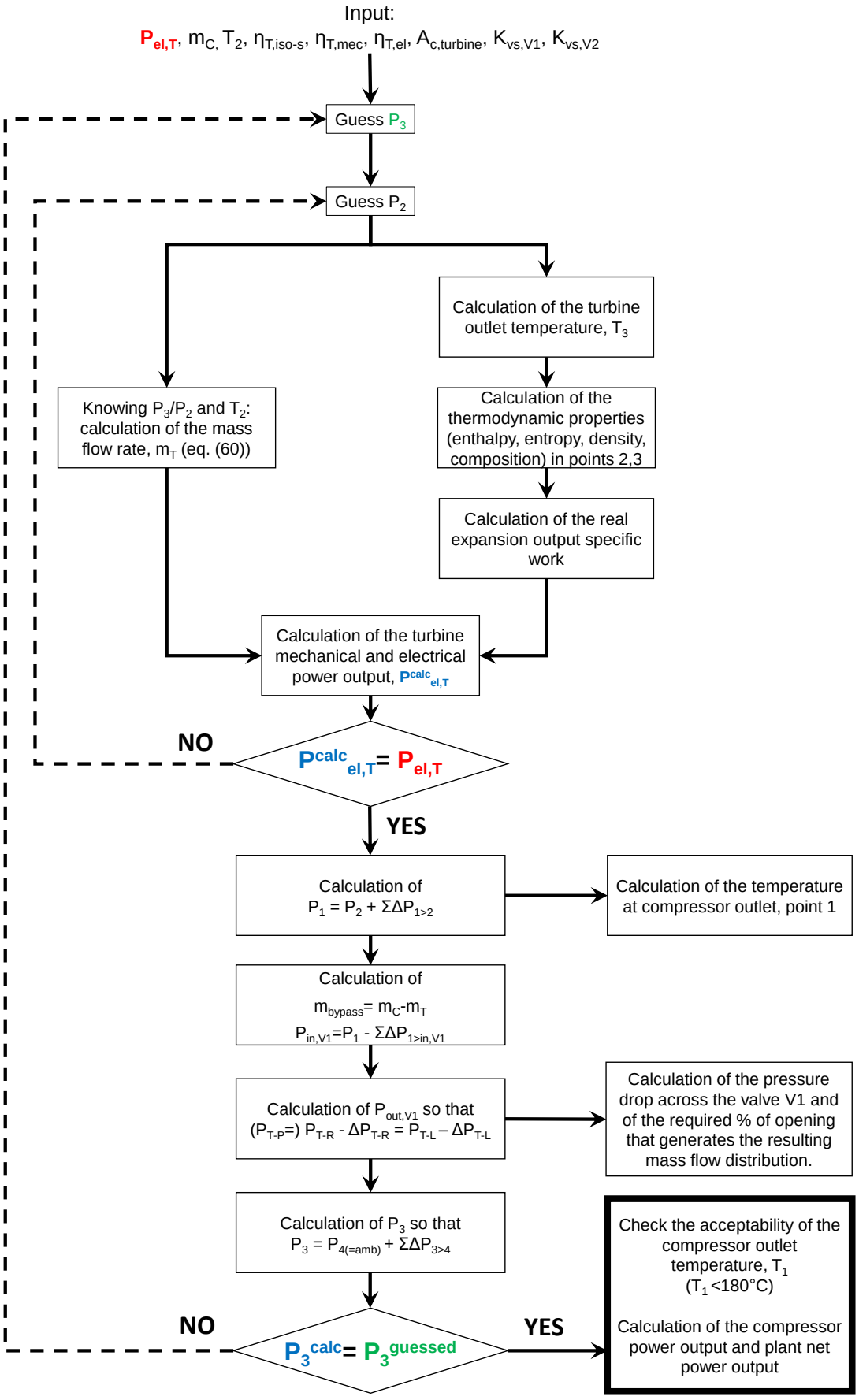

Figure 69. Procedure applied for the pilot operation in open cycle configuration.

The results of these calculations in the different case studies, also considering the importance of not exceeding 180 °C at the compressor outlet, have allowed the selection of valves with a maximum K_{vs} = 16.

If we fix a compressor mass flow rate of **42 g/s**, the calculations with pure N_2 say that:

- When V1 and V2 are 100% open, the mass flow rate passing in the turbine is about 8 g/s and the generator produces 30 W (a very low power, as desired), and the outlet pressure of the compressor is 1.09 bar, slightly higher than the input inlet pressure of 1 bar.
- When V1 is totally closed and V2 is 100% open, the compressor pressure outlet is 3 bar (and the temperature about 180 °C) and the generator should produce 2.2 kW.

The different operating conditions, with the various opening positions of the valves, are currently under determination.

This part of the work has been in collaboration with Alexis Sesmat, engineer at General Electric and contributor to this work on a volunteer basis as a member of the association APSIIS ("Association de préfiguration de sociétés d'intégration et ingéniuerie systèmes").

The operation of the cycle in closed loop (Figure 56) still has to be modelled.

5.3.5. The complete vision of the pilot

The services SERM (Service Etudes et Réalisation Mécanique - *Mechanical Design and Production Department*) and SIEL (Service Instrumentation et Electronique du Laboratoire - *Instrumentation and Electronics Department*) of the laboratory LRGP are working with the applicant to the physical realization of the pilot. The compete vision of the pilot (current version) is shown in Figure 70. The overall size is 3.42 m x 2.82 m x 2.05 m (H).

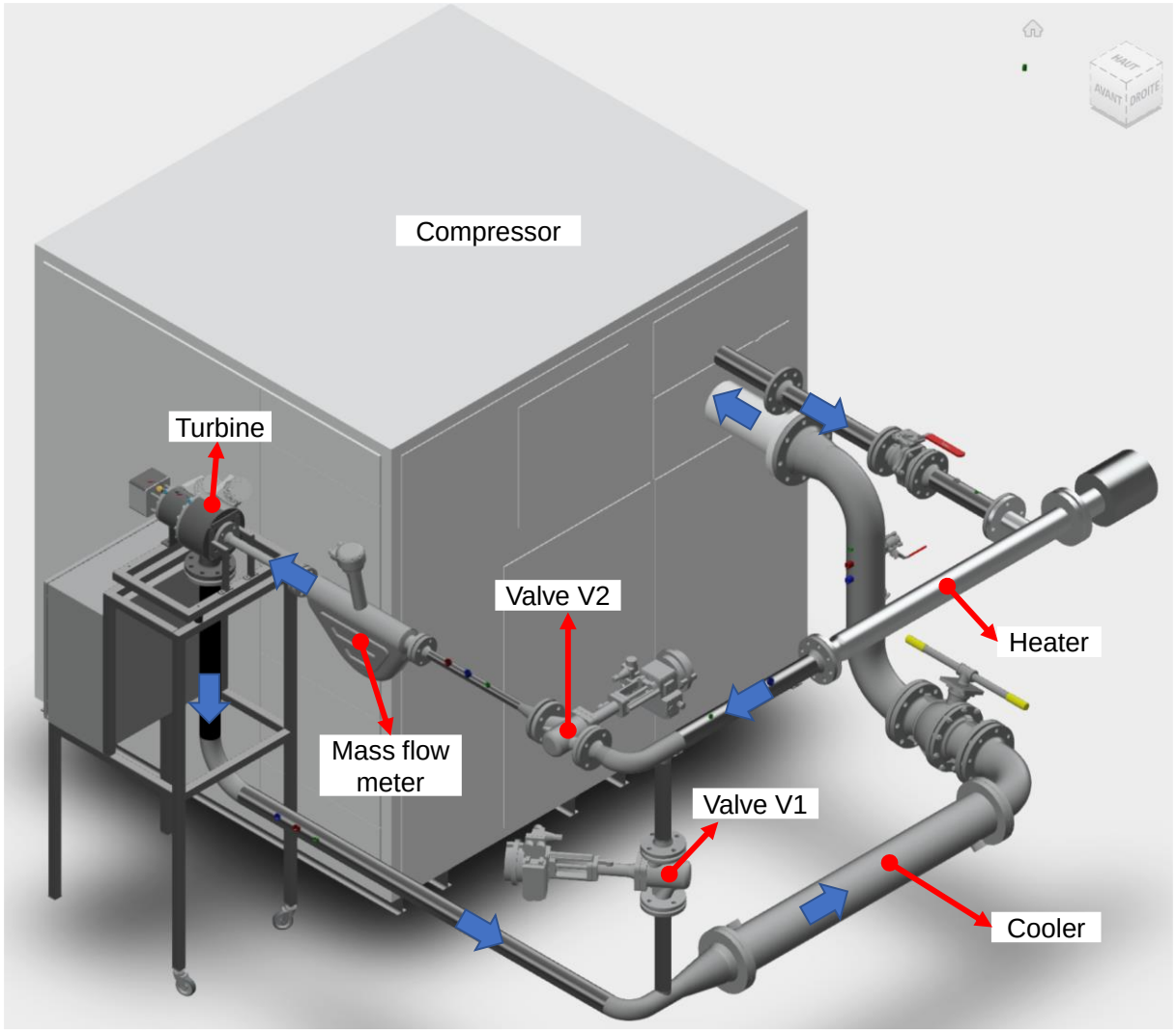

Figure 70. Layout of the pilot.

The pilot realization will be completed in April 2024 and the first tests in open loop will be realized in May 2024.

5.3.6. Procedure to charge the closed cycle

The precise procedures that will be followed to fill the cycle with the working fluid is outlined in the following.

I. Calculate the **total mass of gas** that must be introduced in the cycle to guarantee normal operation in stationary conditions:
   a. With the sizes of the pilot elements, calculate the **volume of the gas** (m^3) occupied in the piping and in the unit operations;

b. Calculate the **density of the gas** (kg/m^3) in each pipe and unit operations, in stationary -nominal- operation of the pilot (knowing by simulations the temperature and pressure in each point of the cycle).
c. From point a) and b), calculate the **total mass of gas** that must be introduced in the cycle (=density*volume).

II. When the pilot is switched off, the volume of the gas fills all the loop at a uniform temperature (the ambient one) and pressure. To charge the gas, we need to compress the gas in the whole pilot loop up to the pressure level that ensures the charging of the total mass of gas previously calculated. This pressure level can be calculated directly from the density of the gas and its -ambient- temperature. In turn, the density is calculated from the total volume and mass of gas obtained in I.a and I.c. Finally, the determined pressure is the searched pressure level at which the gas must be charged.

However, the leakages of the compressor will imply the necessity of refilling the cycle during operation. This necessity will be investigated during the first running of the closed cycle with pure nitrogen.

Conclusion

During ten years of research since the beginning of her PhD, the applicant had the possibility to deepen her knowledge in different fields of Energy and Chemical Engineering. She contributed to the improvement in modelling the thermodynamics of CO_2-based mixtures treated by carbon capture processes, air and quantum fluids (e.g., hydrogen) in cryogenic units, and working fluids of -conventional and novel- thermodynamic cycles for power- and tri-generation. Also, she has been working on the development of methodologies for the selection of pure fluids, or even the design of inert mixtures or novel reactive fluids used as working media for thermodynamic cycles, in general.

To thoroughly develop these topics, she needed to complement her Energy Engineering background with Chemical Engineering knowledge. She thus looked for research collaborations worldwide. The most fruitful ones which marked her research track have been tighten with the team "Thermodynamique et Energie"-ThermE, where she is currently working, the Group of Energy Conversion Systems - GECOS of "Politecnico di Milano" (Italy), the Mechanical Department of the "Università di Brescia" (Italy), the research group directed by Prof. Thijs Vlugt at TU Delft (Holland), the partners involved in the European project REGEN-by-2, prof. Ø. Wilhelmsen and his collaborators at NTNU (Norway). Thanks to the multiple collaborations that she has been able to establish, the research work that the applicant has developped has been rewarded with one fellowship and four prizes.

The present research activities of the applicant mainly aim to investigate the impact of using reactive -instead of inert- working fluids in thermodynamic cycles. The breakthrough character of this -fundamental and applicative- research field has been funded by two grants of excellence: **ANR- Jeune-Chercheur-Jeune-Chercheuse – 2021**, funding of over 230.000€, which was awarded to the applicant by the French National Scientific Research Agency; **ERC-Starting Grant – 2021**, funding of 1.5M€, which was also awarded to the applicant by the European Research Council. To avoid double funding, due to the overlapping of some of the topics treated in the two funded projects, the applicant had to decline the ANR-JCJC funding.

The ERC funding gave to the applicant the possibility of hiring five researchers (2 doctoral students and 3 postdoctoral students), who are currently co-working with here to develop the project, under her supervision. In parallel, the applicant is currently involved in the co-direction of 2 more PhD thesis, one about the development of thermodynamic measurements and models for CO_2 storage, and the other one about the coupling of quantum mechanics and artificial intelligence. The applicant is gaining supervision experience, from both the scientific and

human viewpoint, from the daily and intense work with a very international (and extremely multi-cultural) team, and thanks to the precious advices of her mentor, prof. Jean-Noël Jaubert.

In the period January-March 2024, the applicant is submitting three more research projects, in response to the call for project: 1) “France2030-i-démo3”, in collaboration with two Industries (General Electric and NEEXT Engineering, the coordinator), with the aim to develop a power plant of 1 MW_{el} operating with reactive working fluids; 2) “ERC Proof of Concept”, to develop a residential heat pump operating with reactive working fluids, at TRL4; 3) “PEPR SPLEEN”, to develop high-temperature (higher than 200 °C) heat pumps for industrial heating processes, whose improvement currently represents one of the main industrial need.

For completeness, it is highlighted that the applicant is also a teacher at the Chemical Engineering school ENSIC and in the Master programme DENSYS (Decentralised Energy conversion Systems), both part of University of Lorraine. She has the chance to *teach* some of the topics of her daily research (Energy conversion systems, at DENSYS, Thermodynamics, at ENSIC). Also, at ENSIC, she is (or, has been) involved in the *teaching* of Fortran language, process control and monitoring, techno-economic optimisation of processes, *practical works* in distillation, liquid-liquid extraction, pressure drop calculations, heat exchangers. Due to the intense research activity, the applicant had to reduce her teaching hours, from about 250 to 80 hours/year, but in perspective she would love to have the possibility of being much more involved in the Thermodynamics teachings at ENSIC.

To conclude, this application for the “authorisation to conduct research” is motivated by the applicant’s desire to carry out, within a short period of time, multiple and intensive research aimed at contributing to the urgent need to improve the efficiency of energy conversion processes.

Resumé en français

Le domaine de la « thermodynamique des systèmes de conversion d'énergie » représente le cœur des activités couvertes par la formation universitaire, les études doctorales et postdoctorales de la candidate, Silvia Lasala. Actuellement, elle est maître de conférences à l'Université de Lorraine, elle enseigne à l'École Nationale Supérieure des Industries Chimiques (ENSIC) et effectue ses recherches au Laboratoire Réactions et Génie des Procédés (LRGP), unité mixte de recherche du CNRS (Centre National de la Recherche Scientifique) et de l'Université de Lorraine.

La candidate a obtenu les titres d'ingénieur et docteur en « Sciences et technologies énergétiques et nucléaires » à l'Ecole Polytechnique de Milan. Elle a été initiée au domaine de la recherche en 2011, avec la préparation de sa thèse de Master dans le département R&D « Combustion and Casings » de Rolls-Royce plc, au Royaume-Uni. En effet, conscient de la nécessité de réduire les émissions d'oxydes d'azote de ses moteurs aéronautiques et d'aborder le problème des instabilités de combustion qui en découle, Rolls-Royce avait fait appel à l'école Polytechnique de Milan. Dans ce contexte, la candidate a été sélectionnée pour développer une chambre de combustion expérimentale et un modèle semi-empirique pour prédire l'apparition de modes instables de combustion se produisant dans les chambres annulaires des turbines aéronautiques fonctionnant avec du kérosène liquide. Traitant de la compréhension des interactions entre la thermo-acoustique de la chambre de combustion et la dynamique de la flamme, ce sujet a permis à la candidate de se familiariser avec le domaine et la rigueur de la recherche scientifique.

En 2012, elle a commencé une thèse de doctorat européen [1] sous la direction du professeur Paolo Chiesa, de l'école Polytechnique de Milan, et en collaboration avec le professeur Jean-Noël Jaubert, de l'ENSIC-LRGP. Sa recherche doctorale a porté sur l'étude théorique et expérimentale de la thermodynamique des fluides impliqués dans les technologies de captage et de stockage du CO_2. Les quatre contributions majeures de ces activités de recherche doctorale [2–7] sont : **1) L'amélioration des équations d'état cubiques.** Visant à définir une équation d'état cubique qui soit à la fois précise et cohérente d'un point de vue thermodynamique, ce travail a corrigé deux des incohérences théoriques de cette famille d'équations d'état affectant la modélisation des fluides purs et des mélanges. Plus précisément, le développement théorique des équations d'état pour les fluides purs a consisté en la dérivation et l'application de critères théoriques pour définir la relation fonctionnelle entre le paramètre énergétique d'une équation d'état et la température [2,4]; en ce qui concerne la modélisation des mélanges, cette étude a

quantifié la précision de nouvelles règles de mélange avancées qui couplent une équation d'état cubique avec la partie résiduelle de l'énergie d'Helmholtz d'excès calculée à partir du modèle de Wilson (règles de mélange notées "EoS/$a^{E\text{-}Wilson}{}_{res}$" dans ce qui suit) [3]. **2) La mesure des propriétés thermodynamiques des mélanges en équilibre liquide-vapeur.** L'optimisation et la validation du modèle thermodynamique proposé (et de tous les modèles thermodynamiques disponibles aujourd'hui) nécessitent des données expérimentales. En raison de l'insuffisance des données disponibles, une campagne expérimentale a été menée dans ce travail afin de déterminer les propriétés thermodynamiques des mélanges CO_2-O_2, CO_2-N_2, CO_2-Ar, CO_2-N_2-O_2, CO_2-N_2-Ar en équilibre liquide-vapeur pour des températures comprises entre 223 K et 293 K et des pressions allant de 10 à 200 bar. **3) L'optimisation et la validation de l'équation d'état développée dans cette étude.** La thèse présente l'optimisation et la comparaison de deux modèles : l'équation d'état de Peng-Robinson modifiée par l'application des règles de mélange "EoS/$a^{E\text{-}Wilson}{}_{res}$" développée au cours de l'étude (nouveau modèle) et l'équation d'état de Peng-Robinson standard (modèle de comparaison couramment utilisé). Ces deux modèles ont été optimisés sur des données expérimentales d'équilibre liquide-vapeur disponibles parmi les 36 mélanges binaires résultant de la combinaison de 9 composés typiquement présents dans les effluents des procédés de captage du CO_2 : H_2, N_2, CO, Ar, O_2, CH_4, CO_2, H_2S, H_2O. Compte tenu des données disponibles dans la littérature et de celles acquises dans cette étude, il a été possible d'optimiser le modèle sur 23 mélanges binaires. La validation et la comparaison des deux modèles ont été effectuées à l'aide de données disponibles sur des mélanges ternaires en équilibre liquide-vapeur et de données d'enthalpies et de densités de mélange. Les résultats ont confirmé la supériorité du modèle proposé dans cette étude. **4) L'évaluation de l'impact industriel de la précision du modèle thermodynamique développé**. Les effets de la précision de l'équation d'état ont été quantifiés lors du dimensionnement et du calcul des performances d'une unité de purification et de compression de mélanges issus des procédés de postcombustion, de précombustion et d'oxycombustion. Les études menées ont concerné : (1) la purification du CO_2 par liquéfaction et distillation ; (2) la détermination de la pression du CO_2 pour garantir son transport à l'état liquide ou supercritique ; (3) le calcul de l'énergie nécessaire pour pressuriser le mélange à base de CO_2 jusqu'à la pression de transport. L'effet le plus important lié à la précision du modèle thermodynamique utilisé a été observé lors du calcul du nombre de plateaux dans une colonne de distillation pour réduire à 100 ppm le niveau d'oxygène présent dans le flux de CO_2 capté : l'équation d'état introduite dans cette étude, contrairement aux modèles couramment utilisés, prédit un nombre de plateaux nécessaires pour atteindre l'objectif qui est divisé par deux.

Au cours de ses études doctorales et au début de ses recherches postdoctorales, la candidate a également étudié, avec des collègues de l'école Polytechnique de Milan et de l'Université de Brescia, certains moyens d'accroître l'efficacité des cycles de puissance utilisés pour valoriser le contenu énergétique de sources de chaleur disponibles à basse température (max. 400 °C) et, éventuellement, de sources froides à haute température (supérieure à 30 °C). Plus précisément, elle a contribué à la conception, à la caractérisation expérimentale et à la modélisation thermodynamique des fluides de travail pour les cycles de puissance. Elle s'est tout d'abord concentrée sur la comparaison de cycles fonctionnant avec du CO_2 ou des molécules organiques, en considérant différentes caractéristiques de la source de chaleur (température maximale et degré de refroidissement). Les résultats ont été cartographiés de manière à mettre en évidence le fluide de travail et la configuration du cycle les mieux adaptés aux caractéristiques de la source de chaleur. Cependant, la détermination de la stabilité thermique des fluides de travail (c'est-à-dire leur capacité à conserver leur structure moléculaire à une température spécifiée) était peu fiable car la limite de stabilité thermique des molécules organiques est rarement connue. Grâce à la collaboration avec le professeur Invernizzi, la candidate a pu effectuer, à l'université de Brescia, la caractérisation expérimentale de la limite de stabilité thermique de différentes molécules d'intérêt pour des cycles organiques de Rankine (perfluorohexane, n-pentane, cyclopentane et toluène [8,9]), ou pour être mélangées à du CO_2 pour une utilisation dans des cycles de puissance transcritiques [10]. Bien qu'elle ait conçu un système pour mesurer la stabilité thermique des mélanges, cette activité expérimentale s'est malheureusement limitée à l'étude de la stabilité thermique des fluides purs. A ce stade, soulignons que l'étude expérimentale de la stabilité thermique des fluides de travail pour les cycles de puissance et les pompes à chaleur, ainsi que l'impact d'un faible degré (acceptable ?) d'instabilité moléculaire sur les performances des installations, sont des domaines de recherche insuffisamment étudiés, qui mériteraient davantage d'attention de la part de la communauté scientifique.

En 2016, juste après avoir soutenue sa thèse de doctorat, la candidate a débuté un stage postdoctoral de deux ans au LRGP. Ce stage, financé par Air Liquide, comportait deux volets principaux. Le premièr consistait à modéliser les propriétés thermodynamiques et de transport des fluides impliqués dans les procédés cryogéniques de séparation des principaux composants de l'air (azote, oxygène et argon) [11]. Un deuxième volet était la réalisation d'une étude bibliographique sur l'état de l'art des procédés catalytiques de liquéfaction de l'hydrogène. En effet, l'hydrogène existe sous forme de deux isomères de spin appelés ortho-hydrogène (o-H_2)

et para-hydrogène (p-H_2). La proportion entre ces deux formes, dictée par l'équilibre thermodynamique de la réaction o-H_2 ⇄ p-H_2, varie avec la température. Au début du processus de liquéfaction de l'hydrogène (à température ambiante), le mélange gazeux se compose de 75 % d'o-H_2 et de 25 % de p-H_2 (un mélange connu sous le nom d'"hydrogène normal") ; à la température de stockage (20 K), le mélange liquide se compose de 99,8 % de p-H_2. La transformation de l'o-H_2 en p-H_2 est exothermique et se caractérise par un taux de conversion très faible. En raison de cette cinétique lente, l'hydrogène reste sous sa forme "normale" tout au long du processus de liquéfaction, jusqu'à la température de stockage (20 K) ; le liquide ainsi obtenu, composé à 75 % de o-H_2, subit une lente transformation exothermique spontanée qui convertit ces 75 % de o-H_2 en p-H_2 avec un dégagement de chaleur qui produit une évaporation partielle indésirable de l'hydrogène liquéfié. Pour remédier à cet inconvénient, la conversion de l'hydrogène ortho/para doit être effectuée pendant la liquéfaction à l'aide d'un catalyseur approprié qui augmente la vitesse de la réaction de conversion. Il avait été demandé à la candidate d'analyser en détail l'état de l'art relatif à la thermodynamique et la cinétique de la réaction ortho-hydrogène ⇄ para-hydrogène [12] et à l'effet catalytique de l'oxyde ferrique Fe_2O_3 sur la cinétique de la réaction. Elle a également développé un sous-programme contenant le modèle cinétique retenu, préalablement optimisé par Wilhelmsen et al [13], qui est actuellement utilisé dans le simulateur de procédé (ProSim) utilisé par Air Liquide pour les simulations de liquéfaction d'hydrogène.

La recherche sur la modélisation thermodynamique de l'hydrogène a ensuite été poursuivie en collaboration avec le professeur Ø. Wilhelmsen, de l'université norvégienne NTNU [14]. Il a proposé de collaborer dans le but de développer une équation d'état cubique précise et thermodynamiquement cohérente (c'est-à-dire respectant les critères de cohérence des fonctions α développés dans la thèse de la candidate et dans celle de Le Guennec et al. [4]) en appliquant une correction quantique au covolume de l'hydrogène. Cette correction a été étendue à d'autres fluides quantiques et a permis d'améliorer sensiblement la précision de la modélisation des fluides quantiques purs et de leurs mélanges.

Parallèlement au sujet postdoctoral susmentionné, la candidate a commencé à développer son propre projet de recherche, qu'elle a défendu à l'occasion de l'attribution de son poste actuel de maître de conférences, en 2018. Ce projet s'articule autour d'une question posée en 1957 par le professeur Lighthill [15] et reprise ensuite par divers auteurs, dont le professeur Angelino [16] de l'école Polytechnique de Milan : y-a-t-il un intérêt à détendre dans une turbine, ou à

comprimer dans un compresseur, des fluides réactifs, c'est-à-dire sièges d'une réaction chimique réversible ? En d'autres termes, quel est l'effet de la conversion simultanée de l'énergie thermique (physique) et chimique en travail mécanique dans les opérations unitaires présentes dans les cycles thermodynamiques ?

Pour répondre à cette question de manière générale (c'est-à-dire non spécifique à un fluide), la candidate a proposé de définir des fluides de travail réactifs fictifs et assimilés à des gaz parfaits afin d'évaluer l'impact de la thermochimie et de la stœchiométrie de chaque réaction sur les performances du cycle. Les premières conclusions, obtenues pour des cycles de Brayton, ont permis de mettre en évidence le fort potentiel de ces fluides réactifs [17]. Cette étude a alors été étendue à d'autres cycles thermodynamiques (pompes à chaleur basées sur le cycle de Brayton, cycles de pompes à chaleur et cycles de puissance de Stirling) qui sont actuellement étudiés par une doctorante sous la (co-)supervision de la candidate [18]. Les résultats prometteurs, d'une part, et la disponibilité limitée de fluides réactifs appropriés, d'autre part, ont incité la candidate à soumettre (et à obtenir) un projet de recherche ERC-Starting Grant (REACHER) visant à concevoir et à caractériser des fluides de travail réactifs appropriés, à concevoir les architectures optimales des cycles thermodynamiques et à valider ce potentiel prometteur des fluides réactifs en construisant une microcentrale électrique.

D'autres recherches ont été entreprises ces dernières années, en collaboration avec d'autres groupes de recherche nationaux et internationaux. Ce manuscrit présente les principales contributions passées, présentes et futures de la candidate, dans le domaine de la thermodynamique appliquée aux procédés énergétiques. Leur présentation suit un ordre thématique (non-chronologique), regroupé en cinq chapitres.

- *Chapitre 1.* Contributions à la caractérisation thermodynamique des fluides inertes purs et multi-constituants.
- *Chapitre 2.* Contributions à l'amélioration de l'efficacité des cycles thermodynamiques conventionnels.
- *Chapitre 3.* Étude et développement de cycles thermodynamiques fonctionnant avec des fluides de travail réactifs. Le projet ERC REACHER : des fluides de travail réactifs fictifs aux fluides de travail réactifs réels.
- *Chapitre 4.* Modélisation des mélanges réactifs (premiers résultats du projet ERC REACHER, présenté au chapitre 3).

- *Chapitre 5.* Conception d'une microcentrale électrique pour valider les résultats de REACHER (une deuxième série de résultats issus du projet REACHER, introduit au chapitre 3).

References

[1] S. Lasala, Advanced cubic equations of state for accurate modelling of fluid mixtures. Application to CO_2 capture systems, Politecnico di Milano, 2016.

[2] S. Lasala, Y. Le Guennec, R. Privat, J.-N. Jaubert, The role of alpha functions in the thermodynamic modeling of supercritical pure components, in: JETC 2015 - 13th Joint European Thermodynamics Conference, Nancy, 2015.

[3] S. Lasala, P. Chiesa, R. Privat, J.-N. Jaubert, VLE properties of CO2 - Based binary systems containing N2, O2 and Ar: Experimental measurements and modelling results with advanced cubic equations of state, Fluid Phase Equilibria 428 (2016) 18–31. https://doi.org/10.1016/j.fluid.2016.05.015.

[4] Y. Le Guennec, S. Lasala, R. Privat, J.-N. Jaubert, A consistency test for α-functions of cubic equations of state, Fluid Phase Equilibria 427 (2016). https://doi.org/10.1016/j.fluid.2016.07.026.

[5] S. Lasala, P. Chiesa, R. Privat, J.-N. Jaubert, Modeling the thermodynamics of fluids treated by CO2 capture processes with Peng-Robinson + residual Helmholtz energy-based mixing rules, Industrial and Engineering Chemistry Research 56 (2017). https://doi.org/10.1021/acs.iecr.6b04190.

[6] S. Lasala, P. Chiesa, R. Privat, J.-N. Jaubert, Measurement and prediction of multi-property data of CO2-N2-O2-CH4 mixtures with the "Peng-Robinson + residual Helmholtz energy-based" model, Fluid Phase Equilibria 437 (2017) 166–180. https://doi.org/10.1016/j.fluid.2017.01.016.

[7] S. Lasala, P. Chiesa, R. Privat, J.-N. Jaubert, Optimizing Thermodynamic Models: The Relevance of Molar Fraction Uncertainties, Journal of Chemical & Engineering Data 62 (2017) 825–832. https://doi.org/10.1021/acs.jced.6b00853.

[8] S. Lasala, C. Invernizzi, P. Iora, P. Chiesa, E. Macchi, Thermal Stability Analysis of Perfluorohexane, in: Energy Procedia, 2015: pp. 1575–1582. https://doi.org/10.1016/j.egypro.2015.07.358.

[9] C.M. Invernizzi, P. Iora, G. Manzolini, S. Lasala, Thermal stability of n-pentane, cyclo-pentane and toluene as working fluids in organic Rankine engines, Applied Thermal Engineering 121 (2017). https://doi.org/10.1016/j.applthermaleng.2017.04.038.

[10] S. Lasala, P. Chiesa, E. Macchi, Binary mixtures of carbon dioxide and fluorocarbons: review of thermodynamic data and their modelling, in: Lyon, France, 2014. https://doi.org/10.13140/RG.2.2.14853.58084.

[11] S. Lasala, R. Privat, J.-N. Jaubert, P. Arpentinier, Modelling the thermodynamics of air-component mixtures (N2, O2 and Ar): Comparison and performance analysis of available models, Fluid Phase Equilibria 458 (2018). https://doi.org/10.1016/j.fluid.2017.10.033.

[12] S. Lasala, R. Privat, P. Arpentinier, J.-N. Jaubert, Note on the inconsistent definition assigned in the literature to the heat capacity of the so-called "equilibrium hydrogen" mixture, Fluid Phase Equilibria 504 (2020) 112325. https://doi.org/10.1016/j.fluid.2019.112325.

[13] Ø. Wilhelmsen, D. Berstad, A. Aasen, P. Nekså, G. Skaugen, Reducing the exergy destruction in the cryogenic heat exchangers of hydrogen liquefaction processes, International Journal of Hydrogen Energy 43 (2018) 5033–5047. https://doi.org/10.1016/j.ijhydene.2018.01.094.

[14] A. Aasen, M. Hammer, S. Lasala, J.-N. Jaubert, Ø. Wilhelmsen, Accurate quantum-corrected cubic equations of state for helium, neon, hydrogen, deuterium and their

mixtures, Fluid Phase Equilibria 524 (2020) 112790. https://doi.org/10.1016/j.fluid.2020.112790.

[15] M.J. Lighthill, Dynamics of a dissociating gas. Part I: Equilibrium flow., Journal of Fluid Mechanics 2 (1957) 1–32.

[16] G. Angelino, Performance of N2O4 gas cycles for solar power applications, Proceedings of the Institution of Mechanical Engineers 1847-1982 (Vols 1-196) 193 (1979) 313–320. https://doi.org/10.1243/PIME_PROC_1979_193_033_02.

[17] S. Lasala, R. Privat, O. Herbinet, P. Arpentinier, D. Bonalumi, J.-N. Jaubert, Thermo-chemical engines: Unexploited high-potential energy converters, Energy Conversion and Management 229 (2021) 113685. https://doi.org/10.1016/j.enconman.2020.113685.

[18] A. Barakat, S. Lasala, P. Arpentinier, J.-N. Jaubert, The original and impactful exploitation of chemical energy in heat pumps, Chemical Engineering Journal Advances 12 (2022) 100400. https://doi.org/10.1016/j.ceja.2022.100400.

[19] IEAGHG, Effects of imputrities on geological storage of CO2, 2011.

[20] N.I. Diamantonis, G.C. Boulougouris, E. Mansoor, D.M. Tsangaris, I.G. Economou, Evaluation of cubic, SAFT, and PC-SAFT equations of state for the vapor-liquid equilibrium modeling of CO2 mixtures with other gases, Industrial and Engineering Chemistry Research 52 (2013) 3933–3942. https://doi.org/10.1021/ie303248q.

[21] H. Li, J. Yan, Evaluating cubic equations of state for calculation of vapor–liquid equilibrium of CO2 and CO2-mixtures for CO2 capture and storage processes, Applied Energy 86 (2009) 826–836. https://doi.org/10.1016/j.apenergy.2008.05.018.

[22] X. Xu, S. Lasala, R. Privat, J.-N. Jaubert, E-PPR78: a proper cubic EoS for modeling fluids involved in the design and operation of carbon dioxide capture and storage (CCS) processes, International Journal of Greenhouse Gas Control 56 (2017) 126–154.

[23] A. Anderko, Equations of State for Fluids and Fluid Mixtures, 2000. https://doi.org/10.1016/S1874-5644(00)80015-6.

[24] S.W. Løvseth, H.G.J. Stang, A. Austegard, S.F. Westman, R. Span, R. Wegge, Measurements of CO2-rich mixture properties: Status and CCS needs, in: Energy Procedia, 2016: pp. 469–478. https://doi.org/10.1016/j.egypro.2016.01.048.

[25] G.M. Kontogeorgis, G.K. Folas, Thermodynamic Models for Industrial Applications: From Classical and Advanced Mixing Rules to Association Theories, 2009. https://doi.org/10.1002/9780470747537.

[26] J.N. Jaubert, R. Privat, Thermodynamic Models for Chemical Engineering. Design, Develop, Analyse and Optimise., 1st edition, ISTE Press - Elsevier, 2021.

[27] G. Soave, Equilibrium constants from a modified Redlich-Kwong equation of state, Chemical Engineering Science 27 (1972) 1197–1203. https://doi.org/10.1016/0009-2509(72)80096-4.

[28] B.E. Poling, J.M. Prausnitz, J.P. O apos Connell, Properties of Gases and Liquids, in: Experimental Thermal and Fluid Science, 2007: pp. 1–803. https://doi.org/10.1036/0070116822.

[29] E. Neau, I. Raspo, J. Escandell, C. Nicolas, O. Hernández-Garduza, The Soave, Twu and Boston-Mathias alpha functions in cubic equations of state. Part II. Modeling of thermodynamic properties of pure compounds, Fluid Phase Equilibria 276 (2009) 156–164. https://doi.org/10.1016/j.fluid.2008.10.010.

[30] C.H. Twu, J.E. Coon, J.R. Cunningham, A new generalized alpha function for a cubic equation of state Part 1. Peng-Robinson equation, Fluid Phase Equilibria 105 (1995) 49–59. https://doi.org/10.1016/0378-3812(94)02601-V.

[31] G.M. Wilson, Vapor-Liquid Equilibrium. XI. A New Expression for the Excess Free Energy of Mixing, Journal of the American Chemical Society 86 (1964) 127–130. https://doi.org/10.1021/ja01056a002.

[32] H. Renon, J.M. Prausnitz, Local compositions in thermodynamic excess functions for liquid mixtures, AIChE Journal 14 (1968) 135–144. https://doi.org/10.1002/aic.690140124.

[33] D.S. Abrams, J.M. Prausnitz, Statistical thermodynamics of liquid mixtures: A new expression for the excess Gibbs energy of partly or completely miscible systems, AIChE Journal 21 (1975) 116–128. https://doi.org/10.1002/aic.690210115.

[34] H.-J. Huron, J. Vidal, New mixing rules for cubic equations of state for strongly nonideal mixtures, Fluid Phase Equilibria 3 (1979) 255–271.

[35] M.L. Michelsen, A modified Huron-Vidal mixing rule for cubic equations of state, Fluid Phase Equilibria 60 (1990) 213–219. https://doi.org/10.1016/0378-3812(90)85053-D.

[36] D.S.H. Wong, S.I. Sandler, A theoretically correct mixing rule for cubic equations of state, AIChE Journal 38 (1992) 671–680. https://doi.org/10.1002/aic.690380505.

[37] G.M. Kontogeorgis, P. Coutsikos, Thirty Years with EoS/GE Models - What Have We Learned?, Ind. Eng. Chem. Res. 51 (2012) 4119–4142.

[38] C. Coquelet, A. Valtz, F. Dieu, D. Richon, P. Arpentinier, F. Lockwood, Isothermal P, x, y data for the argon + carbon dioxide system at six temperatures from 233.32 to 299.21 K and pressures up to 14 MPa, Fluid Phase Equilib. 273 (2008) 38–43. https://doi.org/10.1016/j.fluid.2008.08.010.

[39] J.-N. Jaubert, R. Privat, Cubic equations of state: what's new since Van der Waals? Which future?, 26th European Symposium On Applied Thermodynamics Place: Potsdam, Germany, (2012).

[40] G. Dohrn, Ralf; Brunner, High pressure fluid-phase equilibria: Experimental methods and systems investigated, Fluid Phase Equilibria 106 (1995) 213–282.

[41] M. Christov, R. Dohrn, High-pressure fluid phase equilibria: Experimental methods and systems investigated (1994-1999), Fluid Phase Equilibria 202 (2002) 153–218. https://doi.org/10.1016/S0378-3812(02)00096-1.

[42] R. Dohrn, S. Peper, J.M.S. Fonseca, Fluid Phase Equilibria High-pressure fluid-phase equilibria: Experimental methods and systems investigated (2000–2004), Fluid Phase Equilibria 288 (2010) 1–54. https://doi.org/10.1016/j.fluid.2009.08.008.

[43] J.M.S. Fonseca, R. Dohrn, S. Peper, High-pressure fluid-phase equilibria: Experimental methods and systems investigated (2005-2008), Fluid Phase Equilibria 300 (2011) 1–69. https://doi.org/10.1016/j.fluid.2010.09.017.

[44] P. Stephanie, R. Dohrn, Sampling from fluid mixtures under high pressure: Review, case study and evaluation, The Journal of Supercritical Fluids 66 (2012).

[45] C.H. Twu, D. Bluck, J.R. Cunningham, J.E. Coon, A cubic equation of state with a new alpha function and a new mixing rule, Fluid Phase Equilibria 69 (1991) 33–50. https://doi.org/10.1016/0378-3812(91)90024-2.

[46] Y. Le Guennec, Développement d'équations d'état cubiques adaptées à la représentation de mélanges contenant des molécules polaires (eau, alcools, amines …) et des hydrocarbures, Ph.D. thesis, Université de Lorraine, 2018. http://www.theses.fr/2018LORR0245 (accessed September 25, 2021).

[47] R. Privat, M. Visconte, A. Zazoua-Khames, J.N. Jaubert, R. Gani, Analysis and prediction of the alpha-function parameters used in cubic equations of state, Chemical Engineering Science 126 (2015) 584–603. https://doi.org/10.1016/j.ces.2014.12.040.

[48] Y. Le Guennec, R. Privat, S. Lasala, J.N. Jaubert, On the imperative need to use a consistent α-function for the prediction of pure-compound supercritical properties with a cubic equation of state, Fluid Phase Equilibria 445 (2017) 45–53. https://doi.org/10.1016/j.fluid.2017.04.015.

[49] A. Pina-Martinez, Y. Le Guennec, R. Privat, J.-N. Jaubert, P.M. Mathias, Analysis of the combinations of property data that are suitable for a safe estimation of consistent Twu α-function parameters: updated parameter values for the translated-consistent *tc*-PR and *tc*-RK cubic equations of state, Journal of Chemical & Engineering Data 63 (2018) 3980–3988. https://doi.org/10.1021/acs.jced.8b00640.

[50] H.A. Lorentz, Ueber die Anwendung des Satzes vom Virial in der kinetischen Theorie der Gase, Annalen Der Physik 248 (1881) 127–136.

[51] S. Lasala, P. Chiesa, D. Di Bona, S. Consonni, Vapour – Liquid Equilibrium Measurements of CO2 based Mixtures: Experimental Apparatus and Testing Procedures, Energy Procedia 45 (2014) 1215–1224. https://doi.org/10.1016/j.egypro.2014.01.127.

[52] S. Lasala, P. Chiesa, R. Privat, J.-N. Jaubert, Modelling the thermodynamics of fluids treated by CO2-capture processes with "Peng-Robinson + residual Helmholtz energy-based mixing rules," Accepted for Publication on Industrial & Engineering Chemistry Research (2016).

[53] J.R. Elliott, V. Diky, T.A. Knotts, W.V. Wilding, The properties of gases and liquids, Sixth edition, McGraw Hill, New York Chicago San Francisco, 2023.

[54] Y. Le Guennec, R. Privat, J.-N. Jaubert, Development of the translated-consistent *tc*-PR and *tc*-RK cubic equations of state for a safe and accurate prediction of volumetric, energetic and saturation properties of pure compounds in the sub- and super-critical domains, Fluid Phase Equilibria 429 (2016) 301–312. https://doi.org/10.1016/j.fluid.2016.09.003.

[55] A. Pina-Martinez, R. Privat, J. Jaubert, Use of 300,000 pseudo-experimental data over 1800 pure fluids to assess the performance of four cubic equations of state: SRK, PR, *tc*-RK, and *tc*-PR, AIChE Journal 68 (2022) e17518. https://doi.org/10.1002/aic.17518.

[56] J.-N. Jaubert, Y. Le Guennec, A. Pina-Martinez, N. Ramirez-Velez, S. Lasala, B. Schmid, I.K. Nikolaidis, I.G. Economou, R. Privat, Benchmark database containing binary-system-high-quality-certified data for cross-comparing thermodynamic models and assessing their accuracy, Ind. Eng. Chem. Res. 59 (2020) 14981–15027. https://doi.org/10.1021/acs.iecr.0c01734.

[57] B. Creton, C. Nieto-Draghi, T. de Bruin, V. Lachet, E. El Ahmar, A. Valtz, C. Coquelet, S. Lasala, R. Privat, J.-N. Jaubert, Thermodynamic study of binary systems containing sulphur dioxide and nitric oxide: Measurements and modelling, Fluid Phase Equilibria 461 (2018). https://doi.org/10.1016/j.fluid.2017.12.036.

[58] J.-N. Jaubert, F. Mutelet, VLE predictions with the Peng-Robinson equation of state and temperature dependent kij calculated through a group contribution method, Fluid Phase Equilibria 224 (2004) 285–304. https://doi.org/10.1016/j.fluid.2004.06.059.

[59] J.-N. Jaubert, J.-W. Qian, S. Lasala, R. Privat, The impressive impact of including enthalpy and heat capacity of mixing data when parameterising equations of state. Application to the development of the E-PPR78 (Enhanced-Predictive-Peng-Robinson-78) model., Fluid Phase Equilibria 560 (2022) 113456. https://doi.org/10.1016/j.fluid.2022.113456.

[60] K. Saadallah, V. Lachet, B. Creton, M.-C. Caumon, A. Randi, J. Sterpenich, Solubility study of binary systems containing sulfur dioxide and water: A combination of Raman spectroscopy and Monte Carlo molecular simulation, Fluid Phase Equilibria 574 (2023) 113901. https://doi.org/10.1016/j.fluid.2023.113901.

[61] N. Juntarachat, P.D. Beltran Moreno, S. Bello, R. Privat, J.-N. Jaubert, Validation of a new apparatus using the dynamic and static methods for determining the critical properties of pure components and mixtures, Journal of Supercritical Fluids 68 (2012) 25–30. https://doi.org/10.1016/j.supflu.2012.04.004.

[62] S. Quoilin, M.V.D. Broek, S. Declaye, P. Dewallef, V. Lemort, Techno-economic survey of Organic Rankine Cycle (ORC) systems, Renewable and Sustainable Energy Reviews 22 (2013) 168–186. https://doi.org/10.1016/j.rser.2013.01.028.

[63] E. Wang, C.N. Markides, Y. Lu, V. Lemort, Editorial: Organic Rankine Cycle for Efficiency Improvement of Industrial Processes and Urban Systems, Front. Energy Res. 8 (2020). https://doi.org/10.3389/fenrg.2020.569868.

[64] A. Mota-Babiloni, P. Makhnatch, R. Khodabandeh, Recent investigations in HFCs substitution with lower GWP synthetic alternatives: Focus on energetic performance and environmental impact, International Journal of Refrigeration 82 (2017) 288–301. https://doi.org/10.1016/j.ijrefrig.2017.06.026.

[65] T.E.P. and the C. of the E. Union, Regulation (EU) No 517/2014 of the European Parliament and the Council of 16 April 2014 on fluorinated greenhouse gases and repealing Regulation (EC) No 842/2006, Off. J. Eur. Union (2014) 195–230.

[66] ASHRAE, ANSI/ASHRAE 34-2019, Designation and Safety Classification of Refrigerants, Atlanta, USA, 2019.

[67] M.O. McLinden, A.F. Kazakov, J.S. Brown, P.A. Domanski, A thermodynamic analysis of refrigerants: Possibilities and tradeoffs for Low-GWP refrigerants, International Journal of Refrigeration-Revue Internationale Du Froid 38 (2014) 80–92. https://doi.org/10.1016/j.ijrefrig.2013.09.032.

[68] M.O. McLinden, J.S. Brown, R. Brignoli, A.F. Kazakov, P.A. Domanski, Limited options for low-global-warming-potential refrigerants, Nature Communications 8 (2017) 14476. https://doi.org/10.1038/ncomms14476.

[69] M.O. McLinden, M.L. Huber, The (R)Evolution of Refrigerants: How Did We Get Here? Where Are We Going?, IIR Rankine Conference 2020, Boulder, Colorado, 2020.

[70] Regulation (EC) No 1005/2009 of the European Parliament and of the Council of 16 September 2009 on substances that deplete the ozone layer (Text with EEA relevance), (2009). https://eur-lex.europa.eu/eli/reg/2009/1005/oj/eng (accessed April 1, 2021).

[71] J.M. Cullen, J.M. Allwood, Theoretical efficiency limits for energy conversion devices, Energy 35 (2010) 2059–2069. https://doi.org/10.1016/j.energy.2010.01.024.

[72] M. Astolfi, D. Alfani, S. Lasala, E. Macchi, Comparison between ORC and CO2 power systems for the exploitation of low-medium temperature heat sources, Energy 161 (2018) 1250–1261. https://doi.org/10.1016/j.energy.2018.07.099.

[73] M. Astolfi, S. Lasala, E. Macchi, Selection maps for ORC And CO2 systems for low-medium temperature heat sources, Energy Procedia 129 (2017) 971–978. https://doi.org/10.1016/j.egypro.2017.09.217.

[74] REGEN-BY-2, (n.d.). https://www.regen-by-2.eu/.

[75] D. Bonalumi, E. Macchi, S. Lasala, CO2-based mixture for energy production, US 2020/0270496, n.d.

[76] S. Lasala, D. Bonalumi, E. Macchi, R. Privat, J.N. Jaubert, The design of CO2-based working fluids for high-temperature heat source power cycles, in: Energy Procedia, 2017: pp. 947–954. https://doi.org/10.1016/j.egypro.2017.09.125.

[77] D. Bonalumi, S. Lasala, E. Macchi, CO2-TiCl4 working fluid for high-temperature heat source power cycles and solar application, Renewable Energy 147 (2020) 2842–2854. https://doi.org/10.1016/j.renene.2018.10.018.

[78] S. Lasala, A. Pina-Martinez, J.-N. Jaubert, A predictive equation of state to perform an extending screening of working fluids for power and refrigeration cycles, in: S. Lasala (Ed.), Organic Rankine Cycles for Waste Heat Recovery - Analysis and Applications, IntechOpen, 2020. https://doi.org/10.5772/intechopen.92173.

[79] S.A. Gornati, D. Di Bona, P. Chiesa, New experimental VLE data for the binary mixture of carbon dioxide + perfluorohexane (CO2 + C6F14) from 273 K to 333 K, Fluid Phase Equilibria 498 (2019) 94–103. https://doi.org/10.1016/j.fluid.2019.06.024.

[80] US Patent Application for CO2-BASED MIXTURES AS WORKING FLUID IN THERMODYNAMIC CYCLES Patent Application (Application #20220056328 issued February 24, 2022) - Justia Patents Search, (n.d.). https://patents.justia.com/patent/20220056328 (accessed January 16, 2024).

[81] Supercritical CARbon dioxide/Alternative fluids Blends for Efficiency Upgrade of Solar power plants | SCARABEUS Project | Fact Sheet | H2020, CORDIS | European Commission (n.d.). https://cordis.europa.eu/project/id/814985/fr (accessed January 16, 2024).

[82] G. Di Marcoberardino, E. Morosini, D. Di Bona, P. Chiesa, C. Invernizzi, P. Iora, G. Manzolini, Experimental characterisation of CO2 + C6F6 mixture: Thermal stability and vapour liquid equilibrium test for its application in transcritical power cycle, Applied Thermal Engineering 212 (2022) 118520. https://doi.org/10.1016/j.applthermaleng.2022.118520.

[83] O.A. Aqel, M.T. White, M.A. Khader, A.I. Sayma, Sensitivity of transcritical cycle and turbine design to dopant fraction in CO2-based working fluids, Applied Thermal Engineering 190 (2021) 116796. https://doi.org/10.1016/j.applthermaleng.2021.116796.

[84] Next REnewable multi-GENeration technology enabled by TWO-phase fluids machines | REGEN-BY-2 Project | Fact Sheet | H2020, CORDIS | European Commission (n.d.). https://cordis.europa.eu/project/id/851541/fr.

[85] S. Briola, PLANT AND METHOD FOR THE SUPPLY OF ELECTRIC POWER AND/OR MECHANICAL POWER, HEATING POWER AND/OR COOLING POWER, WO 2017/158511, n.d. https://www.patentguru.com/assignee/briola-stefano (accessed January 16, 2024).

[86] S. Briola, P. Di Marco, R. Gabbrielli, Thermodynamic sensitivity analysis of a novel trigeneration thermodynamic cycle with two-phase expanders and two-phase compressors, Energy 127 (2017) 335–350. https://doi.org/10.1016/j.energy.2017.03.135.

[87] A. Pina-Martinez, S. Lasala, R. Privat, V. Falk, J.-N. Jaubert, Design of promising working fluids for emergent combined cooling, heating, and power (CCHP) systems, ACS Sustainable Chem. Eng. 9 (2021) 11807–11824. https://doi.org/10.1021/acssuschemeng.1c03362.

[88] Y. Le Guennec, R. Privat, J.-N. Jaubert, Development of the translated-consistent tc-PR and tc-RK cubic equations of state for a safe and accurate prediction of volumetric, energetic and saturation properties of pure compounds in the sub- and super-critical domains, Fluid Phase Equilibria 429 (2016) 301–312. https://doi.org/10.1016/j.fluid.2016.09.003.

[89] A.K. Krasin, V.B. Nesterenko, Dissociating Gases: A New Class of Coolants and Working Substances for Large Power Plants, Atomic Energy Review 9 (1971) 177.

[90] W.J. Bradley, Recouping the thermal-to-electric conversion loss by the use of waste heat, in: Low-Grade Heat: A Resource in Cold Climates, Chalk River Nuclear Laboratories, 1976: pp. 535–558.

[91] A. Sorokin, Dissociating Nitrogen Dioxide (N2O4) as a working fluid in thermodynamic cycles, Nuclear Science and Engineering 72 (1979) 330–346.

[92] K. Kesavan, J.F. Osterle, Split-Flow Nuclear Gas Turbine Cycle Using Dissociating N2O4, in: American Society of Mechanical Engineers Digital Collection, 1982. https://doi.org/10.1115/82-GT-181.

[93] H. Cheung, Dissociating gas as a working fluid for space plant, Energy Conversion 8 (1968) 125–128.

[94] K. Kesavan, J.F. Osterle, Brayton cycle using dissociating nitrosyl chloride, (1981) 2204–2209.

[95] K. Kesavan, The use of dissociating gases as the working fluid in thermodynamic power conversion cycles, Carnegie-Mellon University, 1978.

[96] H.M. Huang, R. Govind, Use of Dissociating Gases in Brayton Cycle Space Power Systems, Ind. Eng. Chem. Res. 27 (1988) 803–810.

[97] H.-M. Huang, R. Govind, Optimisation of power plants using dissociating gases as working fluids, in: Proceedings of the 20th Intersociety Energy Conversion Engineering Conference, Warrendale, PA 15096, 1985: pp. 620–629.

[98] H.-M. Huang, R. Govind, Studies on power plants using dissociating gases as working fluids, Chem. Eng. Comm. 72 (1988) 95–119.

[99] E.P. Gyftopoulos, G.P. Beretta, Thermodynamics - Foundations and Applications, 2005.

[100] H.B. Callen, Thermodynamics and an Introduction to Thermostatistic, 2nd editio, John Wiley & Sons, Inc., 1985.

[101] J.M. Smith, H.C.V. Ness, M.M. Abbott, Introduction to chemical engineering thermodynamics, 7 edizione, McGraw-Hill Education, Boston, 2004.

[102] E. Althaus, M. Jakubith, Memofix – Chemistry and Chemical Engineering, Wiley VCH, Weinheim ; New York, 1993.

[103] M. Chys, M. van den Broek, B. Vanslambrouck, M. De Paepe, Potential of zeotropic mixtures as working fluids in organic Rankine cycles, Energy 44 (2012) 623–632. https://doi.org/10.1016/j.energy.2012.05.030.

[104] A. Barakat, S. Lasala, P. Arpentinier, P. Tobaly, J.-N. Jaubert, Understanding the thermodynamic effects of chemically reactive working fluids in the Stirling engine, Submitted to Energy Conversion and Management X (n.d.).

[105] B. Schmid, J. Gmehling, Revised parameters and typical results of the VTPR group contribution equation of state, Fluid Phase Equilibria 317 (2012) 110–126. https://doi.org/10.1016/j.fluid.2012.01.006.

[106] D. Frenckel, B. Smit, Understanding Molecular Simulation. From Algorithms to Applications., 3rd Edition, 2002.

[107] R. Hens, A. Rahbari, S. Caro-Ortiz, N. Dawass, M. Erdős, A. Poursaeidesfahani, H.S. Salehi, A.T. Celebi, M. Ramdin, O.A. Moultos, D. Dubbeldam, T.J.H. Vlugt, Brick-CFCMC: Open Source Software for Monte Carlo Simulations of Phase and Reaction Equilibria Using the Continuous Fractional Component Method, Journal of Chemical Information and Modeling 60 (2020) 2678–2682. https://doi.org/10.1021/acs.jcim.0c00334.

[108] S. Lasala, K. Samukov, H. Mert Polat, V. Lachet, O. Herbinet, R. Privat, J.-N. Jaubert, O.A. Moultos, K. De Ras, T. J. H. Vlugt, Application of thermodynamics at different scales to describe the behaviour of fast reacting binary mixtures in vapour-liquid equilibrium, Chemical Engineering Journal (2024) 148961. https://doi.org/10.1016/j.cej.2024.148961.

[109] H.M. Polat, S. Lasala, F. De Meyer, C. Houriez, O.A. Moultos, Scaling Towards the Critical Point in the Combined Reaction/Gibbs Ensemble, Submitted to Fluid Phase Equilibria (n.d.).

[110] COSMOTherm Reference Manual, (2021).

[111] S. Stephan, M. Thol, J. Vrabec, H. Hasse, Thermophysical Properties of the Lennard-Jones Fluid: Database and Data Assessment, J. Chem. Inf. Model. 59 (2019) 4248–4265. https://doi.org/10.1021/acs.jcim.9b00620.

[112] Radiative Efficiency Estimation of Organic Substance Based on Group Contribution Method, Energy Procedia 61 (2014) 492–495. https://doi.org/10.1016/j.egypro.2014.11.1156.

[113] Ø. Hodnebrog, M. Etminan, J.S. Fuglestvedt, G. Marston, G. Myhre, C.J. Nielsen, K.P. Shine, T.J. Wallington, Global warming potentials and radiative efficiencies of halocarbons and related compounds: A comprehensive review, Reviews of Geophysics 51 (2013) 300–378. https://doi.org/10.1002/rog.20013.

[114] G. Schneider, K.-H. Baringhaus, Molecular Design: Concepts and Applications, WILEY-VCH, Weinheim, 2008.

[115] Q. Zhao, Conception and optimization of supercritical CO2 Brayton cycles for coal-fired power plant application, These de doctorat, Université de Lorraine, 2018. http://www.theses.fr/2018LORR0080 (accessed April 6, 2021).

[116] PROCESS ENGINEERING FOR ENERGY - white book of LRGP, LRGP - CNRS, n.d.

[117] NIST Standard Reference Database 103b, NIST (2010). https://www.nist.gov/mml/acmd/trc/thermodata-engine/srd-nist-tde-103b (accessed April 6, 2021).

[118] https://www.aiche.org/dippr/events-products/801-database, (n.d.). DIPPR 801 Database.

[119] Dortmund Data Bank, (2023). http://www.ddbst.com.

[120] C. Trinh, Y. Tbatou, S. Lasala, O. Herbinet, D. Meimaroglou, On the Development of Descriptor-Based Machine Learning Models for Thermodynamic Properties: Part 1—From Data Collection to Model Construction: Understanding of the Methods and Their Effects, Processes 11 (2023) 3325. https://doi.org/10.3390/pr11123325.

[121] C. Trinh, S. Lasala, O. Herbinet, D. Meimaroglou, On the Development of Descriptor-Based Machine Learning Models for Thermodynamic Properties: Part 2—Applicability Domain and Outliers, Algorithms 16 (2023) 573. https://doi.org/10.3390/a16120573.

[122] E.T. Chang, N.A. Gokcen, Thermodynamic Properties of Gases in Propellants and Oxidizers. I. Solubilities of He, N2, O2, Ar, and N2O3 in Liquid N2O4, J. Phys. Chem. 70 (1966) 2394–2399. https://doi.org/10.1021/j100879a050.

[123] H.M. Huang, R. Govind, Use of dissociating gases in Brayton Cycle space power systems, Ind. Eng. Chem. Res. 27 (1988) 803–810. https://doi.org/10.1021/ie00077a015.

[124] M. Blander, L.G. Epel, A.P. Fraas, R.F. Newton, Aluminum chloride as a thermodynamic working fluid and heat transfer medium, Oak Ridge National Laboratory, Union Carbide Corporation, U.S. Atomic Energy Commission, 1959.

[125] K. Kesavan, The use of dissociating gases as the working fluid in thermodynamic power conversion cycles, Nuclear Science and Engineering Division, Carnegie-Mellon University, 1978.

[126] T.A. Jacobs, J.R. Lloyd, The Influence of the Equilibrium Dissociation of a Diatomic Gas on Brayton-Cycle Performance, Journal of Applied Mechanics (1963) 288–290.

[127] V.B. Nesterenko, V.P. Bubnov, E.N. Bunin, N.M. Shiryaeva, Thermodynamic cycles on chemically reacting fluids, Vesci Akad. Navuk BSSR, Ser. Fiz.-Energ. Navuk (1970) 74–76.

[128] R. Stochl, Potential performance improvement using a reacting gas (nitrogen tetroxide) as the working fluid in a closed Brayton cycle, DOE/NASA/1060-79/3, 1979. https://doi.org/10.2172/5746805.

[129] M.A. Bazhin, V.P. Bubnov, V.B. Nesterenko, N.M. Shiryaeva, Optimisation of parameters of power plants using dissociating working fluids., Nauka i Tehnika, Minsk, 1970.

[130] S. Lasala, R. Privat, O. Herbinet, P. Arpentinier, D. Bonalumi, J.-N. Jaubert, Thermo-chemical engines: Unexploited high-potential energy converters, Energy Convers. Manag. 229 (2021) 113685. https://doi.org/10.1016/j.enconman.2020.113685.

[131] Dissociating gases as coolants and working substances in power plants (Proceedings of All-Union Conference), Nauka i Tehnika, Minsk, 1970.

[132] K. Zhang, Y. Shen, C. Duwig, Identification of heat transfer intensification mechanism by reversible N2O4 decomposition using direct numerical simulation, International Journal of Heat and Mass Transfer 182 (2022) 121946. https://doi.org/10.1016/j.ijheatmasstransfer.2021.121946.

[133] K. Zhang, A. Laitinen, Y. Shen, V. Vuorinen, C. Duwig, Reactive cooling simulation of electronic components, Applied Thermal Engineering 228 (2023) 120519. https://doi.org/10.1016/j.applthermaleng.2023.120519.

[134] S. Lasala, Reactive fluids for intensified thermal energy conversion, Project Repository Journal 13 (2022) 102–105. https://doi.org/10.54050/PRJ1318808.

[135] S. Lasala, ERC-REACHER, (2022). https://www.univ-lorraine.fr/erc-reacher/.

[136] V. Diky, C. Muzny, A. Smolyanitsky, A. Bazileva, R. Chirico, J. Magee, Y. Paulechka, A. Kazakov, S. Townsend, E. Lemmon, M. Frenkel, K. Kroenlein, ThermoData Engine (TDE) Version 10.1 (Pure Compounds, Binary Mixtures, Ternary Mixtures, and Chemical Reactions): NIST Standard Reference Database 103b, National Institute of Standards and Technology, Gaithersburg, MD, 2016.

[137] D.F. Stai, F. Bizjak, S.E. Stephanou, Thermodynamic properties of nitrogen tetroxide, Journal of Spacecraft and Rockets 2 (1965) 742–745. https://doi.org/10.2514/3.28272.

[138] D.N. Seshadri, D.S. Viswanath, N.R. Kuloor, Thermodynamic properties of the system $N_2O_4 \leftrightarrows 2NO_2 \leftrightarrows 2NO + O_2$, AIChE J. 16 (1970) 420–425. https://doi.org/10.1002/aic.690160319.

[139] O.A. Hougen, K.M. Watson, Chemical Process Principles, John Wiley & Sons, Inc., New York, 1952.

[140] R.D. McCarty, H.-U. Steurer, C.M. Daily, The thermodynamic properties of nitrogen tetroxide, Thermophysics Division, Center for Chemical Engineering, National Engineering Laboratory, National Bureau of Standards, Boulder, 1986.

[141] M. Binotti, C.M. Invernizzi, P. Iora, G. Manzolini, Dinitrogen tetroxide and carbon dioxide mixtures as working fluids in solar tower plants, Solar Energy 181 (2019) 203–213. https://doi.org/10.1016/j.solener.2019.01.079.

[142] G. Manzolini, M. Binotti, D. Bonalumi, C. Invernizzi, P. Iora, CO_2 mixtures as innovative working fluid in power cycles applied to solar plants. Techno-economic assessment, Solar Energy 181 (2019) 530–544. https://doi.org/10.1016/j.solener.2019.01.015.

[143] L.E.S. de Souza, U.K. Deiters, Modeling of the N_2O_4–NO_2 reacting system, Phys. Chem. Chem. Phys. 2 (2000) 5606–5613. https://doi.org/10.1039/b005464j.

[144] A. Belkadi, F. Llovell, V. Gerbaud, L.F. Vega, Modeling the vapor–liquid equilibrium and association of nitrogen dioxide/dinitrogen tetroxide and its mixtures with carbon dioxide, Fluid Phase Equilib. 266 (2008) 154–163. https://doi.org/10.1016/j.fluid.2008.01.026.

[145] E.W. Lemmon, A.H. Harvey, J.M. Young, Thermodynamic Model for the Reactive Mixture Comprising Dinitrogen Tetroxide (N2O4), Nitrogen Dioxide (NO2), Nitric Oxide (NO), and Oxygen (O2), (2022).

[146] E. Bourasseau, V. Lachet, N. Desbiens, J.-B. Maillet, J.-M. Teuler, P. Ungerer, Thermodynamic Behavior of the CO_2 + NO_2/N_2O_4 Mixture: A Monte Carlo Simulation Study, J. Phys. Chem. B 112 (2008) 15783–15792. https://doi.org/10.1021/jp8068255.

[147] J.K. Johnson, A.Z. Panagiotopoulos, K.E. Gubbins, Reactive canonical Monte Carlo, Molecular Physics 81 (1994) 717–733. https://doi.org/10.1080/00268979400100481.

[148] W.R. Smith, B. Triska, The reaction ensemble method for the computer simulation of chemical and phase equilibria. I. Theory and basic examples, The Journal of Chemical Physics 100 (1994) 3019–3027. https://doi.org/10.1063/1.466443.

[149] J.K. Shah, E. Marin-Rimoldi, R.G. Mullen, B.P. Keene, S. Khan, A.S. Paluch, N. Rai, L.L. Romanielo, T.W. Rosch, B. Yoo, E.J. Maginn, Cassandra: An open source Monte Carlo package for molecular simulation, Journal of Computational Chemistry 38 (2017) 1727–1739. https://doi.org/10.1002/jcc.24807.

[150] M.J. Molina, S.B. Rodriguez-Reartes, M.S. Zabaloy, A theoretical study on the simultaneous vapor-liquid and chemical equilibria in a highly restricted system, Fluid Phase Equilibria 557 (2022) 113439. https://doi.org/10.1016/j.fluid.2022.113439.

[151] M.J. Molina, S.B. Rodriguez-Reartes, M.S. Zabaloy, Computation and analysis of reactive isopleths involving fluid phases, Fluid Phase Equilibria 574 (2023) 113889. https://doi.org/10.1016/j.fluid.2023.113889.

[152] F.E.C. Scheffer, J.P. Treub, Determinations of the vapour tension of nitrogen tetroxide, KNAW, Proceedings (1912) 166–178.

[153] H.H. Reamer, B.H. Sage, Volumetric Behavior of Nitrogen Dioxide in the Liquid Phase, Ind. Eng. Chem. 44 (1952) 185–187. https://doi.org/10.1021/ie50505a052.

[154] DECHEMA, DIPPR 801 database, (2023). https://dechema.de/en/dippr801.html.

[155] D.-Y. Peng, D.B. Robinson, The characterization of the heptanes and heavier fractions for the GPA Peng-Robinson programs, Gas Processors Association, 1978.

[156] S. Lasala, P. Chiesa, R. Privat, J.-N. Jaubert, VLE properties of CO_2–based binary systems containing N_2, O_2 and Ar: experimental measurements and modelling results with advanced cubic equations of state, Fluid Phase Equilibria 428 (2016) 18–31. https://doi.org/10.1016/j.fluid.2016.05.015.

[157] J.W. Qian, R. Privat, J.N. Jaubert, P. Duchet-Suchaux, Enthalpy and heat capacity changes on mixing: Fundamental aspects and prediction by means of the PPR78 cubic equation of state, Energy and Fuels 27 (2013) 7150–7178. https://doi.org/10.1021/ef401605c.

[158] P. Ungerer, B. Tavitian, A. Boutin, Applications of Molecular Simulation in the Oil and Gas Industry - Monte-carlo Methods, Editions TECHNIP, 2005.

[159] Gaussian 09, n.d. https://gaussian.com/.

[160] A. Miyoshi, GPOP software, 2002. http://akrmys.com/gpop/.

[161] J.A. Montgomery, M.J. Frisch, J.W. Ochterski, G.A. Petersson, A complete basis set model chemistry. VI. Use of density functional geometries and frequencies, Journal of Chemical Physics 110 (1999) 2822–2827. https://doi.org/10.1063/1.477924.

[162] A.D. Becke, Density-functional thermochemistry. III. The role of exact exchange, Journal of Chemical Physics 98 (1993) 5648–5652. https://doi.org/10.1063/1.464913.

[163] K.S. Pitzer, W.D. Gwinn, Energy Levels and Thermodynamic Functions for Molecules with Internal Rotation I. Rigid Frame with Attached Tops, The Journal of Chemical Physics 10 (2004) 428–440. https://doi.org/10.1063/1.1723744.

[164] M.P. Allen, D.J. Tildesley, Computer Simulation of Liquids, 2nd edition, Oxford University Press, 2017.

[165] W. Shi, E.J. Maginn, Continuous Fractional Component Monte Carlo: An Adaptive Biasing Method for Open System Atomistic Simulations, J Chem Theory Comput 3 (2007) 1451–1463. https://doi.org/10.1021/ct7000039.

[166] W. Shi, E.J. Maginn, Improvement in molecule exchange efficiency in Gibbs ensemble Monte Carlo: Development and implementation of the continuous fractional component move, Journal of Computational Chemistry 29 (2008) 2520–2530. https://doi.org/10.1002/jcc.20977.

[167] A. Rahbari, R. Hens, M. Ramdin, O.A. Moultos, D. Dubbeldam, T.J.H. Vlugt, Recent advances in the continuous fractional component Monte Carlo methodology, Molecular Simulation 47 (2021) 804–823. https://doi.org/10.1080/08927022.2020.1828585.

[168] H.M. Polat, H.S. Salehi, R. Hens, D.O. Wasik, A. Rahbari, F. De Meyer, C. Houriez, C. Coquelet, S. Calero, D. Dubbeldam, O.A. Moultos, T.J.H. Vlugt, New Features of the Open Source Monte Carlo Software Brick-CFCMC: Thermodynamic Integration and Hybrid Trial Moves, Journal of Chemical Information and Modeling 61 (2021) 3752–3757. https://doi.org/10.1021/acs.jcim.1c00652.

[169] A. Poursaeidesfahani, A. Torres-Knoop, D. Dubbeldam, T.J.H. Vlugt, Direct Free Energy Calculation in the Continuous Fractional Component Gibbs Ensemble, J. Chem. Theory Comput. 12 (2016) 1481–1490. https://doi.org/10.1021/acs.jctc.5b01230.

[170] F. Wang, D.P. Landau, Efficient, Multiple-Range Random Walk Algorithm to Calculate the Density of States, Phys. Rev. Lett. 86 (2001) 2050–2053. https://doi.org/10.1103/PhysRevLett.86.2050.

[171] A. Poursaeidesfahani, R. Hens, A. Rahbari, M. Ramdin, D. Dubbeldam, T.J.H. Vlugt, Efficient Application of Continuous Fractional Component Monte Carlo in the Reaction Ensemble, J. Chem. Theory Comput. 13 (2017) 4452–4466. https://doi.org/10.1021/acs.jctc.7b00092.

[172] H.M. Polat, F. de Meyer, C. Houriez, O.A. Moultos, T.J.H. Vlugt, Solving Chemical Absorption Equilibria using Free Energy and Quantum Chemistry Calculations: Methodology, Limitations, and New Open-Source Software, Journal of Chemical Theory and Computation 19 (2023) 2616–2629. https://doi.org/10.1021/acs.jctc.3c00144.

[173] A.Z. Panagiotopoulos, Direct determination of phase coexistence properties of fluids by Monte Carlo simulation in a new ensemble, Molecular Physics 61 (1987) 813–826. https://doi.org/10.1080/00268978700101491.

[174] V. Lachet, T. de Bruin, P. Ungerer, C. Coquelet, A. Valtz, V. Hasanov, F. Lockwood, D. Richon, Thermodynamic behavior of the CO2+SO2 mixture: Experimental and Monte Carlo simulation studies, Energy Procedia 1 (2009) 1641–1647. https://doi.org/10.1016/j.egypro.2009.01.215.

[175] V. Lachet, B. Creton, T. de Bruin, E. Bourasseau, N. Desbiens, Ø. Wilhelmsen, M. Hammer, Equilibrium and transport properties of CO2+N2O and CO2+NO mixtures: Molecular simulation and equation of state modelling study, Fluid Phase Equilibria 322–323 (2012) 66–78. https://doi.org/10.1016/j.fluid.2012.03.011.

[176] J.S. Rowlinson, F.L. Swinton, Liquids and liquid mixtures, 3rd edition, Butterworths, 1982.

[177] C. Heath Turner, J.K. Brennan, M. Lísal, W.R. Smith, J. Karl Johnson, K.E. Gubbins, K.E. Gubbins, Simulation of chemical reaction equilibria by the reaction ensemble Monte

Carlo method: a review, Molecular Simulation 34 (2008) 119–146. https://doi.org/10.1080/08927020801986564.

[178] S.C. Glotzer, D. Stauffer, N. Jan, Monte Carlo simulations of phase separation in chemically reactive binary mixtures, Phys. Rev. Lett. 72 (1994) 4109–4112. https://doi.org/10.1103/PhysRevLett.72.4109.

[179] Y. Mo, W. Wu, Q. Zhang, Valence bond studies of N2O4, Journal of Molecular Structure: THEOCHEM 315 (1994) 173–178. https://doi.org/10.1016/0166-1280(94)03778-J.

[180] NIST, WebBook de Chimie NIST, (n.d.). https://doi.org/10.18434/T4D303.

[181] A. Mittasch, E. Kuss, H. Schlueter, Dichten und Dampfdrucke von wäßrigen Ammoniaklösungen und von flüssigem Stickstofftetroxyd für das Temperatur-gebiet 0° bis 60°, Z. Anorg. Allg. Chem. 159 (1927) 1–36. https://doi.org/10.1002/zaac.19261590102.

[182] N.G. Polikhronidi, R.G. Batyrova, I.M. Abdulagatov, Isochoric heat capacity measurements of nitrogen tetroxide system at temperatures between 410 and 484 K and pressures up to 35 MPa, Fluid Phase Equilibria 175 (2000) 153–174. https://doi.org/10.1016/S0378-3812(00)00457-X.

[183] A.B. Verzhinskaya, V.I. Tsurbelev, P.M. Klepatskiy, Impact of nitrogen monooxide on shape of the coexistence curve of N_2O_4 and vicinity of the critical point liquid-vapor, in Application of mathematical methods for description and studying of the phisico-chemical equilibria (extended abstracts of reports), in: Novosibirsk, 1985.

[184] P. Gray, P. Rathbone, Dissociation of liquid dinitrogen tetroxide; Henry's law coefficients, heats and entropies of solution, and the thermodynamics of homolytic dissociation in the pure liquid, J. Chem. Soc. (1958) 3550. https://doi.org/10.1039/jr9580003550.

[185] C.C. Addison, B.C. Smith, Volume changes on mixing organic liquids with dinitrogen tetroxide: comparison with sulphur dioxide systems, J. Chem. Soc. (1958) 3664. https://doi.org/10.1039/jr9580003664.

[186] R. Privat, J.-N. Jaubert, Classification of global fluid-phase equilibrium behaviors in binary systems, Chemical Engineering Research and Design 91 (2013) 1807–1839. https://doi.org/10.1016/j.cherd.2013.06.026.

[187] J.-N. Jaubert, R. Privat, Y. Le Guennec, L. Coniglio, Note on the properties altered by application of a Péneloux–type volume translation to an equation of state, Fluid Phase Equilibria 419 (2016) 88–95. https://doi.org/10.1016/j.fluid.2016.03.012.

[188] R. Privat, J.-N. Jaubert, Y. Le Guennec, Incorporation of a volume translation in an equation of state for fluid mixtures: which combining rule? Which effect on properties of mixing?, Fluid Phase Equilibria 427 (2016) 414–420. https://doi.org/10.1016/j.fluid.2016.07.035.

[189] I.E. Idel'cik, Memento des pertes de charge: Coefficients de pertes de charge singulières et de perte de charge par frottement., 2e ed., Eyrolles, Paris, 1986.

Currculum Vitae

■ PERSONAL INFORMATION

Family name, First name:	**Lasala, Silvia**
Researcher unique identifiers:	ORCID: 0000-0002-4013-9336
Date of birth:	10/05/1988
Nationality:	Italian
Professional address:	1, rue Grandville, Nancy (France)
Professional email:	silvia.lasala@univ-lorraine.fr
Professional phone number:	+33 3 72 74 37 64

■ CURRENT POSITION

From 2018 Assistant professor, titular teacher at the **Chemical Engineering School (ENSIC)** and researcher at **Reaction and Chemical Engineering Laboratory (LRGP)**.
ENSIC-LRGP, University of Lorraine (Nancy, France).

■ EDUCATION

2016 **Ph.D. in "Energy and Nuclear Science and Technology"**, cum laude (with honours).

Ph.D. thesis entitled "Advanced cubic equations of state for accurate modelling of fluid mixtures. Application to CO_2 capture systems" (doi: 10.13140/RG.2.1.2948.9041)
Energy Department, Politecnico di Milano, Milano, Italy
Name of PhD Supervisor: Professor P. Chiesa

2012 **Master in "Energy Engineering"**, cum laude (with honours)
Politecnico di Milano, Milano (Italy)

2010 **Bachelor in "Energy Engineering"**, cum laude (with honours)
Politecnico di Milano, Milano (Italy)

■ PREVIOUS POSITIONS

2016 – 2018 Postdoctoral researches funded by Air Liquide investigating, mainly: 1) the modelling of the thermodynamics and the kinetics of the reaction ortho-H_2=para-H_2, in **hydrogen liquefaction** processes; 2) the improvement of algorithms used in REFPROP for **VLE modelling of mixtures of N_2, Ar and O_2**; 3) the optimal selection of working fluids for power cycles.

LRGP - Centre National de la Recherche Scientifique (CNRS), France.

2011 Six-month internship with the aim to model the **interactions between combustion instabilities, combustor acoustics and flame characteristics** in rich-burn and lean-burn aerospace engines.

Combustion & Casings department, Rolls-Royce, Derby, United Kingdom.

■ PRIZES AND FELLOWSHIPS

2016 Prize: Ph.D. thesis awarded with **"Ermanno Grinzato" prize, by *Associazione Italiana Proprietà Termofisiche*** (AIPT), at XXII congress of AIPT, Bologna, Italy.

2017 Prize: Ph.D. thesis awarded by the ***European Federation of Chemical Engineering*** **(EFCE)** with the **second prize "Excellence Award in Thermodynamics and Transport Properties"**, at 29th European Symposium on Applied Thermodynamics, Bucarest, Romania

2017 Fellowship of $9000 awarded by *the* ***Knowledge Centre on Organic Rankine Cycles*** (KCORC) to support postdoctoral researches on ORC technologies - link

2022 Prize "**Susanne Zivi**" conferred by the ***Académie de Stanislas*** to award young researchers of University of Lorraine. Nancy, France - link

2023 Prize "**Médaille de Bronze**" of the French CNRS (***National Center of Scientific Research)*** - link

■ MAIN TEACHING ACTIVITIES

Since 2020 *Master Erasmus Mundus DENSYS (Decentralizes smart Energy Systems), University of Lorraine, France* (70 hours/year): Responsible of the courses "Energy Storage", "Case based module".

Since 2018 ENSIC, *University of Lorraine, Nancy, France* (300 hours/year): lecturer in different courses or exercise sessions: "Thermodynamics", "Informatics" (Fortran and Matlab programming), "Techno-economic processes optimisation", practical works in "Distillation".

Since 2018 *Conservatoire National d'Arts et Métiers* (CNAM): lecturer in "Thermodynamics" and "Mixtures and phase diagrams".

Since 2022, my teaching activity is reduced to 77h because I have received a discharge of teaching duties due to the obtention of an ERC grant (see session RESEARCH GRANTS).

■ RESEARCH GRANTS

- **Current grants I obtained as Principal Investigator (Coordinator)**

Project Title	Funding source	Amount	Period
Reactive fluids for intensified thermal energy conversion (REACHER)	**ERC Starting Grant (Individual Project)** funded by European Union (Programme Horizon Europe) https://www.univ-lorraine.fr/erc-reacher/	~ 1.5 M€	April 2022 – March 2027
Fluides réactifs pour intensifier la conversion de l'énergie thermique (REACHER)	**ANR-JCJC (Individual Project)** funded by the French Council of Scientific Research (ANR) - https://anr.fr/Projet-ANR-21-CE50-0014 *I had to decline this funding because, both, it overlaid with the ERC Starting Grant and the overall declared personal implication in the two projects would have exceeded 100%.*	~ 300 k€	February 2022 – January 2026

- **Current grants as Partner (CNRS)**

Project Title	Funding source	Amount	Period
Next REnewable multi-GENeration technology enabled by TWO-phase fluids machines (REGEN-BY-2)	**Collaborative European project**, funded by European Union (Programme H2020) https://www.regen-by-2.eu/	5 419 328 € (total budget) 225 624 € (our -of partner CNRS-budget in the project)	September 2020 – August 2024

■ SUPERVISION ACTIVITY

Summary of the supervised researchers (ref. to "Supervision_activities.pdf" for more details):

- **5** postdoctoral researchers
- **3** PhD students (+ **2** starting in March 2024)
- **10** research internships (Master students and visiting PhDs)

■ SUMMARY OF THE SCIENTIFIC PRODUCTION

Metrics overview: N. of citations = 700, h-index = 14 (source: Google Scholar).

- 25 papers (12 as first and/or corresponding author)
- 5 publications in conference proceedings
- 3 international patents
- 4 chapters in books
- 1 edited book
- 38 oral communications and 8 posters, mostly in International Conferences.

■ REVIEWING ACTIVITIES

2019 - 2024 Expert evaluator for European Commission (for Marie-Curie fellowships, H2020 and Horizon Europe programmes), with 2/3 participations per year.

2018 - 2022 Editor-in-chief of the *International Journal of Energy, Environment and Economics*.

Since 2016 Peer reviewer of more than 20 international journals (10 review/year): *Fluid Phase Equilibria, Applied Energy, Energy, Applied Thermal Engineering, Journal of Chemical & Engineering Data, Industrial & Engineering Chemistry Research, Journal of Chemical Thermodynamics, Journal of Cleaner Production, Oil & Gas Science and Technology, Journal of the Brazilian Society of Mechanical Sciences and Engineering, Cryogenics, Molecules, Sugar Tech, Thermochimica Acta, Textile Research Journal, Review in Chemical Engineering, Journal of the Taiwan Institute of Chemical Engineers, Journal of Thermal Science, International Journal of Refrigeration, Energy Conversion and Management, SoftwareX, SN Applied Sciences*.

■ INVESTISSEMENT POUR LA COLLECTIVITE ET RAYONNEMENT

- I have been involved in delivering lectures to the general public and politicians (in 2022 : 1 – at the Night of researchers; 2 - at the Italian Ambassy in Paris, 3 - for the adviser of the Minister for Europe and Foreign Affairs Clément Beaune, 4 - for the French General Secretary for the Investment Bruno Bonnell) or to industrials (invited by General Electric, la *Vallée de l'Energie*, NEEXT Engineering, BDR Thermea, ENI). Also, I have recently delivered different interviews to national and regional French and Italian journals (for

example, in *Est Republicain*, *France 3*, *Usine Nouvelle*, *Radio 24* in *Smart City* by *Maurizio Melis*).

- ❖ Since 2022, I have supported French, Norwegian and Polish researchers who submitted a proposal for an ERC Starting grant, advising them in the project drafting process and in the preparation of their interview.
- ❖ Since 2022, I contribute to the writing of national position papers in ANCRE (*Alliance Nationale de Coordination de la Recherche sur l'Energie*) on waste heat recovery and valorisation, aiming at defining the research national guidelines towards the carbon neutrality by 2050.

■ OTHER ACADEMIC RESPONSIBILITIES

Since 2021, I am **academic responsible** for ENSIC students going in our partner Universities (2 in Italy, 4 in Germany, 3 in Portugal) in **ERASMUS+ programme**. I have also driven the establishment of a new academic collaboration between ENSIC and Politecnico di Milano.

List of publications, patents and communications

PUBLICATIONS

[The asterisk (*) indicates the corresponding author].

List of publications in international peer-reviewed journals

1) Silvia Lasala*, Paolo Chiesa, Romain Privat, Jean-Noël Jaubert, **VLE properties of CO_2 – based binary systems containing N_2, O_2 and Ar: Experimental measurements and modelling results with advanced cubic equations of state**. *Fluid Phase Equilibria* 2016, 428, 18-31.

2) Yohann Le Guennec, Silvia Lasala, Romain Privat, Jean-Noël Jaubert*, **A consistency test for α-functions of cubic equations of state**. *Fluid Phase Equilibria* 2016, 427, 513-538.

3) Silvia Lasala*, Paolo Chiesa, Romain Privat, Jean-Noël Jaubert. **Optimizing thermodynamic models: the relevance of molar fraction uncertainties.** *Journal of Chemical & Engineering Data* 2017, 62, 825−832.

4) Xiaochun Xu, Silvia Lasala, Romain Privat, Jean-Noël Jaubert*. **E-PPR78: a proper cubic EoS for modeling fluids involved in the design and operation of carbon dioxide capture and storage (CCS) processes**. *International Journal of Greenhouse Gas Control* 2017, 56, 126-154.

5) Silvia Lasala*, Paolo Chiesa, Romain Privat, Jean-Noël Jaubert. **Modelling the thermodynamics of fluids treated by CO_2-capture processes with "Peng-Robinson + residual Helmholtz energy-based mixing rules"**. *Industrial and Engineering Chemistry Research* 2017, 56, 2259-2276.

6) Silvia Lasala*, Paolo Chiesa, Romain Privat, Jean-Noël Jaubert. **Measurement and prediction of multi-property data of CO_2-N_2-O_2-CH_4 mixtures with the "Peng-Robinson + residual Helmholtz energy-based" model**. *Fluid Phase Equilibria* 2017, 437, 166-180.

7) Costante M. Invernizzi*, Paolo Iora, Giampaolo Manzolini, Silvia Lasala. **Thermal stability of n-pentane, cyclo-pentane and toluene as working fluids in organic Rankine engines**. *Applied Thermal Engineering* 2017, 121, 172-179.

8) Yohann Le Guennec, Romain Privat, Silvia Lasala, Jean-Noël Jaubert*. **On the imperative need to use a consistent α-function for the prediction of pure-compound supercritical properties with a cubic equation of state**. *Fluid Phase Equilibria* 2017, 445, 45-53.

9) Silvia Lasala*, Romain Privat, Jean-Noël Jaubert, Philippe Arpentinier. **Modelling the thermodynamics of air-component mixtures (N_2, O_2 and Ar). Comparison and performance analysis of available models**. *Fluid Phase Equilibria* 2018, 458, 278-287.

10) Carlos Nieto-Draghi, Theodorus de Bruin, Véronique Lachet, Elise El Ahmar, Alain Valtz; Christophe Coquelet, Silvia Lasala, Romain Privat, Jean-Noël Jaubert*. **Thermodynamic study of binary systems containing sulphur dioxide and nitric oxide: measurements and modelling.** *Fluid Phase Equilibria* 2018, 461, 84-100.

11) Silvia Lasala*, Paolo Chiesa, Romain Privat, Jean-Noël Jaubert. **Sizing and operating units for the purification and compression of CO_2-based streams: the impact of thermodynamic model accuracy**. *The Journal of Supercritical Fluids* 2018, 140, 336-347.

12) Marco Astolfi*, Dario Alfani, Silvia Lasala, Ennio Macchi. **Comparison between ORC and CO_2 Systems for the exploitation of Low-Medium Temperature Heat Sources**. *Energy* 2018, 161, 1250-1261.

13) Davide Bonalumi*, Silvia Lasala, Ennio Macchi. **CO_2-$TiCl_4$ working fluid for high-temperature heat-source power cycles and solar applications**. *Renewable Energy* 2020, 147, 2842-2854.

14) Silvia Lasala*, Romain Privat, Philippe Arpentinier, Jean-Noël Jaubert*. **Note on the inconsistent definition assigned in the literature to the heat capacity of the so-called "equilibrium hydrogen" mixture.** *Fluid Phase Equilibria* 2020, 504, 112325.

15) Ailo Aasen, Morten Hammer, Silvia Lasala, Jean-Noël Jaubert, Øivind Wilhelmsen*. **Accurate quantum-corrected cubic equations of state for helium, neon, hydrogen, deuterium and their mixtures.** *Fluid Phase Equilibria* 2020, 524, 112790.

16) Jean-Noël Jaubert*, Yohann Le Guennec, Andrés Piña-Martinez, Nicolas Ramirez-Velez, Silvia Lasala, Bastian Schmid, Ilias K. Nikolaidis, Ioannis G. Economou, and Romain Privat. **Benchmark Database Containing Binary-System-High-Quality-Certified Data for Cross-Comparing Thermodynamic Models and Assessing Their Accuracy.** *Industrial & Engineering Chemistry Research.* 2020, 59, 33, 14981–15027.

17) Andrés Piña-Martinez, Romain Privat, Silvia Lasala, Giorgio Soave, Jean-Noël Jaubert*. **Search for the optimal expression of the volumetric dependence of the attractive contribution in cubic equations of state.** *Fluid Phase Equilibria* 2020, 522, 112750.

18) Silvia Lasala*, Romain Privat, Olivier Herbinet, Philippe Arpentinier, Davide Bonalumi, Jean-Noël Jaubert. **Thermo-Chemical Engines: Unexploited High-Potential Energy Converters.** *Energy Conversion and Management* 2021, 229, 113685.

19) Andrés Piña-Martinez, Silvia Lasala*, Romain Privat, Véronique Falk, and Jean-Noël Jaubert*. **Design of Promising Working Fluids for Emergent Combined Cooling, Heating, and Power (CCHP) Systems.** *ACS Sustainable Chemistry & Engineering* 2021, 9 (35), 11807-11824.

20) Jean-Noel Jaubert*, Jun-Wei Qian, Silvia Lasala, Romain Privat*, **The impressive impact of including enthalpy and heat capacity of mixing data when parameterising equations of state. Application to the development of the E-PPR78 (Enhanced-Predictive-Peng-Robinson-78) model.** *Fluid Phase Equilibria*. 2022, 113456.

21) Aya Barakat, Silvia Lasala*, Philippe Arpentinier, Jean-Noel Jaubert, **The original and impactful exploitation of chemical energy in heat pumps.** *Chemical Engineering Journal Advances*, 2022, 100400.

22) Cindy Trinh, Youssef Tbatou, Silvia Lasala, Olivier Herbinet, Dimitrios Meimaroglou*. **On the Development of Descriptor-Based Machine Learning Models for Thermodynamic Properties: Part 1—From Data Collection to Model Construction: Understanding of the Methods and Their Effects.** Processes 2023, 11(12), 3325.

23) Cindy Trinh, Silvia Lasala, Olivier Herbinet, Dimitrios Meimaroglou*. **On the Development of Descriptor-Based Machine Learning Models for Thermodynamic Properties: Part 2—Applicability Domain and Outliers.** Algorithms 2023, 16(12), 573.

24) Silvia Lasala*, Konstantin Samukov, H. Mert Polat, Véronique Lachet, Olivier Herbinet, Romain Privat, Jean-Noël Jaubert, Othonas A. Moultos, Kevin De Ras, and Thijs J. H. Vlugt*. **Application of thermodynamics at different scales to describe the behaviour of fast reacting binary mixtures in vapour-liquid equilibrium.** Chemical Engineering Journal, 2024, 148961.

25) Aya Barakat, Silvia Lasala*, Philippe Arpentinier, Pascal Tobaly, Jean-Noël Jaubert. **Understanding the thermodynamic effects of chemically reactive working fluids in a Stirling heat pump**. Submitted to Energy Conversion and Management X.

List of publications in refereed conference proceedings

1) Silvia Lasala*, Paolo Chiesa, Daniele Di Bona, Stefano Consonni. **Vapour Liquid Equilibrium Measurements of CO_2 based Mixtures: Experimental Apparatus and Testing Procedures**, Energy Procedia, Volume 45, 2014, pages 1215-1224. A contribution to the 68th Conference of Associazione Termotecnica Italiana - ATI2013.

2) Silvia Lasala*, Costante Invernizzi, Paolo Iora, Paolo Chiesa, Ennio Macchi, **Thermal stability analysis of per-fluorohexane**, Energy Procedia, Volume 75, August 2015, pages 1575-1582. A contribution to the 7th International Conference on Applied Energy - ICAE2015.

3) Marco Astolfi*, Silvia Lasala, Ennio Macchi. **Selection maps for ORC and CO_2 Systems for low-medium temperature heat sources.** Energy Procedia, Volume 129, September 2017, pages 971–978. A contribution to the IV International Seminar on ORC Power Systems, ORC2017

4) Silvia Lasala*, Davide Bonalumi, Ennio Macchi, Romain Privat, Jean-Noel Jaubert. **The design of CO_2-based working fluids for high-temperature heat source power cycles**. Energy Procedia, Volume 129, September 2017, pages 947–954. A contribution to the IV International Seminar on ORC Power Systems, ORC2017

5) Cindy Trinh, Dimitrios Meimaroglou*, Silvia Lasala, Olivier Herbinet. **Machine Learning for the prediction of the thermochemical properties (enthalpy and entropy of formation) of a molecule from its molecular descriptors.** Computer-Aided Chemical Engineering, Volume 51, pages 1471-1476. A contribution to the 32nd European Symposium on Computer-Aided Process Engineering - ESCAPE32.

List of chapters and books

1) Lasala, S., Privat, R., & Jaubert, J. N. (2018). **The Impact of Thermodynamic Model Accuracy on Sizing and Operating CCS Purification and Compression Units**. Cutting-Edge Technology for Carbon Capture, Utilization, and Storage, 317-359.

2) Silvia Lasala, Romain Privat and Jean-Noël Jaubert (2018) **Inert and Reactive Working Fluids for Closed Power Cycles: Present Knowledge, Applications and Open Researches.** Chapitre publié sur " Organic Rankine Cycle Technology for Heat Recovery". IntechOpen.

3) **Organic Rankine Cycles for Waste Heat Recovery - Analysis and Applications.** Silvia Lasala. IntechOpen 2020. ISBN: 978-1-78985-474-9.

4) Silvia Lasala, Andrés-Piña Martinez and Jean-Noël Jaubert. (2020). **A Predictive Equation of State to Perform an Extending Screening of Working Fluids for Power and Refrigeration Cycles.** Chapitre publié sur "Organic Rankine Cycles for Waste Heat Recovery - Analysis and Applications". IntechOpen.

PATENTS

D. Bonalumi, E. Macchi, S. Lasala, inventors. Politecnico di Milano, applicant. "CO2-based mixtures as working fluid in thermodynamic cycles". International patent. IPN: WO 2019/053550 A1. International publication date : 21 March 2019.

2 Patents under finalisation (one patent – related to the second one - has already been filed in December with the number EP 23307265.1)

SCIENTIFIC COMMUNICATIONS

[The asterisk (*) indicates the presenter at the conference].

List of oral presentations at international conferences (unless otherwise indicated)

1) Silvia Lasala*, Paolo Chiesa, Daniele Di Bona, Stefano Consonni, "Vapour-Liquid Equilibrium Measurements of CO2 based Mixtures: Experimental Apparatus and Testing Procedures", ATI2013 - 68th Conference of the Italian Thermal Machines Engineering Association. September 2013, Bologna, Italy. (National conference)

2) Marco Astolfi, Silvia Lasala*, Carlo De Servi, Ennio Macchi, "Comparison between the use of pure fluids and mixtures for the exploitation of variable temperature heat sources", ASME ORC, International Seminar on ORC Power Systems, 7-8 October 2013, The Netherlands.

3) Silvia Lasala*, Paolo Chiesa, "Vapour – liquid equilibrium measurements of CO2 based ternary mixtures containing Ar, O2 and N2", JEEP - Journées d'Etudes des Equilibres entre Phases, 26 - 28 March 2014, France.

4) Silvia Lasala*, Costante Invernizzi, Paolo Iora, Paolo Chiesa, Ennio Macchi, "Thermal stability analysis of per-fluorohexane", ICAE - International Conference on Applied Energy, 28 - 31 March 2015, United Arab Emirates.

5) Silvia Lasala*, Yohann Le Guennec, Romain Privat, Jean-Noël Jaubert. "The role of alpha functions in the thermodynamic modeling of supercritical pure components", JETC - Joint European Thermodynamics Conference. 20 - 22 May 2015, France.

6) Silvia Lasala*, Romain Privat, Jean-Noël Jaubert. "Modelling Vapour – Liquid Equilibria of CO2 Mixtures with Equations of State / Excess Helmholtz Energy models", ECCE10 - European Congress of Chemical Engineering. 27 September - 1 October 2015, France.

7) Silvia Lasala*. "Towards a clever optimization of thermodynamic models". **Keynote lecture** at the seminar "Données thermodynamiques : production, cohérence et impact sur le dimensionnement des procédés industriels" organized by IFP Energies nouvelles – GT Thermodynamique des Procédés de la SFGP. 1 avril 2016, Rueil-Malmaison, France. (National congress)

8) Romain Privat, Silvia Lasala, Yohann Le Guennec, Jean-Noël Jaubert*. "Optimal design of the cohesive parameter in cubic equations of state", PPEPPD–International Conference on Properties and Phase Equilibria for Product and Process Design. 22 – 26 May 2016, Portugal.

9) Jean-Noël Jaubert*, Romain Privat, Silvia Lasala, Yohann Le Guennec, "Mathematical constraints for an optimal design of temperature-dependent attractive parameter expressions in cubic equations of state". **Keynote lecture**, CHISA – International Congress of Chemical and Process Engineering. 27 – 31 August 2016, Czech Republic.

10) Silvia Lasala*, "Advanced Cubic Equations of State for Accurate Modelling of Fluid Mixtures. Application to CO2 Capture Systems". XXII congress A.I.P.T. – "Associazione Italiana Proprietà Termofisiche". 23 September 2016, Reggio Emilia, Italy. (National congress)

11) Jean-Noël Jaubert*, Romain Privat, Yohann Le Guennec, Silvia Lasala, "A new Pure-Component Equation of State Designed for Accurate Reproduction of Phase-Equilibrium, Caloric and Volumetric Properties with Emphasis on Supercritical-Property Prediction". **Keynote lecture**, 2016 AIChE Annual Meeting, 13 – 18 November 2016, San Francisco.

12) Silvia Lasala, Romain Privat, Jean- Noël Jaubert*, Philippe Arpentinier, "Modelling the thermodynamics of mixtures of N2, O2, Ar. The state-of-the-art of available models". TPTPR - Conference on Thermophysical Properties and Transfer Process of Refrigerants, 23 – 26 April 2017, South Korea.

13) Silvia Lasala*, Paolo Chiesa, Romain Privat, Jean-Noël Jaubert. “Accurate modelling of high-pressure phase-equilibria of mixtures containing non-condensable components.” ESAT – European Symposium on Applied Thermodynamics, 18-21 May 2017, Romania.

14) Silvia Lasala*, Paolo Chiesa, Romain Privat, Jean-Noël Jaubert. “The impact of thermodynamic model accuracy on sizing and operating CCS purification and compression units”. CETCCUS - Cutting-Edge Technology for Carbon Capture, Utilization and Storage, 24-27 September 2017, France.

15) Jean-Noël Jaubert*, Silvia Lasala. “Carbon dioxide capture and storage (CCS) processes: influence of the thermodynamic model on performance calculations and sizing considerations”. Plenary lecture, RICCCE - Romanian International Conference on Chemistry and Chemical Engineering, 6-9 September 2017, Romania.

16) Marco Astolfi*, Silvia Lasala, Ennio Macchi. “Selection maps for ORC and CO2 Systems for low-medium temperature heat sources”. International Seminar on ORC Power Systems, 13-15 September 2017, Italy.

17) Silvia Lasala, Davide Bonalumi*, Ennio Macchi, Romain Privat, Jean-Noel Jaubert. “The design of CO2-based working fluids for high-temperature heat source power cycles”. International Seminar on ORC Power Systems, 13-15 September 2017, Italy.

18) Romain Privat*, Jean-Noël Jaubert, Silvia Lasala, Yohann Le Guennec, Xiauchun Xu. “New horizons for cubic equations of state”. TEEP - Thermodynamique des équilibres entre phases, 7-8 December 2017, Clermont-Ferrand, France.

19) Øivind Wilhelmsen*, Ailo Aasen, Morten Hammer, Jean-Noël Jaubert and Silvia Lasala. “Simple Quantum Corrections Improve the Accuracy of Cubic Equations of State for Mixtures That Contain Hydrogen, Helium, Neon and Deuterium”. Twenty-first symposium on thermophysical properties. June 20-25 2021, Boulder, USA.

20) Silvia Lasala*, Jean-Noël Jaubert. “The exploitation of reactive working fluids in a closed thermodynamic cycle. A breakthrough high-energy conversion system”. ESAT – European Symposium on Applied Thermodynamics, 4-7 July 2021, Paris (virtual form).

21) Cindy Trinh*, Dimitrios Meimaroglou, Silvia Lasala, Olivier Herbinet. “Machine Learning for the prediction of the thermochemical properties (enthalpy and entropy of formation) of a molecule from its molecular descriptors”. 32nd European Symposium on Computer-Aided Process Engineering - ESCAPE32. 12-15 June 2022, Toulouse, France.

22) Aya Barakat*, Silvia Lasala, Jean-Noel Jaubert. “The efficient exploitation of chemical energy in heat pumps”. The 35th International Conference on Efficiency, Cost, Optimization, Simulation and Environmental Impact of Energy Systems - ECOS 2022, 3-7 July 2022, Copenhagen, Denmark.

23) Andrés Pina-Martinez*, Silvia Lasala, Romain Privat, Véronique Falk, Jean-Noël Jaubert. “Apport de la méthodologie Product Design pour identifier le fluide de travail optimal d’un cycle de trigénération (chaleur, électricité, froid)”. 18ème Congrès de la Société Française De Génie Des Procédés - SFGP2022. 7-10 Nov. 2022, Toulouse, France. (National congress)

24) Andrés Pina-Martinez*, Silvia Lasala, Romain Privat, Jean-Noël Jaubert. “Design of Promising Working Fluids for Emergent Combined Cooling, Heating, and Power (CCHP) Systems”. PPEPPD 2022, Properties & Phase Equilibria for Product & Process Design. 21-25 May 2023, Tarragona, Spain.

25) Silvia Lasala*, Jean-Noel Jaubert, Konstantin Samukov, Cindy Trinh, Dimitrios Meimaroglou, Olivier Herbinet. “Computing the thermodynamic properties of equilibrated reactive mixtures by means of equations of state: the necessary appeal to Quantum Chemistry and molecular

Monte Carlo simulations." 14th European Congress of Chemical Engineering (ECCE-2023). 10-13 September 2023, Berlin, Germany.

26) Aya Barakat*, Silvia Lasala, Jean-Noël Jaubert. "Understanding the thermodynamic effects of reactive working fluids in the Stirling engine". 14th European Congress of Chemical Engineering (ECCE-2023). 10-13 September 2023, Berlin, Germany.

27) Cindy Trinh*, Dimitrios Meimaroglou, Silvia Lasala, Olivier Herbinet. "Machine learning prediction of thermodynamic properties from molecular descriptors: towards a general and automatic approach in presence of high dimensional data sets and limited knowledge". 14th European Congress of Chemical Engineering (ECCE-2023). 10-13 September 2023, Berlin, Germany.

28) Dimitrios Meimaroglou*, Cindy Trinh, Olivier Herbinet, Silvia Lasala. "On the effect of the different choices along the implementation of a machine-learning approach to a product engineering problem: Example of the prediction of thermodynamic properties of molecules." **Keynote lecture** at IGSMP INTERNATIONAL. 13 May 2023. Virtual event.

29) Silvia Lasala*, "A still unexploited solution to boost efficiency of power plants, heat pumps and refrigeration cycles (?)". **Keynote lecture** at Science Days of Silesian University of Technology. 4-5 July 2023, Gliwice, Pologne.

30) Silvia Lasala*, Jean-Noël Jaubert. "The fundamental role of multi-scale thermodynamics. An application to reactive media proposed as working fluids for thermodynamic cycles". **Keynote lecture** at 22nd European Conference on Thermophysical Properties (ECTP). 10-13 September 2023, Venise (Italy).

31) Konstantin Samukov*, Silvia Lasala, Jean-Noël Jaubert, Romain Privat. "Calculating phase equilibrium properties of the reactive N2O4-NO2 system". 22nd European Conference on Thermophysical Properties (ECTP). 10-13 September 2023, Venise (Italy).

32) Aya Barakat*, Silvia Lasala, Jean-Noël Jaubert. "The thermodynamic effects of using reactive working fluids in the Stirling cycle". 22nd European Conference on Thermophysical Properties (ECTP). 10-13 September 2023, Venise, Italy.

33) Aya Barakat*, Silvia Lasala, Jean-Noël Jaubert. "Understanding the thermodynamic effects of reactive working fluids in the Stirling engine". ECCE2023. 17-21 September 2023, Berlin, Germany.

34) Silvia Lasala*, Jean-Noël Jaubert, Romain Privat, Konstantin Samukov, Cindy Trinh, Dimitrios Meimaroglou, Olivier Herbinet. "Computing the thermodynamic properties of mixtures by means of equations of state: the necessary appeal to Quantum Chemistry and molecular Monte Carlo simulations". ECCE2023. 17-21 September 2023, Berlin, Germany.

35) Dimitrios Meimaroglou*, Cindy Trinh, Silvia Lasala, Olivier Herbinet. "Machine learning prediction of thermodynamic properties from molecular descriptors: towards a general and automatic approach in presence of high dimensional data sets and limited knowledge". ECCE2023. 17-21 September 2023, Berlin, Germany.

36) Konstantin Samukov*, Silvia Lasala, Romain Privat, Véronique Lachet, Jean-Noël Jaubert, "Calculation of the thermodynamic properties of the reactive fluid N2O4 ↔ 2 NO2 and its mixtures with inert gases". JEEP - Journées d'Etudes des Equilibres entre Phases, 4-6 October 2023, France. (National congress)

37) Silvia Lasala*, Romain Privat, Konstantin Samukov, Jean-Noël Jaubert, H. Mert Polat, Thijs J. H. Vlugt. Modelling the thermodynamic properties of reactive working fluids for thermodynamic cycles. 22nd Symposium on Thermophysical Properties. 23-28 June, 2024, University of Colorado, Boulder.

38) Silvia Lasala, Romain Privat, Konstantin Samukov, Jean-Noël Jaubert*, H. Mert Polat, Thijs J. H. Vlugt. How the synergy between quantum mechanics simulations, Monte Carlo simulations and an equation of state can be used to describe the behaviour of reacting binary mixtures in vapour-liquid equilibrium. ESAT 2024. 9-12 June 2024, Edinburgh, UK.

List of poster communications

1) Silvia Lasala*, Paolo Chiesa, Ennio Macchi, "Binary mixtures of carbon dioxide and fluorocarbons: review of thermodynamic data and their modelling", JEEP 2014 - 40ième Journées d'Etudes des Equilibres entre Phases, 26 - 28 March 2014, Lyon, France.

2) Silvia Lasala*, Romain Privat, Jean-Noël Jaubert. "Vapour – Liquid Equilibrium Modelling and Experimental Data: The Role of Molar Fraction Uncertainties", ECCE10 – 10th European Congress of Chemical Engineering. 27 September - 1 October 2015, Nice, France.

3) Silvia Lasala*, Romain Privat, Jean-Noël Jaubert, "Modélisation de systèmes rencontrés dans les procédés de capture et stockage du CO2 à l'aide d'une équation d'état cubique munie de règles de mélange complexes". JNSC 2016. 9 – 10 June 2016, Bordeaux, France.

4) Silvia Lasala*, Romain Privat, Jean-Noël Jaubert, Philippe Arpentinier. The state-of-the-art of available thermodynamic models for N2-O2-Ar mixtures. ESAT 2017 – European Symposium on Applied Thermodynamics, 18-21 May 2017, Bucharest, Romania

5) Silvia Lasala*, Romain Privat, Jean-Noël Jaubert. The thermodynamics of mixtures characterized by discontinuous critical points loci. ESAT 2017 – European Symposium on Applied Thermodynamics, 18-21 May 2017, Bucharest, Romania

6) Philippe Arnoux*, Silvia Lasala, Olivier Herbinet, Sarena Loulha, Ryma Benrabah, Pierre-Alexandre Glaude, Baptiste Sirjean, Saad Nader, Yann Le Brech, Anthony Dufour. "Fluorescence and Raman spectroscopy applications in the field of biomass, combustion and energy". MECAREACT 2023, 18-23 June, Paris, France. (National congress)

7) Aya Barakat*, Silvia Lasala, and Jean-Noël Jaubert. "Understanding the thermodynamic effects of chemically reactive working fluids in the Stirling engine". JEEP - Journées d'Etudes des Equilibres entre Phases, 4-6 October 2023, France. (National congress)

8) Rachid Hadjadj*, Olivier Herbinet, Silvia Lasala. "Molecular design of reactive fluids for thermodynamic cycles". JEEP - Journées d'Etudes des Equilibres entre Phases, 4-6 October 2023, France. (National congress)